



PALACKÝ UNIVERSITY IN OLOMOUC

Faculty of Science

Laboratory of Growth Regulators

**Metabolic profiling of phytohormones
in subcellular compartments using LC-MS
techniques**

Ph.D. thesis

Author:	Mgr. Vladimír Skalický
Study programme:	P1527 / Biology
Study branch:	1501V019 Experimental biology
Form:	Daily
Supervisor:	doc. Mgr. Ondřej Novák, Ph.D.
Consultant:	Dr. Ioanna Antoniadis
Date of submitting:	27. 9. 2021

Bibliografická identifikace

Jméno a příjmení autora	Vladimír Skalický
Název práce	Metabolické profilování rostlinných hormonů v buněčných organelách pomocí LC-MS technik
Typ práce	Disertační
Pracoviště	Laboratoř růstových regulátorů
Vedoucí práce	doc. Ondřej Novák, Ph.D.
Rok obhajoby práce	2021
Abstrakt	<p>Auxiny a cytokininy jsou dvě hlavní skupiny fytohormonů, které regulují a kontrolují většinu aspektů růstu, vývoje a plasticity rostlin. Jejich distribuce v rostlinných orgánech případně pletivech je již popsána. Zastoupení fytohormonů na úrovni buněčných typů či organel se stále intenzivně studuje. Mimoto odlišná lokalizace enzymů zapojených do biosyntézy a degradace fytohormonů, receptorů a transportérů naznačuje intracelulární regulaci jejich umístění v buňce. Objasnění subcelulární distribuce obou fytohormonů umožní lepší pochopení udržování vnitřní rovnováhy rostlinných buněk a časoprostorovou percepci fytohormonů. Proto byla optimalizována hustotně-gradientová centrifugace a vyvinuta inovativní metoda pro frakcionaci organel, založená na principech průtokové cytometrie zvaná vícecestné průtokové třídění organel na základě aktivované fluorescence (FAMOS z angl. Fluorescence-activated multi-Organelle Sorting). Kombinace FAMOS s hmotnostní spektrometrií poskytuje unikátní a robustní techniku nejen pro studování profilů rostlinných hormonů na úrovni organel, ale i proteomů či metabolomů.</p>
Klíčová slova	Auxin, cytokinin, subcelulární homeostáza, subcelulární frakcionace, průtoková cytometrie, LC-MS/MS
Počet stran	61
Počet příloh	6
Jazyk	Anglický

Bibliographical identification

Author's first name and surname	Vladimír Skalický
Title of thesis	Metabolic profiling of phytohormones in subcellular compartments using LC-MS techniques
Type of thesis	Ph.D.
Department	Laboratory of Growth Regulators & Institute of Experimental Botany AS CR & Faculty of Science of Palacký University
Supervisor	doc. Ondřej Novák, Ph.D.
The year of presentation	2021
Abstract	<p>Auxins and cytokinins are two major families of phytohormones which control and regulate most aspects of plant growth, development, and plasticity. Their distribution within plant organs or tissues is already well studied but the importance of cell-type-specific and intracellular phytohormone homeostasis is still under intense investigation. Further, distinct localization of transporters, receptors and enzymes related to auxin and cytokinin suggests control of their allocation within the plant cell. Gaining knowledge on the intracellular distribution of both phytohormones can enable deeper understanding of their homeostasis maintenance and spatial-temporal signalling in plants. Hence, density-gradient ultracentrifugation was optimised and Fluorescence-activated multi-Organelle Sorting (FAmOS), the innovative subcellular compartment separating technique based on principles of flow cytometry was developed. Combination of the subcellular fractionation with the mass spectrometry-based analysis provide a unique and powerful tool for studying organelle-specific phytohormone profiles as well as proteomes and metabolomes.</p>
Keywords	Auxin, cytokinin, subcellular homeostasis, subcellular fractionation, flow cytometry, LC-MS/MS
Number of pages	61
Number of appendices	6
Language	English

Declaration of originality

I hereby, declare that the presented dissertation thesis summarizes original results obtained during my Ph.D. under the great supervision of doc. Mgr. Ondřej Novák, Ph.D. and Dr. Ioanna Antoniadí. The literature used is listed in the References section.

Olomouc

Mgr. Vladimír Skalický

Acknowledgement

This research was performed at the Laboratory of Growth Regulators (LGR), Faculty of Science, Palacký University in Olomouc under the great supervision of doc. Mgr. Ondřej Novák, Ph.D. I thank him for his expert advices, patience, encouragement, and friendly discussion of results. My special thanks belong to Dr. Ioanna Antoniadou for her inspiration, English editing, and mainly for great collaboration which turned to close friendship. I thank also to Mgr. Aleš Pěňčík, Ph.D., RNDr. Martin Kubeš, Ph.D., prof. Karin Ljung, Mgr. Karel Doležal, Dr., DSc. and prof. Ing. Miroslav Strnad, CSc. DSc. for scientific and academic support during the studies. I would like to express big thanks to my colleagues from LGR and Umeå Plant Science Centre (UPSC) who participate in research projects and other lab members who created friendly and inspirational environment.

I would like to thank my family, friends for their great support and continual encouragement.

This work was supported by the Czech Foundation Agency (GA17-21581Y), by the Internal Grant Agency of Palacký University (IGA_PrF_2021_011, IGA_PrF_2021_016), and partially by Endowment fund of Palacký University in Olomouc.

Content

List of papers	1
Contribution report	2
Abbreviations	3
1 Introduction	5
2 Aims and scopes	6
3 Literature review	7
3.1 Plant hormones	7
3.2 Auxins	7
3.2.1 Auxin metabolism	8
3.2.2 Auxin transport	11
3.2.3 Auxin signalling	12
3.3 Cytokinins	13
3.3.1 Cytokinin metabolism	14
3.3.2 Cytokinin transport	17
3.3.3 Cytokinin signalling	19
3.4 Subcellular fractionation	20
3.4.1 Plant tissue homogenization	20
3.4.2 Fractionation based on centrifugation	21
3.4.3 Flow cytometry	23
3.4.4 Affinity purification	26
3.4.5 Free-flow electrophoresis	27
3.5 Phytohormone profiling at subcellular level	27
4 Materials and methods	29
4.1 Chemicals	29
4.2 Plant material and growth conditions	29
4.3 Equipment	30
5 Survey of results	32
5.1 Revealing auxin metabolome in the endoplasmic reticulum isolated by density-gradient ultracentrifugation	32
5.2 Comparison of isolation methods for auxin metabolome determination in nucleus ..	35
5.3 Auxin and cytokinin subcellular map	37
6 Conclusion and perspectives	41
7 References	42
8 Supplements I – VI	61

List of papers

This thesis summarizes and links the following papers that are referred in the text by Roman numerals I-VI and are attached at the end of the thesis in the Supplementary section.

- I **Skalický V**¹, Kubeš M¹, Napier R, Novák O. (2018) Auxins and cytokinins—the role of subcellular organization on homeostasis. *Int. J. Mol. Sci.* **19** (10), 3115.
- II Galbraith D, Loureiro J, Antoniadis I, Bainard J, Bureš P, Cápál P, Castro M, Castro S, Čertner M, Čertnerová D, Chumová Z, Doležel J, Giorgi D, Husband BC, Kolář F, Koutecký P, Kron P, Leitch IJ, Ljung K, Lopes S, Lučanová M, Lucretti S, Ma W, Melzer S, Molnár I, Novák O, Poulton N, **Skalický V**, Sliwinska E, Šmarda P, Smith TW, Sun G, Talhinas P, Tárnok A, Temsch EM, Trávníček P, Urfus T. (2021) Best practices in plant cytometry. *Cytometry A.* **99** (4), 311-317.
- III Antoniadis I, **Skalický V**, Sun G, Ma W, Galbraith DW, Novák O, Ljung K. (2021) Fluorescence Activated Cell Sorting – A selective tool for plant cell isolation and analysis. *Cytometry A.* **99** (Online ahead of print) doi: 10.1002/cyto.a.24461.
- IV Včelařová L¹, **Skalický V**¹, Chamrád I, Lenobel R, Kubeš FM, Pěňčík A, Novák O. (2021) Auxin metabolome profiling in the Arabidopsis endoplasmic reticulum using an optimised organelle isolation protocol. *Int. J. Mol. Sci.* **22** (17), 9370.
- V **Skalický V**, Vojtková T, Pěňčík A, Vrána J, Katarzyna J, Koláčková V, Sedlářová M, Napier R, Kubeš MF, Novák O. (2021) Auxin profiling in isolated intact plant nuclei. *Int. J. Mol. Sci.* (submitted)
- VI **Skalický V**¹, Antoniadis I¹, Pěňčík A, Chamrád I, Lenobel R, Kubeš FM, Strnad M, Ljung K, Novák O. (2021) Fluorescence-activated multi-organelle sorting: A smart tool for subcellular mapping of auxins and cytokinins. (in preparation)

¹ These authors contributed equally to the presented works.

Contribution report

- I As the first author, VS performed literature review of subcellular cytokinin homeostasis and organelle-specific phytohormone profiling.

- II As a co-author, VS participated on writing the review and text editing.

- III As a co-author, VS participated on conceptualization, visualization, wrote a part of original draft, reviewed, and edited the text.

- IV As the first joined author, VS developed and optimised an isolation of endoplasmic reticulum (ER), optimized sample processing for auxin and protein analysis. VS set an evaluation method for determination of ER enrichment. VS also wrote the manuscript.

- V As the first author, VS developed and optimized isolation of nuclei. VS evaluated purity and enrichment of nuclear fraction. VS also wrote the manuscript.

- VI As the first author, VS developed flow cytometric method for plant organelle sorting. VS performed control and *in vivo* labelling experiments with subsequent organelle sorting. VS evaluated enrichment of sorted organelle populations. VS also wrote the manuscript.

Abbreviations

AA	amino acid
ABCB	ATP-binding cassette subfamily B
ABCG	ATP-binding cassette subfamily G
ABP1	AUXIN BINDING PROTEIN1
AFB	AUXIN SIGNALING F-BOX
AHK	ARABIDOPSIS HISTIDINE KINASE
AHP	ARABIDOPSIS HISTIDINE PHOSPHOTRANSFER
AP	affinity purification
APT	ADENINE PHOSPHORIBOSYLTRANSFERASE
ARF	AUXIN RESPONSE FACTOR
ARR	ARABIDOPSIS RESPONSE REGULATOR
Asp	aspartic acid
AUX1/LAX	AUXIN RESISTANT1/LIKE AUX1
BA	<i>N</i> ⁶ -benzyladenine
BY-2	<i>Nicotiana tabacum</i> cv. Bright Yellow 2 cell line
CHASE	cyclase/histidine kinase associated sensory extracellular domain
CK	cytokinin
CKX	CYTOKININ OXIDASE/DEHYDROGENASE
Col-0	<i>Arabidopsis thaliana</i> ecotype Columbia
CRISPR	clustered regularly interspaced short palindromic repeats
CYP	CYTOCHROME P450
<i>cZ</i>	<i>cis</i> -zeatin ((2 <i>Z</i>)-2-methyl-4-(9 <i>H</i> -purin-6-ylamino)but-2-en-1-ol)
DAO1	DIOXYGENASE FOR AUXIN OXIDATION 1
DAPI	4',6-diamidino-2-phenylindole
DC	differential centrifugation
DGU	density-gradient ultracentrifugation
DHZ	dihydrozeatin (2-methyl-4-(7 <i>H</i> -purin-6-ylamino)butan-1-ol)
ELISA	enzyme-linked immunosorbent assay
ENT	EQUILIBRATIVE NUCLEOSIDE TRANSPORTER
ER	endoplasmic reticulum
FACS	fluorescence-activated cell sorting
FAmOS	fluorescence-activated multi-organelle sorting
FCM	flow cytometry
FFE	free-flow electrophoresis
GFP	GREEN FLUORESCENT PROTEIN
GH3	GRETCHEN HAGEN 3
glc	glucose
Glu	glutamic acid
IAA	indole-3-acetic acid
IAN	indole-3-acetonitrile
IBA	indole-3-butyric acid
iP	<i>N</i> ⁶ -isopentenyladenine (6-(γ,γ -dimethylallylamino)purine)

iPR	<i>N</i> ⁶ -isopentenyladenosine
iPRDP	<i>N</i> ⁶ -isopentenyladenosine-5'-diphosphate
iPRTP	<i>N</i> ⁶ -isopentenyladenosine-5'-triphosphate
IPT	ISOPENTENYL TRANSFERASE
IPyA	indole-3-pyruvic acid
LC-MS/MS	liquid chromatography combined with tandem mass spectrometry
<i>Ler</i>	<i>Arabidopsis thaliana</i> ecotype Landsberg <i>erecta</i>
LOG	LONELY GUY
MeIAA	indole-3-acetic acid methyl ester
oxIAA	2-oxindole-3-acetic acid
PAT	polar auxin transport
PILS	PIN-LIKES
PIN	PIN-FORMED
PM	plasma membrane
PUP	PURINE PERMEASE
RIA	radioimmunoassay
SCF	S-PHASE KINASE ASSOCIATED PROTEIN 1 - CULLIN 1 - F-BOX
SKP2A	S-PHASE KINASE-ASSOCIATED PROTEIN 2A
TAA1	TRYPTOPHAN AMINOTRANSFERASE OF ARABIDOPSIS1
TARs	TAA1-RELATED proteins
TIR1	TRANSPORT INHIBITOR RESPONSE1
TRA	tryptamine
Trp	tryptophan
<i>tZ</i>	<i>trans</i> -zeatin ((<i>E</i>)-2-methyl-4-(7 <i>H</i> -purin-6-ylamino)but-2-en-1-ol)
<i>tZR</i>	<i>trans</i> -zeatin riboside
UGT	UDP-GLYCOSYLTRANSFERASE
WAT1	WALLS ARE THIN1
WT	wild type
YUC	YUCCA

1 Introduction

Auxins and cytokinins (CKs) are the best-described plant hormones that regulate a variety of physiological processes in plants. Therefore, they play a crucial role in proper plant development and growth. Homeostasis of these phytohormones is tightly regulated by coordination of biosynthesis, transport, and metabolism. This leads to different distributions of auxin and CK within the plant body, organ, or tissue. In addition, the distinct enzymes and transporters' localization involved in the maintenance of homeostasis within the cell indicates a further level of complex regulation. To date, the organelle-specific profile of auxin or CK has only been described in chloroplasts and vacuoles. Nevertheless, a comprehensive view of this issue is still missing.

Several subcellular fractionation approaches such as differential centrifugation, density-gradient ultracentrifugation (DGU), affinity purification, and flow cytometric sorting have been developed. However, many of them focus only on one type of organelle. In addition, DGU is the gold standard for organelle isolation, but its resolving power may not be appropriate for phytohormone profiling.

This doctoral thesis describes the development of a method of subcellular fractionation based on DGU and flow cytometry (FCM) followed by profiling of phytohormones in isolated organelles by sensitive mass spectrometric methods. Flow cytometric method enabled simultaneous sorting of chloroplasts, nuclei, mitochondria, and endoplasmic reticulum (ER) from one sample. Combination of these approaches can shed light on the regulation mechanisms that maintain phytohormone homeostasis within the plant cell.

2 Aims and scopes

Auxins and CKs are master regulators of myriad physiological and developmental processes *in planta*. Their distribution within plant organs and tissues is already well described, but the importance of cell-type specific phytohormone homeostasis is currently under intense investigation. Moreover, intracellular auxin and CK dislocation and mechanisms of homeostasis maintenance are still elusive. Therefore, this doctoral thesis deals with auxin and CK metabolic profiling at the subcellular level.

The main aims of the work described and discussed in this thesis were as follows:

- to review the homeostasis of auxin and CK at the subcellular level and subcellular fractionation approaches,
- to develop and optimize protocols for subcellular compartments isolation with view to subsequent phytohormone analysis,
- to optimize the purification protocol for auxin and CKs analysis from isolated organelles,
- to analyse the profiles of auxin and CK in particular plant organelles,
- to create the subcellular map of auxin and CK concentrations.

3 Literature review

3.1 Plant hormones

Plant hormones (phytohormones) are central players in growth, development, and plasticity *in planta*. They represent signalling molecules that regulate physiological processes as a reaction to exogenous as well as to endogenous stimuli. Phytohormones are determined as naturally occurring organic compounds that act at extremely low concentrations and are perceived and transduced through specialized receptors (Davies, 2010). Nine phytohormonal groups have been described so far, including auxins, CKs, gibberellins, abscisates, ethylene, brassinosteroids, jasmonates, salicylic acid, and the most recently discovered strigolactones (Tarkowská et al., 2014). Each member of the phytohormone groups can regulate physiological responses in the plants by acting either alone or in cooperation with other phytohormone(s), also known as hormonal crosstalk. The latter enables fine-tuning of hormonal responses depending on the plant's developmental or biological context. Furthermore, phytohormones can act synergistically as well as antagonistically to regulate plant functions (Schaller et al., 2015; Hurný et al., 2020) and mutual influence on their homeostasis has been also shown (Šimášková et al., 2015; Di Mambro et al., 2019).

3.2 Auxins

Auxins were the first phytohormonal group discovered back in 19th century (Darwin and Darwin, 1880). In general, when auxin is mentioned, it concerns the most well-known representative active compound, indole-3-acetic acid (IAA) (Figure 1). However, other endogenous auxin-active compounds, such as 4-chloroindole-3-acetic acid or phenylacetic acid, have been also described (Simon and Petrášek, 2011). Commonly, auxins are weak organic acids consisting of a planar aromatic ring and a carboxyl group side chain critical which drives their activity (Bielešzová et al., 2018).

Auxins have great impact on plant growth and influence plenty developmental and physiological processes such as tropisms, shoot apical dominance, leaf abscission, embryogenesis, organogenesis, tissue patterning, cell division, expansion and differentiation (reviewed in Schaller et al., 2015; Casanova-Sáez et al., 2021; Gomes and Scortecci, 2021). Therefore, it is essential for the plants to keep an accurate spatio-temporal occurrence of auxin during their entire plant life span. Differential auxin distributions within the plant

body, organs, or tissues are indispensable for organogenesis and development of all land plants (Vanneste and Friml, 2009). Homeostasis of IAA is strictly controlled and balanced by coordination of their biosynthesis, metabolism and transport, which will be described in the following chapters.

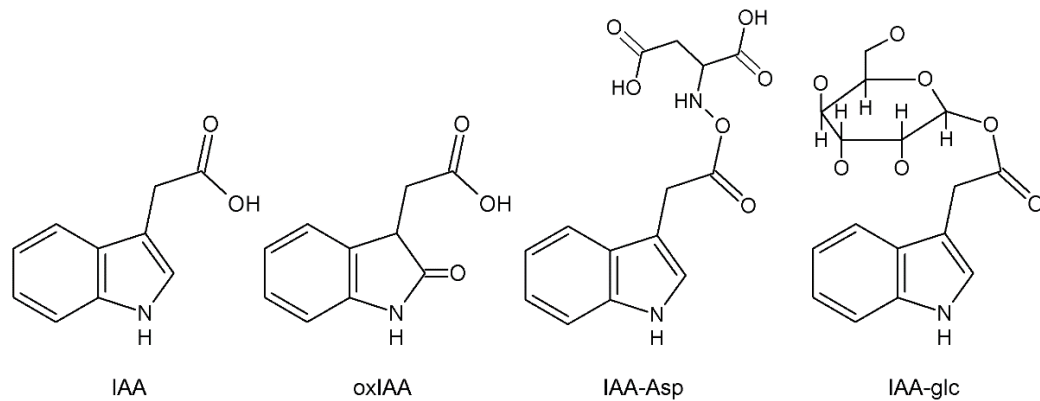


Figure 1 Chemical structures of indole-3-acetic acid (IAA) and its metabolites: oxIAA – 2-oxindole-3-acetic acid, IAA-Asp – IAA-aspartic acid, IAA-glc – IAA-glucose.

3.2.1 Auxin metabolism

Auxins play irreplaceable role in plant growth and development. Therefore, IAA is synthesised mainly in young developing organs or tissues such as apical meristems. Several biosynthetic pathways of this crucial phytohormone have been described so far. Firstly, tryptophan (Trp)-dependent auxin biosynthesis starts in chloroplasts by production of Trp via the shikimate pathway (Figure 2) (Maeda and Dudareva, 2012). Then the Trp-dependent pathway is branching to other 4 parallel routes named according to the first metabolite formed from Trp as follows: indole-3-pyruvic acid (IPyA), indole-3-acetamide, tryptamine and indole-3-acetaldoxime pathways (reviewed in Ljung, 2013).

The two-step IPyA pathway is believed to be prevailing in Arabidopsis and is the only pathway that has been fully described (Casanova-Sáez and Voß, 2019; Casanova-Sáez et al., 2021). In this IAA biosynthesis pathway, Trp is converted to IPyA by TRYPTOPHAN AMINOTRANSFERASE OF ARABIDOPSIS1 (TAA1) or TAA1-RELATED proteins (TARs) (Stepanova et al., 2008; Tao et al., 2008). Subsequently, YUCCAs (YUCs), the flavin-contained monooxygenase enzymes, transform IPyA to active IAA (Mashiguchi et al., 2011; Stepanova et al., 2011). TAA1 and YUCs were localized to the cytosol (Kim et al., 2007; Tao et al., 2008). However, YUC4 may be anchored to ER membrane and facing to the cytosol depending on alternative splicing regulation (Figure 2) (Kriechbaumer et al.,

2012). Interestingly, Kriechbaumer et al. (2016) described that the TAA1/YUC enzyme complex resides at ER. However, the YUC enzymes family comprises several enzymes whose localization yet remains unclear. The other Trp-dependent parallel pathways can be plant species-specific and many are not fully understood (Casanova-Sáez et al., 2021). Finally, IAA can be also synthesized by a Trp-independent pathway. This route was proposed based on the detection of IAA in Trp-synthesis defective mutants in maize and Arabidopsis (Wright et al., 1991; Normanly et al., 1993). In agreement with this, a cytosolic indole synthase converting indole-3-glycerol phosphate to indole was described (Zhang et al., 2008; Wang et al., 2015). However, this pathway is still poorly understood as the subsequent key enzymes producing IAA from indole remain unknown (Casanova-Sáez et al., 2021).

The pool of free active IAA is well-regulated by biosynthesis and metabolism processes. These two mechanisms of auxin homeostasis maintenance involve enzymes that are distinctly localized within plant cell bringing an additional level of regulation complexity (Kriechbaumer et al., 2012). IAA can be reversibly inactivated by conjugation with sugars, amino acids (AAs), peptides or proteins as a storage form, which can be hydrolysed back or irreversibly deactivated to auxin catabolites (Ljung, 2013). Conjugation of IAA with AAs is catalysed by Group II members of GRETCHEN HAGEN 3 (GH3) family (Staswick et al., 2005). *GH3* genes are rapidly induced upon IAA treatment and act as a negative feedback loop resulting in reduction of IAA levels (Ludwig-Müller, 2011). Although GH3 enzymes are important for IAA steady-state level maintenance, their subcellular localization is not fully revealed. Nevertheless, Di Mambro et al. (2019) recently published that GH3.17 occurs in cytosol. Various IAA-AAs conjugates that have been detected *in planta* comprise the following AAs: aspartic (Asp) and glutamic acid (Glu), glycine, leucine, phenylalanine, valine and alanine (Kowalczyk and Sandberg, 2001; Pěnčík et al., 2009). However, IAA-Asp (Figure 1) and IAA-Glu are the most abundant IAA-AA forms in Arabidopsis (Novák et al., 2012). Moreover, these two IAA-AA conjugates are considered to be resistant or not efficiently cleaved to IAA by amidohydrolases (LeClere et al., 2002). Other IAA-AAs can be hydrolysed in the ER (Sanchez Carranza et al., 2016; Fu et al., 2019).

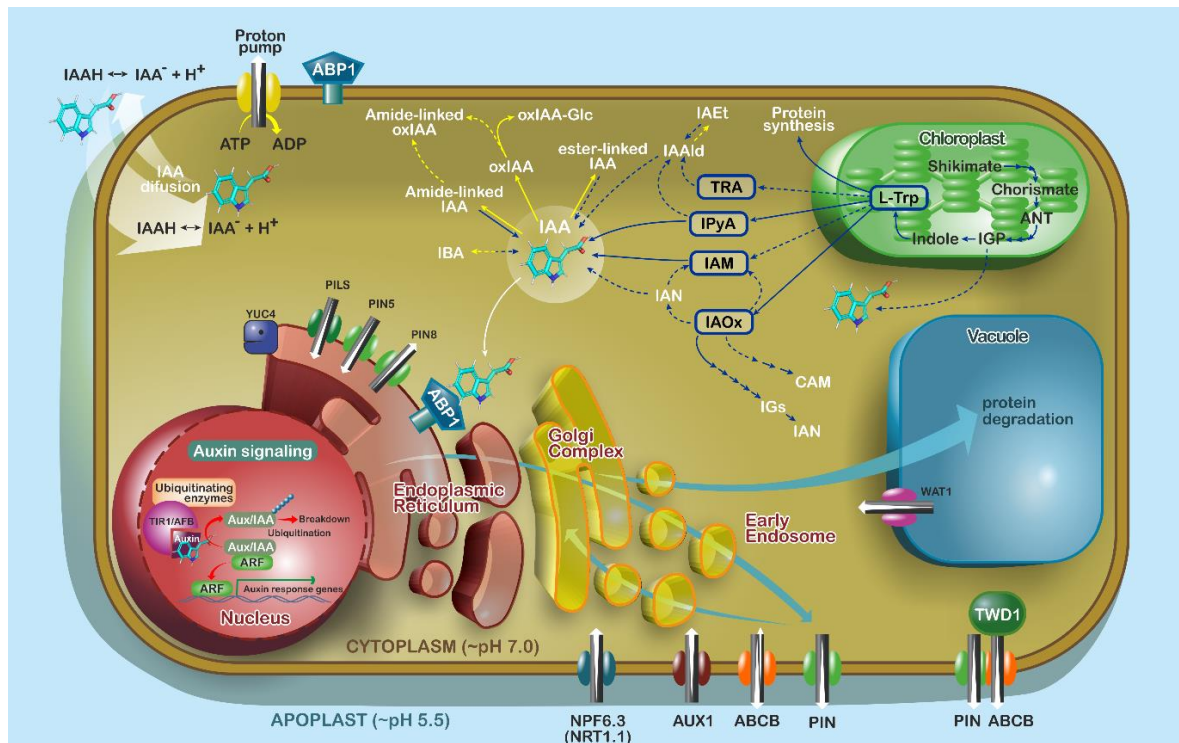


Figure 2 Model of cellular and subcellular auxin homeostasis (Skalický et al., 2018).

Furthermore, IAA levels can be modulated via a reversible conjugation with glucose (glc) (Figure 1) catalysed by UDP-GLUCOSYL TRANSFERASEs (UGTs) (Jin et al., 2013a). IAA-glc ester is believed to be an IAA storage form which is enriched in vacuoles (Ranocha et al., 2013). Methyl ester of IAA (MeIAA) and indole-3-butyric acid (IBA) are also considered putative storage forms of IAA (Qin et al., 2005; Zolman et al., 2008; Casanova-Sáez and Voß, 2019). Qin et al. (2005) discovered that MeIAA is formed by *Arabidopsis* IAA CARBOXYL METHYLTRANSFERASE1 and can be hydrolysed back by METHYLESTERASE17 (Yang et al., 2008). While the origin of IBA still remains unclear, its catabolism to IAA can occur in peroxisomes by β -oxidation (Zolman et al., 2008). Nevertheless, the biological relevance of IBA is still under discussion in the scientific community, mainly because IBA has been endogenously undetectable in several plant species, e.g. *Arabidopsis*, poplar and wheat (Novák et al., 2012).

Finally, the activity of IAA can be abolished by its conversion to 2-oxindole-3-acetic acid (oxIAA) (Figure 1) via the cytosolic DIOXYGENASE FOR AUXIN OXIDATION 1 (DAO1) (Porco et al., 2016; Zhang et al., 2016). Nevertheless, oxIAA can be further glycosylated to oxIAA-glc (Tanaka et al., 2014). IAA oxidation is a constitutive catabolic process in *Arabidopsis* to keep balance of endogenous levels of IAA (Mellor et al., 2016; Zhang et al., 2016). Interestingly, *dao1* mutants showed elevated levels of IAA-AAs whereas

concentration of free IAA remained close to the wild type (WT) levels (Mellor et al., 2016; Porco et al., 2016; Zhang et al., 2016).

3.2.2 Auxin transport

A pivotal component of auxin homeostasis is IAA transport. As mentioned above, IAA is not distributed equally within the plant body, organs and tissues (Vanneste and Friml, 2009). IAA can be transported within the plant over long distances through the phloem and xylem (Gomes and Scortecci, 2021). IAA distribution, facilitated by active cell-to-cell transport over short distances, in the apical meristems has been also described as polar auxin transport (PAT) (Friml, 2003). Overall, auxin can be transported in various ways described below.

Firstly, IAA as a weak acid can be protonated at low pH occurring in apoplast or vacuole (Gao et al., 2004; Martinière et al., 2013). Protonation causes decreasing of IAA polarity and enables its diffusion through membranes (Figure 2). On the other hand, IAA becomes too polar to diffuse due to deprotonation in pH-neutral environment of the cytosol (Ljung, 2013). In that case, the “trapped” within cell IAA can be translocated by specific transporters (Figure 2).

Many transporters residing at the plasma membrane (PM) can mediate active auxin influx or efflux in and out of the cell, respectively. Their asymmetrical positioning leads to PAT and results in the auxin gradient that was previously shown in the root apex (Pettersson et al., 2009; Pěnčík et al., 2013). PAT is regulated by the coordination of the AUXIN RESISTANT1/LIKE AUX1 (AUX1/LAX), the ATP-binding cassette subfamily B (ABCB), and the PIN-FORMED (PIN) transporters. AUX1/LAX carriers, facilitating IAA and proton import, localizes polarly at the PM (Swarup et al., 2001; Friml, 2010; Péret et al., 2012). The ABCB energy-dependent transporters are localized uniformly at the PM mediating both IAA influx and efflux (Yang and Murphy, 2009; Kubeš et al., 2012). Finally, the PIN proteins are crucial transporters responsible for IAA efflux. The PIN family includes 8 members that can be divided into two subgroups according to their length of central hydrophilic loop. Importantly, this loop determines the PIN localization. The unequal localization of “long” PINs (PIN1-4, and PIN7) at PM regulates direction of IAA flux (Tanaka et al., 2006; Vieten et al., 2007; Křeček et al., 2009), whereas PIN5, PIN6 and PIN8 are localized in the membranes of intercellular compartments (Barbez and Kleine-Vehn, 2013).

While the subcellular distribution of IAA still remains elusive, several subcellular auxin transporters have been described. WALLS ARE THIN1 (WAT1) auxin transport facilitator at tonoplast mediates IAA export from vacuole (Ranocha et al., 2013). PIN5 and

PIN8 transporters reside mainly at the ER membrane (Figure 2). PIN5 loads IAA into the ER lumen while PIN8 acts antagonistically to PIN5 action (Mravec et al., 2009; Dal Bosco et al., 2012; Ding et al., 2012). PIN6 mediates IAA export from the cell but it has shown dual localization both at the PM and ER membrane (Simon et al., 2016). Further, PIN-LIKES transporters (PILS) also contribute to auxin subcellular compartmentation by importing IAA into the ER (Barbez et al., 2012). Surprisingly, it has been shown that ER-to-nuclei auxin flux dominate compared to cytosol-to-nuclei flux (Middleton et al., 2018). Although the activity of ER residing transporters has direct impact on auxin signalling and developmental processes (Béziat et al., 2017; Feraru et al., 2019; Lee et al., 2020), the regulation mechanisms of auxin intracellular distribution still remain unclear. Overall, the formation of auxin maxima and minima are crucial for many plant developmental aspects (Peer et al., 2011; Di Mambro et al., 2017).

3.2.3 Auxin signalling

Auxin levels are strictly regulated by coordination of biosynthesis, transport, and catabolism (Korasick et al., 2013). Moreover, it seems that auxin subcellular distribution also plays important role in homeostasis and IAA perception (Kriechbaumer et al., 2012; Skalický et al., 2018). Canonical auxin signalling occurs in nucleus and regulates the downstream transcriptional responses, respectively (Figure 2) (Dharmasiri et al., 2005; Kepinski and Leyser, 2005). IAA acts as a “chemical glue”, which stabilises the protein complexes TRANSPORT INHIBITOR RESPONSE1/ AUXIN SIGNALING F-BOX (TIR1/AFB). TIR1/AFBs are F-box proteins and contain S-PHASE KINASE ASSOCIATED PROTEIN 1 - CULLIN 1 - F-BOX (SCF)-type E3 ubiquitin ligase. Formation of SCF^{TIR1} protein complex leads to ubiquitination of AUXIN/INDOLE-3-ACETIC ACID (Aux/IAA) proteins, the auxin transcriptional repressors. Subsequent degradation of Aux/IAA by the 26S proteasome results in the release of AUXIN RESPONSE FACTORS (ARFs) and transcription of auxin-responsive genes. At low levels of IAA, Aux/IAA proteins repress gene transcription by blocking the ARFs (reviewed in Ljung, 2013). Auxin signalling cascade comprises of 5 AFBs binding in the TIR1 receptor, 29 Aux/IAA response genes and 22 ARFs. These numbers and combinations possibilities highlight the complexity of auxin response which is important for regulating plethora of developmental and physiological processes in Arabidopsis (Vernoux et al., 2011; Calderón-Villalobos et al., 2012). Furthermore, Fendrych et al. (2018) recently showed that TIR1/AFB can mediate root

growth inhibition as a rapid non-canonical auxin response. This response is too fast (dozens of sec) to trigger gene expression leading to physiological changes.

S-PHASE KINASE-ASSOCIATED PROTEIN 2A (SKP2A) and AUXIN BINDING PROTEIN1 (ABP1) have been also suggested to act as auxin receptors (Powers and Strader, 2016). SKP2A, the F-box protein of SFC complex, can mediate the canonical auxin response similarly to TIR1/ABF. SKP2A regulating G1/M transition during cell cycle by degradation of antiproliferation factors (Jurado et al., 2010; Grones and Friml, 2015). ABP1 has been considered as an important auxin receptor regulating embryogenesis and development due to the lethality of *abp1* loss-of-function mutant embryos (Chen et al., 2001). Although ABP1 resides mainly at the ER membrane, a small portion of it can also be located at the cell wall (Ljung, 2013). The ABP1 portion localized at the cell surface could be active because the lower pH of the extracellular space can cause increase of the IAA affinity to the putative receptor (Jones and Herman, 1993; Tian et al., 1995; Klode et al., 2011). Later, Enders et al. (2015) showed that the original *abp1* mutant contains numerous background mutations. Moreover, the newly prepared *abp1* loss-of-function mutant, generated by Clustered Regularly Interspaced Short Palindromic Repeats (CRISPR) system, showed neither developmental nor morphological defects (Gao et al., 2015). Hence, function of ABP1 in plant development and growth remains elusive.

3.3 Cytokinins

Cytokinins (CKs) are classified as derivatives of adenine substituted at the N^6 position. CKs are divided according to the chemical character of their side chain on the prevalent isoprenoid group. Thus, the four CK active molecules can be divided respectively to *trans*- and *cis*-zeatin (*tZ* and *cZ*), dihydrozeatin (DHZ) and N^6 -isopentenyladenine (iP) (Figure 3). Same classification applies to an aromatic group, N^6 -benzyladenine (BA) or topolins, which are also active CKs (Miller et al., 1955a, 1955b; Horgan et al., 1973, 1975; Strnad, 1997). Another group of naturally occurring CKs are the adenine derivatives modified at position C^2 by a methylthio group (Vreman et al., 1974). Finally, there are synthetic CK-like compounds with recorded bioactivity such as urea and thiourea derivatives, e.g., thidiazuron or N, N'-diphenylurea (Thomas and Katterman, 1986).

CKs stimulate cell division, inhibit shoot apical dominance, delay senescence, promote cell differentiation, and regulate a wide variety of other physiological processes (reviewed in Schaller et al., 2015; Zürcher and Müller, 2016; Kieber and Schaller, 2018;

Nedvěd et al., 2021). For this reason, CKs mainly occur in young leaves, root apical meristem and developing tissues. Their distribution is not uniform throughout the plant body and depends on specific tissues and developmental stages (Zürcher and Müller, 2016).

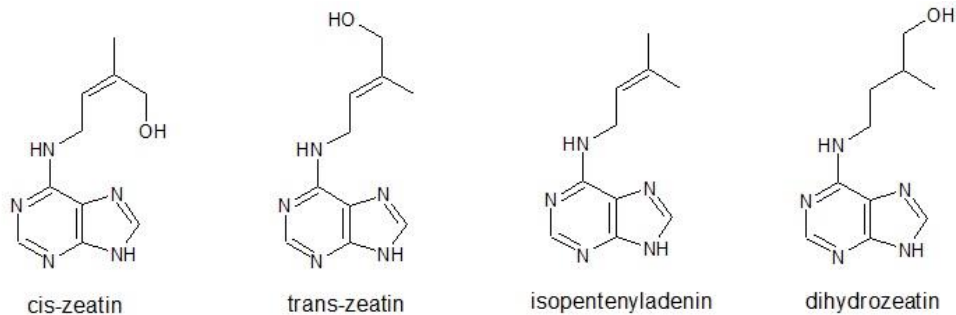


Figure 3 Chemical structures of isoprenoid cytokinin bases (active forms).

3.3.1 Cytokinin metabolism

Key enzymes catalysing the first step of CKs biosynthesis are ISOPENTENYL TRANSFERASEs (IPTs). IPTs mediate binding of the isopentenyl group to the N^6 -position of the adenine ribotide in order to form isopentenyladenosine-5'-di- or -triphosphate (iPRDP or iPRTP, respectively). This type of enzymatic reaction was initially observed in a slime mold (*Dictyostelium discoideum*) (Taya et al., 1978). Several gene homologs encoding for IPTs (IPT1-9), were identified also in *Arabidopsis thaliana* (Kakimoto, 2001; Takei et al., 2001; Miyawaki et al., 2006). IPT2 and 9 catalyse isopentenylation of tRNA, which provides a source for *cZ*-type CKs and have thus cytosolic localization (Miyawaki et al., 2006). IPT1, 3 and 5 fused with GREEN FLUORESCENT PROTEIN (GFP), were localized in the chloroplasts of mesophyll cells (Kasahara et al., 2004). However, IPT3 has shown also nuclear localization, depending on respective posttranslational modifications such as farnesylation, which strongly determines protein localization despite the presence of chloroplast transit peptide (Figure 4) (Galichet et al., 2008). Signal localization of IPT2 and IPT4, fluorescently labelled with GFP, has been detected in the cytosol (Kasahara et al., 2004). This finding agrees with the idea that IPT4 may utilize the isoprenoid precursor synthesized via mevalonate pathway in cytosol. Finally, GFP fluorescence of IPT7 was observed in mitochondria (Figure 4) (Kasahara et al., 2004).

Synthesis of iPRDP and iPRTP occurs via transmission of isoprenoid moiety to adenosine. These ribotides are then hydroxylated producing *tZ* type CKs. The hydroxylation reaction is catalysed by the CYTOCHROME P450 (CYP) MONOOXYGENASE

CYP735A1 and CYP735A2 (Takei et al., 2004). CK ribotides can get also phosphoribohydrolysed by ‘LONELY GUY’ (LOG) enzyme and thus get directly converted to the highly active free-base forms (Kurakawa et al., 2007). To date, 9 LOG homologues targeted predominantly to nucleus and cytosol have been identified (Figure 4) (Kuroha et al., 2009).

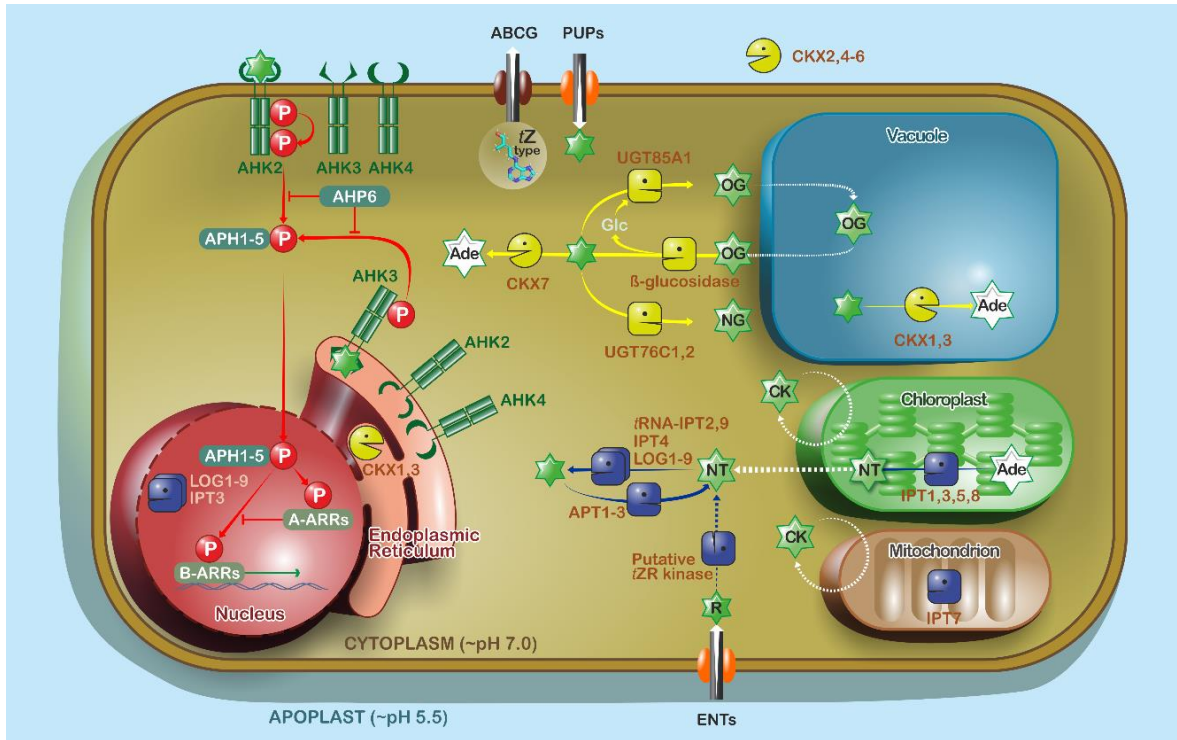


Figure 4 Model of cellular and subcellular cytokinin homeostasis (Skalický et al., 2018).

The metabolism of active free bases is believed to be at least partially regulating CK homeostasis. CK bases can be reversibly conjugated with sugars (e.g., glc or xylose) through their hydroxyl moiety at the N^6 -side chain of *tZ*, *cZ* and *DHZ* via Arabidopsis UGT85A1 located in cytosol (Jin et al., 2013b; Šmehilová et al., 2016). The generated pool of *O*-glucosides can serve as CK storage pool since their rapid conversion back to active CK forms via β -glucosidases is possible, as in the case of N^3 -glucosides (Brzobohatý et al., 1993). Another reversible inactivation of CK active bases can occur via the ADENINE PHOSPHORIBOSYLTRANSFERASEs (APT1-3) enzymes, which appear to be cytosolic and act antagonistically comparing to LOGs (Moffatt et al., 1991; Allen et al., 2002; Zhang et al., 2013). Direct glycosylation at N^7 or N^9 position of the purine skeleton can be catalysed by cytosolic UGT76C1 and UGT76C2 causing irreversible active CKs' inactivation (Mok and Mok, 2001).

CYTOKININ OXIDASES/DEHYDROGENASEs (CKXs) are known as the main enzymes mediating CKs degradation (Pačes et al., 1971; Werner et al., 2006) and play key roles in maintenance of CK endogenous levels. CKX family counts 7 homologs in Arabidopsis with distinct subcellular localizations. It seems that the main site of CKs' inactivation is in the apoplast (extracellular space; Figure 4), where CKX2, CKX4, CKX5 and CKX6 are translocated through the secretory pathway (Werner et al., 2003). While *in silico* experiments initially predicted that CKX1 and CKX3 could be mitochondrial enzymes, (Schmülling et al., 2003), their fusion to GFP revealed that these two enzymes are targeted to the vacuole *in vivo* translocation (Werner et al., 2003). Moreover, the localization of these two dehydrogenases were observed also in the ER, as this compartment mediates their translocation (Werner et al., 2003). Recently, the catalytic activity of CKX1 was confirmed to be localized in the ER lumen (Niemann et al., 2018). Finally, CKX7 localization is estimated to be in the cytosol, mainly due to lack of a signal peptide sequence (Köllmer et al., 2014).

CKX proteins do not differ only in the subcellular localization, but also in their substrate specificity. Generally, CKXs catalyse the removal of CK's aliphatic unsaturated side chain to produce adenine or adenosine and the corresponding aldehyde (Brownlee et al., 1975; Galuszka et al., 2001). While CKXs prefer unsaturated isoprenoid CKs as a substrate, aromatic CKs could be also degraded but with lower turnover rate (Galuszka et al., 2007; Kowalska et al., 2010). On the other hand, DHZ, *O*-glucosides are believed to be resistant to Arabidopsis CKXs activity. In a CKX enzymatic activity assay with DHZ as a substrate, there was no 4-hydroxy-3-methylbutanal detected as the expected product of the reaction (Frébortová et al., 2004; Galuszka et al., 2007). The glc molecule residing at the hydroxyl group of the *O*-glucosides' side chain, protects them from CKX-mediated cleavage (Galuszka et al., 2007). Furthermore, *N*⁷-glucosides appear to be resistant to degradation via CKXs (Galuszka et al., 2007). Different structural conformations of *cZ* side chain compared to *tZ* probably worsen its binding access to the active site in most of Arabidopsis dehydrogenases homologues (CKX1-6). Later, Köllmer et al. (2014) proved that CKX7 is exclusively capable in inactivation of *cZ*-types. Apoplastic Arabidopsis CKXs, especially CKX2 and CKX4, catabolize free bases and their related ribosides with higher activity compared to other CKX enzymes (Galuszka et al., 2007). Additionally, CKX6 shows the lowest enzymatic activity in comparison with other extracellular CKXs. CKX1 and CKX7 demonstrated the highest substrate specificity to *N*⁹-glucosides (Galuszka et al., 2007). CKX7 could also degrade free bases and ribosides, whereas CKX3 preferred ribotides and

ribosides as substrates (Galuszka et al., 2007; Kowalska et al., 2010). Additionally, CKX3 is much less enzymatically effective due to low substrate affinity than the other two intracellular dehydrogenases CKX1 and CKX7 (Kowalska et al., 2010).

3.3.2 Cytokinin transport

CKs can act as paracrine or long-distance signal within the plant body. It was observed, that *tZ* riboside (*tZR*) is transported mainly acropetally through the xylem sap, whereas *iP* riboside (*iPR*) is pivotally translocated basipetally via the phloem sap (Corbesier et al., 2003; Hirose et al., 2008; Kudo et al., 2010; Osugi et al., 2017). Despite the importance of CK transport, for long time there was no evidence for a respective facilitator. First indications appeared during the first decade of the 21st century, when three protein groups possessing CK translocation capability were described: the PURINE PERMEASEs (PUPs) (Gillissen et al., 2000), the EQUILIBRATIVE NUCLEOSIDE TRANSPORTERs (ENTs) (Wormit et al., 2004) and the subfamily G of the ATP-binding cassette (ABCG) transporters (Figure 4) (Ko et al., 2014; Zhang et al., 2014). While CK transport seems to be shared with essential nucleobases (Hirose et al., 2008), the molecular basis of CK transport is still poorly understood.

The large PUP family counts 23 members (Gillissen et al., 2000; Zürcher and Müller, 2016). According to the similarity between purine bases and CKs, it was hypothesized, that some PUPs might mediate CK transport through the PM. In agreement with this hypothesis, the yeast mutant PUP1 was deficient in adenine uptake while competitive assays in respective wild type showed that kinetin and *tZ*, but not *tZR*, inhibited adenine uptake (Gillissen et al., 2000). Moreover, both *glc* addition and weak acid environment raised PUP1 activity, whereas presence of proton pump inhibitors reduced it. These findings point to energy dependent and potential proton coupled transport against concentration gradient (Gillissen et al., 2000). Nevertheless, this indirect evidence was not sufficient to pronounce PUP1 as a CK transporter. Only after the transport of radiolabeled *tZ* mediated by PUP1 was confirmed (Bürkle et al., 2003), PUP1 could be established as a CK transporter. Meanwhile, the capability of two more PUPs (PUP2 and PUP3) to transport CKs was indicated. In fact, free bases as kinetin \geq *iP* > BA > *cZ* > *tZ* strongly and *tZR* less effectively inhibited adenine uptake in competitive assay via PUP2. On the contrary, no CK transport activity in yeast was proved for PUP3 (Bürkle et al., 2003). Furthermore, PUPs are promiscuous to other purine related substrates such as caffeine or nicotine (Gillissen et al., 2000; Bürkle et al., 2003). Recently, another PURINE PERMEASE, PUP14, was shown to be involved in early stages

of plant development and transported CK free bases more effectively than PUP1 (Zürcher et al., 2016). Transport of bioactive CKs via PUP14 was not affected in *tZR* presence during competitive assay. In mutants with non-functional PUP14, the CK free bases pool was reduced in apoplastic space (Zürcher et al., 2016) and CK response, mediated by PM-localized CK receptors, was consequently diminished (Kim et al., 2006; Zürcher et al., 2016; Antoniadis et al., 2020).

ENT1 was described as a putative nucleoside transporter based on shared similarity with human ENTs (Li and Wang, 2000). Hydrogen proton-dependent import of nucleosides through ENT1, 3, 6, 7 were later confirmed (Möhlmann et al., 2001; Wormit et al., 2004). Furthermore, ENT1-8 is localized at the PM (Li and Wang, 2000; Li et al., 2003; Wormit et al., 2004). Later, ENT1 was identified in the proteome of the tonoplast (Jaquinod et al., 2007; Bernard et al., 2011). These results were supported by revealing of differences of adenosine content in isolated vacuoles from *ent1* loss-of-function mutant or ENT1 overexpressing line (Bernard et al., 2011). Substrate specificity of some ENTs was examined in an inhibitory assay of adenosine uptake. The results showed that ENT3, 6, 7 and 8 could participate in CK riboside transport. Moreover, ENT6 preferred *iPR* than *tZR* as a substrate and ENT3 and 7 show only weak capability to inhibit adenosine uptake (Sun et al., 2005; Hirose et al., 2008).

The first CK exporter ABCG14 involved in root-to-shoot transport of CKs was discovered in 2014. ABCG14 is highly expressed in Arabidopsis root vascular tissue and loss-of function *abcg14* mutants commemorate CK-deficient phenotypes (Ko et al., 2014; Zhang et al., 2014). Nevertheless, *tZ* -but not *iP*- applied by spraying was able to rescue the dwarf phenotype of *abcg14* mutant (Ko et al., 2014). In *abcg14* mutants, *tZ*-type CK content in shoots was reduced despite the abundant amounts of *tZ*-type CKs in roots. Interestingly, the same plants displayed elevated levels of *iP*-type and *cZ*-type CKs in both shoots and roots. Taken together these findings suggest that in *abcg14* mutant, root-synthesized *tZ*-type CKs translocation to the shoot is irreversibly impaired, while other CK types attempt to compensate for CK intrinsic homeostasis maintenance (Ko et al., 2014; Zhang et al., 2014). Undoubtedly, ABCG14 is so far the only identified transporter responsible for long-distance translocation of CKs.

Recently, it was proved that a member of purine transporter family AZA-GUANINE RESISTANT 2 (AZG2) can also facilitate transport of CKs (Tessi et al., 2021). AZG2 is mainly expressed in the root tissue especially around lateral root primordia. Restricted expression of AZG2 indicated its involvement in lateral root emergence. AZG2 resides at PM and ER membrane and enables CK bidirectional diffusion (Nedvĕd et al., 2021).

3.3.3 Cytokinin signalling

CK signals are delivered via a multistep phosphorelay cascade derived from bacterial two-component system (Parkinson and Kofoed, 1992). Until now, three ARABIDOPSIS HISTIDINE KINASEs (AHK1–4) (Suzuki et al., 2001; Ueguchi et al., 2001), AHK4 also known as CRE1 (Inoue et al., 2001) or WOL (Mähönen et al., 2000), have been described as CK receptors. They are transmembrane proteins functioning as dimers and can recognize free CK bases with high affinity (Wolanin et al., 2002). CKs bind to cyclase/histidine kinase associated sensory extracellular (CHASE) domain of the AHK triggering the signalling machinery (Figure 4) (Anantharaman and Aravind, 2001; Ueguchi et al., 2001). Upon CK perception the receptor gets auto-phosphorylated within the intracellular histidine-kinase domain utilizing ATP. The phosphoryl group is then transferred to a conserved histidine residue of ARABIDOPSIS HISTIDINE PHOSPHOTRANSFERASEs (AHPs), translocating between the cytosol and the nucleus (Hwang and Sheen, 2001; Punwani et al., 2010). Six genes encoding AHP1-6 have been identified so far (Hutchison et al., 2006; Mähönen et al., 2006). All of them, except AHP6, can directly interact with 23 known nuclear ARABIDOPSIS RESPONSE REGULATORS (ARRs) that are transcriptional factors (Dortay et al., 2006; Hutchison et al., 2006; Dortay et al., 2008; Verma et al., 2015). AHP6, with asparagine residue instead of conserved histidine, is a pseudo-phosphotransferase and acts as CK signalling inhibitor (Suzuki et al., 2000; Mähönen et al., 2006). The phosphorylated AHPs further activate downstream ARR, which are split into two main groups: Type A and Type B (Imamura et al., 1999; D'Agostino Ingrid B et al., 2000). Type-B ARRs bind to DNA (Kiba et al., 1999; Mason et al., 2004) and regulate transcription of CK responsive genes while type-A ARRs ensure a negative feedback loop in CK signalling (D'Agostino Ingrid B et al., 2000; Hwang and Sheen, 2001; Rashotte et al., 2003; To et al., 2004).

Importantly, results obtained from ligand binding assays, show distinct ligand specificity of individual receptor homologues. AHK4 binds *iP* and *tZ* with approximately similar affinity, while AHK2 prefers *iP*. On the contrary, AHK3 binds *tZ* rather than *iP* (Spíchal et al., 2004; Stolz et al., 2011; Lomin et al., 2012). Moreover, potential hormonal activity of ribosides derived from isoprenoid CKs agrees with findings that *tZR* and *iPR* are transported from apical meristems through the xylem or phloem saps, respectively, and could be perceived by AHKs at PM (Figure 4) (Kudo et al., 2010). On the other hand, some controversial evidence pointed to the high variability of CK ribosides binding affinity based

on two different heterologous model systems – bacterial and yeast (Yamada et al., 2001; Spíchal et al., 2004; Yonekura-Sakakibara et al., 2004; Romanov et al., 2005, 2006; Stolz et al., 2011; Kuderová et al., 2015). One possible explanation of CK ribosides activity was that *Escherichia coli* could quickly metabolize riboside to corresponding active base, which can then bind to CK receptors. Such uncertainty was finally solved by Lomin et al. (2015) thanks to the data from plant membrane assays, where CK ribosides were unable to bind to CK receptors. Furthermore, it was postulated, that properties of the membrane, in which the receptors are anchored, could change the signal perception (Lomin et al., 2015).

Firstly, it was assumed, that AHKs are PM-resident receptors due to presence of CKs in apoplastic space (Inoue et al., 2001; Ueguchi et al., 2001; Kim et al., 2006), where the receptors could perceive paracrine or long-distance CK signal from apoplastic fluid. Some years later, it was demonstrated that AHKs reside predominantly at the ER membrane instead (Figure 4) (Caesar et al., 2011; Wulfetange et al., 2011) and their ability of CK perception *in situ* was also confirmed (Lomin et al., 2018). Moreover, it was proved, that the CHASE domain is faced to lumen of the ER and the histidine kinase with acceptor domain to cytoplasm (Caesar et al., 2011; Wulfetange et al., 2011).

Zürcher et al. (2016) provided evidence that AHKs may also localized at PM. They showed that *pup14* mutants are defective in export of CK free bases from the cell resulting in decreased levels of CKs in the apoplast and consequent reduced CK signalling. These findings were in agreement with evidence that followed later. These showed that CK signalling could be triggered in Arabidopsis protoplasts after incubation with immobilized CK bases that cannot enter the plant cell to be perceived by intracellular receptors (Antoniadi et al., 2020). Kubiasová et al. (2020) also confirmed colocalization of AHK4 at PM as well as on ER using plant line expressing AHK4 tagged with GFP and fluorescently labelled iP.

3.4 Subcellular fractionation

3.4.1 Plant tissue homogenization

The original idea of intracellular compartments separation to study a participation of a specific enzyme in developmental processes was fostered by De Duve and co-workers in 1950's (1955). Subcellular fractionation usually consists of two steps: disruption of the cellular organization (homogenization) and subsequent separation of compartments mixture to populations of distinct organelles (Robert et al., 2007; Seigneurin-Berny et al., 2008; Wulfetange et al., 2011; Ding et al., 2012).

Plant tissue homogenization is a key step for successful organelles isolation. The choice of a suitable homogenization approach depends on the purpose of isolation with respect to preservation of organelle intactness. General approach for material homogenization is grinding with mortar and pestle under liquid nitrogen (Zhang et al., 1995; Šafář et al., 2004; Kriechbaumer et al., 2016). However, resulting crystals of ice can cause organelle membranes disruption and thereby result in significant drop of fractionation effectiveness (Song et al., 2006). Grinding of plant tissue in buffer with blender is an also frequently used homogenization technique enabling processing of enormous amount of material (Neuburger et al., 1982; Seigneurin-Berny et al., 2008; Petrovská et al., 2014). Despite of the high homogenization efficiency, blending causes organelle damage and large proportion of broken organelles in crude extract affects further subcellular fractionation (Seigneurin-Berny et al., 2008). Smaller amount of plant material can be gently and effectively homogenized by razor blade (Ding et al., 2012; Thibivilliers et al., 2020; Včelařová et al., 2021). Rigid plant tissue can be disrupted by enzymatic cell wall digestion (Somerville et al., 1981; Yoo et al., 2007; Antoniadi et al., 2021). Undoubtedly, enzymatic cell wall digestion and subsequent lysis of protoplast suspension by osmotic or thermal shock is the most delicate method. For example, protoplast isolation is required for vacuoles isolation (Saunders, 1979; Shimaoka et al., 2004; Robert et al., 2007) and it has also been previously utilized for chloroplasts (Somerville et al., 1981) or nuclei (Saxena et al., 1985) isolation.

3.4.2 Fractionation based on centrifugation

Methods based on differential centrifugation (DC) or DGU are popular due to their simplicity, efficiency and high yield (Huber et al., 2003; Lee et al., 2010). Organelle suspension can be fractionated by various centrifugation techniques, where the organelles are separated according to their size and density, which is mainly determined by the ratio of their lipid to protein contents (Lee et al., 2010). In general, organelles are sedimented by centrifugal force in the following order: nuclei, chloroplasts, mitochondria and endomembranes such as ER and Golgi apparatus (Vertommen et al., 2011). Even the simplest DC method can provide enriched fractions of crude organelles (Somerville et al., 1981; Keech et al., 2005). Higher purity of organelle fractions could be achieved by effective DGU using very high centrifugal force ($\geq 100,000 \times g$ for at least 30 min). During this process, the compartments migrate through the viscous medium of rising density, and they are focused at their isopycnic points after centrifugation. Media forming density gradient

usually include sucrose for ER (Ding et al., 2012) and Golgi apparatus (Parsons et al., 2012), Ficoll for vacuoles (Robert et al., 2007), or Percoll for mitochondria (Keech et al., 2005) and chloroplasts (Seigneurin-Berny et al., 2008; Kriechbaumer et al., 2012).

Alternative methods for compartment separation have been also described, such as non-aqueous fractionation (Fürtauer et al., 2016), or two-phase partitioning (Larsson et al., 1987). Two-phase partitioning is generally based on the separation of PM and inner membrane structures in two fractions, which are obtained by mixing and centrifugation of two distinct water-soluble polymers (e.g., polyethylene glycol and dextran) above the critical concentration.

Importantly, all centrifugation-based protocols provide only organelle isolation from organs or whole plant body. Moreover, these approaches may not have appropriate resolving power due to increasing sensitivity of downstream applications. Therefore, other strategies and new advanced techniques have been developed (Table 1).

Table 1. Overview of published isolation methods for a particular organelle. Methods highlighted in bold represent well-established fractionation methods providing high purity of organelle fraction. AP – affinity purification, DC – differential centrifugation, DGU – density-gradient ultracentrifugation, ER – endoplasmic reticulum, FCM – flow cytometry, FFE – free-flow electrophoresis, GA – Golgi apparatus

Compartment	Isolation methods			
	DC	DGU	AP	FCM
Nuclei	(Saxena et al., 1985)	(Folta and Kaufman, 2007)	(Deal and Henikoff, 2011)	(Thibivilliers et al., 2020)
Nucleoli	(McKeown et al., 2008)			
Vacuoles		(Robert et al., 2007)	(Bardy et al., 1998)	
Plastids		(Seigneurin-Berny et al., 2008)		(Wolf et al., 2005)
Mitochondria		(Keech et al., 2005)	(Eubel et al., 2007)	(Boussardon et al., 2020)
ER		(Včelařová et al., 2021)	(Okekeogbu et al., 2019)	
GA		(Muñoz et al., 1996)	(Parsons et al., 2012)	(Wilkop et al., 2019)
Peroxisomes		(Reumann and Lisik, 2017)	(Eubel et al., 2008)	

3.4.3 Flow cytometry

FCM is a powerful technology used to count cells or particles in the suspension and measure plenty of their optical properties at the same time. Acquired data can be further analysed and statistically processed to improve stability and reproducibility of cytometric procedure (Antoniadi et al., 2021).

Initially, suspension of particles is loaded into flow cell where they are hydrodynamically focused within an aqueous stream. Focusing causes an alignment of particles in a stream core (Robinson and Grégori, 2007). This enables spatial separation of particles which are then passing singly through the region where a set of lasers cross the stream (Galbraith et al., 2021). Illuminated particles absorb and scatter light. If the particles carry a fluorochrome, subsequently fluorescence is emitted. The light intensities are recorded for each single particle and a detailed data set can be obtained for the analysed sample. Forward and side scatters are the main parameters providing information about relative size and relative complexity of the analysed particle, respectively. Specific fluorescence is also important for measured particle properties (Doležel et al., 2007). Wide spectrum of various fluorochromes and their combination enables extended applicability of FCM in immunology (Cossarizza et al., 2017) as well as in plant sciences (Galbraith et al., 2021) e.g., cell cycle analysis (Galbraith et al., 1983), DNA and ploidy estimation (Temsch et al., 2021), analysis of pollen and spores (Kron et al., 2021), or microalgae (Čertnerová and Galbraith, 2021).

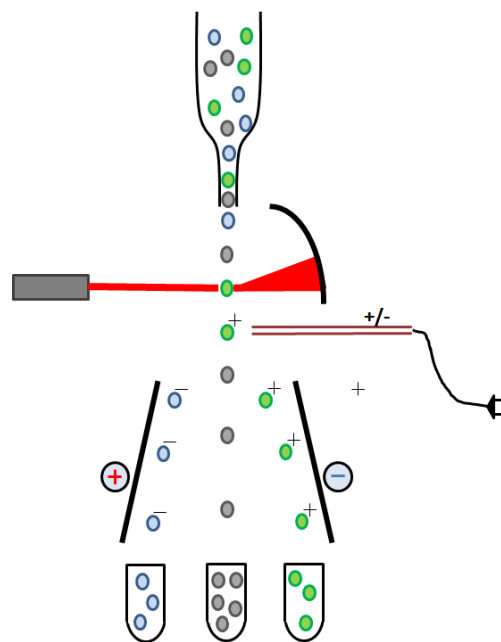


Figure 5 Scheme of flow cytometric sorting.

Flow cytometers equipped with sorting module provide analysis of a heterogenous particle mixture and subsequent separation into different fractions according to selected parameters. When the particle meets the conditions, the particle-containing droplet is charged accordingly and deflected into the respective collecting tube (Figure 5). Fluorescence-activated cell sorting (FACS) is a well-established technique employed in basic and applied plant research. FACS enable analysis at cell-type-specific resolution and has been thus previously employed to unravel developmental processes in specific plant tissues e.g., shoot apical meristem, root cell types, carpel margin meristem, embryo and stomatal lineage cells (Antoniadi et al., 2021). Sorted protoplasts were then subjected to various downstream applications e.g., transcriptomics (Yadav et al., 2009), proteomics (Petricka et al., 2012), metabolomics (Petersson et al., 2015) or plant hormone analysis (Petersson et al., 2009; Pěňčík et al., 2013; Antoniadi et al., 2015). Nevertheless, flow sorting can be applied to separate even smaller particles than plant cells like chromosomes, which simplify genome sequencing (Doležel et al., 2021) or organelles. However, sorting of organelles is quite a novel approach facilitating plant cell compartments fractionation.

Organelle suspension represents a heterogeneous mixture of different intact compartments, broken or impaired organelles, unbroken cells and other cellular debris. Plant organelles have different sizes depending on the cell-type or the plant species origin (Boussardon et al., 2020) e.g., root mitochondria (0.5 – 0.9 μm), chloroplasts (units of μm) or mesophyll vacuoles (dozens of μm). It is difficult to clearly identify organelle populations during cytometric analysis based on their relative size or complexity exclusively.

Specific fluorescence is a suitable parameter for the identification of the organelle population of interest. However, proper, and unique localization of potential fluorochromes is required. Notably, plant cells as well as organelles contain a wide range of autofluorescence compounds (Antoniadi et al., 2021), which can make FCM analysis more challenging. On the other hand, chlorophylls as an endogenous fluorochrome occurring only in chloroplasts may facilitate their identification.

An optimal approach for determination of organelle populations would be to utilize fluorescent marker plant lines (Table 2). These transgenic plants express a protein, or a targeting sequence fused with fluorescent protein specifically in the organelle of interest (Boisnard-Lorig et al., 2001; Grebe et al., 2003; Viotti et al., 2013). It is important to select marker proteins/sequences that localize uniquely in one type of subcellular compartment. Another possible method to identify organelle population using FCM is to exploit fluorescent staining.

Table 2 Overview of organelle-specific markers fused with fluorescent proteins. ER – endoplasmic reticulum, GA – Golgi apparatus.

Compartment	Marker protein/sequence	Shortcut	Reference
Nuclei	Histone 2B	H2B	(Boisnard-Lorig et al., 2001)
Mitochondria	β -ATPase	β -ATPase	(Logan and Leaver, 2000)
Plastids	Snowy cotyledon 1	SCO1	(Albrecht et al., 2006)
ER	HDEL and KDEL anchoring motif	HDEL, KDEL	(Matsushima et al., 2002)
GA	<i>N</i> -acetylglucosaminyl transisferase I	NAG1	(Grebe et al., 2003)
Peroxisomes	PTS1 sequence	PTS1	(Nelson et al., 2007)
Tonoplast	V-type proton ATPase subunit a3	VHA-a3	(Viotti et al., 2013)
Vacuoles	Aquaporins	TIPs	(Ma et al., 2004)
Lytic vacuoles	Aleurain	Aleurain	(Miao et al., 2008)
Storage vacuoles	Chitinase	Chi	(Fluckiger et al., 2003)
Early endosomes	Ras-related protein RABA2a	Rab-A2	(Markham et al., 2011)
Vesicles	Clathrin	CLC	(Ito et al., 2012)

Nowadays, application of fluorescently labelled antibodies against plant proteins is not possible due to the lack of them (Antoniadi et al., 2021). However, application of wide spectrum of organelle specific fluorescent dyes can present an alternative option. Currently, the majority of organelles can be stained with commercially available fluorescent dyes, although they are originally designed for mammalian cells (Table 3). This fact may cause difficulties like dye permeability through cell wall or PM during *in vivo* staining or improper specificity. Nevertheless, some of them have been already successfully used in the field of plant sciences (Cho et al., 2004; Yao et al., 2004; Wolf et al., 2005; Petrovská et al., 2014). It is important to keep in mind the purpose of use and the dye specificity during dye selection. In general, fluorescent dyes are divided into two groups for live or fixed sample staining. Some of dyes can also allow both variants of sample preparation.

FCM as an analytical technique for characterization of heterogenous organelles provides a wide spectrum of applications. A comprehensive data set obtained from cytometric analysis can be used for structural and functional studies of organelles (Rodrigues et al., 2018). For some downstream applications, it is important to select alive organelles. Their viability may be evaluated by shape or size of studied organelles. However, in general more precise selection of undamaged organelles can be achieved by fluorescent dye staining, which is metabolised or actively up taken exclusively by live organelles, e.g., carboxyfluorescein diacetate in case of chloroplasts (Schulz et al., 2004). On the other hand, organelle functionality can be also analysed on single cell basis in protoplasts. Yao and co-workers developed FCM technique to quantitate mitochondrial membrane potential changes

during programmed cell death (Yao et al., 2004). One of the most widespread applications dealing with subcellular compartmentalization is sorting of nuclei for further genome or transcriptome analysis (Šimková et al., 2003; Šafář et al., 2004; Thibivilliers et al., 2020). Nevertheless, FCM was also exploited as a tool for semiautonomous organelle isolation for subsequent chloroplast genome sequencing (Wolf et al., 2005) or non-nuclear genome characterization (Cho et al., 2004).

Table 3 Overview of representative commercially available fluorescent dyes for organelle staining. ER – endoplasmic reticulum, GA – Golgi apparatus.

Compartment	Fluorescent dye	Wavelength (nm)	
		Excitation (laser)	Emission (colour)
Nuclei	DAPI	360 (UV)	460 (violet/blue)
	Hoechst 33342)	361 (UV)	497 (violet/blue)
	Sytox™ Green	504 (blue)	523 (green)
Mitochondria	MitoTracker™ Green FM	490 (blue)	516 (green)
	MitoTracker™ Orange CMTMRos	554 (green-yellow)	576 (yellow)
	MitoTracker™ Red FM	581 (green-orange)	644 (red)
	JC-1	498/593 (blue/ yellow)	525/595 (green/orange)
	MitoTracker™ Deep Red FM	644 (red)	665 (red)
ER	ER-Tracker™ Blue-White DPX	374 (UV)	430–640 (violet-red)
	ER-Tracker™ Green	502 (blue)	511 (green)
	ER-Tracker™ Red	588 (yellow)	615 (orange-red)
GA	BODYPI™ FL C ₅ -Ceramide	502 (blue)	511 (green)
	NBD C ₆ -Ceramide	466 (blue)	536 (green-yellow)
	BODYPI™ TR Ceramide	588 (yellow)	615 (orange-red)

Subcellular fractionation is one of the most frequently used approaches in proteomics resulting in proteome complexity reduction. This is important because while highly abundant proteins are easily detected, more scarce but still important proteins' identification has been previously lost (Huber et al., 2003). Therefore, reducing the complexity of a protein mixture improves the identification of a higher number of proteins (Lee et al., 2010). Proteomic studies of nuclear proteins in barley have shown that FCM is also suitable for this “omics” approach. Moreover, high resolving power of FCM has enabled the separation of nuclei in different stages of the cell cycle (Petrovská et al., 2014; Blavet et al., 2017).

3.4.4 Affinity purification

Affinity purification (AP) procedure is usually based on an ectopically expressed tag anchored in an organelle membrane. This tag is subsequently captured by a respective

interactor which is attached to magnetic microparticles. Biotin-streptavidin binding and epitope-antibody pairing have so far been utilized for affinity purification as two main interactions (Deal and Henikoff, 2010; Chen et al., 2016). Despite the novelty of this approach, AP is now becoming popular instead (Deal and Henikoff, 2011; Chen et al., 2016; Wilkop et al., 2019; Boussardon et al., 2020; Kuhnert et al., 2020). This is mainly due to the rapid isolation and the possibility of site selection for tag expression, which represent the great advantages of this method and increases the spatio-temporal resolution of various downstream analysis, such as transcriptomics (Deal and Henikoff, 2010), proteomics (Kuhnert et al., 2020; Niehaus et al., 2020), metabolomics (Chen et al., 2016), or glycomic analysis (Wilkop et al., 2019).

3.4.5 Free-flow electrophoresis

The principal mechanism of free-flow electrophoresis (FFE) is the organelle separation based on surface charge provided by membrane proteins (Eubel et al., 2007). Intracellular membrane structures isolated by FFE were mainly exploited for revealing of their protein composition. Parsons et al. (2012) used this method after DGU to obtain a highly enriched Golgi fraction from *Arabidopsis*. This method has also been successfully applied for separation of vacuoles (Bardy et al., 1998), mitochondria (Eubel et al., 2007) or peroxisomes (Eubel et al., 2008).

3.5 Phytohormone profiling at subcellular level

Currently, there are only few reports dealing with the determination of phytohormones in live-cell systems (Novák et al., 2017). The study of plant hormones comprises, *inter alia*, their identification and quantification. Therefore, attention was paid to the development of accurate analytical methods enabling phytohormone determination, such as radioimmunoassay (RIA), enzyme-linked immunosorbent assay (ELISA), biosensors, fluorescence- or chemiluminescence-based detection methods (reviewed in Tarkowská et al., 2014). Nowadays, liquid chromatography combined with tandem mass spectrometry (LC-MS/MS) are the most widespread techniques used for phytohormone profiling (Svačinová et al., 2012; Nováková, 2013; Novák et al., 2017; Pěňčík et al., 2018; Šimura et al., 2018). Compared to other compounds, phytohormones occur in extremely low concentration in plant tissues (pg/g of fresh weight) (Tarkowská et al., 2014). Moreover, due

to the high sensitivity and resolution of LC-MS/MS methods, it is currently possible to analyse phytohormones at the subcellular level.

In 1990, a sequential porous-specific filtration through 8 µm and 0.45 µm membranes was used for IAA determination in chloroplasts and mitochondria (Sandberg et al., 1990). The density gradient was also applied to separate chloroplasts using a Percoll solution and determine CKs, IAA and abscisic acid concentrations (Benková et al., 1999; Polanská et al., 2007). Other studies also reported an exploiting of DGU to isolate vacuoles for subsequent MS-based phytohormone analysis (Ranocha et al., 2013; Jiskrová et al., 2016).

Ranocha et al. (2013) characterized a vacuolar auxin transporter WAT1 by measurement of the full profile of IAA and its metabolites in the respective Arabidopsis mutant line. A significant increase in the vacuolar concentration of free IAA, followed by higher levels of oxIAA, demonstrated intracellular IAA transport facilitated by WAT1 and triggering of homeostatic mechanisms (Skalický et al., 2018).

Moreover, recent results suggest that manipulation of active CKs levels by genetic modification could be a very potent tool for plant biotechnology (Zalabák et al., 2013). Therefore, the study of the profile of CK metabolites at the subcellular level was performed not only in the Arabidopsis model plant, but also in the transgenic barley lines (*Hordeum vulgare*) expressing vacuolar *AtCKX1* (Jiskrová et al., 2016). In leaves, isolated protoplasts and vacuoles, the concentration of 25 CK metabolites was determined and ultimately related to extracellular space, cytosol, and vacuoles. Surprisingly, the highest proportion of CKs was located outside the cell (up to 90%, with a majority of CK *O*- and *N*-glucosides), and only about 10% was present in the cytosol and vacuoles. In the overexpressing *AtCKX1* transgenic barley, an extreme decrease in extracellular *tZ9G* and *tZ* was accompanied by a compensatory increased content of *iP* and vacuolar *iPR*. Changes in CKs levels were probably observed as a result of local biosynthesis and maintenance of hormonal balance at the cellular level.

Unfortunately, very little is still known about extra- and intracellular phytohormone distribution, as well as the phytohormone levels in individual cell compartments. As mentioned above, the isolation of organelles is currently achieved through different isolation approaches, and subsequent hormonal profiling requires the usage of extremely sensitive mass spectrometry-based methods. This thesis should help to reveal the missing pieces in the overall picture of the phytohormone distribution in plant cell.

4 Materials and methods

More detailed information about individual methods and equipment parameters are given in the research papers attached in the Supplement section (*Supplement IV-VI*).

4.1 Chemicals

- All chromatographic solvents and chemicals for hormonal analysis were of hypergrade purity from Sigma-Aldrich Chemie GmbH (Steinheim, Germany), Merck Life Science (Darmstadt, Germany) and Roche Diagnostics (Mannheim, Germany) (*Supplement IV-VI*).
- Standards of tested chemicals were obtained from Olchemim Ltd (Olomouc, Czech Republic), Sigma-Aldrich Chemie GmbH (Steinheim, Germany), CDN Isotopes (Quebec, Canada) (*Supplement IV-VI*), or purchased from the Chembridge identification number (*Supplement IV-VI*).
- Chemical used for experiments were purchased from Sigma-Aldrich Chemie GmbH (Steinheim, Germany), Merck Life Science (Darmstadt, Germany), Duchefa Biochemie (Haarlem, Netherlands), Thermo Fisher Scientific (MA, USA), BD Bioscience (NY, USA) (*Supplement IV-VI*).

4.2 Plant material and growth conditions

- Arabidopsis WT – *Arabidopsis thaliana* Columbia ecotype (Col-0)
- Arabidopsis lines expressing organelle-specific markers – β -ATPase-GFP (Logan and Leaver, 2000) in mitochondria, HDEL-GFP in ER (Matsushima et al., 2002), and H2B-YFP in nuclei (Boisnard-Lorig et al., 2001).
- Cell suspension cultures – *A. thaliana* Col-0, *A. thaliana* cv. Landsberg *erecta* (Ler), *Nicotiana tabacum* cv. Bright Yellow 2 cell line (BY-2)
- Arabidopsis seeds were surface-sterilised using a 70% ethanol solution (Merck Life Science, Germany) supplemented with 0.1% Tween-20 (Merck Life Science) for

10 min, rinsed with sterile deionised water. Seeds were sowed on solid Murashige and Skoog medium (4.4 g/L) (Duchefa Biochemie) supplemented with 1% sucrose (Sigma Aldrich) and 1% plant agar (Duchefa Biochemie). After 3 days of stratification at 4 °C in dark, the plates with seeds were arranged vertically and incubated for 10 days under long-day conditions (16 h light/8 h dark) at 22 °C. (*Supplement IV, VI*).

- Cell suspension cultures of *A. thaliana* cv. *Ler* was grown in liquid Murashige-Skoog medium (4.4 g/L) supplemented with 3% sucrose, 0.232 µM kinetin and 5.37 µM 1-naphthaleneacetic acid. BY-2 was grown in Murashige-Skoog medium (4.4 g/L) supplemented with 3 % sucrose, 4 µM thiamine, 555 µM inositol, 1.47 mM KH₂PO₄ and 0.9 µM 2,4-dichlorophenoxyacetic acid. Both cell lines were subcultured weekly into fresh media in volume ratio 1:10. The cells were cultivated at 23 °C in dark and shaken at 120 rpm. 5-day-old cells were used for all experiments. (*Supplement V*)
- Arabidopsis Col-0 cell suspension culture was grown in liquid Murashige and Skoog media with addition of 3% sucrose, pH adjusted to 5.7, in the dark at 22 °C and shaken at 120 rpm. Cells were weekly subcultured into fresh media in ratio 1:10. For all control and sorting experiments, 14-days old cells cultivated under continuous light (150 µmol photons m⁻² s⁻¹) with fully developed chloroplasts were used (Dubreuil et al., 2018). (*Supplement VI*)

4.3 Equipment

Most of the instruments and equipment used are described in *Supplement IV-IV*.

- Subcellular fractionation based on differential centrifugation and DGU was done using Centrifuge Heraeus Biofuge Stratos Thermo Fisher Scientific (MA, USA) and Ultracentrifuge CP 90 WX with swinging-bucket rotor P40ST-2054 Hitachi Koki (Tokyo, Japan).
- Organelle sorting was performed using BD FACSAria II and BD FACSAria III flow cytometer BD Bioscience (NY, USA). The software used for data processing was BD FACSDiva BD Bioscience (NY, USA).

- Auxin quantitative analysis was based on a LC-MS/MS analysis using a 1290 Infinity LC system and a 6495B Triple Quadrupole LC/MS system equipped with Jet Stream and Dual Ion Funnel systems Agilent Technologies (CA, USA) equipped with reversed-phase column (Kinetex C18 100A, length 50 mm, diameter 2.1 mm, particle size 1.7 μm ; Phenomenex; CA, USA) according to Pěňčík et al. (2018). All MS data were processed by MassHunter software Agilent Technologies (CA, USA).
- CK quantitative analysis was performed using an ACQUITY UPLC I-Class system combined with a triple quadrupole mass spectrometer Xevo TQ-S Waters (Manchester, UK) equipped with reversed-phase column (Acquity UPLC BEH C18, 1.7 μm , 2.1 \times 50 mm; Waters, Manchester, UK) according to Svačinová et al. (2012). All MS data were processed by Masslynx software Micromass (Manchester, UK).

5 Survey of results

The current model of auxin and CK homeostasis maintenance at the subcellular level has been fully reviewed in *Supplement I*. The distinct localization of transporters, receptors, and enzymes related to auxin and CK suggests another layer of their complex regulation. The distribution of these phytohormones within plant organs or tissues is already well described but the importance of cell-type specific or intracellular phytohormone homeostasis is still poorly understood.

To shed light on phytohormone distribution within the plant cell, it is necessary to employ subcellular fractionation approaches. Differential centrifugation and DGU are possible conventional methods for isolation of cells and organelles. However, the use of advanced flow cytometric sorting as an ultra-selective tool for cell-type- and organelle-specific resolution analyses has been described in *Supplements II-III*.

This doctoral thesis is focused on the metabolic profiling of phytohormones at the subcellular level utilizing approaches based on (ultra)centrifugation (*Supplements IV-V*) and FCM (*Supplements V-VI*) in combination with ultra-sensitive LC-MS/MS methods. To achieve this, several protocols dealing with organelle isolation were tested and optimised for subsequent phytohormone analysis. Moreover, a cutting-edge subcellular compartment separating technique based on principles of FCM has been developed (*Supplement VI*).

5.1 Revealing auxin metabolome in the endoplasmic reticulum isolated by density-gradient ultracentrifugation

The ER plays a pivotal role in auxin distribution within the plant cell and auxin transport carriers have been identified to reside at this subcellular compartment (Figure 6). To elucidate the involvement of the ER in auxin homeostasis maintenance, an isolation protocol based on DGU has been optimized (*Supplement IV*).

Initially, the effectivity and gentleness of two different homogenization methods were investigated. Grinding of 10-days old Arabidopsis seedlings with mortar and pestle in the presence of quartz crystals showed more efficient organelle extraction compared to razor blade chopping. However, subsequent isolation of the ER via a discontinuous sucrose gradient was unsuccessful because the ER failed to focus properly on the expected interphase. In addition, Western blot analysis showed the presence of other co-migrating organelles, which impaired the purity of the isolated fraction. Finally, ER isolation was more

effective after chopping of the seedling by razor blade as a homogenization method (see *Figure 3 in Supplement IV*).

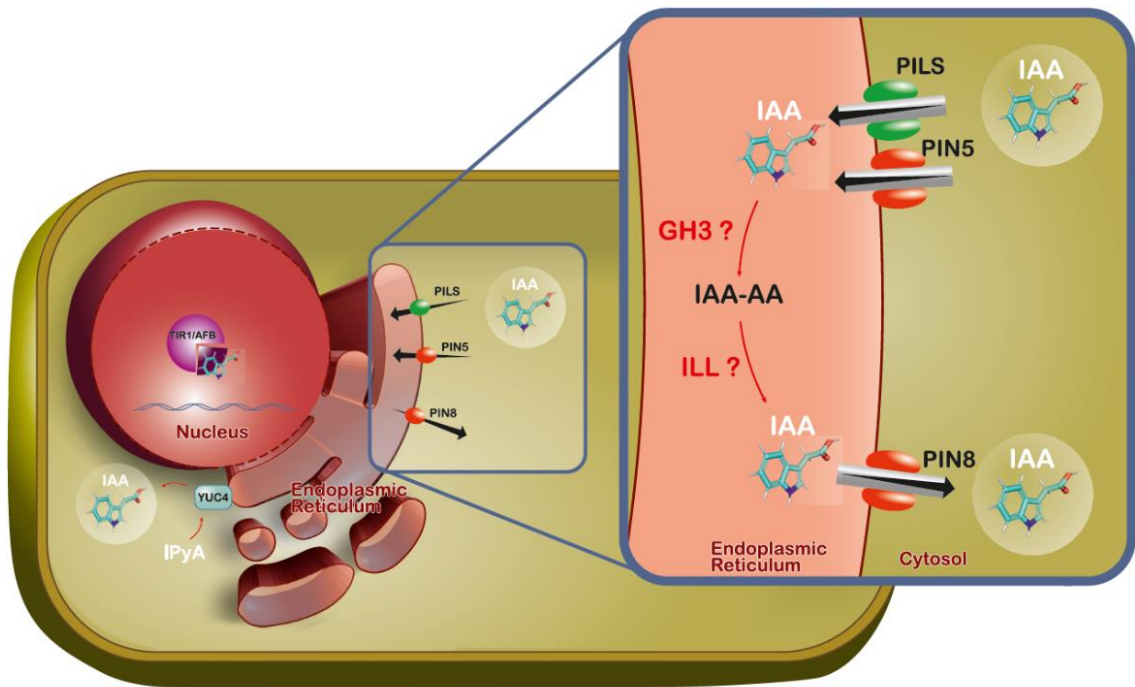


Figure 6 Model of auxin homeostasis in endoplasmic reticulum. IAA – indole-3-acetic acid, IPyA – indole-3-pyruvic acid, IAA-AA – IAA-amino acid conjugate, TIR/AFB – TRANSPORT INHIBITOR RESPONSE1/AUXIN SIGNALING F-BOX, YUC4 – YUCCA4, PIN – PIN-FORMED, PILS – PIN-LIKES, GH3 – GRETCHEN HAGEN 3, ILL – IAA-LEU-RESISTANT1-LIKE.

However, our ER-enriched fraction still contained contaminants, especially chloroplasts or thylakoid membranes. Due to the fact that chloroplasts should be denser than ER, the densities of gradient-forming sucrose solutions were slightly decreased. This resulted in chloroplast sedimentation to the bottom of centrifugal tubes. Finally, the described optimization of the isolation procedure resulted in elimination of unwanted co-migrating organelles in ER-enriched fraction (*Figure 3 in Supplement IV*). The collected ER-enriched fractions were then partitioned to high- and low-molecular weight subfractions containing proteins and auxins, respectively. Subsequent LC-MS/MS analysis of proteins extracted from the isolated ER confirmed the enrichment of the respective fraction with only minor contaminants (*Figure 4 in Supplement IV*).

DGU is a time-consuming process and auxin levels can be undesirably altered during ER isolation. Therefore, a control experiment was designed to examine possible changes. Released organelles from plant material were incubated at the same conditions mimicking the isolation of ER by DGU for 0 h and 3 h, and the relative abundance of individual auxin

metabolites was compared at the selected time points. Importantly, only minimal changes in the auxin profile were observed (*Figure 5 in Supplement IV*). Finally, the ER-specific auxin profile was determined for the first time (*Figure 7*). Interestingly, auxin analysis revealed IAA enrichment in ER fraction compared to crude extract (for more details see *Figure 5 in Supplement IV*). However, the most dominant auxin metabolite in the crude extract (whole seedlings) as well as in the ER-enriched fraction was oxIAA-glc. We found the same relative proportion of oxIAA-glc in both types of samples (79%, *Figure 7*). Altogether, we improved a protocol for ER isolation from *Arabidopsis* seedlings and for the first time reported for the first time the content of auxin and its metabolites in a highly ER-enriched fraction.

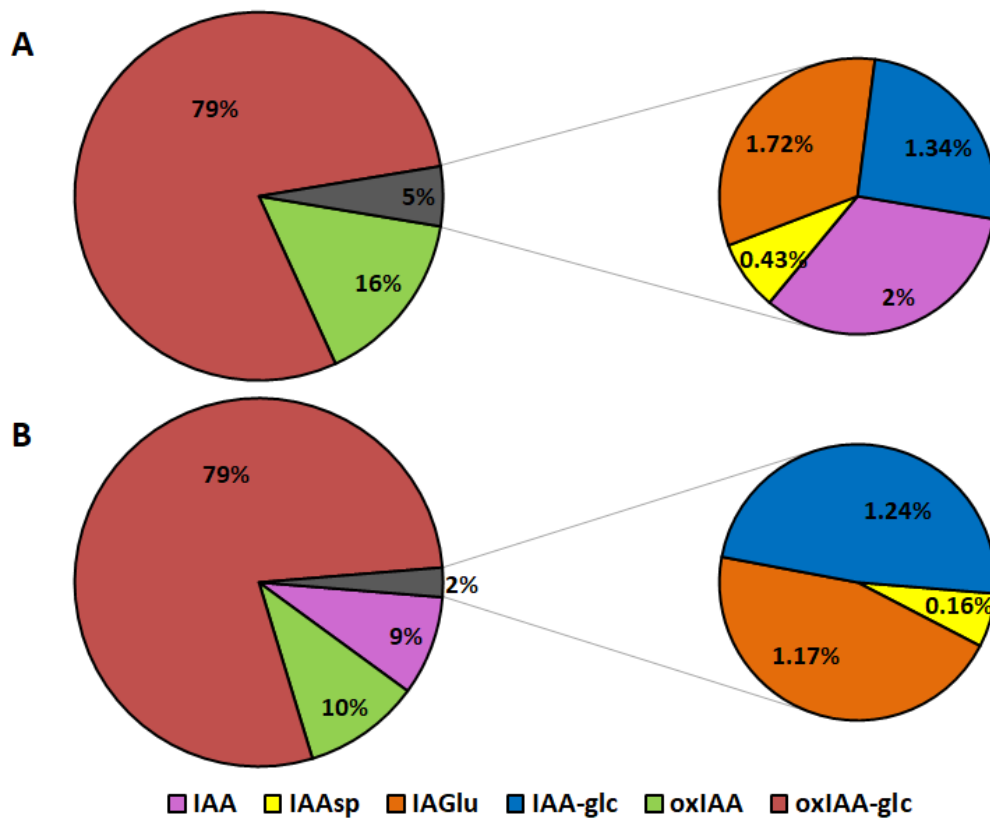


Figure 7 Auxin metabolic profile in crude extract (whole seedlings) (A) and endoplasmic reticulum (B) isolated by density-gradient ultracentrifugation from *A. thaliana* Col-0 10-days old seedling. Auxin metabolite profiles are expressed in percentages showing the relative abundance of each metabolite (n=5). IAA – indole-3-acetic acid, IAA-Asp – IAA-Aspartate, IAA-Glu – IAA-Glutamate, IAA-glc – IAA-glucose, oxIAA – 2-oxoindole-3-acetic acid, oxIAA-glc – oxIAA-glucose.

5.2 Comparison of isolation methods for auxin metabolome determination in nucleus

The bioavailability of active IAA in the nucleus is crucial for triggering canonical auxin signalling. Direct monitoring of IAA levels and related metabolites in the nucleus may unravel a mechanism of spatial homeostasis maintenance. For accurate analysis of nuclear auxin content, two isolation methods were optimized (*Supplement V*). This study aimed to compare the pros and cons of nuclei isolation by conventional differential centrifugation and advanced FCM sorting (Figure 8) from *Arabidopsis* and tobacco cell suspension cultures with respect to subsequent auxin analysis.

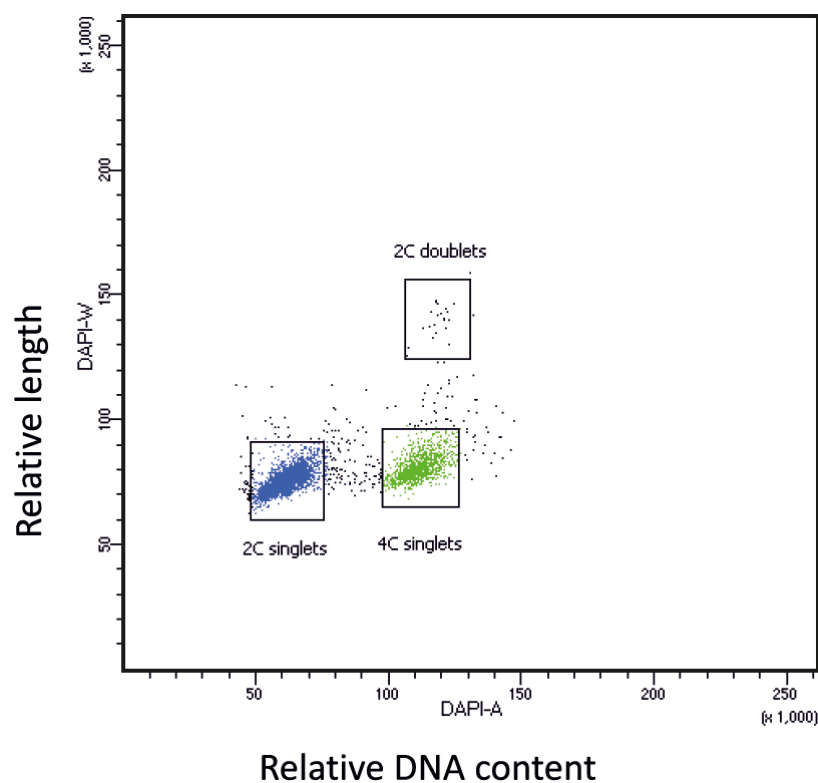


Figure 8 Dot plot graph from sorting of nuclei *Arabidopsis* Ler cell suspension culture. Two massive population of nuclei stained by 4',6-Diamidino-2-phenylindole (DAPI) (2C (blue) and 4C (green) population corresponding to G0/G1 or G2 phase of cell cycle, respectively) was observed due to high resolution of flow cytometer. Doublets of nuclei were excluded from sorting.

The cell suspension culture could not be homogenized by razor blade. Therefore, enzymatic digestion of the rigid cell wall in combination with protoplast lysis by osmotic shock was chosen as a homogenization method leading to gentle release of nuclei. Subsequently, nuclei were isolated by differential centrifugation or FCM. Western blot analysis showed that purer nuclear fractions were obtained after sorting than after

centrifugation-based isolation (*Figure 2 in Supplement V*). Moreover, FCM sorting allowed live monitoring of the organelle's condition changes, high reproducibility and easy quantification of collected organelles. On the other hand, the advantages of differential centrifugation are high yield, simplicity, and low expenses compared to FCM. Nevertheless, the low resolving power of differential centrifugation led to the presence of contaminating organelles in the nuclear fraction, mainly endomembranous compartments such as the ER or Golgi apparatus (*Figure 2a in Supplement V*). Therefore, FCM sorting was chosen as the final isolation technique prior auxin analysis by LC-MS/MS.

In addition to IAA detection, MS-based profiling of the isolated nuclei fractions also revealed the presence of auxin precursors and metabolites (*Figure 9*). The most abundant analyte in both nuclear samples isolated from Arabidopsis and tobacco cell suspension cultures was Trp as a primary metabolite (more than 99 % of relative distribution). Surprisingly, IAA and its metabolites prevailed in Arabidopsis nuclei, whereas auxin precursors predominated mainly in tobacco nuclei (*Figure 4a in Supplement V*).

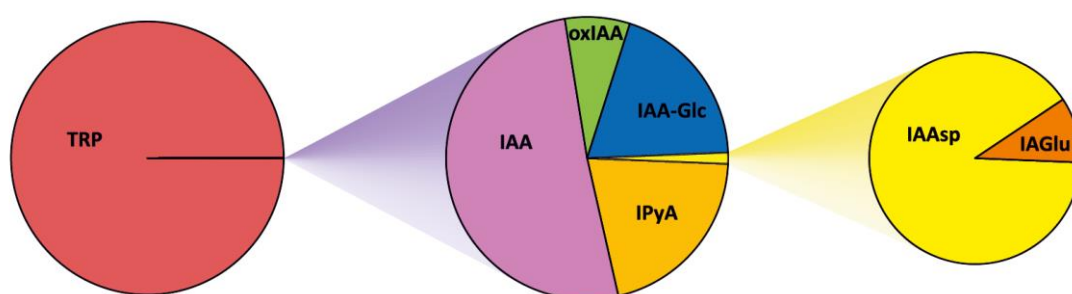


Figure 9 Auxin metabolic profile in intact nuclei isolated by flow cytometric sorting from *Arabidopsis cv. Ler* suspension cell culture. Auxin metabolite profiles are expressed in percentages showing the relative abundance of each metabolite ($n=4$). TRP – tryptophan, IAA – indole-3-acetic acid, IPyA – indole-3-pyruvic acid, IAA-glc – IAA-glucose, oxIAA – 2-oxoindole-3-acetic acid, IAA-Asp – IAA-Aspartate, IAA-Glu – IAA-Glutamate; Compounds below limit of detection: TRA – tryptamine, IAN – indole-3-acetonitrile, oxIAA-glc – oxIAA-glucose.

To confirm the applicability of FCM method, auxin metabolism was further promoted by feeding of the protoplasts with indole – a precursor of Trp – or active IAA. Indole treatment caused a high elevation of IAA precursors levels. Interestingly, only a slight increase in auxin metabolites was observed, but levels of free IAA were not altered in Arabidopsis nuclei. After IAA treatment, levels of IAA as well as other analysed metabolites, such as oxIAA, IAA-Asp and IAA-Glu, were significantly increased (*Figure 4b in Supplement V*). Overall, the combination of FCM with MS-based analysis has been

shown to provide a useful tool for monitoring IAA and its metabolites at the subcellular level. Our methodology should help clarify the regulatory networks involved in plant development processes.

5.3 Auxin and cytokinin subcellular map

Conventional organelle isolation methods focus on only one or a maximum of two types of organelles. Moreover, DGU-based protocols are time consuming (within hours). Therefore, a novel subcellular fractionation technique based on principles of FCM, so-called Fluorescence-Activated multi-Organelle Sorting (FAmOS), has been developed (*Supplement VI*). FAmOS enabled the simultaneous sorting of 4 different organelle populations from one biological sample. Cell suspension culture of Arabidopsis Col-0 was used as a simplified plant model. It was expected that the cell suspension culture exhibits a higher level of uniformity compared to the plant tissue, in which phytohormone gradients between different cell types were described (Petersson et al., 2009; Pěňčík et al., 2013; Antoniadi et al., 2015).

First, a combination of organelle-specific fluorochromes was designed with respect to their excitation, emission, and minimisation of spectra overlap. Organelle populations were then identified based on the specific fluorescent signal of the organelles and the respective negative controls. Thus, the populations of chloroplast, nuclei, mitochondria, and ER were identified and a hierarchical gating strategy for their selection and subsequent sorting was established (*Figure 1* and *Figure S1* in *Supplement IV*).

Furthermore, the identity of four sorted organelle-enriched fractions was examined by Western blot analysis (*Figure S3* in *Supplement VI*). However, due to the impossibility of detecting all organelle marker proteins, the collected organelle populations were subjected to a much more sensitive LC-MS/MS based proteomic analysis. Importantly, our results showed an enrichment of the individual organelle fractions (*Figure 3* in *Supplement VI*).

To disprove the changes in phytohormone profiles or analyte degradations during FAmOS, a set of control experiments covering the experimental design, from sample preparation to organelle sorting, was performed. The overall auxin profiles were not altered under our experimental conditions. However, levels of CK precursors (nucleotides and ribosides) have been shown to increase rapidly during sample preparation (*Figure 10*). Therefore, the homogenization buffer was supplemented with enzymatic or transport inhibitors to prevent undesirable increase of CK precursors levels (see *Figure S4* in

Supplement VI for more details). Finally, the use of a mixture of phosphatase inhibitors resulted in minimal changes in CK profiles during sample preparation (Figure 10).

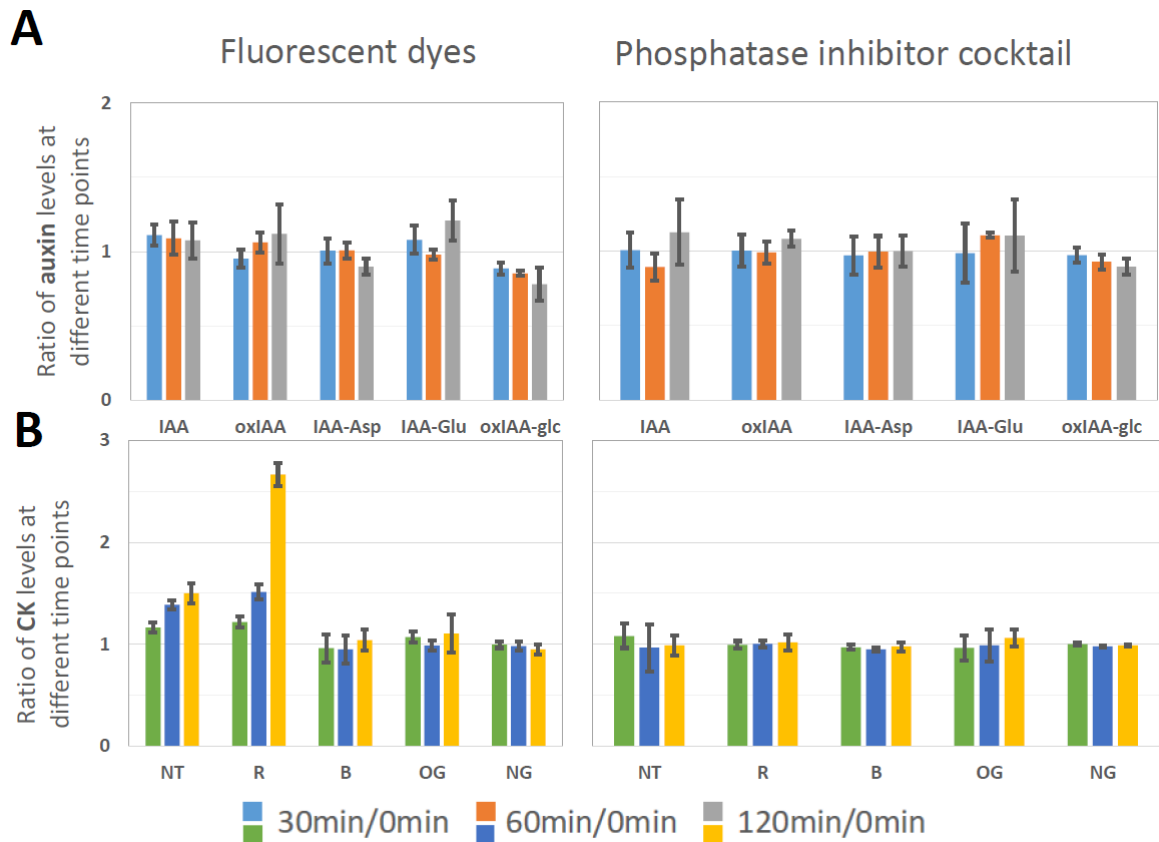


Figure 10 Stability of phytohormonal profile in organelle suspension. Samples were treated with or without a mixture of fluorescent dyes or phosphatase inhibitor cocktail and kept on ice for 2 hours to mimic the sorting process. The endogenous concentrations of auxin (A) and CK (B) were calculated as fmol per 1,000,000 cells and the respective ratios (concentration at time point/concentration at time point 0 min) were calculated ($n=4$). IAA-glucose was not detected. IAA – indole-3-acetic acid; oxIAA – 2-oxindole-3-acetic acid; IAA-Asp – IAA-Aspartate; IAA-Glu – IAA-Glutamate; oxIAA-glc – oxIAA-glucose; NT – CK nucleotides; R – CK ribosides; B – free bases; OG – O-glucosides and NG – N-glucosides.

In addition, samples were spiked with isotopically labelled [$^{13}\text{C}_6$]IAA and [$^{15}\text{N}_4$]iP prior homogenization or sorting to monitor metabolic turn-over. The results showed that some negligible enzymatic activity persisted (Figure 4 in Supplement VI). As a further measure to avoid altering the endogenous phytohormonal profile, the whole procedure was shortened to the minimum possible time. This was mainly achieved by preparing a fresh sample every half hour, followed by only 30 min of sorting (Figure 11). The sorted samples were then sub-fractionated for protein and phytohormone analyses using Amicon filters. Each fraction was purified and analysed separately by LC-MS/MS methods. Finally, our FAMOS

workflow was optimised to achieve high-resolution intracellular information about auxin and CK levels from a single sorted sample.



Figure 11 Workflow of organelle sorting. From left to right: (i) 14-days-old *Arabidopsis* cell suspension culture, (ii) cell homogenization and staining with fluorescent dyes (20 min), (iii) FACS instrument for analysing and sorting the organelles (30 min), (iv) phytohormone in-tip micro solid-phase extraction (μ SPE) purification (3 h), and (v) liquid chromatography-tandem mass spectrometry (LC-MS/MS) analysis (10 – 15 min).

The FAMOS procedure was utilized to separate and collect the population of chloroplasts, nuclei, mitochondria, and ER. To create an overall phytohormonal map of a plant cell, vacuoles were isolated in parallel by a well-established DGU method (Robert et al., 2007). Employing ultra-sensitive MS-based methods, phytohormones were detected in only 200,000 pieces of collected organelles. Due to the different organelle sizes, the levels of measured phytohormones concentrations were finally normalized according to each compartment's protein content and calculated in fmol/ μ g proteins. The concentration gradient of phytohormones was then expressed as subcellular heat maps of the ratio of auxin and CK levels to the level of respective analyte in chloroplasts (Figure 12). Interestingly, auxins and CKs revealed different subcellular distributions within the plant cell. The highest concentration of IAA and CKs was detected in vacuoles. In detail, CK *O*-glucosides, IAA-Asp and IAA-Glu were observed only in this organelle (Figure 5 and Figure S5 in Supplement VI). Our findings point to a potential role of vacuoles as auxin and CK storage compartments. Furthermore, CKs were enriched in the ER, the place of their perception, while higher concentrations of IAA were measured in chloroplasts (Figure 12). The lowest concentrations of CKs and IAA were found in mitochondria.

In conclusion, the combination of efficient FAMOS with a sensitive LC-MS/MS provides a unique approach for phytohormone profiling at the subcellular level. Our results present a way to simultaneously sort four different organelle populations based on the compartment-specific fluorescence parameters. Moreover, control experiments showed that neither sorting nor application of fluorescent dyes caused significant changes in both auxin

and CK profiles. Due to the high resolution of FAMOS, we also expect further use of this method for multiple “omics” approaches.

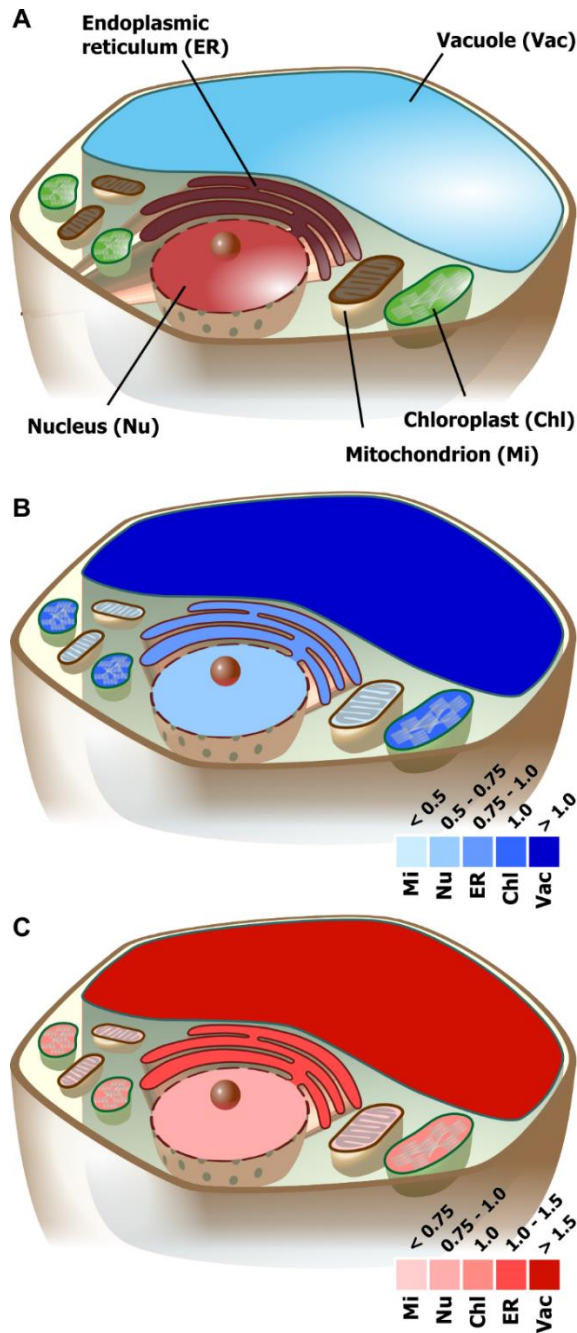


Figure 12 Subcellular phytohormone map. (A) Model of plant cell, (B) total cytokinin and (C) IAA distribution within plant cell. Intensities express ratio of analyte level (expressed as fmol/ug of proteins) to level of respective analyte in chloroplasts. Aliquot of 200.000 pcs of organelles was used for phytohormonal analysis by LC-MS/MS (n=4-5).

6 Conclusion and perspectives

This thesis deals with development and optimization of subcellular fractionation methods for subsequent high-resolution organelle-specific analysis of auxin and CK profiles. The combination of highly resolving fractionation techniques with ultra-sensitive LC-MS/MS analysis supplemented with modern approaches of molecular biology can elucidate the spatiotemporal coordination of phytohormone homeostasis maintenance at the subcellular level.

The most important outcomes of the described work are:

- Optimised isolation of ER by DGU can be utilized for phytohormone profiling. Auxin analysis revealed considerably higher levels of IAA in the ER-enriched fraction than in the whole plant (*Supplement IV*).
- The FCM method provided higher purity of sorted nuclei than the differential centrifugation approach. Surprisingly, not only IAA but also related precursors and metabolites were detected in the nuclear fraction. However, Arabidopsis nuclei contains a higher relative distribution of IAA and its metabolites, whereas IAA precursors predominate in tobacco nuclei (*Supplement V*).
- Subcellular fractionation based on FCM enabled simultaneous sorting of 4 organelles. Moreover, FAmOS is a suitable tool for phytohormone profiling at the organelle level (*Supplement VI*).
- One collected sample of sorted organelles can be subjected to auxin, CK and proteomic analysis.
- A subcellular heat map of auxin and CKs revealed concentration gradients between different organelles.

Revealed concentration gradients of analysed phytohormones within the plant cell support our hypothesis that the distribution of phytohormones is in good agreement with relevant enzymes' and transporters' localizations (Skalický et al., 2018). However, the future involvement of respective loss-of-function mutants or overexpression lines of phytohormone transporters, receptors, biosynthetic or metabolic enzymes in profiling at the subcellular level may further shed light on the regulation of homeostasis maintenance. The developed FAmOS is an innovative technique and a valuable tool not only for subcellular phytohormone analysis, but also for other “omics” approaches in plant sciences.

7 References

- Albrecht, V., Ingenfeld, A., and Apel, K.** (2006). Characterization of the Snowy Cotyledon 1 Mutant of *Arabidopsis thaliana*: The Impact of Chloroplast Elongation Factor G on Chloroplast Development and Plant Vitality. *Plant Mol. Biol.* **60**: 507–18.
- Allen, M., Qin, W., Moreau, F., and Moffatt, B.** (2002). Adenine phosphoribosyltransferase isoforms of *Arabidopsis* and their potential contributions to adenine and cytokinin metabolism. *Physiol. Plant.* **115**: 56–68.
- Anantharaman, V. and Aravind, L.** (2001). The CHASE domain: A predicted ligand-binding module in plant cytokinin receptors and other eukaryotic and bacterial receptors. *Trends Biochem. Sci.* **26**: 579–82.
- Antoniadi, I. et al.** (2020). Cell-surface receptors enable perception of extracellular cytokinins. *Nat. Commun.* **11**: 4284.
- Antoniadi, I., Plačková, L., Simonovik, B., Doležal, K., Turnbull, C., Ljung, K., and Novák, O.** (2015). Cell-Type-Specific Cytokinin Distribution within the *Arabidopsis* Primary Root Apex. *Plant Cell* **27**: 1955–67.
- Antoniadi, I., Skalický, V., Sun, G., Ma, W., Galbraith, D.W., Novák, O., and Ljung, K.** (2021). Fluorescence activated cell sorting—A selective tool for plant cell isolation and analysis. *Cytom. Part A: cyto.a.24461*.
- Barbez, E. et al.** (2012). A novel putative auxin carrier family regulates intracellular auxin homeostasis in plants. *Nature* **485**: 119–22.
- Barbez, E. and Kleine-Vehn, J.** (2013). Divide Et Impera—cellular auxin compartmentalization. *Curr. Opin. Plant Biol.* **16**: 78–84.
- Bardy, N., Carrasco, A., Galaud, J.P., Pont-Lezica, R., and Canut, H.** (1998). Free-flow electrophoresis for fractionation of *Arabidopsis thaliana* membranes. *Electrophoresis* **19**: 1145–53.
- Benková, E., Witters, E., Van Dongen, W., Kolář, J., Motyka, V., Brzobohatý, B., Van Onckelen, H.A., and Macháčková, I.** (1999). Cytokinins in tobacco and wheat chloroplasts. Occurrence and changes due to light/dark treatment. *Plant Physiol.* **121**: 245–52.
- Bernard, C., Traub, M., Kunz, H.-H., Hach, S., Trentmann, O., and Möhlmann, T.** (2011). Equilibrative nucleoside transporter 1 (ENT1) is critical for pollen germination and vegetative growth in *Arabidopsis*. *J. Exp. Bot.* **62**: 4627–37.
- Béziat, C., Barbez, E., Feraru, M.I., Lucyshyn, D., and Kleine-Vehn, J.** (2017). Light triggers PILS-dependent reduction in nuclear auxin signalling for growth transition. *Nat. plants* **3**: 17105.
- Bielešzová, K., Pařízková, B., Kubeš, M., Husičková, A., Kubala, M., Ma, Q., Sedlářová, M., Robert, S., Doležal, K., Strnad, M., Novák, O., and Žukauskaitė, A.** (2018). New fluorescently labeled auxins exhibit promising anti-auxin activity. *N. Biotechnol.*

48: 44–52.

- Blavet, N., Uřinová, J., Jeřábková, H., Chamrád, I., Vrána, J., Lenobel, R., Beinhauer, J., Šebela, M., Doležel, J., and Petrovská, B.** (2017). UNcleProt (Universal Nuclear Protein database of barley): The first nuclear protein database that distinguishes proteins from different phases of the cell cycle. *Nucleus* **8**: 70–80.
- Boisnard-Lorig, C., Colon-Carmona, A., Bauch, M., Hodge, S., Doerner, P., Bancharel, E., Dumas, C., Haseloff, J., and Berger, F.** (2001). Dynamic analyses of the expression of the HISTONE::YFP fusion protein in arabidopsis show that syncytial endosperm is divided in mitotic domains. *Plant Cell* **13**: 495–509.
- Boussardon, C., Przybyla-Toscano, J., Carrie, C., and Keech, O.** (2020). Tissue-Specific Isolation of Arabidopsis/plant Mitochondria- IMTACT (Isolation of Mitochondria Tagged in specific Cell Types). *Plant J.* **103**: 459–73.
- Brownlee, B.G., Hall, R.H., and Whitty, C.D.** (1975). 3-Methyl-2-butenal: an enzymatic degradation product of the cytokinin, N-6-(delta-2 isopentenyl)adenine. *Can. J. Biochem.* **53**: 37–41.
- Brzobohatý, B., Moore, I., Kristoffersen, P., Bako, L., Campos, N., Schell, J., and Palme, K.** (1993). Release of active cytokinin by a beta-glucosidase localized to the maize root meristem. *Science* **262**: 1051–4.
- Bürkle, L., Cedzich, A., Döpke, C., Stransky, H., Okumoto, S., Gillissen, B., Kühn, C., and Frommer, W.B.** (2003). Transport of cytokinins mediated by purine transporters of the PUP family expressed in phloem, hydathodes, and pollen of Arabidopsis. *Plant J.* **34**: 13–26.
- Caesar, K., Thamm, A.M.K., Witthöft, J., Elgass, K., Huppenberger, P., Grefen, C., Horak, J., and Harter, K.** (2011). Evidence for the localization of the Arabidopsis cytokinin receptors AHK3 and AHK4 in the endoplasmic reticulum. *J. Exp. Bot.* **62**: 5571–80.
- Calderón-Villalobos, L.I.A. et al.** (2012). A combinatorial TIR1/AFB-Aux/IAA co-receptor system for differential sensing of auxin. *Nat. Chem. Biol.* **8**: 477–85.
- Casanova-Sáez, R., Mateo-Bonmatí, E., and Ljung, K.** (2021). Auxin Metabolism in Plants. *Cold Spring Harb. Perspect. Biol.*: a039867.
- Casanova-Sáez, R. and Voß, U.** (2019). Auxin Metabolism Controls Developmental Decisions in Land Plants. *Trends Plant Sci.* **24**: 741–54.
- Čertnerová, D. and Galbraith, D.W.** (2021). Best practices in the flow cytometry of microalgae. *Cytom. Part A* **99**: 359–64.
- Chen, J.-G., Ullah, H., Young, J.C., Sussman, M.R., and Jones, A.M.** (2001). ABP1 is required for organized cell elongation and division in Arabidopsis embryogenesis. *Genes Dev.* **15**: 902–11.
- Chen, W.W., Freinkman, E., Wang, T., Birsoy, K., and Sabatini, D.M.** (2016). Absolute Quantification of Matrix Metabolites Reveals the Dynamics of Mitochondrial

- Metabolism. *Cell* **166**: 1324–37.e11.
- Cho, H.S., Lee, S.S., Kim, K.D., Hwang, I., Lim, J.-S., Park, Y.-I., and Pai, H.-S.** (2004). DNA Gyrase Is Involved in Chloroplast Nucleoid Partitioning. *Plant Cell* **16**: 2665–82.
- Corbesier, L., Prinsen, E., Jacqumard, A., Lejeune, P., Van Onckelen, H.A., Périlleux, C., and Bernier, G.** (2003). Cytokinin levels in leaves, leaf exudate and shoot apical meristem of *Arabidopsis thaliana* during floral transition. *J. Exp. Bot.* **54**: 2511–7.
- Cossarizza, A. et al.** (2017). Guidelines for the use of flow cytometry and cell sorting in immunological studies. *Eur. J. Immunol.* **47**: 1584–797.
- D’Agostino Ingrid B, Deruère, J., and Kieber, J.J.** (2000). Characterization of the response of the *Arabidopsis* response regulator gene family to cytokinin. *Plant Physiol.* **124**: 1706–17.
- Dal Bosco, C. et al.** (2012). The endoplasmic reticulum localized PIN8 is a pollen-specific auxin carrier involved in intracellular auxin homeostasis. *Plant J.* **71**: 860–70.
- Darwin, C. and Darwin, F.** (1880). *The power of movement in plants*. John Murray, London.
- Davies, P.J.** (2010). The Plant Hormones: Their Nature, Occurrence, and Functions. In *Plant Hormones: Biosynthesis, Signal Transduction, Action!* 3rd Edition, P.J. Davies, ed (Kluwer Academic Publishers: Dordrecht, Netherlands), pp. 5–15.
- Deal, R.B. and Henikoff, S.** (2010). A simple method for gene expression and chromatin profiling of individual cell types within a tissue. *Dev. Cell* **18**: 1030–40.
- Deal, R.B. and Henikoff, S.** (2011). The INTACT method for cell type-specific gene expression and chromatin profiling in *Arabidopsis thaliana*. *Nat. Protoc.* **6**: 56–68.
- Dharmasiri, N., Dharmasiri, S., and Estelle, M.** (2005). The F-box protein TIR1 is an auxin receptor. *Nature* **435**: 441–5.
- Ding, Z. et al.** (2012). ER-localized auxin transporter PIN8 regulates auxin homeostasis and male gametophyte development in *Arabidopsis*. *Nat. Commun.* **3**: 941.
- Doležel, J., Greilhuber, J., and Suda, J.** (2007). Flow Cytometry with Plants: an Overview. In *Flow Cytometry with Plants*, J. Doležel, J. Greilhuber, and J. Suda, eds (John Wiley & Sons, Ltd: Weinheim, Germany), pp. 41–65.
- Doležel, J., Lucretti, S., Molnár, I., Cápál, P., and Giorgi, D.** (2021). Chromosome analysis and sorting. *Cytom. Part A* **99**: 328–42.
- Dortay, H., Gruhn, N., Pfeifer, A., Schwerdtner, M., Schmölling, T., and Heyl, A.** (2008). Toward an interaction map of the two-component signaling pathway of *Arabidopsis thaliana*. *J. Proteome Res.* **7**: 3649–60.
- Dortay, H., Mehnert, N., Bürkle, L., Schmölling, T., and Heyl, A.** (2006). Analysis of protein interactions within the cytokinin-signaling pathway of *Arabidopsis thaliana*. *FEBS J.* **273**: 4631–44.

- Dubreuil, C., Jin, X., Barajas-López, J. de D., Hewitt, T.C., Tanz, S.K., Dobrenel, T., Schröder, W.P., Hanson, J., Pesquet, E., Grönlund, A., Small, I., and Strand, Å.** (2018). Establishment of Photosynthesis through Chloroplast Development Is Controlled by Two Distinct Regulatory Phases. *Plant Physiol.* **176**: 1199–214.
- De Duve, C., Pressman, B.C., Gianetto, R., Wattiaux, R., and Appelmans, F.** (1955). Tissue fractionation studies. 6. Intracellular distribution patterns of enzymes in rat-liver tissue. *Biochem. J.* **60**: 604–17.
- Enders, T.A., Oh, S., Yang, Z., Montgomery, B.L., and Strader, L.C.** (2015). Genome Sequencing of *Arabidopsis* *abp1-5* Reveals Second-Site Mutations That May Affect Phenotypes. *Plant Cell* **27**: 1820–6.
- Eubel, H., Lee, C.P., Kuo, J., Meyer, E.H., Taylor, N.L., and Millar, A.H.** (2007). Free-flow electrophoresis for purification of plant mitochondria by surface charge. *Plant J.* **52**: 583–94.
- Eubel, H., Meyer, E.H., Taylor, N.L., Bussell, J.D., O’Toole, N., Heazlewood, J.L., Castleden, I., Small, I.D., Smith, S.M., and Millar, A.H.** (2008). Novel proteins, putative membrane transporters, and an integrated metabolic network are revealed by quantitative proteomic analysis of *Arabidopsis* cell culture peroxisomes. *Plant Physiol.* **148**: 1809–29.
- Fendrych, M., Akhmanova, M., Merrin, J., Glanc, M., Hagihara, S., Takahashi, K., Uchida, N., Torii, K.U., and Friml, J.** (2018). Rapid and reversible root growth inhibition by TIR1 auxin signalling. *Nat. plants* **4**: 453–9.
- Feraru, E., Feraru, M.I., Barbez, E., Waidmann, S., Sun, L., Gaidora, A., and Kleine-Vehn, J.** (2019). PILS6 is a temperature-sensitive regulator of nuclear auxin input and organ growth in *Arabidopsis thaliana*. *Proc. Natl. Acad. Sci. U. S. A.* **116**: 3893–8.
- Fluckiger, R., De Caroli, M., Piro, G., Dalessandro, G., Neuhaus, J.-M., and Di Sanebastiano, G.-P.** (2003). Vacuolar system distribution in *Arabidopsis* tissues, visualized using GFP fusion proteins. *J. Exp. Bot.* **54**: 1577–84.
- Folta, K.M. and Kaufman, L.S.** (2007). Isolation of *Arabidopsis* nuclei and measurement of gene transcription rates using nuclear run-on assays. *Nat. Protoc.* **1**: 3094–100.
- Frébortová, J., Fraaije, M.W., Galuszka, P., Šebela, M., Peč, P., Hrbáč, J., Novák, O., Bilyeu, K.D., English, J.T., and Frébort, I.** (2004). Catalytic reaction of cytokinin dehydrogenase: preference for quinones as electron acceptors. *Biochem J* **380**: 121–30.
- Friml, J.** (2003). Auxin transport - shaping the plant. *Curr. Opin. Plant Biol.* **6**: 7–12.
- Friml, J.** (2010). Subcellular trafficking of PIN auxin efflux carriers in auxin transport. *Eur. J. Cell Biol.* **89**: 231–5.
- Fu, Y., Yang, Y., Chen, S., Ning, N., and Hu, H.** (2019). *Arabidopsis* IAR4 modulates primary root growth under salt stress through ros-mediated modulation of auxin distribution. *Front. Plant Sci.* **10**: 522.

- Fürtauer, L., Weckwerth, W., and Nägele, T.** (2016). A Benchtop Fractionation Procedure for Subcellular Analysis of the Plant Metabolome. *Front. Plant Sci.* **7**: 1912.
- Galbraith, D.W. et al.** (2021). Best practices in plant cytometry. *Cytom. Part A* **99**: 311–7.
- Galbraith, D.W., Harkins, K.R., Maddox, J.M., Ayres, N.M., Sharma, D.P., and Firoozabady, E.** (1983). Rapid flow cytometric analysis of the cell cycle in intact plant tissues. *Science* **220**: 1049–51.
- Galichet, A., Hoyerová, K., Kamínek, M., and Gruissem, W.** (2008). Farnesylation directs AtIPT3 subcellular localization and modulates cytokinin biosynthesis in Arabidopsis. *Plant Physiol.* **146**: 1155–64.
- Galuszka, P., Frébort, I., Šebela, M., Sauer, P., Jacobsen, S., and Peč, P.** (2001). Cytokinin oxidase or dehydrogenase? Mechanism of cytokinin degradation in cereals. *Eur. J. Biochem.* **268**: 450–61.
- Galuszka, P., Popelková, H., Werner, T., Frébortová, J., Pospíšilová, H., Mik, V., Köllmer, I., Schmülling, T., and Frébort, I.** (2007). Biochemical Characterization of Cytokinin Oxidases/Dehydrogenases from Arabidopsis thaliana Expressed in Nicotiana tabacum L. *J. Plant Growth Regul.* **26**: 255–67.
- Gao, D., Knight, M.R., Trewavas, A.J., Sattelmacher, B., and Plieth, C.** (2004). Self-reporting Arabidopsis expressing pH and [Ca²⁺] indicators unveil ion dynamics in the cytoplasm and in the apoplast under abiotic stress. *Plant Physiol.* **134**: 898–908.
- Gao, Y., Zhang, Y., Zhang, D., Dai, X., Estelle, M., and Zhao, Y.** (2015). Auxin binding protein 1 (ABP1) is not required for either auxin signaling or Arabidopsis development. *Proc. Natl. Acad. Sci. U. S. A.* **112**: 2275–80.
- Gillissen, B., Bürkle, L., André, B., Kühn, C., Rentsch, D., Brandl, B., and Frommer, W.B.** (2000). A new family of high-affinity transporters for adenine, cytosine, and purine derivatives in Arabidopsis. *Plant Cell* **12**: 291–300.
- Gomes, G.L.B. and Scortecci, K.C.** (2021). Auxin and its role in plant development: structure, signalling, regulation and response mechanisms. *Plant Biol.* **11**: 2170.
- Grebe, M., Xu, J., Möbius, W., Ueda, T., Nakano, A., Geuze, H.J., Rook, M.B., and Scheres, B.** (2003). Arabidopsis sterol endocytosis involves actin-mediated trafficking via ARA6-positive early endosomes. *Curr. Biol.* **13**: 1378–87.
- Grones, P. and Friml, J.** (2015). Auxin transporters and binding proteins at a glance. *J. Cell Sci.* **128**: 1–7.
- Hirose, N., Takeji, K., Kuroha, T., Kamada-Nobusada, T., Hayashi, H., and Sakakibara, H.** (2008). Regulation of cytokinin biosynthesis, compartmentalization and translocation. *J. Exp. Bot.* **59**: 75–83.
- Horgan, R., Hewett, E.W., Horgan, J.M., Purse, J., and Wareing, P.F.** (1975). A new cytokinin from Populus x robusta. *Phytochemistry* **14**: 1005–8.
- Horgan, R., Hewett, E.W., Purse, J., and Wareing, P.F.** (1973). A new cytokinin from

- Populus - robusta*. *Tetrahedron Lett.*: 2827–8.
- Huber, L.A., Pfaller, K., and Vietor, I.** (2003). Organelle Proteomics: Implications for Subcellular Fractionation in Proteomics. *Circ. Res.* **92**: 962–8.
- Hurný, A. et al.** (2020). SYNERGISTIC ON AUXIN AND CYTOKININ 1 positively regulates growth and attenuates soil pathogen resistance. *Nat. Commun.* **11**: 2170.
- Hutchison, C.E., Li, J., Argueso, C., Gonzalez, M., Lee, E., Lewis, M.W., Maxwell, B.B., Perdue, T.D., Schaller, G.E., Alonso, J.M., Ecker, J.R., and Kieber, J.J.** (2006). The Arabidopsis histidine phosphotransfer proteins are redundant positive regulators of cytokinin signaling. *Plant Cell* **18**: 3073–87.
- Hwang, I. and Sheen, J.** (2001). Two-component circuitry in Arabidopsis cytokinin signal transduction. *Nature* **413**: 383–9.
- Imamura, A., Hanaki, N., Nakamura, A., Suzuki, T., Taniguchi, M., Kiba, T., Ueguchi, C., Sugiyama, T., and Mizuno, T.** (1999). Compilation and characterization of Arabidopsis thaliana response regulators implicated in His-Asp phosphorelay signal transduction. *Plant Cell Physiol.* **40**: 733–42.
- Inoue, T., Higuchi, M., Hashimoto, Y., Seki, M., Kobayashi, M., Kato, T., Tabata, S., Shinozaki, K., and Kakimoto, T.** (2001). Identification of CRE1 as a cytokinin receptor from Arabidopsis. *Nature* **409**: 1060–3.
- Ito, E., Fujimoto, M., Ebine, K., Uemura, T., Ueda, T., and Nakano, A.** (2012). Dynamic behavior of clathrin in Arabidopsis thaliana unveiled by live imaging. *Plant J.* **69**: 204–16.
- Jaquinod, M., Villiers, F., Kieffer-Jaquinod, S., Hugouvieux, V., Bruley, C., Garin, J., and Bourguignon, J.** (2007). A proteomics dissection of Arabidopsis thaliana vacuoles isolated from cell culture. *Mol. Cell. Proteomics* **6**: 394–412.
- Jin, S.-H., Ma, X.-M., Han, P., Wang, B., Sun, Y.-G., Zhang, G.-Z., Li, Y.-J., and Hou, B.-K.** (2013a). UGT74D1 is a novel auxin glycosyltransferase from Arabidopsis thaliana. *PLoS One* **8**: e61705.
- Jin, S.-H., Ma, X.-M., Kojima, M., Sakakibara, H., Wang, Y.W., and Hou, B.-K.** (2013b). Overexpression of glucosyltransferase UGT85A1 influences trans-zeatin homeostasis and trans-zeatin responses likely through O-glucosylation. *Planta* **237**: 991–9.
- Jiskrová, E., Novák, O., Pospíšilová, H., Holubová, K., Karády, M., Galuszka, P., Robert, S., and Frébort, I.** (2016). Extra- and intracellular distribution of cytokinins in the leaves of monocots and dicots. *N. Biotechnol.* **33**: 735–42.
- Jones, A.M. and Herman, E.M.** (1993). KDEL-Containing Auxin-Binding Protein Is Secreted to the Plasma Membrane and Cell Wall. *Plant Physiol.* **101**: 595–606.
- Jurado, S., Abraham, Z., Manzano, C., López-Torrejón, G., Pacios, L.F., and Del Pozo, J.C.** (2010). The Arabidopsis cell cycle F-box protein SKP2A binds to auxin. *Plant Cell* **22**: 3891–904.

- Kakimoto, T.** (2001). Identification of plant cytokinin biosynthetic enzymes as dimethylallyl diphosphate:ATP/ADP isopentenyltransferases. *Plant Cell Physiol.* **42**: 677–85.
- Kasahara, H., Takei, K., Ueda, N., Hishiyama, S., Yamaya, T., Kamiya, Y., Yamaguchi, S., and Sakakibara, H.** (2004). Distinct Isoprenoid Origins of cis- and trans-Zeatin Biosyntheses in *Arabidopsis*. *J. Biol. Chem.* **279**: 14049–54.
- Keech, O., Dizengremel, P., and Gardeström, P.** (2005). Preparation of leaf mitochondria from *Arabidopsis thaliana*. *Physiol. Plant.* **124**: 403–9.
- Kepinski, S. and Leyser, H.M.O.** (2005). The *Arabidopsis* F-box protein TIR1 is an auxin receptor. *Nature* **435**: 446–51.
- Kiba, T., Taniguchi, M., Imamura, A., Ueguchi, C., Mizuno, T., and Sugiyama, T.** (1999). Differential expression of genes for response regulators in response to cytokinins and nitrate in *Arabidopsis thaliana*. *Plant Cell Physiol.* **40**: 767–71.
- Kieber, J.J. and Schaller, G.E.** (2018). Cytokinin signaling in plant development. *Development* **145**: dev149344.
- Kim, H.J., Ryu, H., Hong, S.H., Woo, H.R., Lim, P.O., Lee, I.C., Sheen, J., Nam, H.-G., and Hwang, I.** (2006). Cytokinin-mediated control of leaf longevity by AHK3 through phosphorylation of ARR2 in *Arabidopsis*. *Proc. Natl. Acad. Sci. U. S. A.* **103**: 814–9.
- Kim, J.I. et al.** (2007). *yucca6*, a dominant mutation in *Arabidopsis*, affects auxin accumulation and auxin-related phenotypes. *Plant Physiol.* **145**: 722–35.
- Klode, M., Dahlke, R.I., Sauter, M., and Steffens, B.** (2011). Expression and Subcellular Localization of *Arabidopsis thaliana* Auxin-Binding Protein 1 (ABP1). *J. Plant Growth Regul.* **30**: 416–24.
- Ko, D. et al.** (2014). *Arabidopsis* ABCG14 is essential for the root-to-shoot translocation of cytokinin. *Proc. Natl. Acad. Sci. U. S. A.* **111**: 7150–5.
- Köllmer, I., Novák, O., Strnad, M., Schmülling, T., and Werner, T.** (2014). Overexpression of the cytosolic cytokinin oxidase/dehydrogenase (CKX7) from *Arabidopsis* causes specific changes in root growth and xylem differentiation. *Plant J.* **78**: 359–71.
- Korasick, D.A., Enders, T.A., and Strader, L.C.** (2013). Auxin biosynthesis and storage forms. *J. Exp. Bot.* **64**: 2541–55.
- Kowalczyk, M. and Sandberg, G.** (2001). Quantitative analysis of indole-3-acetic acid metabolites in *Arabidopsis*. *Plant Physiol.* **127**: 1845–53.
- Kowalska, M., Galuszka, P., Frébortová, J., Šebela, M., Béréš, T., Hluska, T., Šmehilová, M., Bilyeu, K.D., and Frébort, I.** (2010). Vacuolar and cytosolic cytokinin dehydrogenases of *Arabidopsis thaliana*: Heterologous expression, purification and properties. *Phytochemistry* **71**: 1970–8.
- Křeček, P., Skůpa, P., Libus, J., Naramoto, S., Tejos, R., Friml, J., and Zažímalová, E.** (2009). The PIN-FORMED (PIN) protein family of auxin transporters. *Genome Biol.* **10**: 249.

- Kriechbaumer, V., Botchway, S.W., and Hawes, C.** (2016). Localization and interactions between Arabidopsis auxin biosynthetic enzymes in the TAA/YUC-dependent pathway. *J. Exp. Bot.* **67**: 4195–207.
- Kriechbaumer, V., Wang, P., Hawes, C., and Abell, B.M.** (2012). Alternative splicing of the auxin biosynthesis gene YUCCA4 determines its subcellular compartmentation. *Plant J.* **70**: 292–302.
- Kron, P., Loureiro, J., Castro, S., and Čertner, M.** (2021). Flow cytometric analysis of pollen and spores: An overview of applications and methodology. *Cytom. Part A* **99**: 348–58.
- Kubeš, M. et al.** (2012). The Arabidopsis concentration-dependent influx/efflux transporter ABCB4 regulates cellular auxin levels in the root epidermis. *Plant J.* **69**: 640–54.
- Kubiasová, K. et al.** (2020). Cytokinin fluoroprobe reveals multiple sites of cytokinin perception at plasma membrane and endoplasmic reticulum. *Nat. Commun.* **11**: 4285.
- Kuderová, A., Gallová, L., Kuricová, K., Nejedlá, E., Čurdová, A., Micenková, L., Plíhal, O., Šmajš, D., Spíchal, L., and Hejátko, J.** (2015). Identification of AHK2- and AHK3-like cytokinin receptors in Brassica napus reveals two subfamilies of AHK2 orthologues. *J. Exp. Bot.* **66**: 339–53.
- Kudo, T., Kiba, T., and Sakakibara, H.** (2010). Metabolism and long-distance translocation of cytokinins. *J. Integr. Plant Biol.* **52**: 53–60.
- Kuhnert, F., Stefanski, A., Overbeck, N., Drews, L., Reichert, A.S., Stühler, K., and Weber, A.P.M.** (2020). Rapid single-step affinity purification of HA-tagged plant mitochondria. *Plant Physiol.* **182**: 692–706.
- Kurakawa, T., Ueda, N., Maekawa, M., Kobayashi, K., Kojima, M., Nagato, Y., Sakakibara, H., and Kyojuka, J.** (2007). Direct control of shoot meristem activity by a cytokinin-activating enzyme. *Nature* **445**: 652–5.
- Kuroha, T., Tokunaga, H., Kojima, M., Ueda, N., Ishida, T., Nagawa, S., Fukuda, H., Sugimoto, K., and Sakakibara, H.** (2009). Functional analyses of LONELY GUY cytokinin-activating enzymes reveal the importance of the direct activation pathway in Arabidopsis. *Plant Cell* **21**: 3152–69.
- Larsson, C., Widell, S., and Kjellbom, P.** (1987). Preparation of High-Purity Plasma Membranes. *Methods Enzymol.* **148**: 558–68.
- LeClere, S., Tellez, R., Rampey, R.A., Matsuda, S.P.T., and Bartel, B.** (2002). Characterization of a Family of IAA-Amino Acid Conjugate Hydrolases from Arabidopsis. *J. Biol. Chem.* **277**: 20446–52.
- Lee, H., Ganguly, A., Lee, R.D., Park, M., and Cho, H.-T.** (2020). Intracellularly Localized PIN-FORMED8 Promotes Lateral Root Emergence in Arabidopsis. *Front. Plant Sci.* **0**: 1808.
- Lee, Y.H., Tan, H.T., and Chung, M.C.M.** (2010). Subcellular fractionation methods and strategies for proteomics. *Proteomics* **10**: 3935–56.

- Li, G., Liu, K., Baldwin, S.A., and Wang, D.** (2003). Equilibrative nucleoside transporters of *Arabidopsis thaliana*. cDNA cloning, expression pattern, and analysis of transport activities. *J. Biol. Chem.* **278**: 35732–42.
- Li, J. and Wang, D.** (2000). Cloning and in vitro expression of the cDNA encoding a putative nucleoside transporter from *Arabidopsis thaliana*. *Plant Sci.* **157**: 23–32.
- Ljung, K.** (2013). Auxin metabolism and homeostasis during plant development. *Development* **140**: 943–50.
- Logan, D.C. and Leaver, C.J.** (2000). Mitochondria-targeted GFP highlights the heterogeneity of mitochondrial shape, size and movement within living plant cells. *J. Exp. Bot.* **51**: 865–71.
- Lomin, S.N., Krivosheev, D.M., Steklov, M.Y., Arkhipov, D. V, Osolodkin, D.I., Schmülling, T., and Romanov, G.A.** (2015). Plant membrane assays with cytokinin receptors underpin the unique role of free cytokinin bases as biologically active ligands. *J. Exp. Bot.* **66**: 1851–63.
- Lomin, S.N., Krivosheev, D.M., Steklov, M.Y., Osolodkin, D.I., and Romanov, G.A.** (2012). Receptor properties and features of cytokinin signaling. *Acta Naturae* **4**: 31–45.
- Lomin, S.N., Myakushina, Y.A., Arkhipov, D. V, Leonova, O.G., Popenko, V.I., Schmülling, T., and Romanov, G.A.** (2018). Studies of cytokinin receptor–phosphotransmitter interaction provide evidences for the initiation of cytokinin signalling in the endoplasmic reticulum. *Funct. Plant Biol.* **45**: 192.
- Ludwig-Müller, J.** (2011). Auxin conjugates: their role for plant development and in the evolution of land plants. *J. Exp. Bot.* **62**: 1757–73.
- Ma, S., Quist, T.M., Ulanov, A., Joly, R., and Bohnert, H.J.** (2004). Loss of TIP1;1 aquaporin in *Arabidopsis* leads to cell and plant death. *Plant J.* **40**: 845–59.
- Maeda, H. and Dudareva, N.** (2012). The Shikimate Pathway and Aromatic Amino Acid Biosynthesis in Plants. *Annu. Rev. Plant Biol.* **63**: 73–105.
- Mähönen, A.P., Bishopp, A., Higuchi, M., Nieminen, K.M., Kinoshita, K., Törmäkangas, K., Ikeda, Y., Oka, A., Kakimoto, T., and Helariutta, Y.** (2006). Cytokinin Signaling and Its Inhibitor AHP6 Regulate Cell Fate During Vascular Development. *Science* **311**: 94–8.
- Mähönen, A.P., Bonke, M., Kauppinen, L., Riikonen, M., Benfey, P.N., and Helariutta, Y.** (2000). A novel two-component hybrid molecule regulates vascular morphogenesis of the *Arabidopsis* root. *Genes Dev.* **14**: 2938–43.
- Di Mambro, R. et al.** (2017). Auxin minimum triggers the developmental switch from cell division to cell differentiation in the *Arabidopsis* root. *Proc. Natl. Acad. Sci. U. S. A.* **114**: E7641–9.
- Di Mambro, R. et al.** (2019). The Lateral Root Cap Acts as an Auxin Sink that Controls Meristem Size. *Curr. Biol.* **29**: 1199-205.e4.
- Markham, J.E., Molino, D., Gissot, L., Bellec, Y., Hématy, K., Marion, J., Belcram, K.,**

- Palauqui, J.-C., Satiat-Jeunemaître, B., and Faure, J.-D.** (2011). Sphingolipids containing very-long-chain fatty acids define a secretory pathway for specific polar plasma membrane protein targeting in Arabidopsis. *Plant Cell* **23**: 2362–78.
- Martinière, A., Bassil, E., Jublanc, E., Alcon, C., Reguera, M., Sentenac, H., Blumwald, E., and Paris, N.** (2013). In vivo intracellular pH measurements in tobacco and Arabidopsis reveal an unexpected pH gradient in the endomembrane system. *Plant Cell* **25**: 4028–43.
- Mashiguchi, K. et al.** (2011). The main auxin biosynthesis pathway in Arabidopsis. *Proc. Natl. Acad. Sci. U. S. A.* **108**: 18512–7.
- Mason, M.G., Li, J., Mathews, D.E., Kieber, J.J., and Schaller, G.E.** (2004). Type-B Response Regulators Display Overlapping Expression Patterns in Arabidopsis. *Plant Physiol.* **135**: 927–37.
- Matsushima, R., Hayashi, Y., Kondo, M., Shimada, T., Nishimura, M., and Hara-Nishimura, I.** (2002). An Endoplasmic Reticulum-Derived Structure That Is Induced under Stress Conditions in Arabidopsis. *Plant Physiol.* **130**: 1807–14.
- McKeown, P., Pendle, A.F., and Shaw, P.J.** (2008). Preparation of arabidopsis nuclei and nucleoli. *Methods Mol. Biol.* **463**: 67–75.
- Mellor, N. et al.** (2016). Dynamic regulation of auxin oxidase and conjugating enzymes AtDAO1 and GH3 modulates auxin homeostasis. *Proc. Natl. Acad. Sci. U. S. A.* **113**: 11022–7.
- Miao, Y., Li, K.Y., Li, H.-Y., Yao, X., and Jiang, L.** (2008). The vacuolar transport of aleurain-GFP and 2S albumin-GFP fusions is mediated by the same pre-vacuolar compartments in tobacco BY-2 and Arabidopsis suspension cultured cells. *Plant J.* **56**: 824–39.
- Middleton, A.M. et al.** (2018). Data-Driven Modeling of Intracellular Auxin Fluxes Indicates a Dominant Role of the ER in Controlling Nuclear Auxin Uptake. *Cell Rep.* **22**: 3044–57.
- Miller, C.O., Skoog, F., Okumura, F.S., Von Saltza, M.H., and Strong, F.M.** (1955a). Structure and synthesis of kinetin. *J. Am. Chem. Soc.* **77**: 2662–3.
- Miller, C.O., Skoog, F., Von Saltza, M.H., and Strong, F.M.** (1955b). Kinetin, a cell division factor from deoxyribonucleic acid. *J. Am. Chem. Soc.* **77**: 1392.
- Miyawaki, K., Tarkowski, P., Matsumoto-Kitano, M., Kato, T., Sato, S., Tarkowská, D., Tabata, S., Sandberg, G., and Kakimoto, T.** (2006). Roles of Arabidopsis ATP/ADP isopentenyltransferases and tRNA isopentenyltransferases in cytokinin biosynthesis. *Proc. Natl. Acad. Sci. U. S. A.* **103**: 16598–603.
- Moffatt, B., Pethe, C., and Laloue, M.** (1991). Metabolism of Benzyladenine is Impaired in a Mutant of Arabidopsis thaliana Lacking Adenine Phosphoribosyltransferase Activity. *Plant Physiol* **95**: 900–8.
- Möhlmann, T., Mezher, Z., Schwerdtfeger, G., and Neuhaus, H.E.** (2001). Characterisation of a concentrative type of adenosine transporter from Arabidopsis thaliana (ENT1,At).

FEBS Lett. **509**: 370–4.

- Mok, D.W. and Mok, M.C.** (2001). CYTOKININ METABOLISM AND ACTION. *Annu. Rev. Plant Physiol. Plant Mol. Biol.* **52**: 89–118.
- Mravec, J. et al.** (2009). Subcellular homeostasis of phytohormone auxin is mediated by the ER-localized PIN5 transporter. *Nature* **459**: 1136–40.
- Muñoz, P., Norambuena, L., and Orellana, A.** (1996). Evidence for a UDP-glucose transporter in Golgi apparatus-derived vesicles from pea and its possible role in polysaccharide biosynthesis. *Plant Physiol.* **112**: 1585–94.
- Nedvěd, D., Hošek, P., Klíma, P., and Hoyerová, K.** (2021). Differential Subcellular Distribution of Cytokinins: How Does Membrane Transport Fit into the Big Picture? *Int. J. Mol. Sci.* **22**: 3428.
- Nelson, B.K., Cai, X., and Nebenführ, A.** (2007). A multicolored set of in vivo organelle markers for co-localization studies in Arabidopsis and other plants. *Plant J.* **51**: 1126–36.
- Neuburger, M., Journet, E.P., Bligny, R., Carde, J.P., and Douce, R.** (1982). Purification of plant mitochondria by isopycnic centrifugation in density gradients of Percoll. *Arch. Biochem. Biophys.* **217**: 312–23.
- Niehaus, M., Straube, H., Künzler, P., Rugen, N., Hegermann, J., Giavalisco, P., Eubel, H., Witte, C.P., and Herde, M.** (2020). Rapid Affinity Purification of Tagged Plant Mitochondria (Mito-AP) for Metabolome and Proteome Analyses. *Plant Physiol.* **182**: 1194–210.
- Niemann, M.C.E., Weber, H., Hluska, T., Leonte, G., Anderson, S.M., Novák, O., Senes, A., and Werner, T.** (2018). The cytokinin oxidase/dehydrogenase CKX1 is a membrane-bound protein requiring homooligomerization in the endoplasmic reticulum for its cellular activity. *Plant Physiol.* **176**: 2024–39.
- Normanly, J., Cohen, J.D., and Fink, G.R.** (1993). Arabidopsis thaliana auxotrophs reveal a tryptophan-independent biosynthetic pathway for indole-3-acetic acid. *Proc. Natl. Acad. Sci. U. S. A.* **90**: 10355–9.
- Novák, O., Hényková, E., Sairanen, I., Kowalczyk, M., Pospíšil, T., and Ljung, K.** (2012). Tissue-specific profiling of the Arabidopsis thaliana auxin metabolome. *Plant J.* **72**: 523–36.
- Novák, O., Napier, R., and Ljung, K.** (2017). Zooming In on Plant Hormone Analysis: Tissue- and Cell-Specific Approaches. *Annu. Rev. Plant Biol.* **68**: 323–48.
- Nováková, L.** (2013). Challenges in the development of bioanalytical liquid chromatography–mass spectrometry method with emphasis on fast analysis. *J. Chromatogr. A* **1292**: 25–37.
- Okekeogbu, I.O., Aryal, U.K., Fernández-Niño, S.M.G., Penning, B.W., Heazlewood, J.L., McCann, M.C., and Carpita, N.C.** (2019). Differential distributions of trafficking and

- signaling proteins of the maize ER-Golgi apparatus. *Plant Signal. Behav.* **14**: 1672513.
- Osugi, A., Kojima, M., Takebayashi, Y., Ueda, N., Kiba, T., and Sakakibara, H.** (2017). Systemic transport of trans-zeatin and its precursor have differing roles in Arabidopsis shoots. *Nat. Plants* **3**: 17112.
- Pačes, V., Werstiuk, E., and Hall, R.H.** (1971). Conversion of N-(Delta-Isopentenyl)adenosine to Adenosine by Enzyme Activity in Tobacco Tissue. *Plant Physiol.* **48**: 775–8.
- Parkinson, J.S. and Kofoed, E.C.** (1992). Communication Modules in Bacterial Signaling Proteins. *Prospects* **26**: 71–112.
- Parsons, H.T. et al.** (2012). Isolation and Proteomic Characterization of the Arabidopsis Golgi Defines Functional and Novel Components Involved in Plant Cell Wall Biosynthesis. *Plant Physiol.* **159**: 12–26.
- Peer, W.A., Blakeslee, J.J., Yang, H., and Murphy, A.S.** (2011). Seven Things We Think We Know about Auxin Transport. *Mol. Plant* **4**: 487–504.
- Pěňčík, A. et al.** (2013). Regulation of auxin homeostasis and gradients in Arabidopsis roots through the formation of the indole-3-acetic acid catabolite 2-oxindole-3-acetic acid. *Plant Cell* **25**: 3858–70.
- Pěňčík, A., Casanova-Sáez, R., Pilařová, V., Žukauskaitė, A., Pinto, R., Luis Micol, J., Ljung, K., and Novák, O.** (2018). Ultra-rapid auxin metabolite profiling for high-throughput mutant screening in Arabidopsis. *J. Exp. Bot.* **69**: 2569–79.
- Pěňčík, A., Rolčík, J., Novák, O., Magnus, V., Barták, P., Buchtík, R., Salopek-Sondi, B., and Strnad, M.** (2009). Isolation of novel indole-3-acetic acid conjugates by immunoaffinity extraction. *Talanta* **80**: 651–5.
- Péret, B. et al.** (2012). AUX/LAX genes encode a family of auxin influx transporters that perform distinct functions during Arabidopsis development. *Plant Cell* **24**: 2874–85.
- Peterson, S. V., Johansson, A.I., Kowalczyk, M., Makoveychuk, A., Wang, J.Y., Moritz, T., Grebe, M., Benfey, P.N., Sandberg, G., and Ljung, K.** (2009). An Auxin Gradient and Maximum in the Arabidopsis Root Apex Shown by High-Resolution Cell-Specific Analysis of IAA Distribution and Synthesis. *Plant Cell* **21**: 1659–68.
- Peterson, S. V., Lindén, P., Moritz, T., and Ljung, K.** (2015). Cell-type specific metabolic profiling of Arabidopsis thaliana protoplasts as a tool for plant systems biology. *Metabolomics* **11**: 1679–89.
- Petricka, J.J., Schauer, M.A., Megraw, M., Breakfield, N.W., Thompson, J.W., Georgiev, S., Soderblom, E.J., Ohler, U., Moseley, M.A., Grossniklaus, U., and Benfey, P.N.** (2012). The protein expression landscape of the Arabidopsis root. *Proc. Natl. Acad. Sci. U. S. A.* **109**: 6811–8.
- Petrovská, B., Jeřábková, H., Chamrád, I., Vrána, J., Lenobel, R., Uřinová, J., Šebela, M., and Doležel, J.** (2014). Proteomic analysis of barley cell nuclei purified by flow sorting.

Cytogenet. Genome Res. **143**: 78–86.

- Polanská, L., Vičánková, A., Nováková, M., Malbeck, J., Dobrev, P.I., Brzobohatý, B., Vaňková, R., and Macháčková, I.** (2007). Altered cytokinin metabolism affects cytokinin, auxin, and abscisic acid contents in leaves and chloroplasts, and chloroplast ultrastructure in transgenic tobacco. *J. Exp. Bot.* **58**: 637–49.
- Porco, S. et al.** (2016). Dioxygenase-encoding AtDAO1 gene controls IAA oxidation and homeostasis in Arabidopsis. *Proc. Natl. Acad. Sci. U. S. A.* **113**: 11016–21.
- Powers, S.K. and Strader, L.C.** (2016). Up in the air: Untethered Factors of Auxin Response. *F1000Research* **5**: 133.
- Punwani, J.A., Hutchison, C.E., Schaller, G.E., and Kieber, J.J.** (2010). The subcellular distribution of the Arabidopsis histidine phosphotransfer proteins is independent of cytokinin signaling. *Plant J.* **62**: 473–82.
- Qin, G., Gu, H., Zhao, Y., Ma, Z., Shi, G., Yang, Y., Pichersky, E., Chen, H., Liu, M., Chen, Z., and Qu, L.-J.** (2005). An Indole-3-Acetic Acid Carboxyl Methyltransferase Regulates Arabidopsis Leaf Development. *Plant Cell* **17**: 2693–704.
- Ranocha, P. et al.** (2013). Arabidopsis WAT1 is a vacuolar auxin transport facilitator required for auxin homeostasis. *Nat. Commun.* **4**: 2625.
- Rashotte, A.M., Carson, S.D.B., To, J.P.C., and Kieber, J.J.** (2003). Expression profiling of cytokinin action in Arabidopsis. *Plant Physiol.* **132**: 1998–2011.
- Reumann, S. and Lisik, P.** (2017). Isolation of Arabidopsis leaf peroxisomes and the peroxisomal membrane. *Methods Mol. Biol.* **1511**: 97–112.
- Robert, S., Zouhar, J., Carter, C.J., and Raikhel, N.** (2007). Isolation of intact vacuoles from Arabidopsis rosette leaf-derived protoplasts. *Nat. Protoc.* **2**: 259–62.
- Robinson, J.P. and Grégori, G.** (2007). Principles of Flow Cytometry. In *Flow Cytometry with Plant Cells*, J. Doležel, J. Greilhuber, and J. Suda, eds (John Wiley & Sons, Ltd: Weinheim, Germany), pp. 19–40.
- Rodrigues, J.M.P., Pereira, C.S., Fontes, N., Gerós, H., and Côte-Real, M.** (2018). Flow Cytometry and Fluorescence Microscopy as Tools for Structural and Functional Analysis of Vacuoles Isolated from Yeast and Plant Cells. *Methods Mol. Biol.* **1789**: 101–15.
- Romanov, G.A., Lomin, S.N., and Schmölling, T.** (2006). Biochemical characteristics and ligand-binding properties of Arabidopsis cytokinin receptor AHK3 compared to CRE1/AHK4 as revealed by a direct binding assay. *J. Exp. Bot.* **57**: 4051–8.
- Romanov, G.A., Spíchal, L., Lomin, S.N., Strnad, M., and Schmölling, T.** (2005). A live cell hormone-binding assay on transgenic bacteria expressing a eukaryotic receptor protein. *Anal. Biochem.* **347**: 129–34.
- Šafář, J., Noa-Carrizana, J.C., Vrána, J., Bartoš, J., Alkhimova, O., Sabau, X., Šimková, H., Lheureux, F., Caruana, M.-L., Doležel, J., and Piffanelli, P.** (2004). Creation of a BAC

- resource to study the structure and evolution of the banana (*Musa balbisiana*) genome. *Genome* **47**: 1182–91.
- Sanchez Carranza, A.P., Singh, A., Steinberger, K., Panigrahi, K., Palme, K., Dovzhenko, A., and Dal Bosco, C.** (2016). Hydrolases of the ILR1-like family of *Arabidopsis thaliana* modulate auxin response by regulating auxin homeostasis in the endoplasmic reticulum. *Sci. Rep.* **6**: 24212.
- Sandberg, G., Gardeström, P., Sitbon, F., and Olsson, O.** (1990). Presence of indole-3-acetic acid in chloroplasts of *Nicotiana tabacum* and *Pinus sylvestris*. *Planta* **180**: 562–8.
- Saunders, J.A.** (1979). Investigations of vacuoles isolated from tobacco: I. Quantitation of nicotine. *Plant Physiol.* **64**: 74–8.
- Saxena, P.K., Fowke, L.C., and King, J.** (1985). An efficient procedure for isolation of nuclei from plant protoplasts. *Protoplasma* **128**: 184–9.
- Schaller, G.E., Bishopp, A., and Kieber, J.J.** (2015). The yin-yang of hormones: cytokinin and auxin interactions in plant development. *Plant Cell* **27**: 44–63.
- Schmülling, T., Werner, T., Riefler, M., Krupková, E., and Bartrina y Manns, I.** (2003). Structure and function of cytokinin oxidase/dehydrogenase genes of maize, rice, *Arabidopsis* and other species. *J. Plant Res.* **116**: 241–52.
- Schulz, A., Knoetzel, J., Scheller, H. V, and Mant, A.** (2004). Uptake of a fluorescent dye as a swift and simple indicator of organelle intactness: import-competent chloroplasts from soil-grown *Arabidopsis*. *J. Histochem. Cytochem.* **52**: 701–4.
- Seigneurin-Berny, D., Salvi, D., Dorne, A.-J., Joyard, J., and Rolland, N.** (2008). Percoll-purified and photosynthetically active chloroplasts from *Arabidopsis thaliana* leaves. *Plant Physiol. Biochem.* **46**: 951–5.
- Shimaoka, T., Ohnishi, M., Sazuka, T., Mitsuhashi, N., Hara-Nishimura, I., Shimazaki, K.-I., Maeshima, M., Yokota, A., Tomizawa, K.-I., and Mimura, T.** (2004). Isolation of intact vacuoles and proteomic analysis of tonoplast from suspension-cultured cells of *Arabidopsis thaliana*. *Plant Cell Physiol.* **45**: 672–83.
- Šimášková, M. et al.** (2015). Cytokinin response factors regulate PIN-FORMED auxin transporters. *Nat. Commun.* **6**: 8717.
- Šimková, H., Číhalíková, J., Vrána, J., Lysák, M.A., and Doležel, J.** (2003). Preparation of HMW DNA from plant nuclei and chromosomes isolated from root tips. *Biol. Plant.* **46**: 369–73.
- Simon, S. et al.** (2016). PIN6 auxin transporter at endoplasmic reticulum and plasma membrane mediates auxin homeostasis and organogenesis in *Arabidopsis*. *New Phytol.* **211**: 65–74.
- Simon, S. and Petrášek, J.** (2011). Why plants need more than one type of auxin. *Plant Sci.* **180**: 454–60.
- Šimura, J., Antoniadi, I., Šíroká, J., Tarkowská, D., Strnad, M., Ljung, K., and Novák, O.**

- (2018). Plant Hormonomics: Multiple Phytohormone Profiling by Targeted Metabolomics. *Plant Physiol.* **177**: 476–89.
- Skalický, V., Kubeš, M., Napier, R., and Novák, O.** (2018). Auxins and Cytokinins-The Role of Subcellular Organization on Homeostasis. *Int. J. Mol. Sci.* **19**: 3115.
- Šmehilová, M., Dobrušková, J., Novák, O., Takáč, T., and Galuszka, P.** (2016). Cytokinin-Specific Glycosyltransferases Possess Different Roles in Cytokinin Homeostasis Maintenance. *Front. Plant Sci.* **7**: 1264.
- Somerville, C.R., Somerville, S.C., and Ogren, W.L.** (1981). Isolation of photosynthetically active protoplasts and chloroplasts from *Arabidopsis thaliana*. *Plant Sci. Lett.* **21**: 89–96.
- Song, Y. et al.** (2006). Sample preparation project for the subcellular proteome of mouse liver. *Proteomics* **6**: 5269–77.
- Spíchal, L., Rakova, N.Y., Riefler, M., Mizuno, T., Romanov, G.A., Strnad, M., and Schmülling, T.** (2004). Two cytokinin receptors of *Arabidopsis thaliana*, CRE1/AHK4 and AHK3, differ in their ligand specificity in a bacterial assay. *Plant Cell Physiol.* **45**: 1299–305.
- Staswick, P.E., Serban, B., Rowe, M., Tiryaki, I., Maldonado, M.T., Maldonado, M.C., and Suza, W.** (2005). Characterization of an *Arabidopsis* Enzyme Family That Conjugates Amino Acids to Indole-3-Acetic Acid. *Plant Cell* **17**: 616–27.
- Stepanova, A.N., Robertson-Hoyt, J., Yun, J., Benavente, L.M., Xie, D.Y., Doležal, K., Schlereth, A., Jürgens, G., and Alonso, J.M.** (2008). TAA1-mediated auxin biosynthesis is essential for hormone crosstalk and plant development. *Cell* **133**: 177–91.
- Stepanova, A.N., Yun, J., Robles, L.M., Novák, O., He, W., Guo, H., Ljung, K., and Alonso, J.M.** (2011). The *Arabidopsis* YUCCA1 flavin monooxygenase functions in the indole-3-pyruvic acid branch of auxin biosynthesis. *Plant Cell* **23**: 3961–73.
- Stolz, A., Riefler, M., Lomin, S.N., Achazi, K., Romanov, G.A., and Schmülling, T.** (2011). The specificity of cytokinin signalling in *Arabidopsis thaliana* is mediated by differing ligand affinities and expression profiles of the receptors. *Plant J.* **67**: 157–68.
- Strnad, M.** (1997). The aromatic cytokinins. *Physiol. Plant.* **101**: 674–88.
- Sun, J., Hirose, N., Wang, X., Wen, P., Xue, L., Sakakibara, H., and Zuo, J.** (2005). *Arabidopsis* SOI33/AtENT8 Gene Encodes a Putative Equilibrative Nucleoside Transporter That Is Involved in Cytokinin Transport In Planta. *J. Integr. Plant Biol.* **47**: 588–603.
- Suzuki, T., Miwa, K., Ishikawa, K., Yamada, H., Aiba, H., and Mizuno, T.** (2001). The *Arabidopsis* sensor His-kinase, AHk4, can respond to cytokinins. *Plant Cell Physiol.* **42**: 107–13.
- Suzuki, T., Sakurai, K., Imamura, A., Nakamura, A., Ueguchi, C., and Mizuno, T.** (2000). Compilation and characterization of histidine-containing phosphotransmitters

- implicated in His-to-Asp phosphorelay in plants: AHP signal transducers of *Arabidopsis thaliana*. *Biosci. Biotechnol. Biochem.* **64**: 2486–9.
- Svačinová, J., Novák, O., Plačková, L., Lenobel, R., Holík, J., Strnad, M., and Doležal, K.** (2012). A new approach for cytokinin isolation from *Arabidopsis* tissues using miniaturized purification: pipette tip solid-phase extraction. *Plant Methods* **8**: 17.
- Swarup, R., Friml, J., Marchant, A., Ljung, K., Sandberg, G., Palme, K., and Bennett, M.** (2001). Localization of the auxin permease AUX1 suggests two functionally distinct hormone transport pathways operate in the *Arabidopsis* root apex. *Genes Dev.* **15**: 2648–53.
- Takei, K., Sakakibara, H., and Sugiyama, T.** (2001). Identification of Genes Encoding Adenylate Isopentenyltransferase, a Cytokinin Biosynthesis Enzyme, in *Arabidopsis thaliana*. *J. Biol. Chem.* **276**: 26405–10.
- Takei, K., Yamaya, T., and Sakakibara, H.** (2004). *Arabidopsis* CYP735A1 and CYP735A2 encode cytokinin hydroxylases that catalyse the biosynthesis of trans-Zeatin. *J. Biol. Chem.* **279**: 41866–72.
- Tanaka, H., Dhonukshe, P., Brewer, P.B., and Friml, J.** (2006). Spatiotemporal asymmetric auxin distribution: A means to coordinate plant development. *Cell. Mol. Life Sci.* **63**: 2738–54.
- Tanaka, K., Hayashi, K., Natsume, M., Kamiya, Y., Sakakibara, H., Kawaide, H., and Kasahara, H.** (2014). UGT74D1 catalyzes the glucosylation of 2-oxindole-3-acetic acid in the auxin metabolic pathway in *Arabidopsis*. *Plant Cell Physiol.* **55**: 218–28.
- Tao, Y. et al.** (2008). Rapid synthesis of auxin via a new tryptophan-dependent pathway is required for shade avoidance in plants. *Cell* **133**: 164–76.
- Tarkowská, D., Novák, O., Floková, K., Tarkowski, P., Turečková, V., Grúz, J., Rolčík, J., and Strnad, M.** (2014). Quo vadis plant hormone analysis? *Planta* **240**: 55–76.
- Taya, Y., Tanaka, Y., and Nishimura, S.** (1978). 5'-AMP is a direct precursor of cytokinin in *Dictyostelium discoideum*. *Nature* **271**: 545–7.
- Temsch, E.M., Koutecký, P., Urfus, T., Šmarda, P., and Doležal, J.** (2021). Reference standards for flow cytometric estimation of absolute nuclear DNA content in plants. *Cytom. Part A: cyto.a.24495*
- Tessi, T.M., Brumm, S., Winklbauer, E., Schumacher, B., Pettinari, G., Lescano, I., González, C.A., Wanke, D., Maurino, V.G., Harter, K., and Desimone, M.** (2021). *Arabidopsis* AZG2 transports cytokinins in vivo and regulates lateral root emergence. *New Phytol.* **229**: 979–93.
- Thibivilliers, S., Anderson, D., and Libault, M.** (2020). Isolation of Plant Root Nuclei for Single Cell RNA Sequencing. *Curr. Protoc. Plant Biol.* **5**: e20120.
- Thomas, J.C. and Katterman, F.R.** (1986). Cytokinin Activity Induced by Thidiazuron. *Plant Physiol.* **81**: 681–3.

- Tian, H., Klambt, D., and Jones, A.M.** (1995). Auxin-binding Protein 1 Does Not Bind Auxin within the Endoplasmic Reticulum Despite This Being the Predominant Subcellular Location for This Hormone Receptor. *J. Biol. Chem.* **270**: 26962–9.
- To, J.P.C., Haberer, G., Ferreira, F.J., Deruère, J., Mason, M.G., Schaller, G.E., Alonso, J.M., Ecker, J.R., and Kieber, J.J.** (2004). Type-A Arabidopsis Response Regulators Are Partially Redundant Negative Regulators of Cytokinin Signaling. *Plant Cell* **16**: 658–71.
- Ueguchi, C., Koizumi, H., Suzuki, T., and Mizuno, T.** (2001). Novel family of sensor histidine kinase genes in *Arabidopsis thaliana*. *Plant Cell Physiol* **42**: 231–5.
- Vanneste, S. and Friml, J.** (2009). Auxin: a trigger for change in plant development. *Cell* **136**: 1005–16.
- Včelařová, L., Skalický, V., Chamrád, I., Lenobel, R., Kubeš, M., Pěňčík, A., and Novák, O.** (2021). Auxin Metabolome Profiling in the Arabidopsis Endoplasmic Reticulum Using an Optimised Organelle Isolation Protocol. *Int. J. Mol. Sci.* **22**: 9370.
- Verma, V., Sivaraman, J., Srivastava, A.K., Sadanandom, A., and Kumar, P.P.** (2015). Destabilization of interaction between cytokinin signaling intermediates AHP1 and ARR4 modulates Arabidopsis development. *New Phytol.* **206**: 726–37.
- Vernoux, T. et al.** (2011). The auxin signalling network translates dynamic input into robust patterning at the shoot apex. *Mol. Syst. Biol.* **7**: 508.
- Vertommen, A., Panis, B., Swennen, R., and Carpentier, S.C.** (2011). Challenges and solutions for the identification of membrane proteins in non-model plants. *J. Proteomics* **74**: 1165–81.
- Vieten, A., Sauer, M., Brewer, P.B., and Friml, J.** (2007). Molecular and cellular aspects of auxin-transport-mediated development. *Trends Plant Sci.* **12**: 160–8.
- Viotti, C. et al.** (2013). The Endoplasmic Reticulum Is the Main Membrane Source for Biogenesis of the Lytic Vacuole in Arabidopsis. *Plant Cell* **25**: 3434–49.
- Vreman, H.J., Schmitz, R.Y., Skoog, F., Playtis, A.J., Frihart, C.R., and Leonard, N.J.** (1974). Synthesis of 2-methylthio-cis- and trans-ribosylzeatin and their isolation from *Pisum* tRNA. *Phytochemistry* **13**: 31–7.
- Wang, B., Chu, J., Yu, T., Xu, Q., Sun, X., Yuan, J., Xiong, G., Wang, G., Wang, Y., and Li, J.** (2015). Tryptophan-independent auxin biosynthesis contributes to early embryogenesis in Arabidopsis. *Proc. Natl. Acad. Sci. U. S. A.* **112**: 4821–6.
- Werner, T., Köllmer, I., Bartrina y Manns, I., Holst, K., and Schmölling, T.** (2006). New insights into the biology of cytokinin degradation. *Plant Biol. (Stuttg.)* **8**: 371–81.
- Werner, T., Motyka, V., Laucou, V., Smets, R., Van Onckelen, H.A., and Schmölling, T.** (2003). Cytokinin-deficient transgenic Arabidopsis plants show multiple developmental alterations indicating opposite functions of cytokinins in the regulation of shoot and root meristem activity. *Plant Cell* **15**: 2532–50.
- Wilkop, T., Pattathil, S., Ren, G., Davis, D.J., Bao, W., Duan, D., Peralta, A.G., Domozych,**

- D.S., Hahn, M.G., and Drakakaki, G.** (2019). A hybrid approach enabling large-scale glycomic analysis of post-golgi vesicles reveals a transport route for polysaccharides. *Plant Cell* **31**: 627–44.
- Wolanin, P.M., Thomason, P.A., and Stock, J.B.** (2002). Histidine protein kinases: key signal transducers outside the animal kingdom. *Genome Biol.* **3**: REVIEWS3013.
- Wolf, P.G., Karol, K.G., Mandoli, D.F., Kuehl, J., Arumuganathan, K., Ellis, M.W., Mishler, B.D., Kelch, D.G., Olmstead, R.G., and Boore, J.L.** (2005). The first complete chloroplast genome sequence of a lycophyte, *Huperzia lucidula* (Lycopodiaceae). *GENE* **350**: 117–28.
- Wormit, A., Traub, M., Flörchinger, M., Neuhaus, H.E., and Möhlmann, T.** (2004). Characterization of three novel members of the *Arabidopsis thaliana* equilibrative nucleoside transporter (ENT) family. *Biochem. J.* **383**: 19–26.
- Wright, A.D., Sampson, M.B., Neuffer, M.G., Michalczuk, L., Slovin, J.P., and Cohen, J.D.** (1991). Indole-3-acetic acid biosynthesis in the mutant maize orange pericarp, a tryptophan auxotroph. *Science* **254**: 998–1000.
- Wulfetange, K., Lomin, S.N., Romanov, G.A., Stolz, A., Heyl, A., and Schmülling, T.** (2011). The cytokinin receptors of *Arabidopsis* are located mainly to the endoplasmic reticulum. *Plant Physiol.* **156**: 1808–18.
- Yadav, R.K., Girke, T., Pasala, S., Xie, M., and Reddy, G.V.** (2009). Gene expression map of the *Arabidopsis* shoot apical meristem stem cell niche. *Proc. Natl. Acad. Sci. U. S. A.* **106**: 4941–6.
- Yamada, H., Suzuki, T., Terada, K., Takeji, K., Ishikawa, K., Miwa, K., Yamashino, T., and Mizuno, T.** (2001). The *Arabidopsis* AHK4 histidine kinase is a cytokinin-binding receptor that transduces cytokinin signals across the membrane. *Plant Cell Physiol.* **42**: 1017–23.
- Yang, H. and Murphy, A.S.** (2009). Functional expression and characterization of *Arabidopsis* ABCB, AUX 1 and PIN auxin transporters in *Schizosaccharomyces pombe*. *Plant J.* **59**: 179–91.
- Yang, Y., Xu, R., Ma, C., Vlot, A.C., Klessig, D.F., and Pichersky, E.** (2008). Inactive Methyl Indole-3-Acetic Acid Ester Can Be Hydrolyzed and Activated by Several Esterases Belonging to the AtMES Esterase Family of *Arabidopsis*. *Plant Physiol.* **147**: 1034–45.
- Yao, N., Eisfelder, B.J., Marvin, J., and Greenberg, J.T.** (2004). The mitochondrion—an organelle commonly involved in programmed cell death in *Arabidopsis thaliana*. *Plant J.* **40**: 596–610.
- Yonekura-Sakakibara, K., Kojima, M., Yamaya, T., and Sakakibara, H.** (2004). Molecular characterization of cytokinin-responsive histidine kinases in maize. Differential ligand preferences and response to cis-zeatin. *Plant Physiol.* **134**: 1654–61.
- Yoo, S.-D., Cho, Y.-H., and Sheen, J.** (2007). *Arabidopsis* mesophyll protoplasts: a versatile cell system for transient gene expression analysis. *Nat. Protoc.* **2**: 1565–72.

- Zalabák, D., Pospíšilová, H., Šmehilová, M., Mrízová, K., Frébort, I., and Galuszka, P.** (2013). Genetic engineering of cytokinin metabolism: prospective way to improve agricultural traits of crop plants. *Biotechnol. Adv.* **31**: 97–117.
- Zhang, H.-B., Zhao, X., Ding, X., Paterson, A.H., and Wing, R.A.** (1995). Preparation of megabase-size DNA from plant nuclei. *Plant J.* **7**: 175–84.
- Zhang, J., Lin, J.E., Harris, C., Campos Mastrotti Pereira, F., Wu, F., Blakeslee, J.J., and Peer, W.A.** (2016). DAO1 catalyzes temporal and tissue-specific oxidative inactivation of auxin in *Arabidopsis thaliana*. *Proc. Natl. Acad. Sci. U. S. A.* **113**: 11010–5.
- Zhang, K., Novák, O., Wei, Z., Gou, M., Zhang, X., Yu, Y., Yang, H., Cai, Y., Strnad, M., and Liu, C.-J.** (2014). *Arabidopsis* ABCG14 protein controls the acropetal translocation of root-synthesized cytokinins. *Nat. Commun.* **5**: 3274.
- Zhang, R., Wang, B., Ouyang, J., Li, J., and Wang, Y.** (2008). *Arabidopsis* Indole Synthase, a Homolog of Tryptophan Synthase Alpha, is an Enzyme Involved in the Trp-independent Indole-containing Metabolite Biosynthesis. *J. Integr. Plant Biol.* **50**: 1070–7.
- Zhang, X., Chen, Y., Lin, X., Hong, X., Zhu, Y., Li, W., He, W., An, F., and Guo, H.** (2013). Adenine phosphoribosyl transferase 1 is a key enzyme catalyzing cytokinin conversion from nucleobases to nucleotides in *Arabidopsis*. *Mol. Plant* **6**: 1661–72.
- Zolman, B.K., Martinez, N., Millius, A., Adham, A.R., and Bartel, B.** (2008). Identification and characterization of *Arabidopsis* indole-3-butyric acid response mutants defective in novel peroxisomal enzymes. *Genetics* **180**: 237–51.
- Zürcher, E., Liu, J., di Donato, M., Geisler, M., and Müller, B.** (2016). Plant development regulated by cytokinin sinks. *Science* **353**: 1027–30.
- Zürcher, E. and Müller, B.** (2016). Cytokinin Synthesis, Signaling, and Function-Advances and New Insights. In *International Review of Cell and Molecular Biology*, K.W. Jeon, ed (Academic Press Inc. Elsevier Science: Amsterdam, Netherlands), pp. 1–38.

8 Supplements I – VI

Supplement I

Skalický V¹, Kubeš M¹, Napier R, Novák O. (2018) Auxins and cytokinins—the role of subcellular organization on homeostasis. *Int. J. Mol. Sci.* **19** (10), 3115.

Supplement II

Galbraith D, Loureiro J, Antoniadi I, Bainard J, Bureš P, Cápál P, Castro M, Castro S, Čertner M, Čertnerová D, Chumová Z, Doležel J, Giorgi D, Husband BC, Kolář F, Koutecký P, Kron P, Leitch IJ, Ljung K, Lopes S, Lučanová M, Lucretti S, Ma W, Melzer S, Molnár I, Novák O, Poulton N, **Skalický V**, Sliwinska E, Šmarda P, Smith TW, Sun G, Talhinhos P, Tárnok A, Temsch EM, Trávníček P, Urfus T. (2021) Best practices in plant cytometry. *Cytometry A.* **99** (4), 311-317.

Supplement III

Antoniadi I, **Skalický V**, Sun G, Ma W, Galbraith DW, Novák O, Ljung K. (2021) Fluorescence Activated Cell Sorting – A selective tool for plant cell isolation and analysis. *Cytometry A.* **99** (Online ahead of print) doi: 10.1002/cyto.a.24461.

Supplement IV

Včelařová L¹, **Skalický V¹**, Chamrád I, Lenobel R, Kubeš FM, Pěňčík A, Novák O. (2021) Auxin metabolome profiling in the Arabidopsis endoplasmic reticulum using an optimised organelle isolation protocol. *Int. J. Mol. Sci.* **22** (17), 9370.

Supplement V

Skalický V, Vojtková T, Pěňčík A, Vrána J, Katarzyna J, Koláčková V, Sedlářová M, Napier R, Kubeš MF, Novák O. (2021) Auxin profiling in isolated intact plant nuclei. *Int. J. Mol. Sci.* (submitted).

Supplement VI

Skalický V¹, Antoniadi I¹, Pěňčík A, Chamrád I, Lenobel R, Kubeš FM, Strnad M, Ljung K, Novák O. (2021) Fluorescence-activated multi-organelle sorting: A smart tool for subcellular mapping of auxins and cytokinins. (in preparation).



Review

Auxins and Cytokinins—The Role of Subcellular Organization on Homeostasis

Vladimír Skalický^{1,†} , Martin Kubeš^{2,3,†}, Richard Napier³ and Ondřej Novák^{1,*}

¹ Laboratory of Growth Regulators, Centre of the Region Haná for Biotechnological and Agricultural Research, Institute of Experimental Botany of the Czech Academy of Sciences & Faculty of Science of Palacký University, Šlechtitelů 27, 78371 Olomouc, Czech Republic; vladimir.skalicky@upol.cz

² Department of Chemical Biology and Genetics, Centre of the Region Haná for Biotechnological and Agricultural Research, Faculty of Science of Palacký University, Šlechtitelů 27, 78371 Olomouc, Czech Republic; martin.kubes@upol.cz

³ School of Life Sciences, University of Warwick, Coventry CV4 7AL, UK; richard.napier@warwick.ac.uk

* Correspondence: novako@ueb.cas.cz; Tel.: +420-585-634-853

† These authors contributed equally to this work.

Received: 12 September 2018; Accepted: 9 October 2018; Published: 11 October 2018



Abstract: Plant hormones are master regulators of plant growth and development. Better knowledge of their spatial signaling and homeostasis (transport and metabolism) on the lowest structural levels (cellular and subcellular) is therefore crucial to a better understanding of developmental processes in plants. Recent progress in phytohormone analysis at the cellular and subcellular levels has greatly improved the effectiveness of isolation protocols and the sensitivity of analytical methods. This review is mainly focused on homeostasis of two plant hormone groups, auxins and cytokinins. It will summarize and discuss their tissue- and cell-type specific distributions at the cellular and subcellular levels.

Keywords: auxin; cytokinin; phytohormone metabolism; phytohormone transport; cellular level; subcellular level

1. Introduction

The most well-documented groups of plant hormones are auxins and cytokinins (CKs) (Figure A1) with reasonably well-described signaling, transport, and metabolism (biosynthesis, conjugation, and degradation). Moreover, mutual auxin–cytokinin regulation and/or crosstalk appear to control many developmental processes in plants [1]. Since the 1950s, both CKs and auxins have been known for their ability to effectively determine the type of organs regenerated *in vitro* from undifferentiated callus cultures [2]. High auxin-to-CK ratios stimulate root formation, whereas low ratios promote shoot formation. Müller and Sheen [3] showed that antagonism between CK and auxin is primarily realized at the molecular level and is important for specifying root stem cells during early embryogenesis. Moreover, recent transcriptomic data have shown that meristems reform in positions determined by antagonistic auxin and CK signaling domains during tissue repair [4]. On the other hand, synergistic effects of auxins and CKs have also been reported, an example being shoot apical meristem formation [5,6].

The importance of phytohormone homeostasis at the cellular level has become more prominent with the increasing sensitivity of analytical tools [7]. It is generally accepted that compartmentation is a key feature of eukaryotic cells. Plant cells contain admirably complex, albeit well-organized membrane systems dividing them into organelles or compartments. This partition provides possibilities to create appropriate microenvironments and conditions for specialized metabolic pathways. Thus, unique sets of enzymes, transporters, and other proteins are found separated into organelles.

Current advances in indirect or direct visualization methods and other sensitive analytical techniques enable us to visualize phytohormone distributions in vivo at the cellular and subcellular levels. In this review, the authors have connected homeostasis (transport and metabolism) of auxins and CKs with their tissue- and cell-type specific distributions at the cellular and subcellular levels. They are convinced that this topic will open completely new horizons in understanding how the balance of plant hormones is created and controlled.

2. Organelle-Specific Phytohormone Profiling

Analytical methods for quantitation of auxins and CKs have become increasingly sensitive and capable of discriminating not only the free hormones, but also many of their precursors, metabolites, and catabolites [7,8]. Nevertheless, at the subcellular level, organelle-specific phytohormone profiling is challenging and many factors need to be optimized, such as (i) leakage during isolation; (ii) purity of isolated compartments; and (iii) dynamic metabolic changes during isolation.

2.1. Subcellular Fractionation

The original idea of separating intracellular compartments to study the partition of enzyme processes was developed by De Duve and co-workers in the 1950s [9]. Methods of organelle isolation are mainly based on differential centrifugation or density gradient ultracentrifugation [10–14]. Even the simplest differential centrifugation can provide enriched fractions of crude organelles [15,16]. Higher purity organelle fractions can be achieved by density gradient ultracentrifugation yielding fractions enriched in endoplasmic reticulum (ER) [14], Golgi apparatus [17], vacuoles [11], mitochondria [16], and chloroplasts [12,18].

Alternative methods for compartment separation have been also described, for example, two-phase partitioning [19] and non-aqueous or aqueous fractionation [20,21]. Techniques such as flow cytometry can be used for more rapid sorting of organelles labelled by fluorescent probes, for example, nuclei [22], chloroplasts [23], and mitochondria [24]. Affinity capture or pull down by magnetic microparticles has been also used for isolating nuclei [25] or mitochondria [26].

2.2. Phytohormone Profiling in Organelles

Currently, there are only few reports dealing with the determination of phytohormones in live-cell systems [7]. In addition, little is known about extra- and intracellular phytohormone distribution, or the phytohormone levels in individual cell compartments. Indole-3-acetic acid (IAA) has been determined in chloroplasts and mitochondria [27], whereas CKs, IAA, and abscisic acid concentrations have been determined in chloroplasts [28,29] (Table 1). The full profile of IAA and its metabolites has been described in wild-type *Arabidopsis thaliana* vacuoles [30] with determinations providing, for example, clear functional evidence of the vacuolar auxin transport protein WALLS ARE THIN 1 (WAT1) (Figure 1).

Profiling of CK metabolites at the subcellular level has been performed in both *Arabidopsis* and barley (*Hordeum vulgare*) [31]. Concentrations of 25 CK metabolites were determined from isolated apoplast, cytosol, and vacuoles (Table 1). Surprisingly, the highest proportion of CKs was located outside the cell (up to 90%, with a majority as *O*- and *N*-glucosides), and only about 10% was present in cytosol and vacuoles. In transgenic barley expressing the cytokinin oxidase gene *AtCKX1*, severe decreases in extracellular *trans*-zeatin (*tZ*) and *tZ*-7-glucoside (*tZ7G*) were accompanied by compensatory increases of isopentenyladenine (*iP*) and vacuolar isopentenyladenosine (*iPR*).

All these practical examples indicate that a far richer picture can be drawn of phytohormone homeostasis and fluxes with higher resolution data, but hormone profiling and quantitation remain challenging at the resolution required for reliable data about subcellular compartmentation.

Table 1. Auxin and cytokinin (CK) profiles at the subcellular level. Compounds are ordered according to their abundance in particular organelles. Abbreviations of auxins and CKs are listed in Figure A1.

Organelles (Species ¹)	Auxins	Cytokinins	Reference
Chloroplasts (<i>Nicotiana tabacum</i>)	Precursors (n.a. ²) Active compounds (IAA) Metabolites (n.a.)	Sum of CK bases (B) Sum of CK ribosides (R) Sum of CK N-glucosides (NG) Sum of CK O-glucosides (OG) Sum of CK phosphates (P)	[29]
Chloroplasts (<i>Nicotiana tabacum</i> , <i>Triticum aestivum</i>)	n.a.	B (iP, DHZ) R (ZR, iPR, DHZR) NG (Z9G, DHZ9G, iPNG, Z7G, DHZ7G) OG (n.a.) P (iPRMP, ZRMP, DHZRMP)	[28]
Vacuoles (<i>Arabidopsis</i>)	Precursors (Trp, IAN, ANT, TRA, IAM) Active compounds (IAA) Metabolites (IAA-Glc, oxIAA)	n.a.	[30]
Vacuoles (<i>Arabidopsis</i> , <i>Hordeum vulgare</i>)	n.a.	B (tZ, iP) R (cZR, iPR, tZR) NG (iP7G, tZ7G, DHZ7G, tZ9G, iP9G, cZ9G, DHZ9G) OG (cZROG, cZOG, tZOG, DHZOG, tZROG) P (iPRMP, tZRMP)	[31]

¹ Phytohormone profiles are shown for species in bold. ² "n.a." indicates that the phytohormones were not profiled in the study.

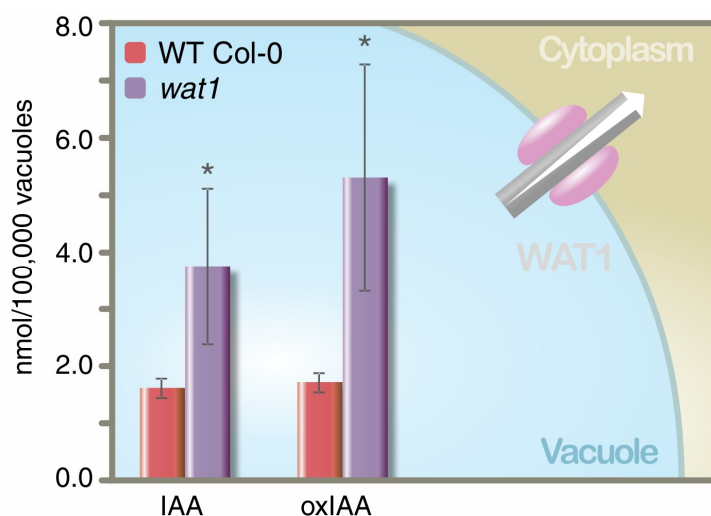


Figure 1. Indole-3-acetic acid (IAA) and 2-oxindole-3-acetic acid (oxIAA) contents were measured in vacuolar fractions isolated by density gradient ultracentrifugation from the wild-type (*Arabidopsis* Col-0) and the vacuolar auxin transporter mutant line (*wat1-1*). Plant tissues were grown, and vacuole isolation was performed as previously described [31]. Samples were purified by in-tip solid-phase microextraction [32] using a minor modification of the protocol described by Pěňčík et al. [33]. Quantification of IAA and oxIAA was performed by LC-MS/MS [34]. The bars represent averages (\pm SD) of four independent biological replicates; the asterisk indicates *p*-values of the genotype comparisons in an ANOVA analysis ($* p < 0.05$). White arrow indicates flux direction.

3. Auxins

It is well described that cellular IAA concentrations are strictly regulated by its transport, biosynthesis, and catabolism [35]. Changes in auxin concentrations and morphogenic gradients are

created in plant tissues and organs as a response to both exogenous and endogenous stimuli, resulting in various developmental events, but how homeostasis is managed in these systems is far from clear. While TRANSPORT INHIBITOR RESPONSE1/AUXIN SIGNALING F-BOX proteins (TIR1/AFBs) are considered as proven auxin receptors, the clear contribution of AUXIN BINDING PROTEIN 1 (ABP1) and S-PHASE KINASE-ASSOCIATED PROTEIN 2A (SKP2A)-dependent perception to auxin signaling still remains controversial [36,37] (Figure 2).

Polar auxin transport (PAT) is a regulated cell-to-cell transport of auxin that provides essential directional and positional information for all vital plant developmental processes, such as vascular differentiation, apical dominance, patterning, organ polarity, embryogenesis, organogenesis, phyllotaxis, and tropisms [38]. Disruption of such directional auxin movement by genetic or pharmacological manipulations results in severe developmental defects [39]. Local auxin production, frequently together with auxin transport, influences lateral root development, embryogenesis, and leaf and fruit development, whereas a strong reduction in auxin levels leads to defects in gravitropism, vasculature development, and reduced apical dominance [40]. All these activities are described at the tissue level, but little is known about how homeostasis, and perturbations to homeostasis, are affected at the subcellular level.

3.1. Locations of Auxin Biosynthesis and Metabolism

The first organelle-specific activity connected with auxin homeostasis described indole-3-butyric acid (IBA) enzymatic conversion to IAA in a peroxisome-dependent reaction [41]. However, whereas IBA has been recorded from a number of plant species [35], other labs have had difficulties detecting IBA or report it at much lower concentrations than IAA [34,42]. Certainly, IBA is a poor ligand for the receptor TIR1 [43,44], but IBA and/or its conjugates might still contribute to IAA homeostasis [45].

The biosynthesis of IAA as a natural auxin could be mediated by two main directions: via an L-tryptophan (L-Trp)-dependent or an L-Trp-independent pathway [46,47] (Figure 2). De novo synthesis through the L-Trp-independent pathway is well described in microorganisms [48] but still discussed in higher plants [49,50]. In contrast, L-Trp-dependent pathways are a significant source of endogenous IAA for higher plants [40], as L-Trp is synthesized by the shikimate pathway localized in the chloroplast stroma. Downstream, IAA biosynthesis is predominantly via the indole-3-pyruvic acid (IPyA) pathway with three main family proteins (Figure 2): TRYPTOPHAN AMIDOTRANSFERASE OF ARABIDOPSIS (TAA1 localized in cytoplasm) and TAA-Related (TAR1 localized on plasma membrane (PM)) that are responsible for the synthesis of IPyA from tryptophan, and flavin monooxygenases from the YUCCA family that are responsible for the conversion of IPyA to IAA [51,52] (Figure 2). The YUCCA enzymes are likely to be cytoplasmic, although *Arabidopsis* YUCCA4 can be localized both to the cytosol and to the cytosolic face of the ER membrane [18]. At least three of the maize auxin biosynthetic proteins are also localized to ER membranes [53] (Figure 2).

The indole-3-acetaldoxime (IAOx) pathway is a unique biosynthetic pathway in *Brassicaceae* with cytochrome P450 enzymes CYP79B2 and CYP79B3 localized in chloroplasts, where their substrate Trp is synthesized [54], converting Trp to IAOx, and then to indole-3-acetamide (IAM) or indole-3-acetonitrile (IAN) downstream. However, the enzymatic steps between IAOx and IAN have yet to be identified. The synthesis of IAM from IAOx has been directly demonstrated in assays with *cyp79b2 cyp79b3* mutants [55,56], and IAM hydrolases have been isolated from *Arabidopsis* and tobacco BY-2 cells (AtAMI1 and NtAMI1) and shown to convert IAM to IAA in vitro, but the subcellular localization of these enzymes remains unclear [57,58], despite some evidence of AtAMI1-green fluorescent protein (GFP) fusion protein in the cytoplasm [59].

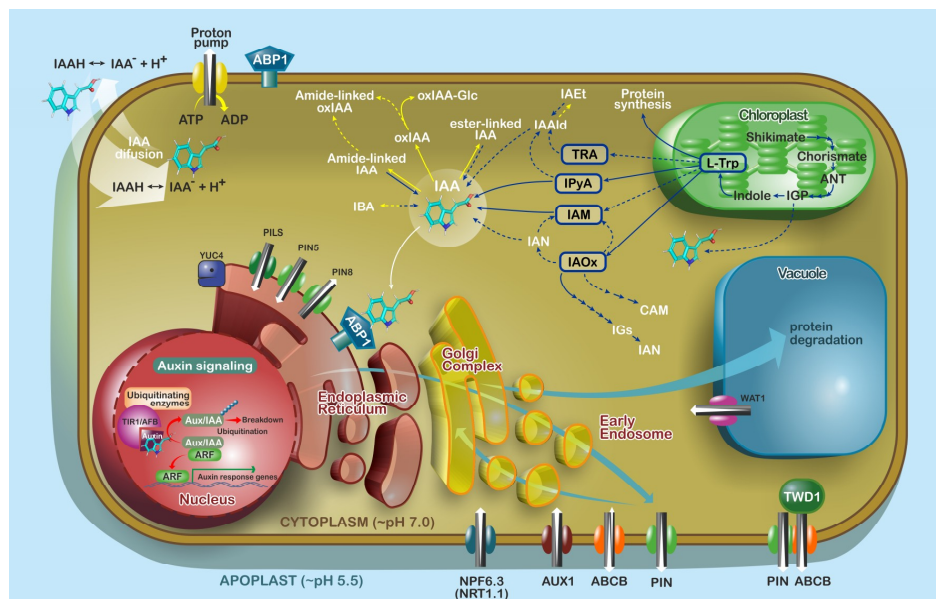


Figure 2. Model of cellular and subcellular auxin homeostasis and signaling in *Arabidopsis*. IAA biosynthesis (indicated by dark blue arrows) could be mediated by L-tryptophan (L-Trp)-dependent or independent biosynthetic pathways [47]. Tryptophan as a substrate for the synthesis of IAA is synthesized in stroma of chloroplast [40]. There are already four described biosynthetic pathways named according to their first intermediates (in dark blue rectangles [60]). In *Arabidopsis*, IAA biosynthesis is running predominantly via the indole-3-pyruvic acid (IPyA) pathway including: cytoplasmic TRYPTOPHAN AMIDOTRANSFERASE OF ARABIDOPSIS (TAA1), TAA-Related (TAR1) localized on plasma membrane (PM), and YUCCA4 attached to the ER membrane [47,52]. Free IAA levels can be modulated via conjugation and/or oxidation, rarely via methylation (metabolic pathways are represented by yellow arrows [59,61]). Four main families of active auxin transporters are described: PM localized AUXIN1/LIKE-AUX1 (AUX1/LAX) auxin influx facilitators, and perhaps also into the ER [62]; PINs efflux carriers [36,63]; ATP-binding cassette type B (ABCB) proteins [64] involved in the influx or efflux of auxin [65,66]; and finally PIN-like (PILS) together with short PIN-FORMED proteins (PINs) (PIN5, 6, and 8) with confirmed localization at ER [67]. WALLS ARE THIN 1 (WAT1) is a recently described tonoplast-localized auxin transporter [30]. Similarly, NPF6.3 (NRT1.1) can control auxin influx (transport is marked by white arrows [68,69]). Nuclear TRANSPORT INHIBITOR RESPONSE1/AUXIN SIGNALING F-BOX proteins (TIR1/AFBs) are considered as proven auxin receptors. However, the strong proof that putative AUXIN BINDING PROTEIN 1 (ABP1) and S-PHASE KINASE-ASSOCIATED PROTEIN 2A (SKP2A) receptors directly mediate auxin signaling still remains contentious (signaling is highlighted by red arrows [37,70]). Light blue arrows indicate protein trafficking. Solid arrows indicate known and well-described pathways, dashed arrows indicate not well-defined pathways. Abbreviations and structures of all IAA metabolites (precursors, catabolites, and conjugates) are listed in Figure A1a.

Free IAA levels are probably managed by activities in the cytoplasm, the compartment of synthesis and of arrival by transport. In the cytoplasm, IAA can be modulated via conjugation and/or oxidation, and rarely via methylation [59]. IAA can be conjugated via ester linkages to glucose by UDP-glucosyl transferases UGT74D1 and UGT84B1 to create 1-O-indole-3-acetyl- β -D-glucose (IAA-Glc) [71], or to amino acids by the GRETCHEN HAGEN 3 (GH3) family of IAA-amido synthases [72,73]. Interestingly, Barbez and Kleine-Vehn [74] later hypothesized that the localization of the GH3 family is in the ER, but this would place them in the same compartment as ILR1-like amidohydrolases (ILR1, ILR2, and ILR3 [75]), which will hydrolyze the products of GH3s. Unfortunately, clear evidence for GH3 localization to the ER is still missing. If IAA conjugates are synthesized in the cytoplasm, the authors can hypothesize that such conjugates are rapidly transported out of the cytoplasm for storage or derivative pathways.

The GH3 enzymes are induced strongly by elevated concentrations of auxin and this provides one level of homeostatic control [76,77], but the role of the ILRs in subsequently releasing free IAA back from amido-conjugates is not known. The steady state concentration of IAA in the cytoplasm is considered to be 5 μM when calculated in system models [78]. Rises in concentration above the steady state in the cytoplasm and nucleus will induce transcription and translation of *GH3s*, among many other genes, and the analysis above suggests that these reside in the cytoplasm ready to react with the elevated free IAA. Consideration of the kinetic properties of these enzymes suggests that GH3s will become increasingly active in the micromolar range of IAA concentrations (K_m for OsGH3-8 = 182 μM , [77]; K_m for AtGH3-5 = 700 μM , [79]). While these K_m values suggest poor activity at the concentrations of IAA likely to be encountered in the cytoplasm, the enzymes do have very high catalytic efficiencies (k_{cat}/K_m) and so free IAA will be rapidly conjugated by resting levels of enzyme, and this will be rapidly supplemented as new enzyme is generated by the auxin response. In the ER, ILRs will become active at somewhat lower concentrations of the conjugates (K_m AtILR1 = 14 μM ; [75]), but the proper location of the conjugates remains to be determined.

IAA oxidation to 2-oxindole-3-acetic acid (oxIAA) is the major IAA catabolic pathway in *Arabidopsis* [34,80,81]. It was later shown that another oxidative metabolite in *Arabidopsis*, oxIAA-glucose (oxIAA-Glc), was synthesized via glycosylation of oxIAA and not via oxidation of IAA-Glc [82,83]. Oxidation of some IAA amides in *Arabidopsis* was also detected [80,84]. The first characterized IAA oxidases, DIOXYGENASE FOR AUXIN OXIDATION (DAO) in dicots, were rice OsDAO homologs in *Arabidopsis* AtDAO1 and AtDAO2 [83,85,86]. These dioxygenases are cytoplasmic [83] and so, again, responses to elevations of IAA concentration are targeted to the cytoplasm and one may expect the cytoplasmic concentration at homeostasis to be micromolar or lower given that OsDAO1 actively oxidized IAA when 1 μM IAA was supplied [85].

AtDAO1 was shown to be a primary determinant of auxin homeostasis [83]. However, the work on oxidases [83,86] showed that the loss of IAA oxidation in *atdao1* mutants did not lead to a significant change in IAA levels, suggesting redundancy in homeostatic mechanisms. Moreover, the mathematical model from Mellor et al. [87] suggests that, in *atdao1* mutant, IAA-aspartate (IAA-Asp) and IAA-glutamate (IAA-Glu) accumulate, compensating for the loss of IAA oxidation.

There are several reports indicating that methylation of IAA is highly relevant for some plant developmental processes, such as leaf development [88] and differential growth in the hypocotyl [89].

Taken together, these results suggest that plants possess redundant and sensitive mechanisms to catabolize cytoplasmic IAA [90]. It will be useful in future to know into which compartment the oxidation and other catabolic products are moved. The presence of the amidohydrolases in the ER suggests that this compartment is important, but it remains possible that this is only involved in feedback control of cytoplasmic IAA concentrations.

3.2. Auxin Transport

There are four main families of active auxin-specific transporters and by their nature, each is localized to specific membranes (Figure 2). Therefore, one can surmise their roles in auxin homeostasis in some detail: (i) AUXIN1/LIKE-AUX1 (AUX1/LAX) auxin- H^+ symporters, responsible for auxin transport from the apoplast into the cell, and perhaps also into the ER [62,91,92]; (ii) PIN-FORMED proteins (PINs) that are gradient-driven secondary transporters (efflux carriers) [63]; (iii) ATP-binding cassette type B proteins (ABCBs) [64] uniformly localized at the PM are involved in the ATP-driven influx or efflux of auxin [65,66]; and (iv) the PIN-like (PILS) protein family with confirmed localization at ER [67] (Figure 2). Additionally, it has been demonstrated that the nitrate transceptor NPF6.3 (NRT1.1, Figure 2), which belongs to the NPF (NRT1/PTR) family in *Arabidopsis* [68,69], is involved in the auxin influx in heterologous systems of *Xenopus* oocytes, yeast, and tobacco BY-2 cells [93–95]. Finally, the tonoplast-localized auxin transporter WAT1 and endomembrane ADP1, that are involved in maintaining the intracellular auxin homeostasis, were also identified [30,96]. Experiments showed

that WAT1 confers auxin efflux to yeast cells and *Xenopus* oocytes [30]. However, it is still not known which auxin-related compound(s) are transported in planta.

In *Arabidopsis*, the PIN family consists of eight members and divides into two subfamilies according to the length of a hydrophilic loop located in the middle of their polypeptide chain. The “long” canonical PINs (PIN1-4, and 7) [97–99] act as auxin efflux carriers and are polarly localized at the PM where they direct auxin flow [100,101]. The “short” non-canonical PINs (PIN5-6 and PIN8) have the hydrophilic loop, either partially (PIN6) or significantly reduced (PIN5 and PIN8) [99]. “Short” PINs are predominantly localized to the ER where they presumably regulate auxin homeostasis by pumping auxin into (PIN5) or out (PIN8) of the ER lumen or hypothetically from the ER lumen into the nucleus (PIN6 and PIN8) [14,102–105]. However, Ganguly et al. [106,107] and Simon et al. [108] revealed dual localizations of PIN5, PIN6, and PIN8 at the PM and ER in *Arabidopsis* epidermal and root hair cells, as well as in tobacco BY-2 cells. PIN5::GFP was predominantly localized to the ER and PIN8::GFP, to the PM. However, in the epidermal and cortical cells of the root meristem region (the PIN2 domain), PIN5 showed a PM localization pattern [106,107]. Finally, Ganguly et al. [107] came up with the hypothesis that both PIN5 and PIN8, with their dual localization property, may act as linkers between the ER-based PILs and the PM-based canonical PINs. It is also clear that PINs do not stay static but undergo constitutive cycling through the clathrin-coated vesicle machinery between the PM and ER compartments [109,110].

ABCB, ABCD, and ABCG protein subfamilies are directly or indirectly involved in auxin transport. There is a clear and well-described functional interaction between members of the ABCB family (ABCB1 and ABCB19) and TWISTED DWARF1 (TWD1) which acts as a chaperone during PM trafficking [111]. Dudler and Hertig [112] were the first to determine the substrate specificity of ABCB1 and later Sidler et al. [113] pointed out the role of ABCB1 in the regulation of hypocotyl elongation and its localization to the PM. ABCB1 and ABCB19 show mainly apolar cellular localizations, although partial apical localization is found in different tissues [114–116]. Interestingly, PAT in *abcb19* was highly reduced, in both inflorescence stems and hypocotyls [117], and by ~70% in the *abcb1 abcb19* double mutant, whereas *pin1* exhibited only a ~30% reduction [118,119]. Similar drastic reductions in PAT were found in *twd1* [120]. This suggests that ABCBs primarily contribute to long-distance auxin transport and do not function in establishing the basal auxin flows that regulate organogenesis [111,118,119,121]. It has also been demonstrated that ABCB4 works as a unique auxin concentration-dependent switchable influx/efflux transporter [65,66], and this will clearly contribute to homeostatic control of cytoplasmic auxin concentrations.

The auxin carriers that are specifically localized to ER provide a clear link between auxin compartmentalization and auxin conjugation-based metabolism. Moreover, the role of auxin intracellular transport (PIN5, PIN8 and PILS) together with compartmentalization of auxin metabolism can be interfaced in maintaining and regulating intracellular auxin homeostasis [74]. Mravec et al. [102] were the first to realize that PIN5 increases cellular auxin retention in *Arabidopsis* protoplasts presumably via auxin transport from the cytosol into the ER lumen. Moreover, PIN5 activity decreases cellular levels of free IAA and increases levels of some auxin conjugates, namely, IAA-Asp, IAA-Glu, and IAA-Glc, suggesting a possible role for PIN5 in compartmentalized auxin metabolism. However, the picture for PIN8 is less clear [14,65,66,74,103]. As for PIN5, PILS2 and PILS5 in the ER increase cellular auxin accumulation, but reduce nuclear auxin signaling, and so one can speculate that they promote the sequestration of cytosolic auxin into the ER, where it is unavailable for nuclear auxin signaling [67].

It is clear that local directed transport activities contribute significantly to the regulation of cellular auxin metabolism. Indeed, Middleton et al. [122] have combined mathematical modelling with time course data from both auxin-mediated nuclear signaling and quantitative phenotyping at the single cell level, to show that an ER-to-nucleus auxin flux represents a major subcellular pathway to directly control nuclear auxin levels. Based on the preceding, the authors can propose that auxin-mediated

responses are controlled by both maintenance of a homeostatic auxin pool in the ER together with regulated rapid auxin fluxes between ER and nucleus.

4. Cytokinins

CKs are divided according to the chemical character of their side chain on the prevalent isoprenoid group, such as *tZ*, *cis*-zeatin (*cZ*), dihydrozeatin (DHZ), and iP. The same classification applies to benzyladenine (BA) and topolins, which occur less in nature, which are CKs carrying an aromatic group instead of the isoprenoid (Figure A1b) [123–127]. Another group of naturally occurring CKs are derivatives modified at position C² by the methylthio group [128]. CKs promote many responses at the cellular level (e.g., cell cycle and division [129], chloroplast development [130]) and are modulators of PIN formation and polarity [131]. These processes are dependent on CK perception mediated by three ARABIDOPSIS HISTIDINE KINASES (AHKs) which trigger a multistep phosphorelay cascade leading to gene transcription. The AHK receptors sit mainly in the ER, but the PM might be relevant in some circumstances as well (described in detail in [132,133]) (Figure 3).

4.1. Locations of Cytokinin Biosynthesis and Metabolism

Key enzymes catalyzing the first step of CK biosynthesis are the isopentenyl transferases (IPTs). IPTs mediate the conjugation of an isopentenyl group to the N⁶-position of the adenine ribotide to form isopentenyladenosine-5'-di- or -triphosphate (iPRDP or iPRTP, respectively). Several IPTs were identified in *Arabidopsis* (AtIPT1-9) [134–136], where AtIPT2 and 9 can also catalyze isopentenylolation of tRNA to provide a source for *cZ*-type CKs [136]. AtIPT1, 3, and 5 fused with GFP were localized to the chloroplasts of mesophyll cells [137], although AtIPT3 appears also in the nucleus. Specific localization depends on posttranslational modifications such as farnesylation, which may overcome the presence of chloroplast transit peptides [138] (Figure 3). GFP fusions of AtIPT2 and AtIPT4 point to cytosolic localization. This finding agrees with the idea that AtIPT4 may utilize isoprenoid precursors synthesized via the mevalonate pathway in the cytosol, but it is likely that the main pool of *tZ* arises from plastids. Additionally, AtIPT7::GFP was observed in mitochondria [137] (Figure 3).

Synthesis of iPRDP and iPRTP nucleotides via transmission of isoprenoid moieties to adenosine is followed by hydroxylation to produce *tZ*-type CKs, a reaction catalyzed by cytochrome P450 monooxygenases CYP735A1 and CYP735A2 [139]. CK nucleotides can get phosphoribohydrolysed by “LONELY GUY” (LOG) enzymes into highly active free-base forms [140]. To date, nine AtLOG homologs targeted predominantly to the nucleus and cytosol have been identified [141].

It is expected that the metabolism of active free bases at least partially regulates CK homeostasis. CK bases can be reversibly conjugated with sugars (e.g., glucose or xylose) through their hydroxyl moiety on the N⁶-side chain of *tZ*, *cZ*, and DHZ via *Arabidopsis* uridine diphosphate glycosyltransferase (AtUGT) 85A1 which is located to the cytosol [142,143] (Figure 3). A pool of *O*-glucosides (OG) could serve as CK storage with the potential of rapid conversion back to active CKs via β -glucosidases [144]. Another reversible inactivation could be mediated by enzymes common with purine metabolism, such as adenine phosphoribosyltransferases (AtAPT1-3), which appear to be cytosolic and act antagonistically to other AtLOGs (Figure 3), switching bioactive CKs back to nucleotides [145–147]. Direct glycosylation at N7 or N9 might also be catalyzed by cytosolic UGT76C1 or UGT76C2, causing irreversible CK inactivation [148].

Cytokinin dehydrogenases/oxidases (CKXs) are recognized as the main enzymes mediating CK degradation [149,150] and they play a key role in the maintenance of endogenous CK levels. The seven CKX homologs in *Arabidopsis* have distinct subcellular localizations. It seems that the main site of CK inactivation is localized in the apoplast by CKX2 and CKX4-6 [151]. CKX1 and 3 were initially predicted as mitochondrial based on in silico experiments [152], although later GFP fusions showed that these two enzymes are predominantly targeted to vacuole, with some observed signal also in ER [151] where they are catalytically active [153]. In the case of CKX7, the lack of a signal peptide suggests that it is localized to the cytosol [154] (Figure 3).

As well as localizations, AtCKXs differ in their substrate specificity adding a level of complexity to cytokinin homeostasis above that for auxin. While CKXs prefer unsaturated isoprenoids, aromatic CKs can also be degraded but with lower turnover rates [155,156] and DHZ, OG, and almost all *cZ*-types are believed to be resistant to AtCKXs.

4.2. Cytokinin Transport

CKs are long-distance signals and the different CK forms appear to be moved differentially. For example, *tZ* riboside (*tZR*) is transported acropetally in xylem sap, whereas *iPR* is mainly transferred basipetally via phloem [157–160]. Despite the importance of CK transport, the facilitator proteins were not discovered until the beginning of the 21st century when three protein groups possessing CK translocation activity were described: purine permeases (PUPs) [161], equilibrative nucleoside transporters (ENTs) [162], and the G subfamily of ATP-binding cassette (ABCG) transporters [163,164] (Figure 3). CK transport seems to be shared with essential nucleobases, although the molecular basis of CK transport is still poorly understood compared with auxin transport.

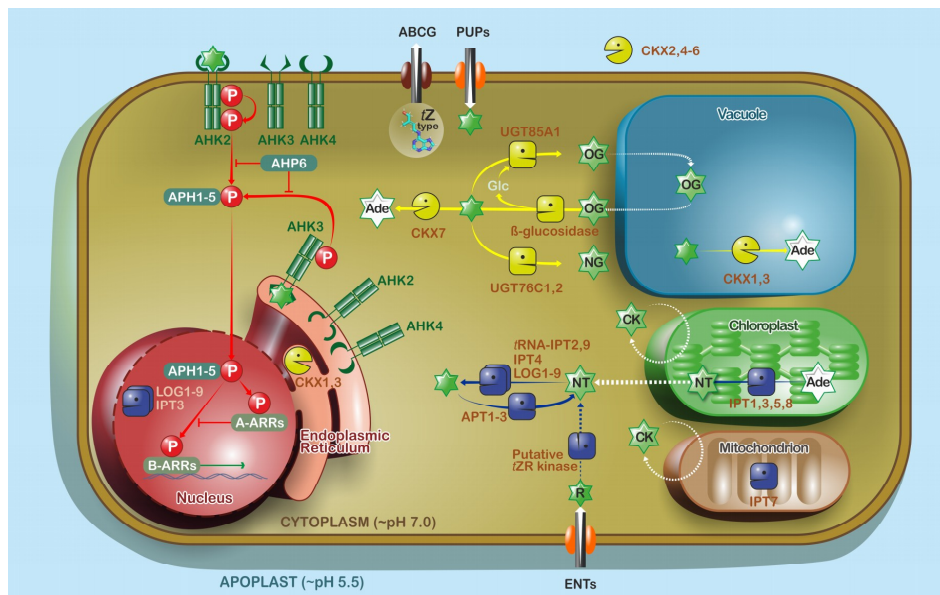


Figure 3. Model of cellular and subcellular CK homeostasis and signaling in *Arabidopsis*. De novo synthesis of CKs is mediated by isopentenyl transferases (IPTs) mainly in chloroplasts; nevertheless, they are localized also in mitochondria, cytosol, and nuclei [137,138]. LONELY GUY enzymes (LOGs) present in cytosol and nuclei are other enzymes, which transform CK nucleotides to active form [140] (biosynthesis is highlighted by dark blue arrows). In contrast, APTs catalyze the opposite reaction [145–147]. Most of the active CKs can be modulated by uridine diphosphate glycosyltransferases (UGTs) [148] or β -glucosidase [144,165] (yellow arrows mark reversible/irreversible inactivation). The terminal degradation product of cytokinin dehydrogenases/oxidases (CKXs) is adenine (Ade, yellow arrows also mark CK degradation). CKXs are prevalent in the apoplast, although three homologs are intracellular [151,153,154]. Transport (represented by white arrows) of CK free bases and their ribosides to cytoplasm is facilitated by purine permeases (PUPs) [161,166,167] and equilibrative nucleoside transporters (ENTs) [158,168], respectively. Lomin et al. [169] proposed a model where ENTs are involved in *tZR* transport to cytosol and its subsequent conversion via a putative kinase and LOG into an active CK base, which enters to ER and triggers signaling. ABCG14 was described and proven as an exporter of *tZ*-types [163,164]. CK signaling pathways (marked by red arrows) are initiated by three ARABIDOPSIS HISTIDINE KINASES (AHKs) localized at PM [170] or ER [13,171]. Signal is transmitted via ARABIDOPSIS HISTIDINE PHOSPHOTRANSFER1-5 (AHP1-5) [172,173] to nuclear type-A ARABIDOPSIS RESPONSE REGULATORS (A-ARRs) or B-ARRs (type-B). AHP6 is inhibitory [174,175].

Activation of B-ARRs leads to transcription [176,177] of CK inducible genes including *A-ARRs* which mediate a negative feedback loop [172,178–180]. Green stars indicate CK species; Glc—glucose; NT—cytokinin nucleotides; NG—cytokinin *N*-glucosides; OG—cytokinin *O*-glucosides; P—phosphate moiety; R—cytokinin riboside. Solid arrows indicate known and well-described pathways, dashed arrows indicate not well-defined pathways.

The PUP family numbers 23 members [132,161] and some PUPs appear to mediate CK uptake at the PM (Figure 3). AtPUP1 was first examined in a yeast mutant deficient in adenine uptake. Results suggested that kinetin and *tZ*, but not *tZR*, were substrates by competitively inhibiting adenine uptake. A mildly acidic apoplast raised AtPUP1 activity, whereas proton pump inhibitors reduced it. These findings point to energy-dependent and potentially proton-coupled transport against the concentration gradient [161], later confirmed by the transport of radiolabeled *tZ* [166]. However, PUPs are promiscuous to other purines and even though PUP14, for example, was shown to be involved in the early stages of plant development [167], their role specifically as CK carriers remains to be elucidated.

AtENT1 was described as a putative nucleoside transporter based on shared similarity with human ENTs [181] and proton-dependent import was confirmed later [162,182]. AtENT1–8 are localized at the PM [162,181,183] (Figure 3), although AtENT1 was also identified in the tonoplast proteome [184]. Substrate specificity of some *Arabidopsis* ENTs has been examined using competition assays of adenosine uptake. As a result, AtENT6 and 8 may participate in CK riboside transport and AtENT6 preferred *iPR* to *tZR* [158,168].

ABCG14 was revealed as the first described CK exporter involved in root-to-shoot transport of CKs. It is highly expressed in *Arabidopsis* root vascular tissue and loss-of function *abcg14* mutants resemble CK-deficient phenotypes [163,164], and measurements showed that mutant shoots contained decreased *tZ*-type CKs, despite abundant *tZs* in roots. Interestingly, *iP*-type and *cZ*-type CK contents were elevated in both shoots and roots, suggesting that the *abcg14* plants are attempting to compensate for the loss of transport of root-synthesized *tZ*-type CKs for intrinsic CK homeostasis [163,164]. Undoubtedly, AtABCG14 represents an important element in the long-distance transport of CKs. Unfortunately, there is little information on local or subcellular compartmentation of cytokinins or cytokinin catabolites.

5. Future Perspectives

In spite of many recent studies on plant hormones, there are still gaps in our knowledge about the mechanisms of homeostasis. For instance, detailed information about intracellular CK transport is still missing. Cell- and organelle-specific distributions of auxin, CK, and their related compounds are also waiting for elucidation. Auxin and CK profiling at the subcellular level will definitely open new insights and provide a better understanding of the regulation of auxin and CK homeostasis, offering more precise inputs for mathematical modelling, the creation of biosensors, and other applications in plant biotechnologies.

Mass spectrometry imaging and living single-cell mass spectrometry analysis could soon provide powerful tools for studying hormone distribution, even though they are still limited for hormone profiling [8]. Cell-specific sorting has been employed to gain more accurate insight into auxin [33,185] and CK [186] distributions in *Arabidopsis* root tips, and flow cytometric techniques for the sorting of organelles may soon provide a better view on subcellular distributions. Another possible approach for visualizing auxin and CK distributions at the cellular or subcellular level is using novel synthetic analogues labelled with 7-nitro-2,1,3-benzoxadiazole (NBD), for example, that have been recently developed to mimic native phytohormones *in vivo* [187–189]. A combination of all these methodologies with the use of mathematical modelling [78,122,190] to parameterize auxin homeostasis at cellular and subcellular levels will undoubtedly lead to far more detailed insights into the secrets of plant developmental control.

Author Contributions: All authors developed the idea and outline of the paper. V.S., M.K. and O.N. wrote the manuscript; R.N. and O.N. revised and edited the manuscript. All authors read the manuscript before submission.

Funding: This work was financially supported by the Ministry of Education, Youth and Sports, Czech Republic (Grant LO1204 from the National Programme of Sustainability I), by the Internal Grant Agency of Palacký University in Olomouc (IGA_PrF_2018_023), and by the Czech Science Foundation (17-21581Y). Vladimír Skalický was supported (in part) by the Endowment fund of Palacký University in Olomouc and Martin Kubeš was supported by the EU MSCA-IF project CrysPINs (792329).

Acknowledgments: The authors are thankful to Ioanna Antoniadis and Markéta Pernisová for their critical reading of the manuscript and to Ota Blahoušek for drawing the figures.

Conflicts of Interest: The authors declare no conflict of interest.

Appendix A

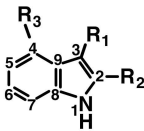
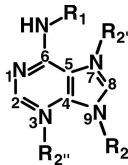
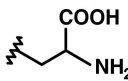
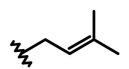
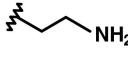
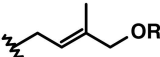
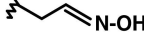
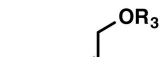
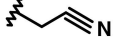
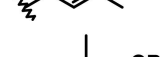
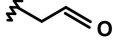
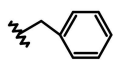
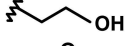
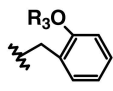
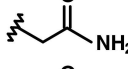
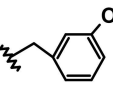
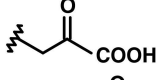
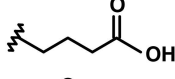
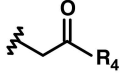
			
R₁	R_{2,3}: H; R₄: OH	R₁	R₂: H; R₃: H
	tryptophan (Trp)		CK Bases isopentenyladenine (iP)
	tryptamine (TRA)		<i>trans</i> -zeatin (<i>tZ</i>)
	indole-3-aldoxime (IAOx)		<i>cis</i> -zeatin (<i>cZ</i>)
	indole-3-acetonitrile (IAN)		dihydrozeatin (DHZ)
	indole-3-acetaldehyde (IAAld)		<i>N</i> ⁶ -benzyladenine (BA)
	indole-3-ethanol (IAEt)		<i>ortho</i> -topolin (<i>oT</i>)
	indole-3-acetamide (IAM)		<i>meta</i> -topolin (<i>mT</i>)
	indole-3-pyruvic acid (IPyA)		
	indole-3-butyric acid (IBA)		
	indole-3-acetic acid (IAA)	R₂: N9-β-D-ribose	Riboside (R)
R₃: -Cl; R₄: OH	4-chloroindole-3-acetic acid (4-Cl-IAA)	R₂: N9-β-D-glucose	9-glucoside (9G)
R₄: -O-R₅	ester-linked IAA	R₂: N7-β-D-glucose	7-glucoside (7G)
R₅: CH₃	IAA-methyl ester (MeIAA)	R₂: N3-β-D-glucose	3-glucoside (3G)
R₅: β-D-glucose	IAA-glucose ester (IAA-Glc)	R₂: N9-β-D-ribose-5'-monophosphate	Riboside-5'-monophosphate (RMP)
R₄: -NH-AA	amide-linked IAA (IAA-AA)	R₃: β-D-glucose	O-glucoside (OG)
AA: Asp, Glu, Ala, Leu, Gly, Phe, Val, Trp		R₂: N9-β-D-ribose; R₃: β-D-glucose	Riboside-O-glucoside (ROG)
R₂: =O; R₄: OH	2-oxindole-3-acetic acid (oxIAA)		
R₂: =O; R₄: -O-R₅	ester-linked oxIAA		
R₅: β-D-glucose	oxIAA-glucose ester (oxIAA-Glc)		
R₂: =O; R₄: -NH-AA	amide-linked oxIAA (oxIAA-AA)		
AA: Asp, Glu, Phe, Val			

Figure A1. Structures, names, and abbreviations of naturally occurring (a) auxins and (b) CKs. Wavy cuts indicate position of substituent attachment.

References

1. Schaller, G.E.; Bishopp, A.; Kieber, J.J. The yin-yang of hormones: Cytokinin and auxin interactions in plant development. *Plant Cell* **2015**, *27*, 44–63. [[CrossRef](#)] [[PubMed](#)]
2. Skoog, F.; Miller, C.O. Chemical regulation of growth and organ formation in plant tissues cultured in vitro. *Symp. Soc. Exp. Biol.* **1957**, *11*, 118–130. [[PubMed](#)]
3. Müller, B.; Sheen, J. Cytokinin and auxin interaction in root stem-cell specification during early embryogenesis. *Nature* **2008**, *453*, 1094–1097. [[CrossRef](#)] [[PubMed](#)]
4. Efroni, I.; Mello, A.; Nawy, T.; Ip, P.-L.; Rahni, R.; DelRose, N.; Powers, A.; Satija, R.; Birnbaum, K.D. Root regeneration triggers an embryo-like sequence guided by hormonal interactions. *Cell* **2016**, *165*, 1721–1733. [[CrossRef](#)] [[PubMed](#)]
5. Leibfried, A.; To, J.P.C.; Busch, W.; Stehling, S.; Kehle, A.; Demar, M.; Kieber, J.J.; Lohmann, J.U. WUSCHEL controls meristem function by direct regulation of cytokinin-inducible response regulators. *Nature* **2005**, *438*, 1172–1175. [[CrossRef](#)] [[PubMed](#)]
6. Zhao, Z.; Andersen, S.U.; Ljung, K.; Doležal, K.; Miotk, A.; Schultheiss, S.J.; Lohmann, J.U. Hormonal control of the shoot stem-cell niche. *Nature* **2010**, *465*, 1089–1092. [[CrossRef](#)] [[PubMed](#)]
7. Novák, O.; Napier, R.; Ljung, K. Zooming In on Plant Hormone Analysis: Tissue- and Cell-Specific Approaches. *Annu. Rev. Plant Biol.* **2017**, *68*, 323–348. [[CrossRef](#)] [[PubMed](#)]
8. Pařízková, B.; Pernisová, M.; Novák, O. What Has Been Seen Cannot Be Unseen—Detecting Auxin In Vivo. *Int. J. Mol. Sci.* **2017**, *18*, 2736. [[CrossRef](#)] [[PubMed](#)]
9. De Duve, C.; Pressman, B.C.; Gianetto, R.; Wattiaux, R.; Appelmans, F. Tissue fractionation studies. 6. Intracellular distribution patterns of enzymes in rat-liver tissue. *Biochem. J.* **1955**, *60*, 604–617. [[CrossRef](#)] [[PubMed](#)]
10. Huber, L.A.; Pfaller, K.; Vietor, I. Organelle Proteomics: Implications for Subcellular Fractionation in Proteomics. *Circ. Res.* **2003**, *92*, 962–968. [[CrossRef](#)] [[PubMed](#)]
11. Robert, S.; Zouhar, J.; Carter, C.J.; Raikhel, N. Isolation of intact vacuoles from *Arabidopsis* rosette leaf-derived protoplasts. *Nat. Protoc.* **2007**, *2*, 259–262. [[CrossRef](#)] [[PubMed](#)]
12. Seigneurin-Berny, D.; Salvi, D.; Dorne, A.-J.; Joyard, J.; Rolland, N. Percoll-purified and photosynthetically active chloroplasts from *Arabidopsis thaliana* leaves. *Plant Physiol. Biochem.* **2008**, *46*, 951–955. [[CrossRef](#)] [[PubMed](#)]
13. Wulfetange, K.; Lomin, S.N.; Romanov, G.A.; Stolz, A.; Heyl, A.; Schmülling, T. The cytokinin receptors of *Arabidopsis* are located mainly to the endoplasmic reticulum. *Plant Physiol.* **2011**, *156*, 1808–1818. [[CrossRef](#)] [[PubMed](#)]
14. Ding, Z.; Wang, B.; Moreno, I.; Dupláková, N.; Simon, S.; Carraro, N.; Reemmer, J.; Pěňčík, A.; Chen, X.; Tejos, R.; et al. ER-localized auxin transporter PIN8 regulates auxin homeostasis and male gametophyte development in *Arabidopsis*. *Nat. Commun.* **2012**, *3*, 941. [[CrossRef](#)] [[PubMed](#)]
15. Somerville, C.R.; Somerville, S.C.; Ogren, W.L. Isolation of photosynthetically active protoplasts and chloroplasts from *Arabidopsis thaliana*. *Plant Sci. Lett.* **1981**, *21*, 89–96. [[CrossRef](#)]
16. Keech, O.; Dizengremel, P.; Gardeström, P. Preparation of leaf mitochondria from *Arabidopsis thaliana*. *Physiol. Plant.* **2005**, *124*, 403–409. [[CrossRef](#)]
17. Parsons, H.T.; Christiansen, K.; Knierim, B.; Carroll, A.; Ito, J.; Batth, T.S.; Smith-Moritz, A.M.; Morrison, S.; McInerney, P.; Hadi, M.Z.; et al. Isolation and Proteomic Characterization of the *Arabidopsis* Golgi Defines Functional and Novel Components Involved in Plant Cell Wall Biosynthesis. *Plant Physiol.* **2012**, *159*, 12–26. [[CrossRef](#)] [[PubMed](#)]
18. Kriechbaumer, V.; Wang, P.; Hawes, C.; Abell, B.M. Alternative splicing of the auxin biosynthesis gene *YUCCA4* determines its subcellular compartmentation. *Plant J.* **2012**, *70*, 292–302. [[CrossRef](#)] [[PubMed](#)]
19. Minami, A.; Takahashi, D.; Kawamura, Y.; Uemura, M. Isolation of plasma membrane and plasma membrane microdomains. In *Methods in Molecular Biology*; Human Press: Clifton, NJ, USA, 2017; Volume 1511, pp. 199–212.
20. Fürtauer, L.; Weckwerth, W.; Nägele, T. A Benchtop Fractionation Procedure for Subcellular Analysis of the Plant Metabolome. *Front. Plant Sci.* **2016**, *7*, 1912. [[CrossRef](#)] [[PubMed](#)]
21. Dietz, K.-J. Subcellular metabolomics: The choice of method depends on the aim of the study. *J. Exp. Bot.* **2017**, *68*, 5695–5698. [[CrossRef](#)] [[PubMed](#)]

22. Petrovská, B.; Jeřábková, H.; Chamrád, I.; Vrána, J.; Lenobel, R.; Uřinová, J.; Šebela, M.; Doležel, J. Proteomic analysis of barley cell nuclei purified by flow sorting. *Cytogenet. Genome Res.* **2014**, *143*, 78–86. [[CrossRef](#)] [[PubMed](#)]
23. Wolf, P.G.; Karol, K.G.; Mandoli, D.F.; Kuehl, J.; Arumuganathan, K.; Ellis, M.W.; Mishler, B.D.; Kelch, D.G.; Olmstead, R.G.; Boore, J.L. The first complete chloroplast genome sequence of a lycophyte, *Huperzia lucidula* (Lycopodiaceae). *Gene* **2005**, *350*, 117–128. [[CrossRef](#)] [[PubMed](#)]
24. Cossarizza, A.; Ceccarelli, D.; Masini, A. Functional heterogeneity of an isolated mitochondrial population revealed by cytofluorometric analysis at the single organelle level. *Exp. Cell Res.* **1996**, *222*, 84–94. [[CrossRef](#)] [[PubMed](#)]
25. Deal, R.B.; Henikoff, S. The INTACT method for cell type-specific gene expression and chromatin profiling in *Arabidopsis thaliana*. *Nat. Protoc.* **2011**, *6*, 56–68. [[CrossRef](#)] [[PubMed](#)]
26. Chen, W.W.; Freinkman, E.; Wang, T.; Birsoy, K.; Sabatini, D.M. Absolute Quantification of Matrix Metabolites reveals the dynamics of mitochondrial metabolism. *Cell* **2016**, *166*, 1324–1337. [[CrossRef](#)] [[PubMed](#)]
27. Sandberg, G.; Gardeström, P.; Sitbon, F.; Olsson, O. Presence of indole-3-acetic acid in chloroplasts of *Nicotiana tabacum* and *Pinus sylvestris*. *Planta* **1990**, *180*, 562–568. [[CrossRef](#)] [[PubMed](#)]
28. Benková, E.; Witters, E.; Van Dongen, W.; Kolář, J.; Motyka, V.; Brzobohatý, B.; Van Onckelen, H.A.; Macháčková, I. Cytokinins in tobacco and wheat chloroplasts. Occurrence and changes due to light/dark treatment. *Plant Physiol.* **1999**, *121*, 245–252. [[CrossRef](#)] [[PubMed](#)]
29. Polanská, L.; Vičánková, A.; Nováková, M.; Malbeck, J.; Dobrev, P.I.; Brzobohatý, B.; Vaňková, R.; Macháčková, I. Altered cytokinin metabolism affects cytokinin, auxin, and abscisic acid contents in leaves and chloroplasts, and chloroplast ultrastructure in transgenic tobacco. *J. Exp. Bot.* **2007**, *58*, 637–649. [[CrossRef](#)] [[PubMed](#)]
30. Ranocha, P.; Dima, O.; Nagy, R.; Felten, J.; Corratgé-Faillie, C.; Novák, O.; Morreel, K.; Lacombe, B.; Martinez, Y.; Pfrunder, S.; et al. *Arabidopsis* WAT1 is a vacuolar auxin transport facilitator required for auxin homeostasis. *Nat. Commun.* **2013**, *4*, 2625. [[CrossRef](#)] [[PubMed](#)]
31. Jiskrová, E.; Novák, O.; Pospíšilová, H.; Holubová, K.; Karády, M.; Galuszka, P.; Robert, S.; Frébort, I. Extra- and intracellular distribution of cytokinins in the leaves of monocots and dicots. *New Biotechnol.* **2016**, *33*, 735–742. [[CrossRef](#)] [[PubMed](#)]
32. Svačinová, J.; Novák, O.; Plačková, L.; Lenobel, R.; Holík, J.; Strnad, M.; Doležal, K. A new approach for cytokinin isolation from *Arabidopsis* tissues using miniaturized purification: Pipette tip solid-phase extraction. *Plant Methods* **2012**, *8*, 17. [[CrossRef](#)] [[PubMed](#)]
33. Pěňčík, A.; Simonovik, B.; Petersson, S.V.; Henyková, E.; Simon, S.; Greenham, K.; Zhang, Y.; Kowalczyk, M.; Estelle, M.; Zažímalová, E.; et al. Regulation of auxin homeostasis and gradients in *Arabidopsis* roots through the formation of the indole-3-acetic acid catabolite 2-oxindole-3-acetic acid. *Plant Cell* **2013**, *25*, 3858–3870. [[CrossRef](#)] [[PubMed](#)]
34. Novák, O.; Hényková, E.; Sairanen, I.; Kowalczyk, M.; Pospíšil, T.; Ljung, K. Tissue-specific profiling of the *Arabidopsis thaliana* auxin metabolome. *Plant J.* **2012**, *72*, 523–536. [[CrossRef](#)] [[PubMed](#)]
35. Korasick, D.A.; Enders, T.A.; Strader, L.C. Auxin biosynthesis and storage forms. *J. Exp. Bot.* **2013**, *64*, 2541–2555. [[CrossRef](#)] [[PubMed](#)]
36. Grones, P.; Friml, J. Auxin transporters and binding proteins at a glance. *J. Cell Sci.* **2015**, *128*, 1–7. [[CrossRef](#)] [[PubMed](#)]
37. Strader, L.C.; Zhao, Y. Auxin perception and downstream events. *Curr. Opin. Plant Biol.* **2016**, *33*, 8–14. [[CrossRef](#)] [[PubMed](#)]
38. Ganguly, A.; Sasayama, D.; Cho, H.-T. Regulation of the polarity of protein trafficking by phosphorylation. *Mol. Cells* **2012**, *33*, 423–430. [[CrossRef](#)] [[PubMed](#)]
39. Friml, J. Auxin transport—Shaping the plant. *Curr. Opin. Plant Biol.* **2003**, *6*, 7–12. [[CrossRef](#)] [[PubMed](#)]
40. Ljung, K. Auxin metabolism and homeostasis during plant development. *Development* **2013**, *140*, 943–950. [[CrossRef](#)] [[PubMed](#)]
41. Zolman, B.K.; Martinez, N.; Millius, A.; Adham, A.R.; Bartel, B. Identification and characterization of *Arabidopsis* indole-3-butyric acid response mutants defective in novel peroxisomal enzymes. *Genetics* **2008**, *180*, 237–251. [[CrossRef](#)] [[PubMed](#)]
42. Liu, X.; Hegeman, A.D.; Gardner, G.; Cohen, J.D. Protocol: High-throughput and quantitative assays of auxin and auxin precursors from minute tissue samples. *Plant Methods* **2012**, *8*, 31. [[CrossRef](#)] [[PubMed](#)]

43. Lee, S.; Sundaram, S.; Armitage, L.; Evans, J.P.; Hawkes, T.; Kepinski, S.; Ferro, N.; Napier, R. Defining binding efficiency and specificity of auxins for SCF(TIR1/AFB)-Aux/IAA co-receptor complex formation. *ACS Chem. Biol.* **2014**, *9*, 673–682. [[CrossRef](#)] [[PubMed](#)]
44. Uzunova, V.V.; Quareshy, M.; Del Genio, C.I.; Napier, R. Tomographic docking suggests the mechanism of auxin receptor TIR1 selectivity. *Open Biol.* **2016**, *6*, 160139. [[CrossRef](#)] [[PubMed](#)]
45. Frick, E.M.; Strader, L.C. Roles for IBA-derived auxin in plant development. *J. Exp. Bot.* **2018**, *69*, 169–177. [[CrossRef](#)] [[PubMed](#)]
46. Woodward, A.W.; Bartel, B. Auxin: Regulation, action, and interaction. *Ann. Bot.* **2005**, *95*, 707–735. [[CrossRef](#)] [[PubMed](#)]
47. Mashiguchi, K.; Tanaka, K.; Sakai, T.; Sugawara, S.; Kawaide, H.; Natsume, M.; Hanada, A.; Yaeno, T.; Shirasu, K.; Yao, H.; et al. The main auxin biosynthesis pathway in *Arabidopsis*. *Proc. Natl. Acad. Sci. USA* **2011**, *108*, 18512–18517. [[CrossRef](#)] [[PubMed](#)]
48. Spaepen, S.; Vanderleyden, J.; Remans, R. Indole-3-acetic acid in microbial and microorganism-plant signaling. *FEMS Microbiol. Rev.* **2007**, *31*, 425–448. [[CrossRef](#)] [[PubMed](#)]
49. Nonhebel, H.M. Tryptophan-independent indole-3-acetic acid synthesis: Critical evaluation of the evidence. *Plant Physiol.* **2015**, *169*, 1001–1005. [[CrossRef](#)] [[PubMed](#)]
50. Wang, B.; Chu, J.; Yu, T.; Xu, Q.; Sun, X.; Yuan, J.; Xiong, G.; Wang, G.; Wang, Y.; Li, J. Tryptophan-independent auxin biosynthesis contributes to early embryogenesis in *Arabidopsis*. *Proc. Natl. Acad. Sci. USA* **2015**, *112*, 4821–4826. [[CrossRef](#)] [[PubMed](#)]
51. Zhao, Y.; Christensen, S.K.; Fankhauser, C.; Cashman, J.R.; Cohen, J.D.; Weigel, D.; Chory, J. A role for flavin monooxygenase-like enzymes in auxin biosynthesis. *Science* **2001**, *291*, 306–309. [[CrossRef](#)] [[PubMed](#)]
52. Stepanova, A.N.; Yun, J.; Robles, L.M.; Novák, O.; He, W.; Guo, H.; Ljung, K.; Alonso, J.M. The *Arabidopsis* YUCCA1 flavin monooxygenase functions in the indole-3-pyruvic acid branch of auxin biosynthesis. *Plant Cell* **2011**, *23*, 3961–3973. [[CrossRef](#)] [[PubMed](#)]
53. Kriechbaumer, V.; Seo, H.; Park, W.J.; Hawes, C. Endoplasmic reticulum localization and activity of maize auxin biosynthetic enzymes. *J. Exp. Bot.* **2015**, *66*, 6009–6020. [[CrossRef](#)] [[PubMed](#)]
54. Hull, A.K.; Vij, R.; Celenza, J.L. *Arabidopsis* cytochrome P450s that catalyze the first step of tryptophan-dependent indole-3-acetic acid biosynthesis. *Proc. Natl. Acad. Sci. USA* **2000**, *97*, 2379–2384. [[CrossRef](#)] [[PubMed](#)]
55. Zhao, Y.; Hull, A.K.; Gupta, N.R.; Goss, K.A.; Alonso, J.M.; Ecker, J.R.; Normanly, J.; Chory, J.; Celenza, J.L. Trp-dependent auxin biosynthesis in *Arabidopsis*: Involvement of cytochrome P450s CYP79B2 and CYP79B3. *Genes Dev.* **2002**, *16*, 3100–3112. [[CrossRef](#)] [[PubMed](#)]
56. Sugawara, S.; Hishiyama, S.; Jikumaru, Y.; Hanada, A.; Nishimura, T.; Koshiba, T.; Zhao, Y.; Kamiya, Y.; Kasahara, H. Biochemical analyses of indole-3-acetaldoxime-dependent auxin biosynthesis in *Arabidopsis*. *Proc. Natl. Acad. Sci. USA* **2009**, *106*, 5430–5435. [[CrossRef](#)] [[PubMed](#)]
57. Pollmann, S.; Neu, D.; Lehmann, T.; Berkowitz, O.; Schäfer, T.; Weiler, E.W. Subcellular localization and tissue specific expression of amidase 1 from *Arabidopsis thaliana*. *Planta* **2006**, *224*, 1241–1253. [[CrossRef](#)] [[PubMed](#)]
58. Nemoto, K.; Hara, M.; Suzuki, M.; Seki, H.; Muranaka, T.; Mano, Y. The *NtAM11* gene functions in cell division of tobacco BY-2 cells in the presence of indole-3-acetamide. *FEBS Lett.* **2009**, *583*, 487–492. [[CrossRef](#)] [[PubMed](#)]
59. Ludwig-Müller, J. Auxin conjugates: Their role for plant development and in the evolution of land plants. *J. Exp. Bot.* **2011**, *62*, 1757–1773. [[CrossRef](#)] [[PubMed](#)]
60. Mano, Y.; Nemoto, K. The pathway of auxin biosynthesis in plants. *J. Exp. Bot.* **2012**, *63*, 2853–2872. [[CrossRef](#)] [[PubMed](#)]
61. Zhang, J.; Peer, W.A. Auxin homeostasis: The DAO of catabolism. *J. Exp. Bot.* **2017**, *68*, 3145–3154. [[CrossRef](#)] [[PubMed](#)]
62. Péret, B.; Swarup, K.; Ferguson, A.; Seth, M.; Yang, Y.; Dhondt, S.; James, N.; Casimiro, I.; Perry, P.; Syed, A.; et al. *AUX/LAX* genes encode a family of auxin influx transporters that perform distinct functions during *Arabidopsis* development. *Plant Cell* **2012**, *24*, 2874–2885. [[CrossRef](#)] [[PubMed](#)]
63. Petrášek, J.; Friml, J. Auxin transport routes in plant development. *Development* **2009**, *136*, 2675–2688. [[CrossRef](#)] [[PubMed](#)]

64. Verrier, P.J.; Bird, D.; Burla, B.; Dassa, E.; Forestier, C.; Geisler, M.; Klein, M.; Kolukisaoglu, H.U.; Lee, Y.; Martinoia, E.; et al. Plant ABC proteins—A unified nomenclature and updated inventory. *Trends Plant Sci.* **2008**, *13*, 151–159. [[CrossRef](#)] [[PubMed](#)]
65. Yang, H.; Murphy, A.S. Functional expression and characterization of *Arabidopsis* ABCB, AUX 1 and PIN auxin transporters in *Schizosaccharomyces pombe*. *Plant J.* **2009**, *59*, 179–191. [[CrossRef](#)] [[PubMed](#)]
66. Kubeš, M.; Yang, H.; Richter, G.L.; Cheng, Y.; Młodzińska, E.; Wang, X.; Blakeslee, J.J.; Carraro, N.; Petrášek, J.; Zažímalová, E.; et al. The *Arabidopsis* concentration-dependent influx/efflux transporter ABCB4 regulates cellular auxin levels in the root epidermis. *Plant J.* **2012**, *69*, 640–654. [[CrossRef](#)] [[PubMed](#)]
67. Barbez, E.; Kubeš, M.; Rolčík, J.; Béziat, C.; Pěnčík, A.; Wang, B.; Rosquete, M.R.; Zhu, J.; Dobrev, P.I.; Lee, Y.; et al. A novel putative auxin carrier family regulates intracellular auxin homeostasis in plants. *Nature* **2012**, *485*, 119–122. [[CrossRef](#)] [[PubMed](#)]
68. Gojon, A.; Krouk, G.; Perrine-Walker, F.; Laugier, E. Nitrate transceptor(s) in plants. *J. Exp. Bot.* **2011**, *62*, 2299–2308. [[CrossRef](#)] [[PubMed](#)]
69. Corratgé-Faillie, C.; Lacombe, B. Substrate (un)specificity of *Arabidopsis* NRT1/PTR FAMILY (NPF) proteins. *J. Exp. Bot.* **2017**, *68*, 3107–3113. [[CrossRef](#)] [[PubMed](#)]
70. Powers, S.K.; Strader, L.C. Up in the air: Untethered Factors of Auxin Response. *F1000Research* **2016**, *5*. [[CrossRef](#)] [[PubMed](#)]
71. Jin, S.-H.; Ma, X.-M.; Han, P.; Wang, B.; Sun, Y.-G.; Zhang, G.-Z.; Li, Y.-J.; Hou, B.-K. UGT74D1 is a novel auxin glycosyltransferase from *Arabidopsis thaliana*. *PLoS ONE* **2013**, *8*, e61705. [[CrossRef](#)]
72. Staswick, P.E.; Serban, B.; Rowe, M.; Tiryaki, I.; Maldonado, M.T.; Maldonado, M.C.; Suza, W. Characterization of an *Arabidopsis* enzyme family that conjugates amino acids to indole-3-acetic acid. *Plant Cell* **2005**, *17*, 616–627. [[CrossRef](#)] [[PubMed](#)]
73. Cano, A.; Sánchez-García, A.B.; Albacete, A.; González-Bayón, R.; Justamante, M.S.; Ibáñez, S.; Acosta, M.; Pérez-Pérez, J.M. Enhanced conjugation of auxin by GH3 enzymes leads to poor adventitious rooting in carnation stem cuttings. *Front. Plant Sci.* **2018**, *9*. [[CrossRef](#)] [[PubMed](#)]
74. Barbez, E.; Kleine-Vehn, J. Divide Et Impera—cellular auxin compartmentalization. *Curr. Opin. Plant Biol.* **2013**, *16*, 78–84. [[CrossRef](#)] [[PubMed](#)]
75. LeClere, S.; Tellez, R.; Rampey, R.A.; Matsuda, S.P.T.; Bartel, B. Characterization of a family of IAA-amino acid conjugate hydrolases from *Arabidopsis*. *J. Biol. Chem.* **2002**, *277*, 20446–20452. [[CrossRef](#)] [[PubMed](#)]
76. Okrent, R.A.; Brooks, M.D.; Wildermuth, M.C. *Arabidopsis* GH3.12 (PBS3) conjugates amino acids to 4-substituted benzoates and is inhibited by salicylate. *J. Biol. Chem.* **2009**, *284*, 9742–9754. [[CrossRef](#)] [[PubMed](#)]
77. Chen, Q.; Westfall, C.S.; Hicks, L.M.; Wang, S.; Jez, J.M. Kinetic basis for the conjugation of auxin by a GH3 family indole-acetic acid-amido synthetase. *J. Biol. Chem.* **2010**, *285*, 29780–29786. [[CrossRef](#)] [[PubMed](#)]
78. Kramer, E.M.; Ackelsberg, E.M. Auxin metabolism rates and implications for plant development. *Front. Plant Sci.* **2015**, *6*, 150. [[CrossRef](#)] [[PubMed](#)]
79. Westfall, C.S.; Sherp, A.M.; Zubieta, C.; Alvarez, S.; Schraft, E.; Marcellin, R.; Ramirez, L.; Jez, J.M. *Arabidopsis thaliana* GH3.5 acyl acid amido synthetase mediates metabolic crosstalk in auxin and salicylic acid homeostasis. *Proc. Natl. Acad. Sci. USA* **2016**, *113*, 13917–13922. [[CrossRef](#)] [[PubMed](#)]
80. Ostin, A.; Kowalczyk, M.; Bhalerao, R.; Sandberg, G. Metabolism of indole-3-acetic acid in *Arabidopsis*. *Plant Physiol.* **1998**, *118*, 285–296. [[CrossRef](#)] [[PubMed](#)]
81. Kowalczyk, M.; Sandberg, G. Quantitative analysis of indole-3-acetic acid metabolites in *Arabidopsis*. *Plant Physiol.* **2001**, *127*, 1845–1853. [[CrossRef](#)] [[PubMed](#)]
82. Tanaka, K.; Hayashi, K.; Natsume, M.; Kamiya, Y.; Sakakibara, H.; Kawaide, H.; Kasahara, H. UGT74D1 catalyzes the glucosylation of 2-oxindole-3-acetic acid in the auxin metabolic pathway in *Arabidopsis*. *Plant Cell Physiol.* **2014**, *55*, 218–228. [[CrossRef](#)] [[PubMed](#)]
83. Porco, S.; Pěnčík, A.; Rashed, A.; Voš, U.; Casanova-Sáez, R.; Bishopp, A.; Golebiowska, A.; Bhosale, R.; Swarup, R.; Swarup, K.; et al. Dioxygenase-encoding *AtDAO1* gene controls IAA oxidation and homeostasis in *Arabidopsis*. *Proc. Natl. Acad. Sci. USA* **2016**, *113*, 11016–11021. [[CrossRef](#)] [[PubMed](#)]
84. Kai, K.; Horita, J.; Wakasa, K.; Miyagawa, H. Three oxidative metabolites of indole-3-acetic acid from *Arabidopsis thaliana*. *Phytochemistry* **2007**, *68*, 1651–1663. [[CrossRef](#)] [[PubMed](#)]

85. Zhao, Z.; Zhang, Y.; Liu, X.; Zhang, X.; Liu, S.; Yu, X.; Ren, Y.; Zheng, X.; Zhou, K.; Jiang, L.; et al. A role for a dioxygenase in auxin metabolism and reproductive development in rice. *Dev. Cell* **2013**, *27*, 113–122. [[CrossRef](#)] [[PubMed](#)]
86. Zhang, J.; Lin, J.E.; Harris, C.; Campos Mastrotti Pereira, F.; Wu, F.; Blakeslee, J.J.; Peer, W.A. DAO1 catalyzes temporal and tissue-specific oxidative inactivation of auxin in *Arabidopsis thaliana*. *Proc. Natl. Acad. Sci. USA* **2016**, *113*, 11010–11015. [[CrossRef](#)] [[PubMed](#)]
87. Mellor, N.; Band, L.R.; Pěnčík, A.; Novák, O.; Rashed, A.; Holman, T.; Wilson, M.H.; Voß, U.; Bishopp, A.; King, J.R.; et al. Dynamic regulation of auxin oxidase and conjugating enzymes AtDAO1 and GH3 modulates auxin homeostasis. *Proc. Natl. Acad. Sci. USA* **2016**, *113*, 11022–11027. [[CrossRef](#)] [[PubMed](#)]
88. Qin, G.; Gu, H.; Zhao, Y.; Ma, Z.; Shi, G.; Yang, Y.; Pichersky, E.; Chen, H.; Liu, M.; Chen, Z.; et al. An Indole-3-Acetic Acid Carboxyl Methyltransferase Regulates *Arabidopsis* Leaf Development. *Plant Cell* **2005**, *17*, 2693–2704. [[CrossRef](#)] [[PubMed](#)]
89. Abbas, M.; Hernández-García, J.; Pollmann, S.; Samodelov, S.L.; Kolb, M.; Friml, J.; Hammes, U.Z.; Zurbriggen, M.D.; Blázquez, M.A.; Alabadí, D. Auxin methylation is required for differential growth in *Arabidopsis*. *Proc. Natl. Acad. Sci. USA* **2018**, *115*, 6864–6869. [[CrossRef](#)] [[PubMed](#)]
90. Stepanova, A.N.; Alonso, J.M. Auxin catabolism unplugged: Role of IAA oxidation in auxin homeostasis. *Proc. Natl. Acad. Sci. USA* **2016**, *113*, 10742–10744. [[CrossRef](#)] [[PubMed](#)]
91. Swarup, R.; Friml, J.; Marchant, A.; Ljung, K.; Sandberg, G.; Palme, K.; Bennett, M. Localization of the auxin permease AUX1 suggests two functionally distinct hormone transport pathways operate in the *Arabidopsis* root apex. *Genes Dev.* **2001**, *15*, 2648–2653. [[CrossRef](#)] [[PubMed](#)]
92. Swarup, K.; Benková, E.; Swarup, R.; Casimiro, I.; Péret, B.; Yang, Y.; Parry, G.; Nielsen, E.; De Smet, I.; Vanneste, S.; et al. The auxin influx carrier LAX3 promotes lateral root emergence. *Nat. Cell Biol.* **2008**, *10*, 946–954. [[CrossRef](#)] [[PubMed](#)]
93. Krouk, G.; Lacombe, B.; Bielach, A.; Perrine-Walker, F.; Malinska, K.; Mounier, E.; Hoyerová, K.; Tillard, P.; Leon, S.; Ljung, K.; et al. Nitrate-regulated auxin transport by NRT1.1 defines a mechanism for nutrient sensing in plants. *Dev. Cell* **2010**, *18*, 927–937. [[CrossRef](#)] [[PubMed](#)]
94. Bouguyon, E.; Brun, F.; Meynard, D.; Kubeš, M.; Pervent, M.; Leran, S.; Lacombe, B.; Krouk, G.; Guiderdoni, E.; Zažímalová, E.; et al. Multiple mechanisms of nitrate sensing by *Arabidopsis* nitrate transporter NRT1.1. *Nat. plants* **2015**, *1*, 15015. [[CrossRef](#)] [[PubMed](#)]
95. Krouk, G. Hormones and nitrate: A two-way connection. *Plant Mol. Biol.* **2016**, *91*, 599–606. [[CrossRef](#)] [[PubMed](#)]
96. Li, R.; Li, J.; Li, S.; Qin, G.; Novák, O.; Pěnčík, A.; Ljung, K.; Aoyama, T.; Liu, J.; Murphy, A.S.; et al. ADP1 affects plant architecture by regulating local auxin biosynthesis. *PLoS Genet.* **2014**, *10*, e1003954. [[CrossRef](#)] [[PubMed](#)]
97. Tanaka, H.; Dhonukshe, P.; Brewer, P.B.; Friml, J. Spatiotemporal asymmetric auxin distribution: A means to coordinate plant development. *Cell. Mol. Life Sci.* **2006**, *63*, 2738–2754. [[CrossRef](#)] [[PubMed](#)]
98. Vieten, A.; Sauer, M.; Brewer, P.B.; Friml, J. Molecular and cellular aspects of auxin-transport-mediated development. *Trends Plant Sci.* **2007**, *12*, 160–168. [[CrossRef](#)] [[PubMed](#)]
99. Křeček, P.; Skůpa, P.; Libus, J.; Naramoto, S.; Tejos, R.; Friml, J.; Zažímalová, E. The PIN-FORMED (PIN) protein family of auxin transporters. *Genome Biol.* **2009**, *10*, 249. [[CrossRef](#)] [[PubMed](#)]
100. Petrášek, J.; Mravec, J.; Bouchard, R.; Blakeslee, J.J.; Abas, M.; Seifertová, D.; Wisniewska, J.; Tadele, Z.; Kubeš, M.; Covanová, M.; et al. PIN proteins perform a rate-limiting function in cellular auxin efflux. *Science* **2006**, *312*, 914–918. [[CrossRef](#)] [[PubMed](#)]
101. Wisniewska, J.; Xu, J.; Seifertová, D.; Brewer, P.B.; Růžička, K.; Blilou, I.; Rouquié, D.; Benková, E.; Scheres, B.; Friml, J. Polar PIN localization directs auxin flow in plants. *Science* **2006**, *312*, 883. [[CrossRef](#)] [[PubMed](#)]
102. Mravec, J.; Skůpa, P.; Bailly, A.; Hoyerová, K.; Křeček, P.; Bielach, A.; Petrášek, J.; Zhang, J.; Gaykova, V.; Stierhof, Y.-D.; et al. Subcellular homeostasis of phytohormone auxin is mediated by the ER-localized PIN5 transporter. *Nature* **2009**, *459*, 1136–1140. [[CrossRef](#)] [[PubMed](#)]
103. Dal Bosco, C.; Dovzhenko, A.; Palme, K. Intracellular auxin transport in pollen. *Plant Signal. Behav.* **2012**, *7*, 1504–1505. [[CrossRef](#)] [[PubMed](#)]
104. Bender, R.L.; Fekete, M.L.; Klinkenberg, P.M.; Hampton, M.; Bauer, B.; Malecha, M.; Lindgren, K.; Maki, J.; Perera, M.A.D.; Nikolau, B.J.; et al. PIN6 is required for nectary auxin response and short stamen development. *Plant J.* **2013**, *74*, 893–904. [[CrossRef](#)] [[PubMed](#)]

105. Sawchuk, M.G.; Edgar, A.; Scarpella, E. Patterning of leaf vein networks by convergent auxin transport pathways. *PLoS Genet.* **2013**, *9*, e1003294. [[CrossRef](#)] [[PubMed](#)]
106. Ganguly, A.; Lee, S.H.; Cho, M.; Lee, O.R.; Yoo, H.; Cho, H.-T. Differential Auxin-Transporting Activities of PIN-FORMED Proteins in *Arabidopsis* Root Hair Cells. *Plant Physiol.* **2010**, *153*, 1046–1061. [[CrossRef](#)] [[PubMed](#)]
107. Ganguly, A.; Park, M.; Kesawat, M.S.; Cho, H.-T. Functional Analysis of the Hydrophilic Loop in Intracellular Trafficking of *Arabidopsis* PIN-FORMED Proteins. *Plant Cell* **2014**, *26*, 1570–1585. [[CrossRef](#)] [[PubMed](#)]
108. Simon, S.; Skůpa, P.; Viaene, T.; Zwiewka, M.; Tejos, R.; Klíma, P.; Čarná, M.; Rolčik, J.; De Rycke, R.; Moreno, I.; et al. PIN6 auxin transporter at endoplasmic reticulum and plasma membrane mediates auxin homeostasis and organogenesis in *Arabidopsis*. *New Phytol.* **2016**, *211*, 65–74. [[CrossRef](#)] [[PubMed](#)]
109. Dhonukshe, P.; Aniento, F.; Hwang, I.; Robinson, D.G.; Mravec, J.; Stierhof, Y.-D.; Friml, J. Clathrin-mediated constitutive endocytosis of PIN auxin efflux carriers in *Arabidopsis*. *Curr. Biol.* **2007**, *17*, 520–527. [[CrossRef](#)] [[PubMed](#)]
110. Kleine-Vehn, J.; Dhonukshe, P.; Sauer, M.; Brewer, P.B.; Wiśniewska, J.; Paciorek, T.; Benková, E.; Friml, J. ARF GEF-dependent transcytosis and polar delivery of PIN auxin carriers in *Arabidopsis*. *Curr. Biol.* **2008**, *18*, 526–531. [[CrossRef](#)] [[PubMed](#)]
111. Geisler, M.; Aryal, B.; di Donato, M.; Hao, P. A Critical View on ABC Transporters and their interacting partners in auxin transport. *Plant Cell Physiol.* **2017**, *58*, 1601–1614. [[CrossRef](#)] [[PubMed](#)]
112. Dudler, R.; Hertig, C. Structure of an *mdr*-like gene from *Arabidopsis thaliana*. Evolutionary implications. *J. Biol. Chem.* **1992**, *267*, 5882–5888. [[PubMed](#)]
113. Sidler, M.; Hassa, P.; Hasan, S.; Ringli, C.; Dudler, R. Involvement of an ABC transporter in a developmental pathway regulating hypocotyl cell elongation in the light. *Plant Cell* **1998**, *10*, 1623–1636. [[CrossRef](#)] [[PubMed](#)]
114. Geisler, M.; Blakeslee, J.J.; Bouchard, R.; Lee, O.R.; Vincenzetti, V.; Bandyopadhyay, A.; Titapiwatanakun, B.; Peer, W.A.; Bailly, A.; Richards, E.L.; et al. Cellular efflux of auxin catalyzed by the *Arabidopsis* MDR/PGP transporter AtPGP1. *Plant J.* **2005**, *44*, 179–194. [[CrossRef](#)] [[PubMed](#)]
115. Terasaka, K.; Blakeslee, J.J.; Titapiwatanakun, B.; Peer, W.A.; Bandyopadhyay, A.; Makam, S.N.; Lee, O.R.; Richards, E.L.; Murphy, A.S.; Sato, F.; et al. PGP4, an ATP binding cassette P-glycoprotein, catalyzes auxin transport in *Arabidopsis thaliana* roots. *Plant Cell* **2005**, *17*, 2922–2939. [[CrossRef](#)] [[PubMed](#)]
116. Cho, M.; Lee, S.H.; Cho, H.-T. P-glycoprotein4 displays auxin efflux transporter-like action in *Arabidopsis* root hair cells and tobacco cells. *Plant Cell* **2007**, *19*, 3930–3943. [[CrossRef](#)] [[PubMed](#)]
117. Noh, B.; Murphy, A.S.; Spalding, E.P. Multidrug resistance-like genes of *Arabidopsis* required for auxin transport and auxin-mediated development. *Plant Cell* **2001**, *13*, 2441–2454. [[CrossRef](#)] [[PubMed](#)]
118. Blakeslee, J.J.; Bandyopadhyay, A.; Lee, O.R.; Mravec, J.; Titapiwatanakun, B.; Sauer, M.; Makam, S.N.; Cheng, Y.; Bouchard, R.; Adamec, J.; et al. Interactions among PIN-FORMED and P-Glycoprotein Auxin Transporters in *Arabidopsis*. *Plant Cell* **2007**, *19*, 131–147. [[CrossRef](#)] [[PubMed](#)]
119. Bandyopadhyay, A.; Blakeslee, J.J.; Lee, O.R.; Mravec, J.; Sauer, M.; Titapiwatanakun, B.; Makam, S.N.; Bouchard, R.; Geisler, M.; Martinoia, E.; et al. Interactions of PIN and PGP auxin transport mechanisms. *Biochem. Soc. Trans.* **2007**, *35*, 137–141. [[CrossRef](#)] [[PubMed](#)]
120. Geisler, M.; Kolukisaoglu, H.U.; Bouchard, R.; Billion, K.; Berger, J.; Saal, B.; Frangne, N.; Koncz-Kalman, Z.; Koncz, C.; Dudler, R.; et al. TWISTED DWARF1, a unique plasma membrane-anchored immunophilin-like protein, interacts with *Arabidopsis* multidrug resistance-like transporters AtPGP1 and AtPGP19. *Mol. Biol. Cell* **2003**, *14*, 4238–4249. [[CrossRef](#)] [[PubMed](#)]
121. Bailly, A.; Sovero, V.; Vincenzetti, V.; Santelia, D.; Bartnik, D.; Koenig, B.W.; Mancuso, S.; Martinoia, E.; Geisler, M. Modulation of P-glycoproteins by auxin transport inhibitors is mediated by interaction with immunophilins. *J. Biol. Chem.* **2008**, *283*, 21817–21826. [[CrossRef](#)] [[PubMed](#)]
122. Middleton, A.M.; Dal Bosco, C.; Chlap, P.; Bensch, R.; Harz, H.; Ren, F.; Bergmann, S.; Wend, S.; Weber, W.; Hayashi, K.-I.; et al. Data-driven modeling of intracellular auxin fluxes indicates a dominant role of the ER in controlling nuclear auxin uptake. *Cell Rep.* **2018**, *22*, 3044–3057. [[CrossRef](#)] [[PubMed](#)]
123. Miller, C.O.; Skoog, F.; Okumura, F.S.; Von Saltza, M.H.; Strong, F.M. Structure and synthesis of kinetin. *J. Am. Chem. Soc.* **1955**, *77*, 2662–2663. [[CrossRef](#)]
124. Miller, C.O.; Skoog, F.; Von Saltza, M.H.; Strong, F.M. Kinetin, a cell division factor from deoxyribonucleic acid. *J. Am. Chem. Soc.* **1955**, *77*, 1392. [[CrossRef](#)]

125. Horgan, R.; Hewett, E.W.; Purse, J.; Wareing, P.F. A new cytokinin from *Populus x robusta*. *Tetrahedron Lett.* **1973**, 2827–2828. [[CrossRef](#)]
126. Horgan, R.; Hewett, E.W.; Horgan, J.M.; Purse, J.; Wareing, P.F. A new cytokinin from *Populus x robusta*. *Phytochemistry* **1975**, *14*, 1005–1008. [[CrossRef](#)]
127. Strnad, M. The aromatic cytokinins. *Physiol. Plant.* **1997**, *101*, 674–688. [[CrossRef](#)]
128. Persson, B.C.; Esberg, B.; Olafsson, O.; Björk, G.R. Synthesis and function of isopentenyl adenosine derivatives in tRNA. *Biochimie* **1994**, *76*, 1152–1160. [[CrossRef](#)]
129. Davies, P.J. *Plant Hormones: Biosynthesis, Signal Transduction, Action!* 3rd ed.; Davies, P.J., Ed.; Kluwer Academic Publishers: Dordrecht, The Netherlands, 2010; ISBN 978-1-4020-2684-3.
130. Cortleven, A.; Schmülling, T. Regulation of chloroplast development and function by cytokinin. *J. Exp. Bot.* **2015**, *66*, 4999–5013. [[CrossRef](#)] [[PubMed](#)]
131. Armengot, L.; Marquès-Bueno, M.M.; Jaillais, Y. Regulation of polar auxin transport by protein and lipid kinases. *J. Exp. Bot.* **2016**, *67*, 4015–4037. [[CrossRef](#)] [[PubMed](#)]
132. Zürcher, E.; Müller, B. *Cytokinin Synthesis, Signaling, and Function—Advances and New Insights*; Elsevier: Amsterdam, The Netherlands, 2016; Volume 324, ISBN 9780128048078.
133. Romanov, G.A.; Lomin, S.N.; Schmülling, T. Cytokinin signaling: From the ER or from the PM? That is the question! *New Phytol.* **2018**. [[CrossRef](#)] [[PubMed](#)]
134. Kakimoto, T. Identification of plant cytokinin biosynthetic enzymes as dimethylallyl diphosphate:ATP/ADP isopentenyltransferases. *Plant Cell Physiol.* **2001**, *42*, 677–685. [[CrossRef](#)] [[PubMed](#)]
135. Takei, K.; Sakakibara, H.; Sugiyama, T. Identification of Genes Encoding Adenylate Isopentenyltransferase, a Cytokinin Biosynthesis Enzyme, in *Arabidopsis thaliana*. *J. Biol. Chem.* **2001**, *276*, 26405–26410. [[CrossRef](#)] [[PubMed](#)]
136. Miyawaki, K.; Tarkowski, P.; Matsumoto-Kitano, M.; Kato, T.; Sato, S.; Tarkowska, D.; Tabata, S.; Sandberg, G.; Kakimoto, T. Roles of *Arabidopsis* ATP/ADP isopentenyltransferases and tRNA isopentenyltransferases in cytokinin biosynthesis. *Proc. Natl. Acad. Sci. USA* **2006**, *103*, 16598–16603. [[CrossRef](#)] [[PubMed](#)]
137. Kasahara, H.; Takei, K.; Ueda, N.; Hishiyama, S.; Yamaya, T.; Kamiya, Y.; Yamaguchi, S.; Sakakibara, H. Distinct Isoprenoid Origins of *cis*- and *trans*-Zeatin Biosyntheses in *Arabidopsis*. *J. Biol. Chem.* **2004**, *279*, 14049–14054. [[CrossRef](#)] [[PubMed](#)]
138. Galichet, A.; Hoyerová, K.; Kamínek, M.; Gruissem, W. Farnesylation directs *AtIPT3* subcellular localization and modulates cytokinin biosynthesis in *Arabidopsis*. *Plant Physiol.* **2008**, *146*, 1155–1164. [[CrossRef](#)] [[PubMed](#)]
139. Takei, K.; Yamaya, T.; Sakakibara, H. *Arabidopsis* CYP735A1 and CYP735A2 encode cytokinin hydroxylases that catalyse the biosynthesis of *trans*-Zeatin. *J. Biol. Chem.* **2004**, *279*, 41866–41872. [[CrossRef](#)] [[PubMed](#)]
140. Kurakawa, T.; Ueda, N.; Maekawa, M.; Kobayashi, K.; Kojima, M.; Nagato, Y.; Sakakibara, H.; Kyozuka, J. Direct control of shoot meristem activity by a cytokinin-activating enzyme. *Nature* **2007**, *445*, 652–655. [[CrossRef](#)] [[PubMed](#)]
141. Kuroha, T.; Tokunaga, H.; Kojima, M.; Ueda, N.; Ishida, T.; Nagawa, S.; Fukuda, H.; Sugimoto, K.; Sakakibara, H. Functional analyses of LONELY GUY cytokinin-activating enzymes reveal the importance of the direct activation pathway in *Arabidopsis*. *Plant Cell* **2009**, *21*, 3152–3169. [[CrossRef](#)] [[PubMed](#)]
142. Jin, S.-H.; Ma, X.-M.; Kojima, M.; Sakakibara, H.; Wang, Y.W.; Hou, B.-K. Overexpression of glucosyltransferase UGT85A1 influences *trans*-zeatin homeostasis and *trans*-zeatin responses likely through O-glucosylation. *Planta* **2013**, *237*, 991–999. [[CrossRef](#)] [[PubMed](#)]
143. Šmehilová, M.; Dobrušková, J.; Novák, O.; Takáč, T.; Galuszka, P. Cytokinin-Specific Glycosyltransferases Possess Different Roles in Cytokinin Homeostasis Maintenance. *Front. Plant Sci.* **2016**, *7*, 1264. [[CrossRef](#)] [[PubMed](#)]
144. Brzobohatý, B.; Moore, I.; Kristoffersen, P.; Bako, L.; Campos, N.; Schell, J.; Palme, K. Release of active cytokinin by a beta-glucosidase localized to the maize root meristem. *Science* **1993**, *262*, 1051–1054. [[CrossRef](#)] [[PubMed](#)]
145. Moffatt, B.; Pethe, C.; Laloue, M. Metabolism of Benzyladenine is Impaired in a Mutant of *Arabidopsis thaliana* Lacking Adenine Phosphoribosyltransferase Activity1. *Plant Physiol.* **1991**, *95*, 900–908. [[CrossRef](#)] [[PubMed](#)]
146. Allen, M.; Qin, W.; Moreau, F.; Moffatt, B. Adenine phosphoribosyltransferase isoforms of *Arabidopsis* and their potential contributions to adenine and cytokinin metabolism. *Physiol. Plant.* **2002**, *115*, 56–68. [[CrossRef](#)] [[PubMed](#)]

147. Zhang, X.; Chen, Y.; Lin, X.; Hong, X.; Zhu, Y.; Li, W.; He, W.; An, F.; Guo, H. Adenine phosphoribosyl transferase 1 is a key enzyme catalyzing cytokinin conversion from nucleobases to nucleotides in *Arabidopsis*. *Mol. Plant* **2013**, *6*, 1661–1672. [[CrossRef](#)] [[PubMed](#)]
148. Mok, D.W.; Mok, M.C. Cytokinin metabolism and action. *Annu. Rev. Plant Physiol.* **2001**, *52*, 89–118. [[CrossRef](#)] [[PubMed](#)]
149. Pačes, V.; Werstiuk, E.; Hall, R.H. Conversion of *N*-(Delta-Isopentenyl)adenosine to adenosine by enzyme activity in tobacco tissue. *Plant Physiol.* **1971**, *48*, 775–778. [[CrossRef](#)] [[PubMed](#)]
150. Werner, T.; Köllmer, I.; Bartrina y Manns, I.; Holst, K.; Schmölling, T. New insights into the biology of cytokinin degradation. *Plant Biol.* **2006**, *8*, 371–381. [[CrossRef](#)] [[PubMed](#)]
151. Werner, T.; Motyka, V.; Laucou, V.; Smets, R.; Van Onckelen, H.A.; Schmölling, T. Cytokinin-deficient transgenic *Arabidopsis* plants show multiple developmental alterations indicating opposite functions of cytokinins in the regulation of shoot and root meristem activity. *Plant Cell* **2003**, *15*, 2532–2550. [[CrossRef](#)] [[PubMed](#)]
152. Schmölling, T.; Werner, T.; Riefler, M.; Krupková, E.; Bartrina y Manns, I. Structure and function of cytokinin oxidase/dehydrogenase genes of maize, rice, *Arabidopsis* and other species. *J. Plant Res.* **2003**, *116*, 241–252. [[CrossRef](#)] [[PubMed](#)]
153. Niemann, M.C.E.; Weber, H.; Hluska, T.; Leonte, G.; Anderson, S.M.; Novák, O.; Senes, A.; Werner, T. The cytokinin oxidase/dehydrogenase CKX1 is a membrane-bound protein requiring homooligomerization in the endoplasmic reticulum for its cellular activity. *Plant Physiol.* **2018**. [[CrossRef](#)] [[PubMed](#)]
154. Köllmer, I.; Novák, O.; Strnad, M.; Schmölling, T.; Werner, T. Overexpression of the cytosolic cytokinin oxidase/dehydrogenase (CKX7) from *Arabidopsis* causes specific changes in root growth and xylem differentiation. *Plant J.* **2014**, *78*, 359–371. [[CrossRef](#)] [[PubMed](#)]
155. Galuszka, P.; Popelková, H.; Werner, T.; Frébortová, J.; Pospíšilová, H.; Mik, V.; Köllmer, I.; Schmölling, T.; Frébort, I. Biochemical Characterization of Cytokinin Oxidases/Dehydrogenases from *Arabidopsis thaliana* Expressed in *Nicotiana tabacum* L. *J. Plant Growth Regul.* **2007**, *26*, 255–267. [[CrossRef](#)]
156. Kowalska, M.; Galuszka, P.; Frébortová, J.; Šebela, M.; Béréš, T.; Hluska, T.; Šmehilová, M.; Bilyeu, K.D.; Frébort, I. Vacuolar and cytosolic cytokinin dehydrogenases of *Arabidopsis thaliana*: Heterologous expression, purification and properties. *Phytochemistry* **2010**, *71*, 1970–1978. [[CrossRef](#)] [[PubMed](#)]
157. Corbesier, L.; Prinsen, E.; Jacquard, A.; Lejeune, P.; Van Onckelen, H.A.; Périlleux, C.; Bernier, G. Cytokinin levels in leaves, leaf exudate and shoot apical meristem of *Arabidopsis thaliana* during floral transition. *J. Exp. Bot.* **2003**, *54*, 2511–2517. [[CrossRef](#)] [[PubMed](#)]
158. Hirose, N.; Takei, K.; Kuroha, T.; Kamada-Nobusada, T.; Hayashi, H.; Sakakibara, H. Regulation of cytokinin biosynthesis, compartmentalization and translocation. *J. Exp. Bot.* **2008**, *59*, 75–83. [[CrossRef](#)] [[PubMed](#)]
159. Kudo, T.; Kiba, T.; Sakakibara, H. Metabolism and long-distance translocation of cytokinins. *J. Integr. Plant Biol.* **2010**, *52*, 53–60. [[CrossRef](#)] [[PubMed](#)]
160. Osugi, A.; Kojima, M.; Takebayashi, Y.; Ueda, N.; Kiba, T.; Sakakibara, H. Systemic transport of *trans*-zeatin and its precursor have differing roles in *Arabidopsis* shoots. *Nat. Plants* **2017**, *3*, 17112. [[CrossRef](#)] [[PubMed](#)]
161. Gillissen, B.; Bürkle, L.; André, B.; Kühn, C.; Rentsch, D.; Brandl, B.; Frommer, W.B. A new family of high-affinity transporters for adenine, cytosine, and purine derivatives in *Arabidopsis*. *Plant Cell* **2000**, *12*, 291–300. [[CrossRef](#)] [[PubMed](#)]
162. Wormit, A.; Traub, M.; Flörchinger, M.; Neuhaus, H.E.; Möhlmann, T. Characterization of three novel members of the *Arabidopsis thaliana* equilibrative nucleoside transporter (ENT) family. *Biochem. J.* **2004**, *383*, 19–26. [[CrossRef](#)] [[PubMed](#)]
163. Ko, D.; Kang, J.; Kiba, T.; Park, J.; Kojima, M.; Do, J.; Kim, K.Y.; Kwon, M.; Endler, A.; Song, W.-Y.; et al. *Arabidopsis* ABCG14 is essential for the root-to-shoot translocation of cytokinin. *Proc. Natl. Acad. Sci. USA* **2014**, *111*, 7150–7155. [[CrossRef](#)] [[PubMed](#)]
164. Zhang, K.; Novák, O.; Wei, Z.; Gou, M.; Zhang, X.; Yu, Y.; Yang, H.; Cai, Y.; Strnad, M.; Liu, C.-J. *Arabidopsis* ABCG14 protein controls the acropetal translocation of root-synthesized cytokinins. *Nat. Commun.* **2014**, *5*, 3274. [[CrossRef](#)] [[PubMed](#)]
165. Kiran, N.S.; Polanská, L.; Fohlerová, R.; Mazura, P.; Válková, M.; Šmeral, M.; Zouhar, J.; Malbeck, J.; Dobrev, P.I.; Macháčková, I.; et al. Ectopic over-expression of the maize β -glucosidase *Zm-p60.1* perturbs cytokinin homeostasis in transgenic tobacco. *J. Exp. Bot.* **2006**, *57*, 985–996. [[CrossRef](#)] [[PubMed](#)]

166. Bürkle, L.; Cedzich, A.; Döpke, C.; Stransky, H.; Okumoto, S.; Gillissen, B.; Kühn, C.; Frommer, W.B. Transport of cytokinins mediated by purine transporters of the PUP family expressed in phloem, hydathodes, and pollen of *Arabidopsis*. *Plant J.* **2003**, *34*, 13–26. [[CrossRef](#)] [[PubMed](#)]
167. Zürcher, E.; Liu, J.; di Donato, M.; Geisler, M.; Müller, B. Plant development regulated by cytokinin sinks. *Science* **2016**, *353*, 1027–1030. [[CrossRef](#)] [[PubMed](#)]
168. Sun, J.; Hirose, N.; Wang, X.; Wen, P.; Xue, L.; Sakakibara, H.; Zuo, J. *Arabidopsis* *SOI33/AtENT8* gene encodes a putative equilibrative nucleoside transporter that is involved in cytokinin transport in *Planta*. *J. Integr. Plant Biol.* **2005**, *47*, 588–603. [[CrossRef](#)]
169. Lomin, S.N.; Myakushina, Y.A.; Arkhipov, D. V.; Leonova, O.G.; Popenko, V.I.; Schmülling, T.; Romanov, G.A. Studies of cytokinin receptor–phosphotransmitter interaction provide evidences for the initiation of cytokinin signalling in the endoplasmic reticulum. *Funct. Plant Biol.* **2018**, *45*, 192. [[CrossRef](#)]
170. Kim, H.J.; Ryu, H.; Hong, S.H.; Woo, H.R.; Lim, P.O.; Lee, I.C.; Sheen, J.; Nam, H.-G.; Hwang, I. Cytokinin-mediated control of leaf longevity by AHK3 through phosphorylation of ARR2 in *Arabidopsis*. *Proc. Natl. Acad. Sci. USA* **2006**, *103*, 814–819. [[CrossRef](#)] [[PubMed](#)]
171. Caesar, K.; Thamm, A.M.K.; Withhöft, J.; Elgass, K.; Huppenberger, P.; Grefen, C.; Horak, J.; Harter, K. Evidence for the localization of the *Arabidopsis* cytokinin receptors AHK3 and AHK4 in the endoplasmic reticulum. *J. Exp. Bot.* **2011**, *62*, 5571–5580. [[CrossRef](#)] [[PubMed](#)]
172. Hwang, I.; Sheen, J. Two-component circuitry in *Arabidopsis* cytokinin signal transduction. *Nature* **2001**, *413*, 383–389. [[CrossRef](#)] [[PubMed](#)]
173. Punwani, J.A.; Hutchison, C.E.; Schaller, G.E.; Kieber, J.J. The subcellular distribution of the *Arabidopsis* histidine phosphotransfer proteins is independent of cytokinin signaling. *Plant J.* **2010**, *62*, 473–482. [[CrossRef](#)] [[PubMed](#)]
174. Mähönen, A.P.; Bishopp, A.; Higuchi, M.; Nieminen, K.M.; Kinoshita, K.; Törmäkangas, K.; Ikeda, Y.; Oka, A.; Kakimoto, T.; Helariutta, Y. Cytokinin signaling and its inhibitor AHP6 regulate cell fate during vascular development. *Science* **2006**, *311*, 94–98. [[CrossRef](#)] [[PubMed](#)]
175. Suzuki, T.; Sakurai, K.; Imamura, A.; Nakamura, A.; Ueguchi, C.; Mizuno, T. Compilation and characterization of histidine-containing phosphotransmitters implicated in His-to-Asp phosphorelay in plants: AHP signal transducers of *Arabidopsis thaliana*. *Biosci. Biotechnol. Biochem.* **2000**, *64*, 2486–2489. [[CrossRef](#)] [[PubMed](#)]
176. Kiba, T.; Taniguchi, M.; Imamura, A.; Ueguchi, C.; Mizuno, T.; Sugiyama, T. Differential expression of genes for response regulators in response to cytokinins and nitrate in *Arabidopsis thaliana*. *Plant Cell Physiol.* **1999**, *40*, 767–771. [[CrossRef](#)] [[PubMed](#)]
177. Mason, M.G.; Li, J.; Mathews, D.E.; Kieber, J.J.; Schaller, G.E. Type-B response regulators display overlapping expression patterns in *Arabidopsis*. *Plant Physiol.* **2004**, *135*, 927–937. [[CrossRef](#)] [[PubMed](#)]
178. D’Agostino Ingrid, B.; Deruère, J.; Kieber, J.J. Characterization of the response of the *Arabidopsis* response regulator gene family to cytokinin. *Plant Physiol.* **2000**, *124*, 1706–1717. [[CrossRef](#)]
179. Rashotte, A.M.; Carson, S.D.B.; To, J.P.C.; Kieber, J.J. Expression profiling of cytokinin action in *Arabidopsis*. *Plant Physiol.* **2003**, *132*, 1998–2011. [[CrossRef](#)] [[PubMed](#)]
180. To, J.P.C.; Haberer, G.; Ferreira, F.J.; Deruère, J.; Mason, M.G.; Schaller, G.E.; Alonso, J.M.; Ecker, J.R.; Kieber, J.J. Type-A *Arabidopsis* response regulators are partially redundant negative regulators of cytokinin signaling. *Plant Cell* **2004**, *16*, 658–671. [[CrossRef](#)] [[PubMed](#)]
181. Li, J.; Wang, D. Cloning and in vitro expression of the cDNA encoding a putative nucleoside transporter from *Arabidopsis thaliana*. *Plant Sci.* **2000**, *157*, 23–32. [[CrossRef](#)]
182. Möhlmann, T.; Mezher, Z.; Schwerdtfeger, G.; Neuhaus, H.E. Characterisation of a concentrative type of adenosine transporter from *Arabidopsis thaliana* (ENT1, *At*). *FEBS Lett.* **2001**, *509*, 370–374. [[CrossRef](#)]
183. Li, G.; Liu, K.; Baldwin, S.A.; Wang, D. Equilibrative nucleoside transporters of *Arabidopsis thaliana*. cDNA cloning, expression pattern, and analysis of transport activities. *J. Biol. Chem.* **2003**, *278*, 35732–35742. [[CrossRef](#)] [[PubMed](#)]
184. Jaquinod, M.; Villiers, F.; Kieffer-Jaquinod, S.; Hugouvieux, V.; Bruley, C.; Garin, J.; Bourguignon, J. A proteomics dissection of *Arabidopsis thaliana* vacuoles isolated from cell culture. *Mol. Cell. Proteom.* **2007**, *6*, 394–412. [[CrossRef](#)] [[PubMed](#)]

185. Petersson, S.V.; Johansson, A.I.; Kowalczyk, M.; Makoveychuk, A.; Wang, J.Y.; Moritz, T.; Grebe, M.; Benfey, P.N.; Sandberg, G.; Ljung, K. An auxin gradient and maximum in the *Arabidopsis* root apex shown by high-resolution cell-specific analysis of IAA distribution and synthesis. *Plant Cell* **2009**, *21*, 1659–1668. [[CrossRef](#)] [[PubMed](#)]
186. Antoniadis, I.; Plačková, L.; Simonovik, B.; Doležal, K.; Turnbull, C.; Ljung, K.; Novák, O. Cell-type-specific cytokinin distribution within the *Arabidopsis* primary root apex. *Plant Cell* **2015**, *27*, 1955–1967. [[CrossRef](#)] [[PubMed](#)]
187. Hayashi, K.; Nakamura, S.; Fukunaga, S.; Nishimura, T.; Jenness, M.K.; Murphy, A.S.; Motose, H.; Nozaki, H.; Furutani, M.; Aoyama, T. Auxin transport sites are visualized *in planta* using fluorescent auxin analogs. *Proc. Natl. Acad. Sci. USA* **2014**, *111*, 11557–11562. [[CrossRef](#)] [[PubMed](#)]
188. Bieleszová, K.; Pařízková, B.; Kubeš, M.; Husičková, A.; Kubala, M.; Ma, Q.; Sedlářová, M.; Robert, S.; Doležal, K.; Strnad, M.; et al. New fluorescently labeled auxins exhibit promising anti-auxin activity. *New Biotechnol.* **2018**. [[CrossRef](#)] [[PubMed](#)]
189. Kubiasová, K.; Mik, V.; Nisler, J.; Hönig, M.; Husičková, A.; Spíchal, L.; Pěkná, Z.; Šamajová, O.; Doležal, K.; Plíhal, O.; et al. Design, synthesis and perception of fluorescently labeled isoprenoid cytokinins. *Phytochemistry* **2018**, *150*, 1–11. [[CrossRef](#)] [[PubMed](#)]
190. Hošek, P.; Kubeš, M.; Laňková, M.; Dobrev, P.I.; Klíma, P.; Kohoutová, M.; Petrášek, J.; Hoyerová, K.; Jiřina, M.; Zažímalová, E. Auxin transport at cellular level: New insights supported by mathematical modelling. *J. Exp. Bot.* **2012**, *63*, 3815–3827. [[CrossRef](#)] [[PubMed](#)]



© 2018 by the authors. Licensee MDPI, Basel, Switzerland. This article is an open access article distributed under the terms and conditions of the Creative Commons Attribution (CC BY) license (<http://creativecommons.org/licenses/by/4.0/>).

EDITORIAL

Best practices in plant cytometry

Flow cytometry (FCM) and flow cytometric sorting (FCS) systems have developed as experimental tools of remarkable power and are enjoying an ever-increasing impact in the general field of biology.¹ Application of these tools to plant biology has developed more slowly given that the natural form of plants infrequently resembles that of the single cell suspension, prototypically the hematopoietic system that drove the original development of FCM/FCS. Nevertheless, these systems have had a profound influence at all levels of plant biology, from the study of single cells and subcellular organelles, to the behavior of populations of plants, and ultimately to the performance of ecosystems. It is safe to say their impact has not plateaued, as further applications of this unique technology are increasingly developed by innovative scientists around the world to address questions both in the basic sciences, and to increasingly confront emerging problems in the applied sector. For example, in addressing the challenges of sustainable production of sufficient food resources based on plant breeding involving ploidy-based approaches (e.g., induction of polyploidy)² for the needs of our future global citizens, FCM, and FCS systems will play central roles in this effort.

The degree to which FCM and FCS systems have impacted plant biology and applied agricultural sciences must not be understated. The major applications of DNA FCM are ploidy level and genome size estimations, and cell cycle analysis/endoreplication (with the later included in a lower percentage of studies). Indeed, FCM is currently/ extensively and almost exclusively employed as the method of choice for measurement of plant genome sizes.^{3,4} Measurements of this type impact agriculture in terms of ploidy estimation, with applications ranging from plant biotechnology, breeding and seed quality testing to taxonomy and population biology. They also impact the fundamental plant sciences in terms of biosystematics, ecology, evolution, genomics, and conservation, among other applications. One of the most startling observations of the angiosperms is the bandwidth occupied by genome size, which spans almost 2400-fold.

Flow sorting of higher plant chromosomes has provided invaluable information regarding the organization of DNA sequences within plant species. It has also greatly facilitated the process of whole-genome sequencing by permitting subdivision of large genomes into samples comprising entire chromosomes or chromosome arms.⁵ FCS methods applied to wall-less cells (protoplasts) expressing fluorescent proteins (FPs) in a cell type-specific manner have allowed elucidation of patterns of co-regulated gene expression and plant hormone gradients identification^{6,7} within organized tissues, such as roots.^{8,9}

The trigger to develop this virtual issue came from the publication, in 2017, of an article entitled “Guidelines for the use of flow cytometry and cell sorting in immunological studies” in the European Journal of Immunology.¹⁰ As noted in that article, one of the advantages of FCM/FCS systems is that they are relatively simple to implement, with some qualifications, which coupled with the development of user-friendly devices and software during the last 15 years led to increasing applications in other areas, such as plant sciences. However, it is also simple to implement and operate the instruments inappropriately. This calls for a comprehensive and collective summary of the best practices when applying FCM/FCS to plants, as was done for immunology.

The first consideration addresses the problem that plants, particularly the vascular plants, in their commonly recognized and utilized forms, exist not as single cell suspensions (typical of immunology) but as complex three-dimensional tissues comprising cells of irregular shapes, different types and functions, that collectively cooperate to produce the final plant form. Optimal methods for producing suspensions of cells, subcellular organelles and other components appropriate for FCM/FCS from these plant tissues and organs, are therefore one of the challenges discussed in this virtual issue. We are fully aware of the mantra that “junk in equals junk out” and having samples of the highest quality prior to FCM/FCS is a critical concern we also addressed here.

The second consideration relates to the vast variety of different plant species found globally, and the recognition of the consummate ability of plants to produce secondary metabolites/products, affecting DNA staining and resulting fluorescence. Again, methods for recognizing and handling the different challenges provided to FCM/FCS methods by the biochemistries of the source samples are required.

The third consideration focuses on the problem of addressing the non-critical application of FCM/FCS methods developed for mammalian cell systems (typically hematopoietic) to plants without careful consideration of their appropriateness. As it will be detailed in this virtual issue, application of FCM/FCS methods to mammalian cell systems almost exclusively occurs in the context of analysis of samples that comprise a majority, often close to 100%, of single cells in suspension. For plants, particularly when using these instruments and methods for the analysis of organelles in tissue homogenates, the objects of interest comprise a very minor subpopulation of the total particles passing through the instrument. Concepts such as placing initial gates around populations defined by forward scatter (FS) versus side scatter (SS), as routinely used to define leukocytes or other

mammalian cells in culture, are at best meaningless and at worst can seriously hamper proper use of the instruments to provide meaningful results. Again, plants are sources of many forms of autofluorescence; in vascular plants, chloroplasts are intensely fluorescent in the red due to the presence of chlorophyll. Phycoerythrin, a red protein-pigment complex from the light-harvesting phycobiliprotein family found in red algae and cryptophytes, is commercially employed as a fluorescent label for antibodies in cytometry. The presence of autofluorescence can restrict the wavelength bandwidths for fluorescence excitation and emission, and this can affect how best to set up FCM/FCS instruments.

In order to define and enunciate best practices, we drew together a network of volunteer authors, experienced in the application of FCM/FCS to plants. We have attempted to make this network as comprehensive as possible, to allow recommendations spanning all relevant life-forms, from the simplest photosynthetic microbes, to the more complex lower and vascular plants, and encompassing also the fungi. In this endeavor, we gratefully acknowledge the support of Wiley and Attila Tarnok, EIC of Cytometry.

As indicated for the Guidelines in Immunology article,⁹ we do wish to keep our recommendations updated. Therefore, please send us your critical comments, new ideas, practical suggestions regarding best practices, and new articles that could be useful for possible future versions of this virtual issue.

To end, we would like to remember that this virtual issue reflects the vision and dream of the late Jan Suda. He has been an inspiration for all of us, and, most certainly, he left us too soon. We are sure that his legacy will persist, not only in his home country, the Czech Republic, but also across the world. We sincerely hope this virtual issue of Cytometry Part A provides an appropriate tribute.

1 | SETTING THE STAGE

Describing how FCCS can be optimally applied to plants requires information in two general areas (a) concerning the samples being prepared and analyzed, in our case focusing on the relevant physical features of plants as organisms, and (b) concerning the instrumentation being used for this analysis, centering on sample requirements imposed by engineering design and implementation.

2 | VASCULAR AND NONVASCULAR PLANTS

Green plants (Viridiplantae) constitute a monophyletic clade within the tree of life and comprise oxygenic photosynthetic eukaryotes.¹¹ The group encompasses green algae and land plants, and further splits into major clades: the Chlorophyta,¹² comprising only algae, and Streptophyta formed by several algal groups (such as Zygnematophyceae and Charophyceae;)^{13,14} and the land plants (Embryophyta). Land plants further split into several groups: the possibly paraphyletic assemblage of three bryophyte lineages (Bryophyta—

mosses, Marchantiophyta—liverworts, and Anthocerotophyta—hornworts) and three sequentially-splitting lineages of vascular plants: lycopods (Lycopodiophyta), ferns and horsetails (Monilophyta) and seed plants (Spermatophyta). The latter group further splits into gymnosperms (Gymnospermae; i.e., conifers, cycads, *Ginkgo*, and gnetophytes) and angiosperms (Angiospermae;).¹⁵⁻¹⁷ The current review is primarily but not exclusively focused on flow cytometric applications in flowering plants, as they represent the most diverse and economically important, and therefore best studied, group of green plants. However, we mention the other green plant lineages where necessary and we also include other organisms that are found in various parts of the Tree of Life (algae in the traditional sense, fungi) and that share certain features of body organization and life style with plants (such as complex tissues or photosynthesis), and have for a long time been a subject of Botany in the broadest sense.

The life cycles of algal groups are highly variable and may comprise stages only with haplophasic (n) or diplophasic ($2n$) chromosome numbers, although in other species both stages are present but in separate generations.¹⁸ All land plants exhibit a characteristic life cycle which alternates between a haplophasic gametophyte and a diplophasic sporophyte. Still, the relative importance of each stage in the life cycle differs between groups: while the gametophyte stage dominates in bryophytes (and is usually the tissue that is analyzed by FCM), the sporophyte stage dominates in the vascular plant groups and is the main focus of flow cytometric investigations. Despite a significant reduction in the size of the gametophyte (comprising only up to 3–4 cells/nuclei in flowering plants), there are flow cytometric applications focused on either the independent gametophyte or the spores of ferns or on pollen grains of seed plants.¹⁹ Unlike vascular plants, fungal life cycles are mostly haplophasic, with a short (often single-celled) diplophasic stage, although most fungi (the Dikarya, i.e., the Ascomycota and the Basidiomycota) are dikaryotic ($n + n$) in part of their life cycles.

The evolution of plant genomes is dynamic, particularly in angiosperms, encompassing a range of genomic processes including multiple rounds of whole genome duplication (polyploidization,^{20,21} chromosomal rearrangements^{22,23} and the turnover and evolution of repetitive DNA (including mobile elements and satellite DNA).^{24,25} This is mirrored in the tremendous variation in nuclear genome sizes across green plants in general (c. 11,850-fold; 2) and flowering plants in particular (2,400-fold variation; 3,4). This has crucial implications for flow cytometric applications both with respect to technical issues (a series of internal standards of different genome size is required) and also as a study topic per se (e.g. what are the mechanisms driving genome size evolution?). Similarly, the relative content of AT versus GC base pairs is highly variable in green plants, although this variation does not strictly correlate with nuclear DNA-content (e.g., 26).

While the algal groups are mostly unicellular, or comprise a rather simple multicellular thallus (e.g., *Ulva*, *Cladophora*, or *Chara*), land plants form complex tissues and organs. The sporophyte of vascular plants typically differentiates into roots, stems and leaves (note that the floral parts of flowering plants are derived from the leaves). Similar (yet haplophasic and thus non-homologous) structures are found in

the gametophytes of bryophytes: rhizoids, cauloids, and phylloids. The specific morphology and anatomy of green plants, as distinct from other eukaryotes, naturally has multiple implications/challenges for flow cytometric analysis. Firstly, we encounter cells having thick cell walls that render flow cytometric analysis of individual cells impossible. Instead, isolated protoplast and, more commonly, nuclear suspensions are used for the analysis of plant tissues.^{26–28} Secondly, two types of endosymbiotic organelles, each with their own genomes, are present in most plant cells, mitochondria and plastids, and FCM applications have been designed to analyze those organelles.^{29–31} Lastly, plants present a wide array of chemical compounds, so-called secondary metabolites, conferring protection against factors both abiotic (e.g., UV-light, frost) and biotic (e.g., herbivores, parasites). Some of these chemical compounds (for example, tannins) directly co-interact with the DNA-binding stains used in FCM, and significantly affect the quality and reliability of such analyses.³²

3 | OVERVIEW OF INSTRUMENTATION AND PRINCIPLES

Flow cytometry and cytometric sorting systems are assembled from distinct engineering modules which collectively function to determine the optical properties of suspensions of biological particles, and selectively isolate these particles, or subsets thereof, for subsequent analysis and processing. The particles are typically constrained hydrodynamically within an aqueous stream to flow singly through regions of intense light, almost exclusively provided by lasers that are focused on the stream. On illumination, the particles absorb and scatter light and, if associated with fluorochromes, subsequently emit fluorescence. The intensities of the scattered and fluorescent light pulses coming from each particle are then measured. Key elements in these modules are (a) a flow cell, which spatially positions and aligns the flow stream containing the particles with the excitation light and detection axes, (b) light scatter and fluorescence detectors, screened by wavelength-appropriate filters and oriented orthogonally to the direction of the flow stream and the excitation light path, (c) electronic circuitry including analog-to-digital converters (ADCs) which convert the voltage pulses emerging from the detectors into digital values corresponding to the outputs from the individual particles, (d) computational architecture to process and store the information from these pulses for further analysis, or to use them immediately for processing sort-related decisions, and (e) mechanisms to implement individual, high-speed sorting of the particles, based on preselected combinations of optical characteristics.

One of the first implementations of flow sorting, and one of the most influential, was described by Bonner et al.³³ for characterization and isolation of various mammalian cell types including those of the hematopoietic system. To date, immunological applications represent the largest fraction of cytometric activities, worldwide. Most flow sorters employ a version of this original implementation, which involves precise conversion of the flow stream into a series of individual droplets, electromechanically synchronized to appear at a fixed

distance below the point of laser interception (Figure 1). Based on the degree of sample dilution, some of these droplets contain the cells of interest, and can be selectively displaced into collection vessels by a process of charging the droplet at the point of its detachment from the flow stream followed by passage through a fixed electrostatic field. The rates of sorting depend on the size of the cells, which determines the size of the flow tip, and the rate of flow of the fluid stream.³⁴

Advances in the area of instrument development have included multiplexed excitation and detection modalities to comprehensively cover the excitation and fluorescence emission spectra of the available fluorochromes.³⁵ Recently, spectral analysis has been demonstrated as an alternative to conventional light filters in FCM.^{36,37} Other advances include the use of flow tips that accommodate cells and biological particles that are larger, and sometimes much larger, than mammalian blood cells, drastic reductions in overall instrument sizes, footprints, and purchase costs, full replacement of analog by digital signal processing and the use of miniaturized fluidics systems with corresponding improvements in accuracy and reliability, and accompanied by reductions in costs of maintenance.

4 | RATIONALE AND TARGET

Flow cytometry and flow cytometric sorting are not new methods. However, their use in Plant Biology has grown dramatically in the last decades, and in some cases, such as genome size measurements, these technologies have come to dominate. At the same time, instruments and associated protocols continue to be improved and expanded (e.g., bead beating, the use of tissues other than leaves, dry tissue). The literature now includes many resources outlining methods, theoretical issues, and limitations of methods (e.g., the “Flow Cytometry with Plant Cells” book,³⁸ ESACP guidelines <http://www.classimed.de/esacflow.html>). However, despite this progress, it is clear from some recent publications that experimental design and manuscript review have not always kept pace with what we know about the application of FCM and cytometric sorting to plants, and this has adversely affected the quality of the results and the conclusions drawn.

Contributing factors include:

1. The practical need of carrying out experiments at centralized flow facilities that are not primarily concerned with, or understand, the characteristics of the input plant materials, or the types of questions (e.g., the large amounts of samples used in population biology) that are being addressed.
2. Effects of “lab culture,” in which poor practices that have become established in laboratories are taught to uncritical novices.
3. Recommendations for “best practices” being scattered across the existing scientific literature: thus, a comprehensive article summarizing key rules for the reliable application of FCM and FCS to plants is still lacking, even for widely used applications such as DNA content measurements (but see 28).

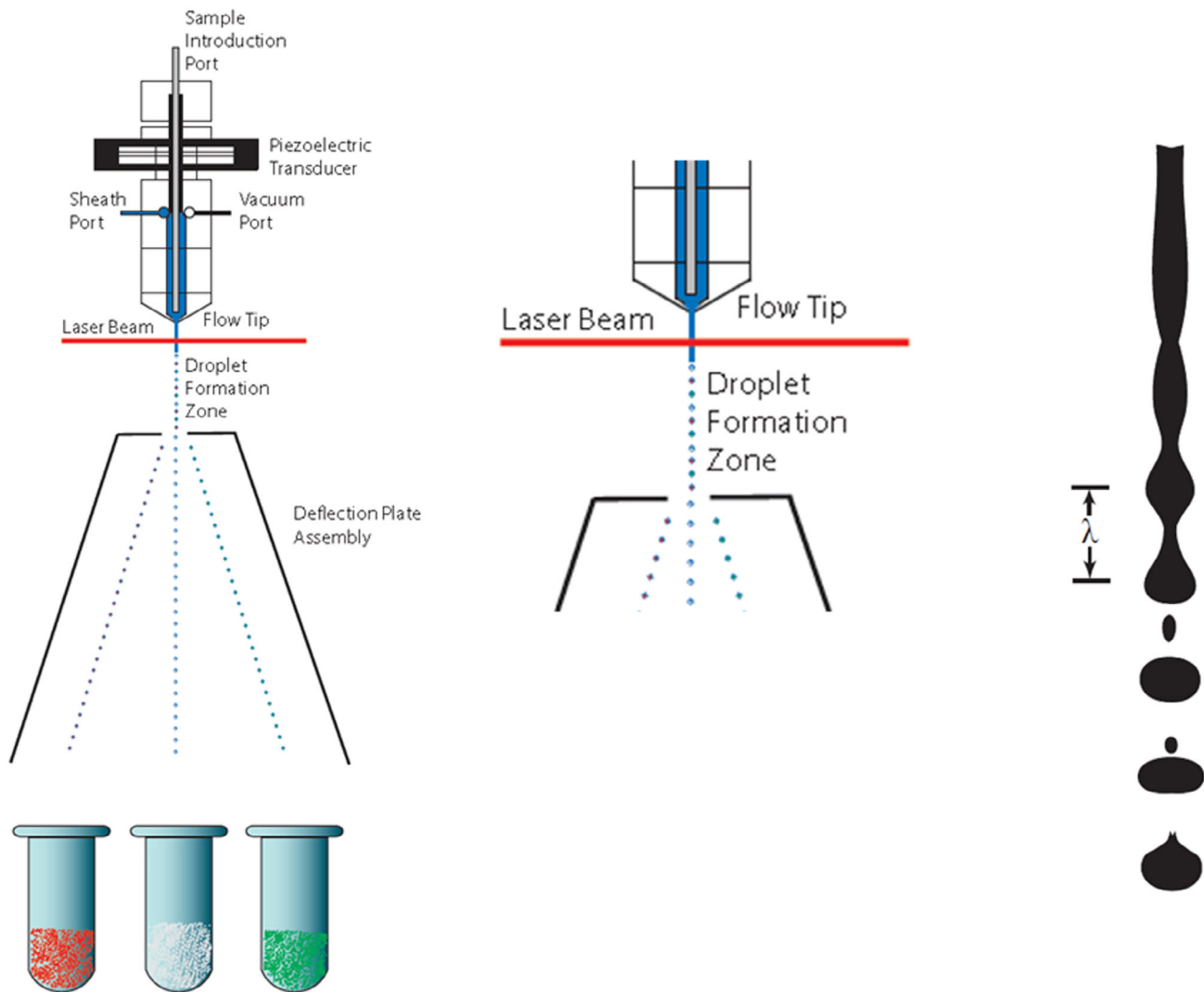


FIGURE 1 Schematic of the process of droplet formation for a typical droplet-in air flow sorter. Droplet formation is synchronized below the point of interception of the flow stream by the laser illumination. The undulation wavelength (λ) is defined by the velocity of the flow stream, and the drive frequency of the piezo-electric oscillator attached to the flow cell. A constant high DC voltage is maintained across the deflection plates. Precise switching of the charge applied to the flow stream at the time of droplet break-off retains that charge on the droplet, which then can be predictably deflected by the electric field

Examples of poor practices and erroneous theories developed as a consequence of these practices, identified by Jan Suda in the original draft, include flax genotrophs and problems with intraspecific variation reports, as reviewed in Greilhuber.³⁵ Recent tendencies in manuscripts to justify the use of dry tissue based on existing literature frequently lack acknowledgment of necessary precautions from the prior literature.

The main objective of this virtual issue is to outline key experimental issues and associated guidelines (under the heading of “Best Practices”) that researchers are recommended to follow, and to provide the rationale for these recommendations, such that the guidelines may be modified with confidence as new applications emerge. We also identify those areas where the establishment of clear guidelines will require additional empirical data or theoretical work. Such guidelines will benefit researchers, facility managers, journal editors,

and reviewers, since they should serve to guarantee high-quality results through elimination (or, at the very least, minimization) of artifactual variation from future research submitted for publication, as well as providing a means to identify artifacts within the published literature.

5 | THE SCOPE OF THIS VIRTUAL ISSUE IS

1. Applications based on the staining of DNA (ploidy, genome size, AT/GC content, cell cycle, including endoreduplication, nuclei and chromosome sorting) which represent a majority of uses.
2. Applications based on sorting single cells (protoplasts) and organelles (nuclei, mitochondria and plastids), based on use of FPs or fluorescent dyes in protoplast/organelle sorting for downstream

omics analyses at the cell-type-specific or organelle-specific level.

3. A focus predominantly on plants, but with separate sections devoted to algae, and to fungi. However, in many cases, the general principles should apply across all organisms; wherever possible, we will extrapolate to other organisms.

The emphasis will be on providing guidelines for reviewers and for experimental design. This will NOT be a methods virtual issue in the sense of providing protocols: these are well-covered elsewhere (e.g.,²⁷ “Flow Cytometry with Plant Cells” book,³⁸ the supplemental material of Kron et al.,³⁹ online resources).

KEYWORDS

best practices, chromosome analysis, cytometry, nuclear suspensions, plant sciences, protoplasts and organelle analysis, single cell suspensions

CONFLICT OF INTEREST

The authors have no conflicts of interest to declare.

AUTHOR CONTRIBUTIONS

David Galbraith: Conceptualization; writing-original draft; writing-review and editing. **João Loureiro:** Conceptualization; writing-original draft; writing-review and editing. **Ioanna Antoniadis:** Writing-review and editing. **Jillian Bainard:** Writing-review and editing. **Petr Bureš:** Writing-review and editing. **Petr Cápál:** Writing-review and editing. **Mariana Castro:** Writing-review and editing. **Sílvia Castro:** Writing-review and editing. **Martin Čertner:** Writing-review and editing. **Dora Čertnerová:** Writing-review and editing. **Zuzana Chumová:** Writing-review and editing. **Jaroslav Doležel:** Writing-review and editing. **Debora Giorgi:** Writing-review and editing. **Brian Husband:** Writing-review and editing. **Filip Kolar:** Writing-review and editing. **Petr Koutecký:** Writing-review and editing. **Paul Kron:** Writing-review and editing. **Ilia Leitch:** Writing-review and editing. **Karin Ljung:** Writing-review and editing. **Sara Lopes:** Writing-review and editing. **Magdalena Lučanová:** Writing-review and editing. **Sergio Lucretti:** Writing-review and editing. **Wen Ma:** Writing-review and editing. **Susanne Melzer:** Writing-review and editing. **István Molnár:** Writing-review and editing. **Ondřej Novák:** Writing-review and editing. **Nicole Poulton:** Writing-review and editing. **Vladimír Skalický:** Writing-review and editing. **Elwira Sliwinska:** Writing-review and editing. **Petr Šmarda:** Writing-review and editing. **Tyler Smith:** Writing-review and editing. **Guilin Sun:** Writing-review and editing. **Pedro Talhinas:** Writing-review and editing. **Attila Tárnok:** Writing-review and editing. **Eva Tamsch:** Writing-review and editing. **Pavel Trávníček:** Writing-review and editing. **Tomas Urfus:** Writing-review and editing.

David Galbraith^{1,2} 

João Loureiro³ 

Ioanna Antoniadis⁴

Jillian Bainard⁵

Petr Bureš⁶

Petr Cápál⁷

Mariana Castro³

Sílvia Castro³

Martin Čertner^{8,9}

Dora Čertnerová⁸

Zuzana Chumová^{8,9}

Jaroslav Doležel⁷

Debora Giorgi¹⁰

Brian C. Husband¹¹

Filip Kolár^{8,9}

Petr Koutecký¹²

Paul Kron¹¹ 

Ilia J. Leitch¹³

Karin Ljung⁴

Sara Lopes³

Magdalena Lučanová^{9,12}

Sergio Lucretti¹⁰

Wen Ma^{1,2}

Susanne Melzer^{14,15}

István Molnár⁷

Ondřej Novák^{4,16}

Nicole Poulton¹⁷

Vladimír Skalický¹⁶

Elwira Sliwinska¹⁸

Petr Šmarda⁶

Tyler W. Smith¹⁹

Guilin Sun^{1,2}

Pedro Talhinas²⁰

Attila Tárnok^{15,21,22}

Eva M. Tamsch²³

Pavel Trávníček⁹

Tomáš Urfus⁸

¹School of Plant Sciences, BIO5 Institute, Arizona Cancer Center, Department of Biomedical Engineering, University of Arizona, Tucson, Arizona, USA

²State Key Laboratory of Cotton Biology, Key Laboratory of Plant Stress Biology, Henan University, School of Life Sciences, State Key Laboratory of Crop Stress Adaptation and Improvement, Kaifeng, China

³Centre for Functional Ecology, Department of Life Sciences, University of Coimbra, Coimbra, Portugal

⁴Umeå Plant Science Centre, Department of Forest Genetics and Plant Physiology, Swedish University of Agricultural Sciences, Umeå, Sweden

⁵Swift Current Research and Development Centre, Agriculture and Agri-Food Canada, Swift Current, Saskatchewan, Canada

⁶Department of Botany and Zoology, Faculty of Science, Masaryk University, Brno, CZ, Czech Republic

⁷Institute of Experimental Botany of the Czech Academy of Sciences, Olomouc, Czech Republic

⁸Department of Botany, Faculty of Science, Charles University, Prague, Czech Republic

- ⁹Czech Academy of Sciences, Institute of Botany, Průhonice, Czech Republic
- ¹⁰Green Biotechnology Laboratory, Biotechnology and Agroindustry Division, Casaccia Research Center, ENEA - Italian National Agency for New Technologies, Energy and Sustainable Economic Development, Rome, Italy
- ¹¹Department of Integrative Biology, University of Guelph, Guelph, Ontario, Canada
- ¹²Department of Botany, Faculty of Science, University of South Bohemia, České Budějovice, Czech Republic
- ¹³Department of Comparative Plant and Fungal Biology, Royal Botanic Gardens, Richmond, UK
- ¹⁴Clinical Trial Centre Leipzig, University Leipzig, Leipzig, Germany
- ¹⁵LIFE-Leipzig Research Center for Civilization Diseases, University of Leipzig, Leipzig, Germany
- ¹⁶Laboratory of Growth Regulators, Institute of Experimental Botany of the Czech Academy of Sciences and Faculty of Science of Palacký University, Olomouc, Czech Republic
- ¹⁷Center for Aquatic Cytometry, Bigelow Laboratory for Ocean Sciences, East Boothbay, Maine, USA
- ¹⁸Laboratory of Molecular Biology and Cytometry, Department of Agricultural Biotechnology, UTP University of Science and Technology, Bydgoszcz, Poland
- ¹⁹Ottawa Research and Development Centre, Agriculture and Agri-Food Canada, Ottawa, Ontario, Canada
- ²⁰LEAF, Linking Landscape, Environment, Agriculture and Food, Instituto Superior de Agronomia, Universidade de Lisboa, Lisbon, Portugal
- ²¹Department of Precision Instruments, Tsinghua University, Beijing, China
- ²²Department for Therapy Validation, Fraunhofer Institute for Cell Therapy and Immunology IZI, Leipzig, Germany
- ²³Department of Botany and Biodiversity Research, University of Vienna, Vienna, Austria

Correspondence

David Galbraith, School of Plant Sciences, BIO5 Institute, Arizona Cancer Center, Department of Biomedical Engineering, University of Arizona, Tucson, AZ, 85721.
 Email: galbraith@email.arizona.edu

David Galbraith and João Loureiro contributed equally to this work.

ORCID

David Galbraith  <https://orcid.org/0000-0003-4020-1635>

João Loureiro  <https://orcid.org/0000-0002-9068-3954>

Paul Kron  <https://orcid.org/0000-0002-1734-5019>





REFERENCES

- Shapiro HM. Practical flow cytometry. 4th ed. New York: John Wiley & Sons Inc.; 2003 736 p.
- Touchell DH, Palmer IE, Ranney TG. In vitro ploidy manipulation for crop improvement. *Front Plant Sci.* 2020;11:722.
- Leitch I, Johnston E, Pellicer J, Hidalgo O, Bennett M. Plant DNA C-values Database (Release 7.1). 2020. <https://cvalues.science.kew.org/>.
- Pellicer J, Leitch IJ. The plant DNA C-values database (release 7.1): an updated online repository of plant genome size data for comparative studies. *New Phytol.* 2020;226:301–5.
- Appels R, Eversole K, Feuillet C, Keller B, Rogers J, Stein N, et al. Shifting the limits in wheat research and breeding using a fully annotated reference genome. *Science.* 2018;36(1):eaar7191.
- Petersson SV, Johansson AI, Kowalczyk M, Makoveychuk A, Wang JY, Moritz T, et al. An auxin gradient and maximum in the Arabidopsis root apex shown by high-resolution cell-specific analysis of IAA distribution and synthesis. *Plant Cell.* 2009;21:1659–68.
- Antoniadi I, Plačková L, Simonovik B, Doležal K, Turnbull C, Ljung K, et al. Cell-type-specific cytokinin distribution within the Arabidopsis primary root apex. *Plant Cell.* 2015;27:1955–67.
- Birnbaum K, Shasha DE, Wang JY, Jung JW, Lambert GM, Galbraith DW, et al. A gene expression map of the Arabidopsis root. *Science.* 2003;302:1956–60.
- Brady SM, Orlando DA, Lee JY, Wang JY, Koch J, Dinneny JR, et al. A high-resolution root spatiotemporal map reveals dominant expression patterns. *Science.* 2007;318:801–6.
- Cossarizza A, Chang HD, Radbruch A, Akdis M, Andrä I, Annunziato F, et al. Guidelines for the use of flow cytometry and cell sorting in immunological studies. *Eur J Immunol.* 2017;47:1584–797.
- Leliaert F, Smith DR, Moreau H, Herron MD, Verbruggen H, Delwiche CF, et al. Phylogeny and molecular evolution of the green algae. *CRC Crit Rev Plant Sci.* 2012;31:1–46.
- Ruggiero MA, Gordon DP, Orrell TM, Bailly N, Bourgoin T, Brusca RC, et al. Kirk PM. A higher level classification of all living organisms. *PLoS One.* 2015;10:e0130114.
- Cheng S, Xian W, Fu Y, Marin B, Keller J, Wu T, et al. Genomes of subaerial Zygnematophyceae provide insights into land plant evolution. *Cell.* 2019;179:1057–1067.e14.
- Guiry MD, Guiry GM. AlgaeBase. World-wide electronic publication. National University of Ireland, Galway. <http://www.algaebase.org/>. 2019.
- Ruhfel BR, Gitzendanner MA, Soltis PS, Soltis DE, Burleigh JG. From algae to angiosperms—inferring the phylogeny of green plants (Viridiplantae) from 360 plastid genomes. *BMC Evol Biol.* 2014;14:23.
- Gitzendanner MA, Soltis PS, Wong GKS, Ruhfel BR, Soltis DE. Plastid phylogenomic analysis of green plants: a billion years of evolutionary history. *Am J Bot.* 2018;105:291–301.
- Leebens-Mack JH, Barker MS, Carpenter EJ, Deyholos MK, Gitzendanner MA, Graham SW, Grosse I, Li Z, Melkonian M, Mirarab S, Porsch M, Quint M, Rensing SA, Soltis DE, Soltis PS, Stevenson DW, Ullrich KK, Wickert NJ, De Gironimo L, Edger PP, Jordon-Thaden IE, Joya S, Liu T, Melkonian B, Miles NW, Pokorny L, Quigley C, Thomas P, Villarreal JC, Augustin MM, Barrett MD, Baucom RS, Beerling DJ, Benstein RM, Biffin E, Brockington SF, Burge DO, Burris JN, Burris KP, Burtet-Sarramegna V, Caicedo AL, Cannon SB, Çebi Z, Chang Y, Chater C, Cheeseman JM, Chen T, Clarke ND, Clayton H, Covshoff S, Crandall-Stotler BJ, Cross H, de Pamphilis CW, Der JP, Determann R, Dickson RC, Di Stilio VS, Ellis S, Fast E, Feja N, Field KJ, Filatov DA, Finnegan PM, Floyd SK, Fogliani B, García N, Gâteblé G, Godden GT, Goh F, Qi Y, Greiner S, Harkess A, Heaney JM, Helliwell KE, Heyduk K, Hibberd JM, Hodel RGJ, Hollingsworth PM, Johnson MTJ, Jost R, Joyce B, Kapralov MV., Kazamia E, Kellogg EA, Koch MA, Von Konrat M, Könyves K, Kutchan TM, Lam V, Larsson A, Leitch AR, Lertz R, Li FW, Lowe AJ, Ludwig M, Manos PS, Mavrodiev E, McCormick MK, McKain M, et al. One thousand plant transcriptomes and the phylogenomics of green plants. *Nature* 2019;574:679–685.

18. Figueroa RI, Estrada M, Garcés E. Life histories of microalgal species causing harmful blooms: haploids, diploids and the relevance of benthic stages. *Harmful Algae*. 2018;73:44–57.
19. Kron P, Husband BC. Using flow cytometry to estimate pollen DNA content: improved methodology and applications. *Ann Bot*. 2012;110:1067–78.
20. Wendel JF. The wondrous cycles of polyploidy in plants. *Am J Bot*. 2015;102:1753–6.
21. Van De Peer Y, Mizrachi E, Marchal K. The evolutionary significance of polyploidy. *Nat Rev Genet*. 2017;18:411–24.
22. Lysák MA, Schubert I. Mechanisms of chromosome rearrangements. In: Greilhuber J, Doležel J, Wendel J, editors. *Plant genome diversity*. Volume 2. Vienna: Springer; 2013. p. 137–47.
23. Mandáková T, Lysak MA. Post-polyploid diploidization and diversification through dysploid changes. *Curr Opin Plant Biol*. 2018;42:55–65.
24. Kejnovsky E, Hawkins JS, Feschotte C. Plant transposable elements: biology and evolution. In: Wendel J, Greilhuber J, Doležel J, Wendel J, Leitch I, editors. *Plant genome diversity*. Volume 21. Vienna: Springer; 2012. p. 17–34.25.
25. Šmarda P, Bureš P, Horová L, Leitch IJ, Mucina L, Pacini E, et al. Ecological and evolutionary significance of genomic GC content diversity in monocots. *Proc Natl Acad Sci U S A*. 2014;111:E4096–102.
26. Galbraith DW, Harkins KR, Maddox JM, Ayres NM, Sharma DP, Firoozabady E. Rapid flow cytometric analysis of the cell cycle in intact plant tissues. *Science*. 1983;220:1049–51.
27. Doležel J, Greilhuber J, Suda J. Estimation of nuclear DNA content in plants using flow cytometry. *Nat Protoc*. 2007;2:2233–44.
28. Li ZY, Xia GM, Chen HM, Guo GQ. Plant regeneration from protoplasts derived from embryogenesis suspension cultures of wheat (*Triticum aestivum* L.). *J. Plant Physiol*. 1992;139:714–8.
29. Monteiro LDB, Davanzo GG, De Aguiar CF, Moraes-Vieira PMM. Using flow cytometry for mitochondrial assays. *MethodsX*. 2020;7:100938.
30. Rowan BA, Oldenburg DJ, Bendich AJ. A high-throughput method for detection of DNA in chloroplasts using flow cytometry. *Plant Methods*. 2007;3:5.
31. Rodríguez E, Azevedo R, Costa A, Serôdio J, Santos C. Chloroplast functionality assessment by flow cytometry: case study with pea plants under Paraquat stress. *Photosynthetica*. 2012;50:197–205.
32. Loureiro J, Rodríguez E, Doležel J, Santos C. Flow cytometric and microscopic analysis of the effect of tannic acid on plant nuclei and estimation of DNA content. *Ann Bot*. 2006;98:515–27.
33. Bonner WA, Hulett HR, Sweet RG, Herzenberg LA. Fluorescence activated cell sorting. *Rev Sci Instrum*. 1972;43:404–9.
34. Galbraith DW, Lucretti S. Large particle sorting. In: Radbruch A, editor. *Flow Cytometry and cell sorting*. Berlin, Heidelberg: Springer; 2000. p. 293–317.
35. Nettey L, Giles AJ, Chattopadhyay PK. OMIP-050: a 28-color/30-parameter fluorescence flow Cytometry panel to enumerate and characterize cells expressing a wide Array of immune checkpoint molecules. *Cytom Part A*. 2018;93:1094–6.
36. Nolan JP, Condello D. Spectral flow cytometry. *Curr Protoc Cytom*. 2013;63:1.27.1–1.27.13.
37. Hawley TS, Hawley RG, Telford WG. Fluorescent proteins for flow cytometry. *Curr Protoc Cytom*. 2017;2017:9.12.1–9.12.20.
38. Doležel J, Greilhuber J, Suda J. *Flow Cytometry with plant cells: analysis of genes, chromosomes and genomes*. Wiley-VCH Verlag: Weinheim; 2007. p. 454.
39. Kron P, Suda J, Husband BC. Applications of flow cytometry to evolutionary and population biology. *Annu Rev Ecol Evol Syst*. 2007;38:847–76.

REVIEW ARTICLE

Fluorescence activated cell sorting—A selective tool for plant cell isolation and analysis

Ioanna Antoniadi¹  | Vladimír Skalický² | Guiling Sun⁴ | Wen Ma⁴ |
 David W. Galbraith^{3,4}  | Ondřej Novák^{1,2}  | Karin Ljung¹ 

¹Umeå Plant Science Center, Department of Forest Genetics and Plant Physiology, Swedish University of Agricultural Sciences, Umeå, Sweden

²Laboratory of Growth Regulators, Institute of Experimental Botany, The Czech Academy of Sciences and Faculty of Science, Palacký University, Olomouc, Czech Republic

³Department of Biomedical Engineering, University of Arizona, School of Plant Sciences, BIO5 Institute, Arizona Cancer Center, Tucson, Arizona, USA

⁴School of Life Sciences, Henan University, Institute of Plant Stress Biology, Kaifeng, China

Correspondence

Karin Ljung, Umeå Plant Science Center, Department of Forest Genetics and Plant Physiology, Swedish University of Agricultural Sciences, SE-901 83 Umeå, Sweden.
 Email: karin.ljung@slu.se

Funding information

Chinese National Key Research and Development Program, the National Natural Science Foundation of China, the Program for Innovative Research Teams in Science and Technology at a University of Henan Province, and the 111 Project of China; Czech Foundation Agency, Grant/Award Number: GA17-21581Y; Endowment fund of Palacký University in Olomouc; European Molecular Biology Organization, Grant/Award Number: EMBO ASTF 297-2013; Internal Grant Agency of Palacký University, Grant/Award Number: IGA_PrF_2021_011; Kempestiftelserna; Ministry of Education, Youth and Sport of the Czech Republic via the ERDF project “Plants as a tool for sustainable global development”, Grant/Award Number: CZ.02.1.01/0.0/0.0/16_019/0000827; Plant Fellows (the International Post doc Fellowship Programme in Plant Sciences, Grant/Award Number: 267423; the Knut and Alice Wallenberg Foundation (KAW); the Swedish Governmental Agency for Innovation Systems (Vinnova); the Swedish Research Council; University of Arizona College of Agriculture and Life Sciences

Abstract

Instrumentation for flow cytometry and sorting is designed around the assumption that samples are single-cell suspensions. However, with few exceptions, higher plants comprise complex multicellular tissues and organs, in which the individual cells are held together by shared cell walls. Single-cell suspensions can be obtained through digestion of the cells walls and release of the so-called protoplasts (plants without their cell wall). Here we describe best practices for protoplast preparation, and for analysis through flow cytometry and cell sorting. Finally, the numerous downstream applications involving sorted protoplasts are discussed.

KEYWORDS

autofluorescence, best practices, plant flow cytometry and sorting, protoplasts, viability and integrity

This is an open access article under the terms of the Creative Commons Attribution-NonCommercial License, which permits use, distribution and reproduction in any medium, provided the original work is properly cited and is not used for commercial purposes.

© 2021 The Authors. *Cytometry Part A* published by Wiley Periodicals LLC on behalf of International Society for Advancement of Cytometry.

1 | PROTOPLAST PREPARATION

Flow cytometric analysis and flow sorting in higher plants requires production of single cell suspensions from three-dimensional tissues and organs comprising multiple interconnected cell types of different function. This is achieved by the digestion of the plant cell walls using microbial enzymes that degrade cellulose, hemicelluloses, and pectin, in the presence of a slightly hypertonic osmoticum such as mannitol. Incubation of the plant tissue in the presence of the cell wall degrading enzymes releases the protoplasts, living plant cells without cell wall, and form a single cell suspension. The released protoplasts can then be pelleted using low centrifugal forces, and re-suspended in the osmoticum (Figure 1).

The preparation of protoplasts, first described in 1960 [1], has since that time been tailored to the plant species, the tissue under study, and the developmental stage of the plant. As a consequence, a large number of protocols for protoplast isolation have been developed [2–8]. In protoplast preparation, variable factors between protocols concern mainly the components of the digestion mixture (composition and concentrations) and the incubation conditions [9–12]. Obtaining healthy and unstressed protoplasts derived from all

the layers of the tissue under study is a key consideration in terms of the efficiency, accuracy, and relevance of flow cytometry and sorting. Protoplast production issues associated with organ type and structure include the obvious, for example, that some organ elements such as mature xylem elements and phloem sieve tubes lack cellular structures that can emerge as protoplasts. Other issues include that the protoplast preparation solutions may not access equally all internal cell types within organized tissues, will penetrate epidermal surfaces covered with waxy cuticles less easily as compared, for example, to the root, and will differ in effectiveness depending on cell wall composition. These issues further relate to the means whereby the starting tissues are prepared, for example whether as sterile plantlets in culture, as plants in growth chambers, as greenhouse-grown materials, or as field materials. Sterile plantlets in culture containers experience very high levels of humidity, which reduces the accumulation of waxes on aerial surfaces, thereby improving access of the protoplasting solutions. Tissue digestibility of organs can also be a function of developmental age and prior manipulation; for example, an initial sampling of leaves can induce systemic wound responses in samples subsequently taken, with notable changes in protoplast release and overall production. Best-practice recommendations include precisely defining the

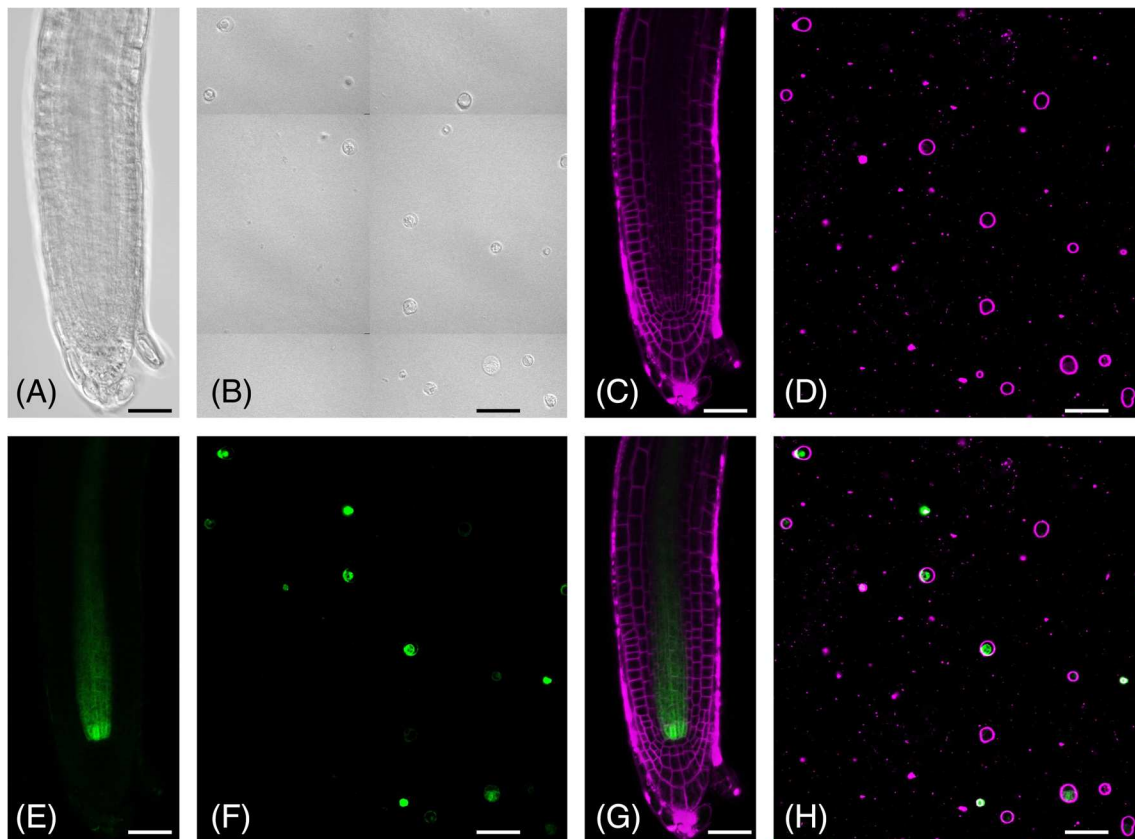


FIGURE 1 Protoplast preparation from the pWOL:GFP transgenic Arabidopsis line. Six-day-old pWOL:GFP seedlings were transferred to microscope slides (A, C, E, and G), while the remaining seedling roots were enzymatically digested to release their corresponding protoplasts (B, D, F, and H). The pWOL:GFP-derived protoplasts are shown in bright field (A and B), according to their fluorescence after staining with the FM4–64 plasma membrane dye (C and D), and their endogenous GFP fluorescence (E and F). G and H provide the merged fluorescent images. Scale bar is 50 μ m

growth conditions of the starting plant materials used for protoplast preparation and employing consistent methods for sampling, manipulating, and incubating these materials in the enzyme solutions.

Following digestion of the cell walls, the emerging protoplasts are osmosensitive, fragile structures (Figure 1). They are also generally larger in diameter than the mammalian cells of the hematopoietic system, around which flow cytometry instruments were originally designed. They therefore should be manipulated with extreme care in order to maintain their integrity. The first step is passage through a nylon filter (these are commercially available with defined mesh sizes from 20 μm upwards, and should evidently be selected dependent on average protoplast diameter) to remove undigested materials. This is followed by centrifugation and washing steps to eliminate residual enzymes, organelles, and other undesired contaminants. Crucial to maintaining protoplast integrity is centrifugation at very low speed in round-bottomed tubes, using a swing out centrifuge rotor, followed by gentle resuspension using wide bore pipette tips. This is one of the most common features found in all protoplast isolation protocols. Less common, but equally important, is purification of the viable protoplasts from the general tissue digest. Sucrose step-gradient flotation via low-speed centrifugation is a convenient way to selectively concentrate viable protoplasts [13, 14]. This step is significantly improving the efficiency, accuracy, and relevance of downstream applications.

After resuspension in the selected resuspension medium, the isolated protoplasts should be finally filtered through a nylon mesh filter of appropriate size to accommodate the average diameters of the protoplasts, prior to sample injection into the cytometer [10, 15]. Protoplasts can be analyzed directly after isolation, but it may be necessary to culture them for longer periods of time, for example to allow gene expression after transfection. Over prolonged culture periods, under optimal conditions, cell wall regeneration will occur, followed by cell expansion and cell division. Since this is not conducive to flow

cytometric analyses of single cells, addition of 2,4-dichlorobenzoic acid can be used to specifically inhibit cell wall regeneration without deleterious effects on cellular metabolism [16]. At all stages, protoplast viability should be determined using fluorescent staining protocols [17–19]. Viability can be measured according to accumulation of a positive signal by viable protoplasts, for example by staining with fluorescein diacetate (FDA, Figure 2, [17–19]). In this case, FDA, which is non-fluorescent and readily permeable to the plasma membrane, is hydrolysed by cytoplasmic esterases to produce fluorescein, which is highly fluorescent, and significantly less permeable to the plasma membrane than FDA. Thus, viable protoplasts accumulate fluorescence, albeit transiently. According to the dye's emission signal and its permeability properties through the plasma membrane, the selection of intact, viable protoplasts for analysis or sorting can also be achieved based on the ability of the intact plasma membrane of viable protoplasts to exclude nuclear staining by 4',6-diamidino-2-phenylindole (DAPI), Hoechst, and/or propidium iodide (PI). Positive and negative viability staining can be combined [20, 21], as illustrated in Figure 2 using FDA and PI. Several additional viability dyes are now commercially available.

In all of these cases, a best practice recommendation is to always include photographic documentation of the protoplast suspension immediately prior to flow analysis.

2 | ENDOGENOUS AND ACQUIRED PROTOPLASTS' FLUORESCENCE

For the desired cell populations to be analyzed using flow cytometry and isolated through sorting, optical signals are required. These are of two types, light that is scattered and detected either parallel to or orthogonally to the excitation beam path, and light emitted as

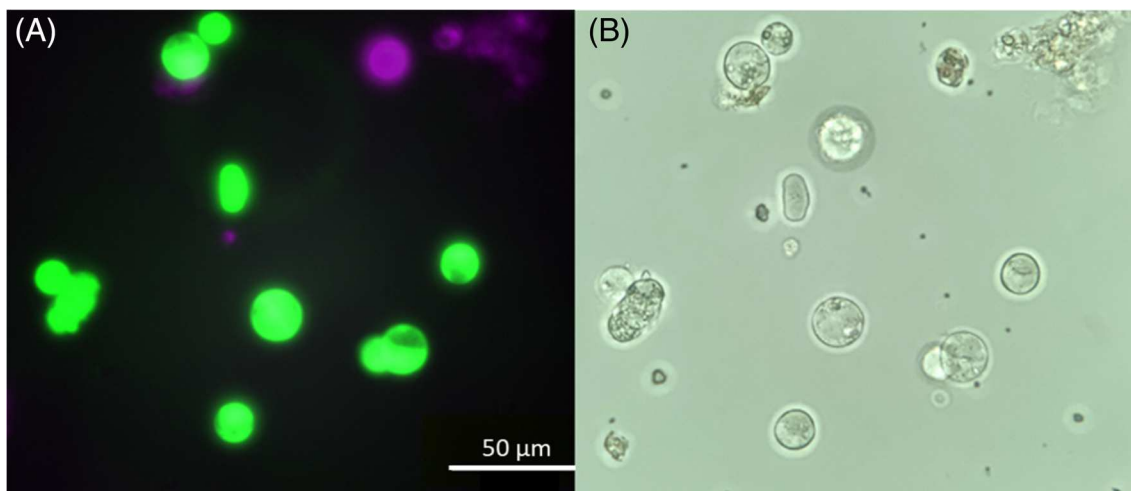


FIGURE 2 Maize epidermal protoplast viability determination via counterstaining with fluorescein diacetate (FDA) and propidium iodide (PI). (A) Protoplasts were stained with 0.20 μM FDA and 74.8 μM PI. Viable protoplasts transiently retain fluorescein, staining green. The plasma membrane of viable protoplasts excludes PI from accessing the nucleus, non-viable protoplasts therefore staining red. Fluorescence microscopy, bar = 50 μm . (B) The same sample under bright-field illumination

fluorescence. Plant protoplasts, as for all cells, contain endogenous compounds that emit autofluorescence when excited, excitation being particularly notable at shorter laser wavelengths [20, 21] (Table 1). Protoplasts derived from green tissues (aerial organs) display high levels of autofluorescence from chlorophyll due to excitation of photopigments within the chloroplasts (Table 1). Taking the above into consideration, fluorophores selection during experimental design is a crucial process that should aim to the reduction of spectra overlap.

Further fluorescent tags can be incorporated into the experimental design by transgenic expression of fluorescent macromolecules (cf. the Fluorescent Proteins; see below) following protoplast transfection or generation of stable transformed lines. As compared to the production of stable transgenic lines, transfection is more fast, efficient, direct, and well-established for some specific cell types, for example mesophyll protoplasts [4]. However, the process of transfection is stressful, and additional centrifugation steps are generally required prior to flow sorting. Another limitation of transfection is that efficiencies could vary depending on the tissue or on the plant species.

An alternative method for fluorescent tagging involves staining with exogenous fluorochromes, either in the form of directly reactive species [22, 23], or fluorescent compounds that can be taken up by the plant as fluorescent hormone analogues [24] or attached to antibody ligands, as widely used in flow cytometric analyses of mammalian cells [25]. Although the latter approach, in principle, is rapid and efficient, and can be extensively multiplexed [26], its application is not at the moment possible using plant protoplasts, since a wide variety of antibodies recognizing cell-surface epitopes, equivalent to the CD-markers on mammalian cells [27], have not been identified and made commercially available. As a consequence, the overwhelming majority of reports of fluorescence labeling of plant cells and protoplasts has focused on the expression of the Fluorescent Proteins, starting with the prototypical Green Fluorescent Protein (GFP), described first for transfected maize leaf protoplasts in 1995 [28, 29]. Methods

for transgenic and transfected expression of Fluorescent Proteins in several plant species are now in widespread use [4, 30, 31]. The most reliable and reproducible method, and thus the most commonly used in plant cytometric analysis and sorting, involves isolation of protoplasts from genetically modified plants [10–12, 32]. An example of combined fluorescent techniques in roots and root-derived protoplasts is shown in Figure 1. In this case, the endogenous GFP fluorescence of the *pWOL:GFP* line (*pWOODEN LEG:GFP*; 9) is combined with staining with the fluorescent dye FM4-64.

3 | PROTOPLASTS ANALYSIS THROUGH FLOW CYTOMETRY

Analysis of protoplast populations via flow cytometry was previously highly challenging, since cytometers and sorters were designed for smaller diameter (10–20 μm) mammalian hematopoietic cells, and the diameters of the original flow tips (50–70 μm) were too small to satisfactorily accommodate plant protoplasts. The first reports of successful sorting and recovery of viable tobacco leaf protoplasts demonstrated the use of larger (200 μm) flow tips, which required modification of the instrument configuration to achieve stable droplet break-off and to accurately determine the point of droplet break-off [33]. Most commercial instruments are now configured with a standard 100 μm flow tip, and several can accommodate flow tips up to 130 μm in diameter, which should be sufficient for many protoplast types. The use of even flow tips larger in diameter (up to 400 μm) is also possible. However, it requires significant alterations to the instrument configuration and their handling to achieve stream stability is exceptionally demanding (discussed in detail below).

Prior to cytometric analysis and sorting, the protoplasts should be gently resuspended in an osmoticum that is compatible with the cytometer sheath fluid. Conventionally, cytometers and sorters

TABLE 1 Autofluorescent compounds naturally occurred in plant cells and most commonly used fluorescent proteins

(Auto)fluorescence compounds	Excitation (nm)	Emission (nm)	Excitation laser/lamp
Flavins	380–490	520–560	Violet and Blue
NADH, NADPH	360–390	440–470	Violet
Lignin	488	530	Blue
Chlorophyll	488	685–740	Blue
Tryptophan	280	300–350	UV
Tyrosine	270	305	UV
Advanced glycation end-products (AGEs)	320–370	385–450	Violet
CFP	380–470	450–570	Violet
GFP	430–510	490–560	Blue
YFP	470–530	510–590	Blue
tdTomato	470–580	550–670	Yellow–green
RFP	500–580	550–680	Yellow–green
mCherry	510–610	580–690	Yellow–green

are operated using various formulations of phosphate-buffered saline (typically 0.9% [154 mM] NaCl, [mostly sodium] phosphate, KCl, and a pH between 5.7 and 7.4). Commercial PBS formulations often contain low levels of detergents as well as antibacterial agents, so caution is needed depending on the downstream application following sorting.

An important warning is to be aware that many media used for protoplast preparation and resuspension contain significant levels (≥ 5 mM) of Ca^{2+} . This will readily precipitate inside the cytometer in the presence of PBS, and therefore non-PBS-based sheath fluids are recommended [11, 12, 34, 35]. A best practice recommendation is to

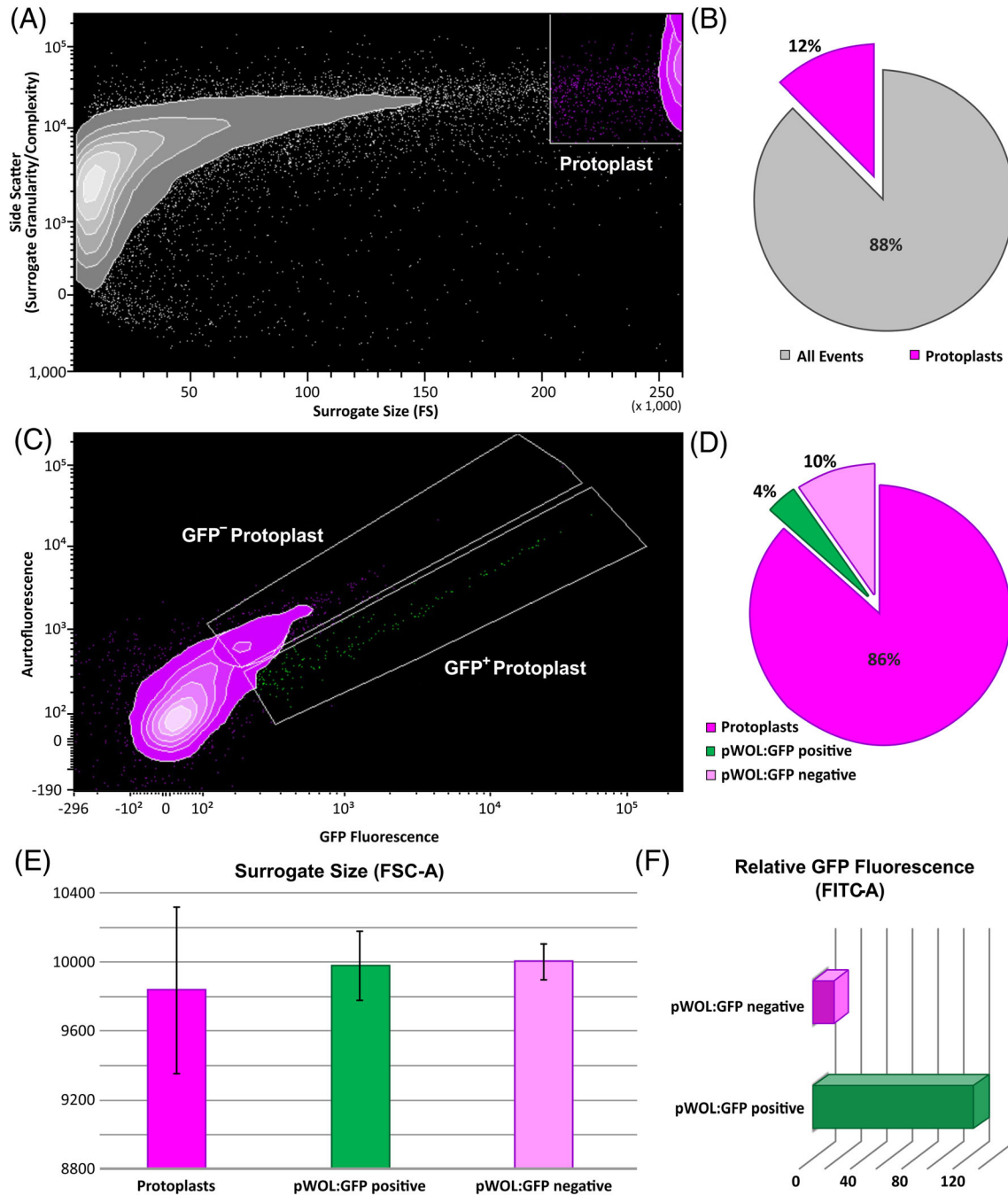


FIGURE 3 Flow cytometric analysis of pWOL:GFP root protoplasts: (A) Biparametric plot of forward and side scatter (surrogate size and granularity/complexity parameters respectively). The protoplasts being the biggest structures in the sample are at the upper-right edge of the chart. (B) The respective abundance percentages of the protoplast population in the sample is shown. (C) The population selected as protoplasts in a (magenta) is then plotted according to its autofluorescence and GFP fluorescence. Two populations are distinguished as GFP-positive (green) and GFP-negative (pink) and are gated respectively. (D) Their respective abundance percentages are shown. (E) The mean of the forward scatters of the three gated populations is plotted, error bars representing standard deviations. (F) The means of the GFP fluorescence of pWOL:GFP positive and negative cells are plotted

empirically explore the effects on protoplast integrity, viability and subsequent growth in culture, when using different sheath fluids and protoplast resuspension media. Osmotica and sheath fluids based on KCl or even NaCl, including 5 mM CaCl₂ but excluding phosphate, and instead using one of the “Good” buffers (MES, MOPS, etc.) that maintain a slightly acidic pH, are excellent places to start. Choice of a lower pH reflects our understanding of the microenvironment of the plant wall/plasma membrane interface, which is dominated by the presence of acidic pectins.

When protoplasts are analyzed through flow cytometry, both background noise and clusters of aggregated protoplasts are to be expected, although purification should greatly reduce their contributions. Exclusion of debris, aggregates and dead protoplasts from the data enables cleaner separation and identification of protoplast populations. Background cytometric signals produced by debris (particles approximately up to 2–5 μm in maximum diameter), mainly derives from ruptured protoplasts, organelles (intact or damaged) liberated from these protoplasts, and general fragments of undigested tissue (Figure 3(A)). Debris can be readily distinguished from protoplasts based on the fact that protoplasts are 10–40 times larger in size. Debris is typically excluded from analysis by use of specific thresholds applied to either the forward light scatter (FS) or the orthogonal side scatter (SS) signals typically used to trigger event detection by the cytometer. This renders the instrument “blind” to the events below this threshold. Application of thresholds can also be done using two-dimensional FS-SS scatter plots, since this can improve discrimination of populations of protoplasts from debris. However, the application of all thresholds should be approached cautiously in flow cytometry and sorting since it can lead to inclusion of undesired but non-detected events along with the objects that are detected and desired for sorting. It should be also noted that the forward and side scatter signals are empirically derived and should rather be considered as surrogates (FS) of size and (SS) of granularity/complexity, since the signals are not monotonically increasing, but rather are complex functions of refractive index, absolute size, pigmentation and so-on. As a reasonable approximation, objects of similar functionality and sizes can be compared, such as protoplasts. If a more precise absolute estimation of protoplast size is required, this can be readily determined via analysis of the features of the pulse-width time-of-flight signal [36].

Although the distinction between debris and protoplasts is in most cases possible in the bi-parametric dot plots of forward and side scatter (Figure 3(A)), it is more difficult to discriminate between healthy and severely stressed or even ruptured protoplasts, since these may not show differences in FS and SS signals. In that situation, viability dyes (FDA, PI, DAPI) can be employed, as previously described, for this discrimination, assuming there are no conflicts with other fluorescent tags involved in the experimental designs (Fluorescent Proteins, antibody labels, etc.). A best practice recommendation is always to purify the protoplasts by gradient flotation [13, 14, 19], and if possible, use dyes singly or in combination to identify viable protoplasts during cytometric analysis and sorting (Figure 2).

After the (healthy) protoplasts have been selected, the population can then be projected in biplot according to their autofluorescence (Table 1) and targeted fluorescence properties. Autofluorescence can be projected in several parameters and can be further distinguished from the targeted fluorescence (labeled protoplasts) by application of compensation and proper band pass filters. Therefore, we select the parameter that facilitates the best population separation between the targeted fluorescence and autofluorescence (Figure 3(C)). The daughter gates are then designed within the gated protoplasts, to define the well-separated negatively and positively fluorescent populations (for targeted fluorescence). (Figure 3(C),(D)). Since in the example provided by Figure 2, a viability stain was not employed, identification and selection of the *pWOL:GFP*-negative cells is driven by the autofluorescence properties of the *pWOL:GFP* positive cells. Since the negative population is much more abundant compared to the positive (Figures 1(C),(E),(G) and 3(C),(D)), it becomes possible to be highly selective. A feature of modern FACS instruments is specialized software that, in parallel to analyzing the events, generates a statistical overview of average signal intensities and association deviation statistics. These data can provide additional information about the sample under analysis or the sorted population and can also be used to confirm the stability and reproducibility of the flow sorting method used over different days of sorting. An example is shown in Figure 3(E),(F). Additional data about the *pWOL:GFP* positive and negative cells gated in Figure 3(C) can be plotted to show that, although these two populations differ substantially in GFP fluorescence (Figure 3(F)), they are very similar in terms of their FS size surrogate (Figure 3(E)) as both populations contain protoplasts.

4 | SORTING OF PROTOPLASTS

The protoplast populations that have been selected by gates for sorting can be readily collected in a purified state by flow sorting into different types of collection tubes, well plates and microscope slides using flow sorters. Most sorters employ the jet-in-air sorting principle. When protoplasts are sorted, preservation during the sort process of their health and integrity, or of their contents of experimental interest, is crucial for meaningful results from downstream applications. Best practice recommendations to achieve this are as follows: firstly, and as already discussed in the flow cytometry section, accommodation of the large plant protoplasts demands flow tips larger in diameter. This requires a reduced system/sheath fluid pressure and a lower maximal drive frequency for droplet formation. On the one hand, lower sheath fluid pressures are beneficial for maintenance of protoplast health and integrity during analysis and sorting, which should improve the quality of biologically-relevant downstream applications as the protoplasts experience less physical stress. On the other hand, the physical constraints on droplet formation, apart from demanding more acute technical FACS expertise, inevitably reduce the upper limit of the sort rate, and the lower sorting yield imposes an extension of sorting hours and costs as compared to handling smaller (i.e., mammalian) cells. Prolonged sorting hours should be carefully planned, and should include

control experiments relevant to the downstream application. This follows largely as a consequence of an enlargement of the time that the sample is loaded into the cytometer and required for collection, the conditions for which may well not be optimal for the protoplasts. One option is to maintain sorting at 4°C (using a chilled sample introduction chamber as well as chilled sorting tubes), to globally reduce the activities of cellular enzymatic reactions and physiological processes [10–12, 15]. Sorting into tubes containing appropriate extraction agents compatible with the downstream applications is also highly appropriate. For example, samples that will be used for transcriptomics can be sorted into tubes preloaded with RNA extraction buffer to optimize the recoveries and integrity of transcripts. An additional suggestion is to load fresh sample in the loading port during long sorting processes as low-quality input will greatly reduce sorting efficiency. The gate design takes place on the beginning of the sorting and thus concerns a freshly loaded protoplasts sample. Therefore, the populations selected for sorting (Figure 3(A),(C)) refer to live protoplasts. If the protoplasts in the loaded sample start to be stressed and rupture, then they will have altered forward and side scatters and will not be selected for sorting as they will not be inside the designed gates anymore. This will have negative effects on the efficiency of the sorting but not on the purity of the sorted populations. Finally, caution is needed in establishing optimal droplet

breakoff points and droplet delay settings [33], in order to maintain sorting purity and reproducibility. In this respect, the best practice is use of commercially available fluorescent microspheres in larger diameter sizes (–25 to 90 μm) or naturally autofluorescent particles (pollen, fungal spores) that are both indestructible and similar in size to the fragile protoplasts that are being sorted, rather than use of standard (2 and 10 μm) fluorospheres, for optimizing instrument calibration and sort settings [14].

5 | APPLICATIONS OF FLOW CYTOMETRIC PROTOPLAST ANALYSIS IN PLANT RESEARCH

Flow cytometry and sorting of viable protoplasts followed by regeneration into plants was first reported in 1984 [14], and subsequently for isolation of somatic hybrid plants recovered by fluorescence-activated sorting of heterokaryons formed by protoplast fusion [19]. Flow analysis and sorting of protoplasts is now routinely employed in basic and applied plant research (Figure 4).

Over the intervening decades, there has been a tremendous increase in FACS-derived data in plant research. Analysis of sorted protoplasts has significantly deepened our understanding in

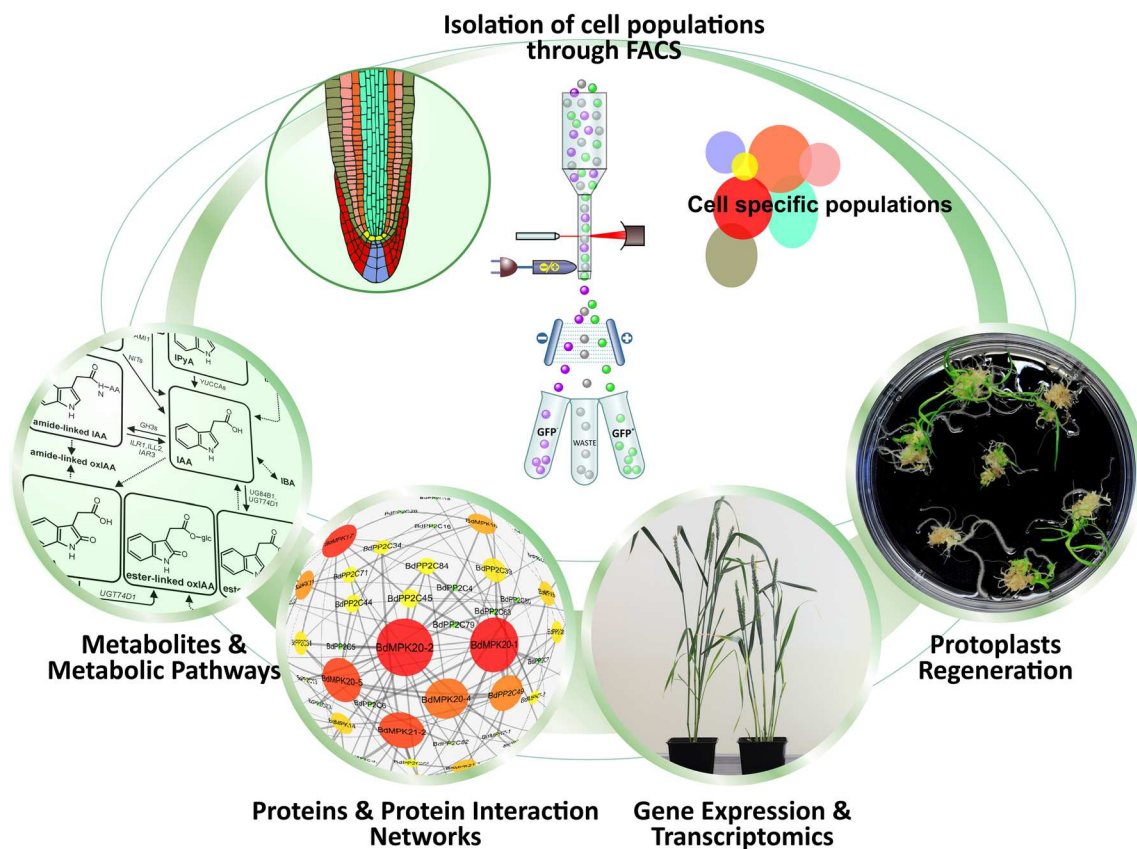


FIGURE 4 Schematics of downstream applications following protoplast isolation and sorting. Isolation of root cell-specific populations by FACS can be followed by applications in protoplast regeneration and different omics technologies, such as transcriptomics, proteomics, and metabolomics

TABLE 2 Selected examples of conditions for preparation and flow sorting of protoplasts

Plant species	Tissue, conditions	Flow cytometry tip	Sorting tip	Downstream application	Reference
At	Root Apex	Sheath fluid: 0.7% NaCl, 20 psi, 100 μ m nozzle	Flow rate 2500–5000 events/s. Sort precision “Purity” mode.	Hormone analysis (auxin and cytokinin metabolites)	[11, 12, 47, 48]
At	Root	30 psi, 100 μ m nozzle	Flow rate 2000–5000 events/s. Protoplasts sorted into Qiagen RLT lysis buffer.	Gene expression profiling (microarrays)	[9, 10, 32]
Nt	Leaf	Machine sterilization, 76 μ m nozzle - 24.5 kHz and 100 μ m nozzle - 14.5 kHz	Flow rate 700 events/s. Sorting in conjunction with the operation of the Autoclone. Protoplasts sorted into KOM medium.	Protoplast growth and plant regeneration	[14]
<i>Nicotiana</i> spp.	Leaf	All settings as Reference [14]. Laser power output 200 mW	All settings as Reference [14]. Flow sorter at 457 nm.	Isolation of somatic hybrids	[22]
Zm	Leaf	Sheath fluid: 0.47 M mannitol, 50 mM KCl, 10mM CaCl_2 , 4 mM MES, pH 5.7. Sheath and flow pressures: 8.0 and 7.3 psi. Sort-sense flow with 100 μ m orifice – 15 kHz. Laser power output 15 mW	Flow rate 50–200 events/s. Sort rate 25–40 cells/s	GFP labeling	[28, 29]
Nt	Leaf	Sheath fluid $\times 3$: DI water, KOM medium and PBS buffer. Fluorescein diacetate stained events selection (viability stain)	Sterile sorting. Laser output 200 mW. Sorting based on time-of-flight analysis of chlorophyll autofluorescence.	Gene expression	[8]
Os and At	Root /Salt stress	Sheath fluid: PBS buffer, 70 μ m (or 100 μ m) nozzle	Sort precision “Purity” mode. Protoplasts sorted into RNA extraction buffer (RLT)	Gene expression profiling (microarrays)	[51]
At	Root apex and emerging lateral root/ Response to Nitrogen	N.S.	Protoplasts sorted into lysis buffer	Gene expression profiling (microarrays)	[52]
At	Leaf	Sheath fluid: TEX buffer, 9 psi, 200 μ m nozzle	Flow rate 6000–15,000 events/s	Gene expression profiling (microarrays)	[54]
At	Roots/Salt and Iron Stress	N.S.	N.S.	Gene expression profiling (microarrays)	[53]
At	Infected and non-infected cells/downy mildew	All settings as Reference [42]	All settings as Reference [42]. Protoplasts sorted into Qiagen RLT lysis buffer with 1% β -mercaptoethanol.	Gene expression profiling (microarrays)	[49]
At	Aerial tissue and seedlings (stomata)	All settings as Reference [51]. 100 μ m nozzle. Forward scatter cutoff: 5000.	Flow rate 2500–3500 events/s, Sort precision “Purity” mode. Protoplasts sorted into RNA extraction buffer (RNeasy™ Micro Kit, QIAGEN).	Gene expression profiling (RNA sequencing and microarrays)	[46]
At and Os	Root tips (root hair)	All settings as Reference [43]	All settings as Reference [43].	Gene expression profiling (RNA sequencing)	[45]

(Continues)

TABLE 2 (Continued)

Plant species	Tissue, conditions	Flow cytometry tip	Sorting tip	Downstream application	Reference
At	Root tip, Root epidermis	N.S.	N.S.	Gene expression profiling (microarrays)	[43]
At	Embryo. Nuclei sorting	Sheath fluid: 1× PBS pH 7.0, ~60.5/~60.0 psi, 70 μM nozzle, ~95 kHz,	1–2 single drop envelope.	Gene expression profiling (microarrays)	[44]
At	Leaf	Sheath fluid: 20 psi (sheath) and 21–21.5 psi (sample), 100 μm nozzle, 39.2 kHz	Flow rate < 4000 events/s. Protoplasts sorted into a lysis buffer containing a reducing agent. Sort time of a single sample limited to 20–30 min.	Gene expression analysis (qRT-PCR) and visual analysis (confocal microscopy)	[42]
At	Roots	Settings as Reference [32]. 20 psi, 70-μm nozzle	Settings as Reference [32]. Flow rate 5000 events/s.		[40]
At	Inflorescence	Settings as Reference [56]. Sheath fluid: 25 psi, 100-μm nozzle. Doublets removal- single cells selection, PI stained events exclusion (viability stain)	Settings as Reference [56]. Flow rate 10,000 events/ s. Protoplasts sorted into Trizol (Invitrogen/Life Technologies). Occasionally agitated during ~40 min of sorting.	Gene expression profiling (mRNA sequencing)	[41]
At	Root apex	Sheath fluid: 0.7% NaCl, 20 psi, 100 μm nozzle.	Flow rate 2000–3000 events/s	Metabolomics analysis	[55]
At	Root/biotic stress (flg22, Pep1)	Sheath fluid: BD FACFlow, 20 psi and 21–21.5 psi, 39.2 kHz, 100 μm nozzle	Flow rate < 4000 events/s. Protoplasts sorted into Qiagen RLT lysis buffer containing 1% (v:v) β-mercaptoethanol.	Gene expression profiling (RNA sequencing)	[50]
At	Root apex	All settings as References [10, 56]	All settings as References [10, 56].	Proteomics analysis (GeLC- MS/MS)	[38]
At	Root Hair	Sheath fluid: 25 psi, 100 μm nozzle	Flow rate 7000 to 8000 events/s.	Gene expression profiling (RNA sequencing)	[37]
Nt	Leaf	Sheath fluid: 6 psi, 204 μm nozzle, Flow velocity 7.9 m/s	Flow rate 50 events/s.	Chlorophyll content and protoplasts size determination	[36]

Abbreviations: At, *Arabidopsis thaliana*; Os, *Oryza sativa*; Nt, *Nicotiana tabacum*; Zm, *Zea mays*; N.S., for conditions not specified.

developmental aspects of highly specific plant tissues and organs [8, 9, 11, 12, 32, 37–50] as well as their interaction with biotic [49, 50] and abiotic [51–55] factors.

Most of these detailed studies on sorted protoplasts have investigated the transcriptome, developmentally, in root cell types [32, 37, 43, 45], shoot apical meristem [9], carpel margin meristem [41], embryo [44] and stomatal lineage cells [48]. Transcriptomic analysis has been also performed in sorted protoplasts subjected to environmentally stressful conditions [53] such as responses to salt [51], nitrogen [52], light [54] and pathogen infections [50, 51]. These data are not only shedding light into plant functions and tissues at uniquely high resolution, but they also certify/confirm that RNA, a molecule that is highly sensitive to degradation, can be reproducibly recovered from sorted protoplasts. This provides additional evidence that FACS, despite its invasive nature as a technique, is a credible method for

obtaining results that can represent endogenous signals in planta discussed also in References [10, 39].

Research does not stop at the transcriptional level though, various groups reporting analysis of proteomes and metabolomes of root protoplast populations isolated via flow sorting. This has included proteome analysis within protoplasts from the different cell types of the root body and in root hairs [38, 45], as well as metabolomics studies [40, 56]. Finally, the distributions of a subgroup of small but highly active molecules, the plant hormones auxin and cytokinin, has been quantified in protoplasts from different cell types of the root apical region [11, 12] revealing high resolution hormonal gradients that are an essential feature of plant growth and development.

The above-mentioned publications, that have equipped FACS technology to achieve high-resolution analyses, have some common settings (Table 2). These being the best practices for protoplasts

sorting include low flow rates, low sheath fluid pressure and sorting of protoplast directly into the buffer that corresponds to the downstream application.

Future challenges will be to combine different 'omics techniques in specific organs and under different treatments or stress conditions in plant lines of specific genotypes, in order to understand their regulation and, for example, identify molecular switches during plant development.

6 | SUMMARY OF BEST PRACTICE RECOMMENDATIONS

- Growing healthy plants is a prerequisite for production of healthy protoplasts. Precise definition of growth conditions is essential for providing sources of protoplasts that respond reproducibly in downstream assays.
- Predefined optimized conditions during protoplast extraction (solutions, incubation times and handling) are essential for success and reproducibility. Verifying in a documented form is essential of the viability and purity of the protoplast populations that will be analyzed via flow cytometry and sorting. The simplest approach involves light and fluorescence microscopy.
- Round-bottom containers and swing-out centrifuges contribute to optimum gentle isolation of protoplasts.
- Choosing the appropriate fluorescent tagging method at the beginning of the experimental setup is a critical factor in experimental design.
- Protoplasts are highly autofluorescent, so selection of fluorochromes with limited spectra overlap is critical.
- Gating strategies should be carefully considered. This includes application of threshold(s) to limit analysis and sorting to the protoplast populations of interest, the use of viability stains for selection of healthy protoplasts, and appropriate positioning of daughter gates to accurately define desired sub-populations.
- Sorting protoplasts directly into an appropriate buffer for the downstream analysis increases the integrity of the investigated molecules and thus the quality of the results.

ACKNOWLEDGMENTS

D.W.G. acknowledges on-going support from the USDA through the University of Arizona College of Agriculture and Life Sciences, and with G.S. and W.M., from the Chinese National Key Research and Development Program, the National Natural Science Foundation of China, the Program for Innovative Research Teams in Science and Technology at a University of Henan Province, and the 111 Project of China. This work was also supported by grants from The Czech Foundation Agency (GA17-21581Y), the Internal Grant Agency of Palacký University (IGA_PrF_2021_011), and the Ministry of Education, Youth and Sport of the Czech Republic via the ERDF project "Plants as a tool for sustainable global development" (CZ.02.1.01/0.0/0.0/16_019/0000827). V.S. was partially supported by the Endowment fund of Palacký University in Olomouc. The authors also acknowledge the European Molecular Biology Organization (EMBO ASTF 297-2013) (I.A.) and Plant Fellows (the International Post doc Fellowship

Program in Plant Sciences, 267423) (I.A.; K.L.), the Swedish Research Council (VR), the VINNOVA (Vinnova), the Knut och Alice Wallenbergs Stiftelse (KAW) and Kempestiftelsema (K.L.).

AUTHOR CONTRIBUTIONS

Ioanna Antoniadis: Conceptualization; visualization; writing-original draft; writing-review & editing. **Vladimir Skalický:** Conceptualization; visualization; writing-original draft; writing-review & editing. **Guling Sun:** Visualization; writing-original draft; writing-review & editing. **Wen Ma:** Visualization; writing-original draft; writing-review & editing. **David Galbraith:** Conceptualization; visualization; writing-original draft; writing-review & editing. **Ondřej Novák:** Conceptualization; visualization; writing-original draft; writing-review & editing. **Karin Ljung:** Conceptualization; funding acquisition; visualization; writing-original draft; writing-review & editing.

CONFLICT OF INTEREST

The authors have no conflicts of interest to declare.

ORCID

Ioanna Antoniadis  <https://orcid.org/0000-0001-9053-2788>

David W. Galbraith  <https://orcid.org/0000-0003-4020-1635>

Ondřej Novák  <https://orcid.org/0000-0003-3452-0154>

Karin Ljung  <https://orcid.org/0000-0003-2901-189X>

REFERENCES

1. Cocking EC. A method for the isolation of plant protoplasts and vacuoles. *Nature*. 1960;187:962–3.
2. Mazarei M, Al-Ahmad H, Rudis MR, Stewart CN Jr. Protoplast isolation and transient gene expression in switchgrass, *Panicum virgatum* L. *Biotechnol J*. 2008;3:354–9.
3. Priyadarshani SVGN, Hu B, Li W, Ali H, Jia H, Zhao L, et al. Simple protoplast isolation system for gene expression and protein interaction studies in pineapple (*Ananas comosus* L.). *Plant Methods*. 2018;14:95.
4. Yoo SD, Cho YH, Sheen J. Arabidopsis mesophyll protoplasts: a versatile cell system for transient gene expression analysis. *Nat Protoc*. 2007;2:1565–72.
5. Davey MR, Anthony P, Power JB, Lowe KC. Plant protoplasts: status and biotechnological perspectives. *Biotechnol Adv*. 2005;23:131–71.
6. Eeckhaut T, Lakshmanan PS, Deryckere D, Van Bockstaele E, Van Huylenbroeck J. Progress in plant protoplast research. *Planta*. 2013; 238:991–1003.
7. Davey M, Anthony P, Patel D, Power J. Plant protoplasts: isolation, culture and plant regeneration. In: Davey M, Anthony P, editors. *Plant cell culture: essential methods*. New York, NY: John Wiley & Sons Inc.; 2010. p. 153–73.
8. Harkins KR, Jefferson RA, Kavanagh TA, Bevan MW, Galbraith DW. Expression of photosynthesis related gene fusions is restricted by cell type in transgenic plants and in transfected protoplasts. *Proc Natl Acad Sci U S A*. 1990;87:816–20.
9. Yadav RK, Girke T, Pasala S, Xie M, Reddy GV. Gene expression map of the Arabidopsis shoot apical meristem stem cell niche. *Proc Natl Acad Sci U S A*. 2009;106:4941–6.
10. Birnbaum K, Shasha DE, Wang JY, Jung JW, Lambert GM, Galbraith DW, et al. A gene expression map of the Arabidopsis root. *Science*. 2003;302:1956–60.
11. Antoniadis I, Plačková L, Simonovik B, Doležal K, Turnbull C, Ljung K, et al. Cell-type-specific cytokinin distribution within the Arabidopsis primary root apex. *Plant Cell*. 2015;27:1955–67.

12. Petersson SV, Johansson AI, Kowalczyk M, Makoveychuk A, Wang JY, Moritz T, et al. An auxin gradient and maximum in the Arabidopsis root apex shown by high-resolution cell-specific analysis of IAA distribution and synthesis. *Plant Cell*. 2009;21:1659–68.
13. Galbraith DW, Mauch TJ. Identification of fusion of plant protoplasts II. *Z Pflanzenphysiol*. 1980;98:129–40.
14. Harkins KR, Galbraith DW. Flow sorting and culture of plant protoplasts. *Physiol Plant*. 1984;60:43–52.
15. Novák O, Antoniadi I, Ljung K. High-resolution cell-type specific analysis of Cytokinins in sorted root cell populations of *Arabidopsis thaliana*. In: Kleine-Vehn J, Sauer M, editors. *Plant hormones: methods and protocols*: 1497. New York, NY: Human Press; 2016. p. 231–48.
16. Galbraith DW, Shields BA. The effects of inhibitors of cell wall synthesis on tobacco protoplast development. *Physiol Plant*. 1982;55:25–30.
17. Jones KH, Senft JA. An improved method to determine cell viability by simultaneous staining with fluorescein diacetate-propidium iodide. *J Histochem Cytochem*. 1985;33:77–9.
18. Huang CN, Cornejo MJ, Bush DS, Jones RL. Estimating viability of plant protoplasts using double and single staining. *Protoplasma*. 1986;135:80–7.
19. Graham JM. Purification of intact plant protoplasts by flotation at 1g. *Sci World J*. 2002;2:1397–9.
20. Donaldson L. Autofluorescence in plants. *Molecules*. 2020;25:2393.
21. Talamond P, Verdeil JL, Conéjéro G. Secondary metabolite localization by autofluorescence in living plant cells. *Molecules*. 2015;20:5024–37.
22. Afonso CL, Harkins KR, Thomas-Compton M, Krejci A, Galbraith DW. Production of somatic hybrid plants through fluorescence activated sorting of protoplasts. *Nat Biotechnol*. 1985;3:811–6.
23. Laughlin ST, Baskin JM, Amacher SL, Bertozzi CR. In vivo imaging of membrane-associated glycans in developing zebrafish. *Science*. 2008;320:664–7.
24. Pařízková B, Žukauskaitė A, Vain T, Gronas P, Raggi S, Kubeš MF, et al. New fluorescent auxin probes visualise tissue-specific and sub-cellular distributions of auxin in Arabidopsis. *New Phytol*. 2021;230:535–49.
25. Vira S, Mekhedov E, Humphrey G, Blank PS. Fluorescent-labeled antibodies: balancing functionality and degree of labeling. *Anal Biochem*. 2010;402:146–50.
26. Mair F, Prlic M. OMIP-044: 28-color immunophenotyping of the human dendritic cell compartment. *Cytometry A*. 2018;93:402–5.
27. Zhang X, Lan Y, Xu J, Quan F, Zhao E, Deng C, et al. CellMarker: a manually curated resource of cell markers in human and mouse. *Nucleic Acids Res*. 2018;47:D721–D728.
28. Sheen J, Hwang S, Niwa Y, Kobayashi H, Galbraith DW. Green fluorescent protein as a new vital marker in plant cells. *Plant J*. 1995;8:777–84.
29. Galbraith DW, Grebenok RJ, Lambert GM, Sheen J. Flow cytometric analysis of transgene expression in higher plants: green fluorescent protein. *Methods Cell Biol*. 1995;50:3–12.
30. Mardanovna ES, Blokhina EA, Tsybalova LM, Peyret H, Lomonosoff GP, Ravin NV. Efficient transient expression of recombinant proteins in plants by the novel pEff vector based on the genome of potato virus X. *Front Plant Sci*. 2017;8:247.
31. Gao L, Shen G, Zhang L, Qi J, Zhang C, Ma C, et al. An efficient system composed of maize protoplast transfection and HPLC–MS for studying the biosynthesis and regulation of maize benzoxazinoids. *Plant Methods*. 2019;15:144.
32. Brady SM, Orlando DA, Lee JY, Wang JY, Koch J, Dinneny JR, et al. A high-resolution root spatiotemporal map reveals dominant expression patterns. *Science*. 2007;318:801–6.
33. Harkins KR, Galbraith DW. Factors governing the flow cytometric analysis and sorting of large biological particles. *Cytometry*. 1987;8:60–71.
34. Galbraith DW. Isolation and flow cytometric characterization of plant protoplasts. In: Darzynkiewicz Z, Crissman HA, editors. *Methods in cell biology*; London: Academic Press. 1990. p. 527–47.
35. Galbraith DW, Bartos J, Dolezel J. Flow cytometry and cell sorting in plant biotechnology. In: Sklar LA, editor. *Flow cytometry in biotechnology*. New York, NY: Oxford University Press; 2005. p. 291–322.
36. Galbraith DW, Harkins KR, Jefferson RA. Flow cytometric characterization of the chlorophyll contents and size distributions of plant protoplasts. *Cytometry A*. 1988;9:75–83.
37. Lan P, Li W, Lin WD, Santi S, Schmidt W. Mapping gene activity of Arabidopsis root hairs. *Genome Biol*. 2013;14:R67.
38. Petricka JJ, Schauer MA, Megraw M, Breakfield NW, Thompson JW, Georgiev S, et al. The protein expression landscape of the Arabidopsis root. *Proc Nat Acad Sci U S A*. 2012;109:6811–8.
39. Ip PL, Birnbaum KD. Tissue-specific gene expression profiling by cell sorting. In: Alonso J, Stepanova A, editors. *Plant functional genomics: methods in molecular biology*, 1284. New York, NY: Humana Press; 2015. p. 175–83.
40. Moussaieff A, Rogachev I, Brodsky L, Malitsky S, Toal TW, Belcher H, et al. High-resolution metabolic mapping of cell types in plant roots. *Proc Nat Acad Sci U S A*. 2013;110:E1232–E1241.
41. Villarino GH, Hu Q, Manrique S, Flores-Vergara M, Sehra B, Robles L, et al. Transcriptomic signature of the SHATTERPROOF2 expression domain reveals the meristematic nature of Arabidopsis Gynoecial medial domain. *Plant Physiol*. 2016;171:42–61.
42. Grønlund JT, Eyres A, Kumar S, Buchanan-Wollaston V, Gifford ML. Cell specific analysis of Arabidopsis leaves using fluorescence activated cell sorting. *J Vis Exp*. 2012;68:4214.
43. Bruex A, Kainkaryam RM, Wieckowski Y, Kang YH, Bernhardt C, Xia Y, et al. A gene regulatory network for root epidermis cell differentiation in Arabidopsis. *PLoS Genet*. 2012;8:e1002446.
44. Slane D, Kong J, Berendzen KW, Kilian J, Henschen A, Kolb M, et al. Cell type-specific transcriptome analysis in the early *Arabidopsis thaliana* embryo. *Development*. 2014;141:4831–40.
45. Huang L, Shi X, Wang W, Ryu KH, Schiefelbein J. Diversification of root hair development genes in vascular plants. *Plant Physiol*. 2017;174:1697–712.
46. Adrian J, Chang J, Ballenger CE, Bargmann BOR, Alassimone J, Davies KA, et al. Transcriptome dynamics of the stomatal lineage: birth, amplification, and termination of a self-renewing population. *Dev Cell*. 2015;33:107–18.
47. Antoniadi I, Novák O, Gelová Z, Johnson A, Plíhal O, Simerský R, et al. Cell-surface receptors enable perception of extracellular cytokinins. *Nat Commun*. 2020;11:4284.
48. Pencík A, Simonovik B, Petersson SV, Henyková E, Simon S, Greenham K, et al. Regulation of auxin homeostasis and gradients in Arabidopsis roots through the formation of the indole-3-acetic acid catabolite 2-oxindole-3-acetic acid. *Plant Cell*. 2013 Oct;25:3858–70.
49. Coker TL, Cevik V, Beynon JL, Gifford ML. Spatial dissection of the *Arabidopsis thaliana* transcriptional response to downy mildew using fluorescence activated cell sorting. *Front Plant Sci*. 2015;6:527.
50. Rich C, Reitz M, Eichmann R, Jacobs S, Jenkins DJ, Esteban E, et al. Cell type identity determines transcriptomic immune responses in *Arabidopsis thaliana* roots. *BioRxiv*. 2018;2018:30244.
51. Evrard A, Bargmann BO, Birnbaum KD, Tester M, Baumann U, Johnson AA. Fluorescence-activated cell sorting for analysis of cell type-specific responses to salinity stress in Arabidopsis and rice. *Methods Mol Biol*. 2012;913:265–76.
52. Gifford ML, Dean A, Gutierrez RA, Coruzzi GM, Birnbaum KD. Cell-specific nitrogen responses mediate developmental plasticity. *Proc Nat Acad Sci U S A*. 2008;105:803–8.
53. Dinneny JR, Long TA, Wang JY, Jung JW, Mace D, Pointer S, et al. Cell identity mediates the response of Arabidopsis roots to abiotic stress. *Science*. 2008;320:942–5.

54. Warnasooriya SN, Montgomery BL. Investigating tissue- and organ-specific phytochrome responses using FACS-assisted cell-type specific expression profiling in *Arabidopsis thaliana*. *J Vis Exp*. 2010;39:1925.
55. Petersson SV, Lindén P, Moritz T, Ljung K. Cell-type specific metabolic profiling of *Arabidopsis thaliana* protoplasts as a tool for plant systems biology. *Metabolomics*. 2015;11:1679–89.
56. Birnbaum K, Jung JW, Wang JY, Lambert GM, Hirst JA, Galbraith DW, et al. Cell type-specific expression profiling in plants via cell sorting of protoplasts from fluorescent reporter lines. *Nat Methods*. 2005;2:615–9.

How to cite this article: Antoniadi I, Skalický V, Sun G, et al. Fluorescence activated cell sorting—A selective tool for plant cell isolation and analysis. *Cytometry*. 2021;1–12. <https://doi.org/10.1002/cyto.a.24461>



Article

Auxin Metabolome Profiling in the Arabidopsis Endoplasmic Reticulum Using an Optimised Organelle Isolation Protocol

Ludmila Včelařová [†], Vladimír Skalický [†] , Ivo Chamrád , René Lenobel, Martin F. Kubeš [‡], Aleš Pěňčík ^{*}
and Ondřej Novák

Laboratory of Growth Regulators, Institute of Experimental Botany of the Czech Academy of Sciences, and Faculty of Science, Palacký University, Šlechtitelů 27, CZ-78371 Olomouc, Czech Republic; ludmila.vcelarova@upol.cz (L.V.); vladimir.skalicky@upol.cz (V.S.); ivo.chamrad@upol.cz (I.C.); rene.lenobel@upol.cz (R.L.); martin.kubes@uhk.cz (M.F.K.); ondrej.novak@upol.cz (O.N.)

* Correspondence: ales.pencik@upol.cz; Tel.: +420-585-634-853

† These authors contributed equally to this work.

‡ Current address: Department of Biology, Faculty of Science, University of Hradec Králové, Rokitanského 62, 500 03 Hradec Králové, Czech Republic.



Citation: Včelařová, L.; Skalický, V.; Chamrád, I.; Lenobel, R.; Kubeš, M.F.; Pěňčík, A.; Novák, O. Auxin Metabolome Profiling in the Arabidopsis Endoplasmic Reticulum Using an Optimised Organelle Isolation Protocol. *Int. J. Mol. Sci.* **2021**, *22*, 9370. <https://doi.org/10.3390/ijms22179370>

Academic Editor:
Jutta Ludwig-Mueller

Received: 31 July 2021

Accepted: 25 August 2021

Published: 29 August 2021

Publisher's Note: MDPI stays neutral with regard to jurisdictional claims in published maps and institutional affiliations.



Copyright: © 2021 by the authors. Licensee MDPI, Basel, Switzerland. This article is an open access article distributed under the terms and conditions of the Creative Commons Attribution (CC BY) license (<https://creativecommons.org/licenses/by/4.0/>).

Abstract: The endoplasmic reticulum (ER) is an extensive network of intracellular membranes. Its major functions include proteosynthesis, protein folding, post-transcriptional modification and sorting of proteins within the cell, and lipid anabolism. Moreover, several studies have suggested that it may be involved in regulating intracellular auxin homeostasis in plants by modulating its metabolism. Therefore, to study auxin metabolome in the ER, it is necessary to obtain a highly enriched (ideally, pure) ER fraction. Isolation of the ER is challenging because its biochemical properties are very similar to those of other cellular endomembranes. Most published protocols for ER isolation use density gradient ultracentrifugation, despite its suboptimal resolving power. Here we present an optimised protocol for ER isolation from *Arabidopsis thaliana* seedlings for the subsequent mass spectrometric determination of ER-specific auxin metabolite profiles. Auxin metabolite analysis revealed highly elevated levels of active auxin form (IAA) within the ER compared to whole plants. Moreover, samples prepared using our optimised isolation ER protocol are amenable to analysis using various “omics” technologies including analyses of both macromolecular and low molecular weight compounds from the same sample.

Keywords: endoplasmic reticulum; auxin; subcellular fractionation; density gradient centrifugation; mass spectrometry

1. Introduction

The endoplasmic reticulum (ER) is a highly dynamic, variable, and extensive nuclear membrane-bound network in eukaryotic cells. It consists of two parallel membranes that form a tangled system of tubules and cisternae, and plays key roles in lipid metabolism and the biosynthesis and sorting of proteins within the cell. Additionally, in plant cells the ER mediates communication between the endomembrane system and non-secretory organelles, such as mitochondria, peroxisomes, and chloroplasts. Proteins in the ER undergo post-translational modifications, such as *N*- and *O*-glycosylation and hydrogen bond formation [1–4]. Studies conducted during the last two decades have also shown that the ER is involved in regulating the distribution of phytohormones and signalling via auxins [5–9], cytokinins [10,11], and ethylene [12].

We have focused on auxin (indole-3-acetic acid, IAA), a key phytohormone regulating a variety of crucial growth and developmental processes, and related metabolites. Recent findings indicate that the ER plays a central role in maintaining subcellular auxin homeostasis by regulating its biosynthesis, subcellular distribution, and metabolism, and also probably regulates its signalling [9]. In this way, the ER significantly affects the tightly

balanced levels of auxin in plant cells and thus the growth and development of plant tissues and organs.

The subcellular redistribution of IAA is facilitated by a complex system of transporters including PIN-FORMED 5, 8 (PIN5, 8) and PIN-LIKES transporters (PILSs) located in the ER [5–8,13,14] (Figure 1), and the vacuolar transporter WALLS ARE THIN 1 (WAT1) [15]. The mechanisms regulating intracellular auxin distribution remain unclear, but the activity of ER-resident transporters directly affects auxin signalling [14,16]. Moreover, it is proven that the main IAA flux to nuclei goes through the ER [9].

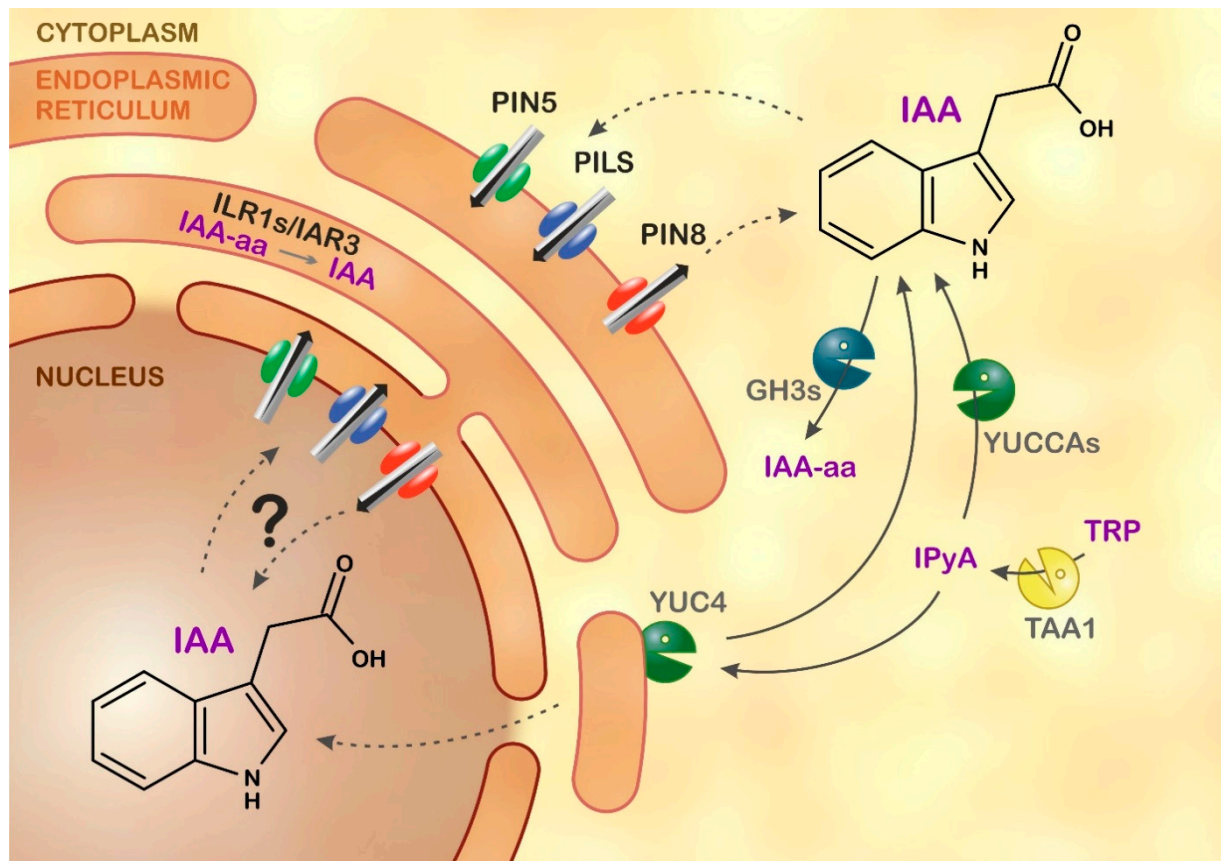


Figure 1. Model of auxin homeostasis in Arabidopsis endoplasmic reticulum (ER). Levels of active indole-3-acetic acid (IAA) are tightly regulated via biosynthesis, transport, and metabolism. Tryptophan (TRP) is converted to IAA via the TRYPTOPHAN AMINOTRANSFERASE OF ARABIDOPSIS/YUCCA (TAA/YUC) biosynthetic pathway, in which a key intermediate is indole-3-pyruvic acid (IPyA). Members of the PIN family of auxin transporter proteins (PIN5, PIN8) and PIN-LIKES (PILS) facilitate intracellular auxin transport. PIN5 mediates auxin flux from the cytosol to the ER lumen, whereas PIN8 acts in the opposite direction. IAA is inactivated by Gretchen Hagen 3 (GH3) proteins, which catalyse the formation of IAA-amino acid conjugates (IAA-aa). ER-localised auxin amidohydrolases (IAR3, ILL2 and ILR1) catalyse the reverse reaction, hydrolysing IAA-aa to active IAA. The ER membrane is in light brown, while the nuclear membrane is in dark brown. Solid and dotted arrows indicate enzymatic conversion or transport, respectively. “?” means putative auxin transport.

Several IAA biosynthetic pathways in Arabidopsis have been reported [17,18]. However, the main pool of active IAA is predominantly synthesised via the TRYPTOPHAN AMINOTRANSFERASE OF ARABIDOPSIS/YUCCA (TAA/YUC) biosynthetic pathway [19,20]. The TAA/YUC complex resides in the ER membrane, but its catalytic domain faces the cytosol [21,22]. Other YUCCA members also co-localise with ER markers or are localised to the cytosol [18]. Newly synthesised IAA must be delivered to its site of action. Auxin perception systems that trigger transcriptional responses are found in the nucleus [23]. However, a key component of the nuclear IAA receptor complex, TRANSPORT INHIBITOR

RESPONSE 1 (TIR1), is also detected in the cytosol, where it may mediate a rapid non-transcriptional response [24].

The distribution and levels of active IAA are strictly controlled and fine-tuned through complex coordination of its biosynthesis and transport, and by its inactivation [25,26]. Reversible inactivation is mediated via conjugation with sugars to form IAA-glucose (IAA-glc), which is catalysed by UDP-glucosyl transferases [27]. Another mode of inactivation is GRETCHEN HAGEN 3 (GH3)-catalysed conjugation of IAA with amino acids to form IAA-amino acid (IAA-aa) conjugates [28,29]. It is currently thought that the two most common IAA-aa forms, IAA-aspartate (IAA_{asp}) and IAA-glutamate (IAA_{glu}), cannot be converted back to free IAA [30,31]. However, less abundant IAA-aa forms, such as conjugates of alanine, leucine or valine, can be hydrolysed back to IAA by ER-localised amidohydrolases, leading to an increased local IAA concentration and thus increased signalling [32]. It has been suggested that IAA-aa are formed in the cytosol by GH3 [33] but hydrolysed in the ER [32]. In Arabidopsis, the dominant catabolic pathway responsible for reducing active IAA levels is regulated by the cytosolic enzyme DIOXYGENASE FOR AUXIN OXIDATION 1 (DAO1), which converts IAA into 2-oxindole-3-acetic acid (oxIAA) [26,34]. Additionally, oxIAA can be conjugated with glucose to form oxIAA-glucose (oxIAA-glc), the most abundant auxin metabolite in Arabidopsis [30,35].

Even though the localisations of many phytohormone-related enzymes, transporters and receptors are known, there is currently no comprehensive subcellular auxin map. Organelle-level auxin and cytokinin profiles have only been determined in vacuoles to date [15,36]. However, IAA was detected in chloroplasts during a cytokinin profiling study [37,38]. Subcellular phytohormone profiling is challenging due to the low abundance of plant hormones, the difficulty of isolating pure organelles, and the frequent use of organelle isolation buffers with high salt concentrations that interfere with subsequent MS-based analysis. Conventional organelle isolation methods generally rely on density gradient (ultra)centrifugation, which requires that organelles be gently and effectively released from plant tissue. This can be achieved by chopping with razor blades [39] or by enzymatic cell wall digestion [40–42]. Organelles are then separated based on the different velocities at which they move through a (dis)continuous sucrose density gradient [43], Ficoll [44], and/or Percoll [45,46]. Organelles become concentrated in the region where their density is equal to that of their surroundings (the so-called isopycnic point), where they stop moving through the gradient [47]. The migration velocity of organelles depends on their density, which in turn depends on their lipid/protein ratio, size and shape [48]. Alternative fractionation methods based on flow cytometry [39,49] or affinity purification have been developed more recently [50,51]. Interestingly, these methods enable the isolation of cell-type-specific organelles, such as nuclei [52] and mitochondria [53]. Despite the existence of advanced subcellular fractionation methods for well-bounded organelles, density-gradient centrifugation remains the gold standard for isolation of the ER, Golgi apparatus (GA), and vacuoles.

Here we present auxin metabolite profile of ER samples from Arabidopsis seedlings obtained using an optimised protocol based on density gradient ultracentrifugation (Figure 2 and Figure S1). Proteomic analysis revealed high ER enrichment in the isolated fractions, and showed that the optimised isolation protocol exhibits good reproducibility. The findings presented herein provide new insights into the subcellular distribution of auxin and IAA homeostasis.

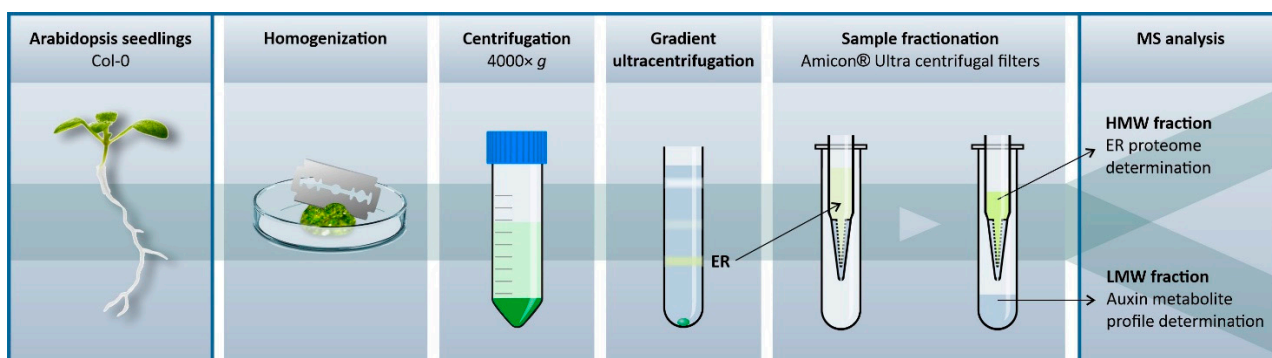


Figure 2. ER isolation workflow. 10-day-old *Arabidopsis* seedlings were placed in a Petri dish on ice and finely chopped with a razor blade in 2 mL of ice-cold homogenisation buffer. The resulting homogenate was filtered through two layers of Miracloth into a 50 mL tube and centrifuged at $4000\times g$ and $4\text{ }^{\circ}\text{C}$ for 10 min. Organelles in the resulting supernatant were fractionated using a discontinuous sucrose density gradient. The ER-enriched fraction was then passed through Amicon[®] Ultra centrifugal filters (cut-off: 3kDa) to obtain a high-molecular weight (HMW) fraction containing proteins and a low-molecular weight (LMW) fraction for auxin metabolite determination by liquid chromatography coupled with tandem mass spectrometry.

2. Results

2.1. Isolation of the ER from *Arabidopsis* Plants

To analyse the ER auxin metabolite profile, it was first necessary to isolate a highly enriched ER fraction containing sufficient material for analytical purposes. Ding et al. [6] studied the mechanism of auxin transport in the ER and developed a method for isolating ER samples from *Arabidopsis* plants by centrifugation in a discontinuous sucrose density gradient. We adapted and optimised this protocol to increase the yield and purity of the product to a level sufficient for analytical determination of auxin metabolites within the ER.

The initial and the most critical step of the isolation process was the homogenisation of the plant material. The homogenisation method must provide a sufficient yield of the isolated compartment while avoiding its disintegration. We therefore compared homogenisation using a razor blade [6] to the method of homogenisation using a mortar and pestle with quartz sand, which was previously shown to be an effective homogenisation method for isolating intact mitochondria from *Arabidopsis* [45]. Gradient fractionation was then performed to assess the efficiency of organelle separation. During the optimisation process, the yields and purities of homogenates and the subsequently isolated ER fractions were evaluated by Western blot analysis, using organelle markers for the ER (Lumena-binding protein, BiP and Calnexin homolog 1/2, CNX1/2), nuclei (Histone 3, H3), Golgi complex (Coatomer subunit gamma, Sec21p) vacuoles (Epsilon subunit of tonoplast H⁺ATPase, V-ATPase), chloroplasts (D1 protein of photosystem II, PsbA), plastids (Glutamine oxoglutarate aminotransferase, GOGAT), mitochondria (H protein of glycine decarboxylase complex, GDC-H), cytosol (actin, ACT) and plasma membrane (plasma membrane H⁺ATPase, H-ATPase).

In general, the strength of all organelle marker signals was higher in the mortar–pestle homogenates than in the razor blade homogenates. However, for both homogenisation methods, the fraction expected to contain the ER (i.e., the fraction located at the 1.1/1.3 M sucrose layer interface) was only slightly enriched in ER markers (Figure 3a). Additionally, chloroplast, vacuole, and Golgi apparatus (GA) markers were detected in these fractions. However, only negligible mitochondrial and nuclear marker signals were detected by Western blotting in the fraction obtained after razor blade homogenisation. The presence of multiple marker signals in the putatively ER-enriched fractions indicates that organelles disintegrated during homogenisation with a mortar and pestle. Overall, these results show that razor blade homogenisation was the superior method for ER isolation (Figure 3a) and that chloroplasts or thylakoids were concentrated in the ER-enriched fraction along with the ER (Figure 3a).

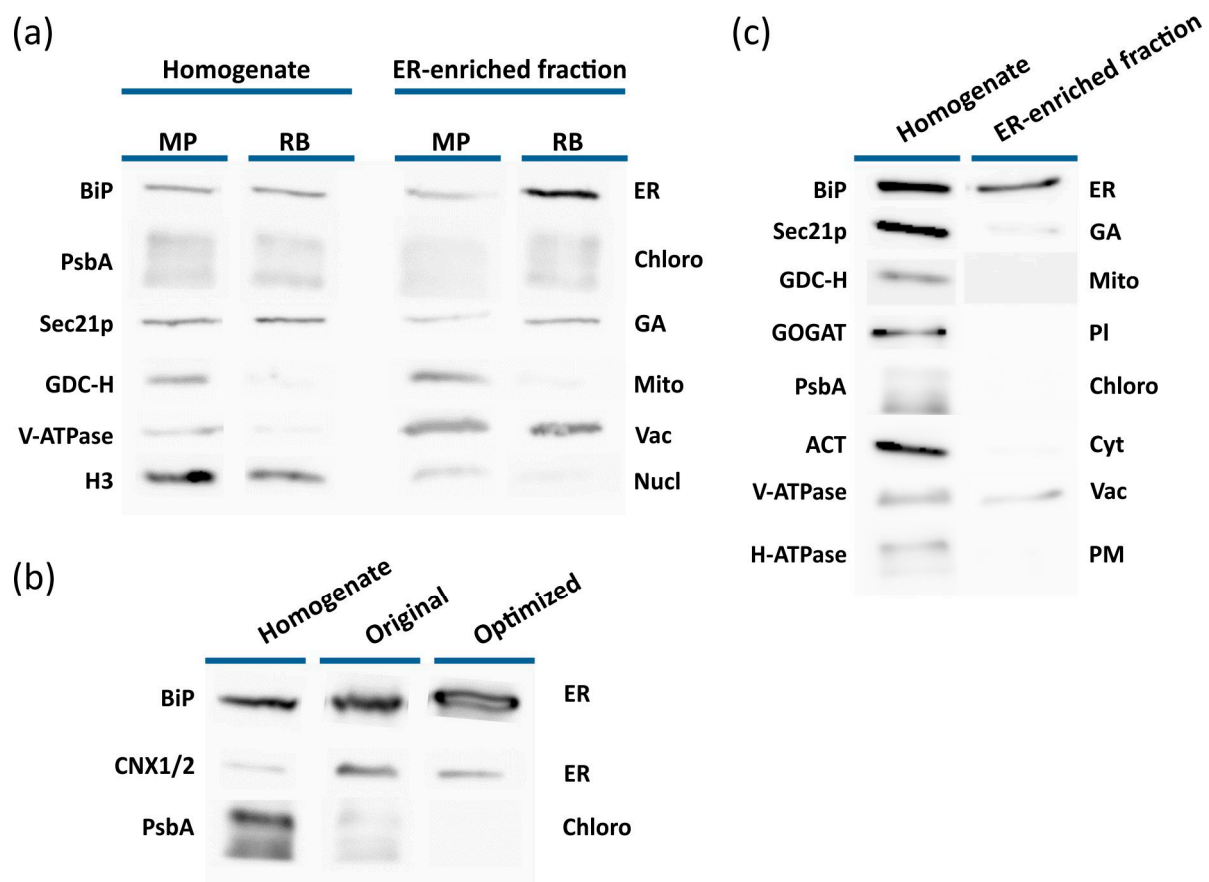


Figure 3. Optimisation of ER isolation from 10-day-old seedlings of *A. thaliana*. The effectiveness and usefulness of each step in the optimisation process was verified by Western blot analysis. (a) Comparison of two homogenisation methods—grinding seedlings using a mortar and pestle (MP) with added quartz sand, and chopping with a razor blade (RB). In both cases, the ER-enriched fraction was isolated using the originally reported sucrose density gradient [6]. (b) Organelle profiles of ER-enriched fractions obtained using various density-gradient ultracentrifugation protocols. Organelles were released by chopping seedlings with razor blade. Microsomal fractions were separated using the original or optimised (reduced sucrose density) gradients; for details, see Materials and Methods, Sections 4.5 and 4.6. (c) Final evaluation of the ER-enriched fraction obtained using the optimised sucrose density gradient. The following organelle-specific markers were immunodetected: Endoplasmic reticulum–ER (Lumena-binding protein, BiP and Calnexin homolog 1/2, CNX1/2), nuclei–Nucl (Histone 3, H3), Golgi apparatus–GA (Coatomer subunit gamma, Sec21p) vacuoles–Vac (Epsilon subunit of tonoplast H+ATPase, V-ATPase), chloroplasts–Chloro (D1 protein of photosystem II, PsbA), plastids–PI (Glutamine oxoglutarate aminotransferase, GOGAT), mitochondria–Mito (H protein of glycine decarboxylase complex, GDC-H), cytosol–Cyt (actin, ACT), and plasma membrane–PM (plasma membrane H+ATPase, H-ATPase).

To address the problem of unwanted organelles co-migrating with the ER, the preparation of samples for density gradient centrifugation was further optimised. First, the initial centrifugation step was optimised by performing centrifugation with centrifugal forces of between 2000 and 12,000 $\times g$. Western blot analyses of the resulting supernatants and the parent homogenate showed that the chloroplast content of the supernatant declined as the centrifugal force increased (Figure S2). However, chloroplasts were not fully removed from the samples during the initial centrifugation under any conditions. Based on the intensity of the chloroplast marker in the Western blot analysis, 4000 $\times g$ was selected as the optimal centrifugal force. Importantly, the signal of the ER marker was not changed (Figure S2). Initial low-speed centrifugation eliminated nuclei from the final ER extract and greatly reduced its content of chloroplasts without appreciably affecting its ER content.

In the next step, the density gradient was optimised to eliminate residual chloroplasts and other contaminating organelles from the ER-enriched fraction (Figure 3b). Since

chloroplasts should have a higher density than ER, the effect of reducing the density of individual layers of the sucrose gradient was tested. It was ultimately found that using a gradient with sucrose solution concentrations of 31%, 27%, 19%, and 8% (*w/w*) caused chloroplast sedimentation to the bottom of the tube, eliminating the chloroplast marker signal from the ER-enriched fraction without affecting the ER yield (Figure 3b). This adjustment of the gradient also affected the migration of vacuoles and GA, which had been additional contaminants of the ER-enriched fraction obtained with the original gradient (Figure 3a,c). Western blot analysis of the ER-enriched fraction isolated using the modified gradient revealed only a weak signal of the GA marker Sec21p (Figure 3c). Aside from the tonoplast marker V-ATPase, no other organelle markers were detected, and the degree of vacuole enrichment was much lower than when using the original gradient (Figure 3a). Optimising the isolation protocol by increasing the initial centrifugation speed and reducing the density of the gradient solutions thus greatly increased the purity of the ER-enriched fraction.

2.2. Confirmation of ER-Enriched Fractions by Proteomic Analysis

To validate our optimised ER isolation procedure, the retentate obtained by partitioning ER-enriched samples using Amicon® filters was subjected to proteomic analysis. On average, 1015 proteins were unambiguously identified per sample, giving over 1300 individual identifications for five biological replicates (Figure 4a, Table S1). Of these, 1003 proteins (about 75 % of the total identifications) were present in at least three replicates (Figure 4a), suggesting that the optimised isolation method exhibits high reproducibility. This was confirmed by pairwise comparisons of protein identifications, which indicated a mean reproducibility of 72.8 % (Figure S3) with a coefficient of variation of 4.6 %.

The ER enrichment of the prepared samples was investigated using two different approaches. First, we investigated the acquired dataset for the presence of proteins commonly used as organelle markers in Western blot experiments. The relative abundance of these markers was subsequently quantified based on the well-established intensity-based absolute quantification (iBAQ) intensities [54]. For comparative purposes, the same quantitative analysis was applied to control samples consisting of a total protein lysate prepared from 10-day-old Arabidopsis seedlings, which was analysed in the same way as ER-enriched isolates. As shown in Figure 4b, the detected ER markers were specifically enriched in the prepared isolates, while most markers for other organelles were significantly more abundant in the control samples. The only exceptions were the plasma membrane H⁺ATPase (AHA1) and vacuolar Epsilon subunit of tonoplast H⁺ATPase (VHA-E1; Figure 4b), consistent with the results obtained by Western blotting (Figure 3c). It should also be noted that some markers (e.g., the nuclei-specific H3) were detected only in the control samples.

Second, we performed a bioinformatic analysis of the ER-related dataset. Seven different algorithms were used to predict the ER localisation of the identified proteins, and the association of these proteins with ER-related processes was assessed based on functional annotation clustering of enriched gene ontology (GO) terms and KEGG pathways. The *in silico* predictions revealed 188 proteins potentially localised to the ER (Table S2), representing over 14 % of the total identifications. Four of the five most enriched GO term clusters were directly connected to the ER, as shown in Figure 4c (Table S3), which was consistent with the KEGG pathway analysis (Table S4, Figure S4). Taken together, these results prove the ER enrichment of the isolated fraction, the high reproducibility of the modified ER isolation protocol based on a discontinuous sucrose density gradient, and its good compatibility with standard proteomic techniques.

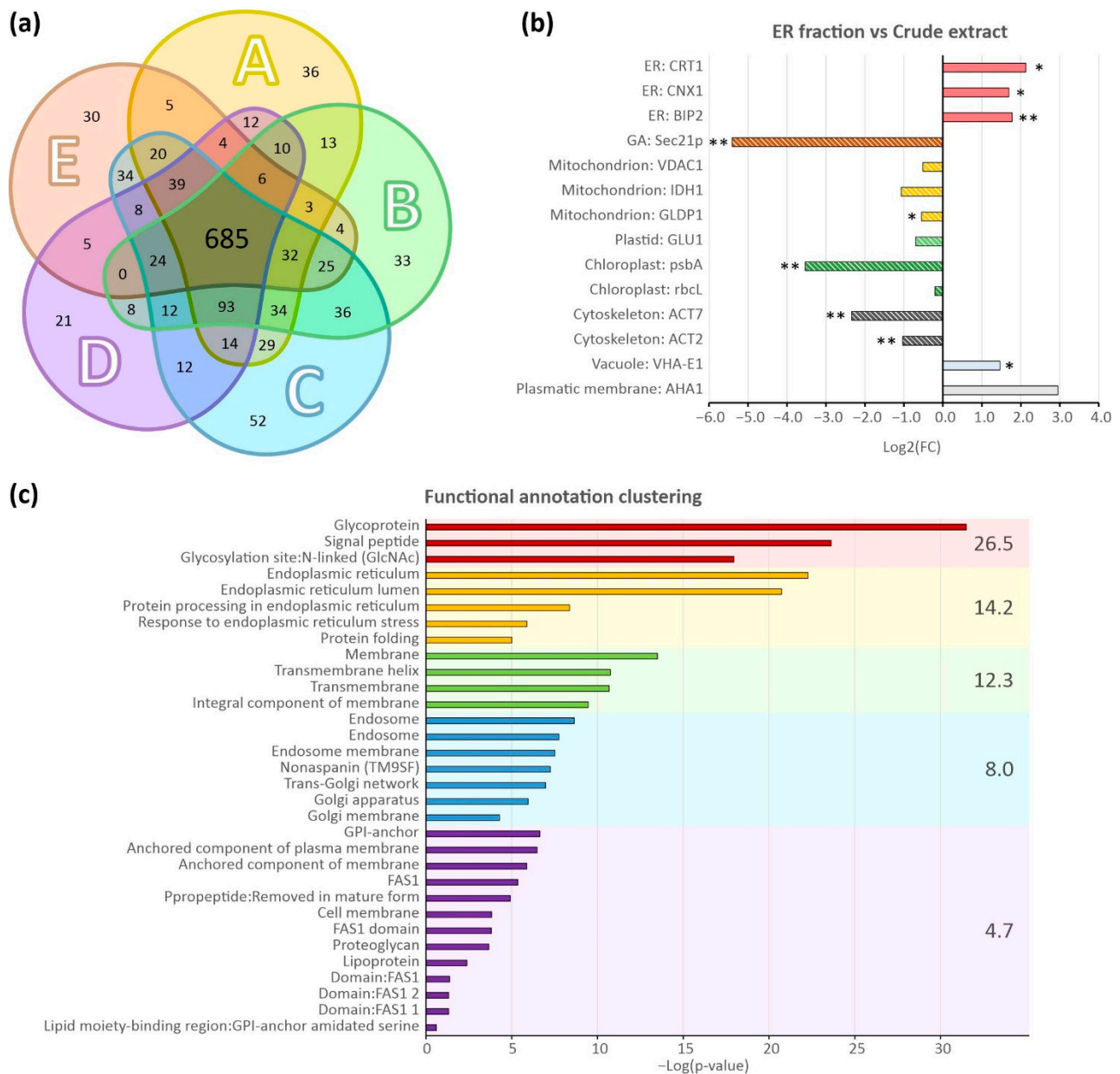


Figure 4. Proteomic analysis of the prepared ER fractions. **(a)** Protein identification overlaps for the analysed independent ER isolates ($n = 5$). The capital letters (A,B,C,D,E) stand for the individual ER isolation replicates. Numbers show the total sums of protein identifications belonging to the particular sections of the Venn diagram. **(b)** Distribution of Log₂ fold changes (FC) of known protein organelle markers. Fold changes were calculated from the ratios of the iBAQ values for the respective markers identified in the analysed ER isolates ($n = 5$) to those in control samples (total protein lysates from 10-days old *Arabidopsis* seedlings; $n = 5$). Asterisks denote significant differences (* for $p \leq 0.05$ and ** for $p \leq 0.01$). **(c)** Clustering of significantly enriched functional annotation terms for the identified proteins whose location was assigned as the ER. The colours of bars and the background indicate the annotation cluster of the protein. The clusters are sorted according to their enrichment score that is presented on the right side of the graph, and the individual functional terms are sorted by the negative log of their p -value. Endoplasmic reticulum (ER), Golgi apparatus (GA).

2.3. Auxin Metabolite Determination in ER

Finally, the ER-specific auxin metabolome was determined in a filtrate containing low-molecular weight metabolites obtained by partitioning ER-enriched samples with Amicon® filters. These filtrates were pure samples containing only minimal quantities of plant matrix. However, because the ER samples were isolated by density gradient centrifugation, they

had a high content of sucrose, which could have adversely affected their analysis by liquid chromatography–tandem mass spectrometry (LC-MS/MS). Solid-phase extraction (SPE) was therefore used to eliminate sucrose from the samples and enrich the target analytes. To maximise extraction efficiency and auxin metabolite recovery, we tested two purification protocols previously developed to isolate IAA metabolites from plant tissue [55,56]. ER buffer samples containing sucrose concentrations ranging from 0.6 M to 1.2 M were spiked with a mixture of auxin standards (1 pmol each) and processed using either reversed-phase Oasis™ hydrophilic lipophilic balance (HLB) columns [55] or an in-tip micro solid-phase extraction (μ SPE) method [56]. Higher extraction efficiencies were obtained using the μ SPE method, for which the average recovery of all tested metabolites was around 60% over the range of tested sucrose concentrations, compared to 30% for the HLB-based method (Figure S5). The μ SPE approach was therefore used to isolate IAA metabolites from the ER-enriched fractions prepared by sucrose density gradient centrifugation.

We next investigated the possibility that undesired changes in endogenous auxin levels might occur during the process of ER enrichment by ultracentrifugation. To this end, a total organelle suspension prepared from 10-day-old *Arabidopsis* seedlings was centrifuged at $4000\times g$ and the resulting supernatant was incubated under identical conditions to those used during the ultracentrifugation step. Samples were collected at the beginning of incubation (0 h) and after 3 h, which corresponds to the duration of ER isolation by ultracentrifugation. Upon comparing the relative abundances of free IAA and auxin metabolites at the beginning and end of the incubation, we observed that the proportion of free IAA increased slightly from 2.3% to 2.8%, while that of IAA-glc decreased slightly from 2.1% to 1.8% (Figure 5a). Additionally, the relative abundance of oxIAA increased from 13.4% to 23% during the incubation, while that of oxIAA-glc decreased by 10%. The relative abundances of the IAA amide conjugates IAAsp and IAGlu remained unchanged during the incubation period (Figure 5a).

The optimised ER isolation procedure and the in-tip μ SPE method were used together with LC-MS/MS to determine the metabolic profile of IAA in the ER. We first determined and compared the proportion of IAA metabolites in the crude *Arabidopsis* seedling extracts, the total organelle suspension, and the ER-enriched fraction (Figure 5b, Table S5). The relative abundance of IAA in the total pool of analytes in the ER-enriched samples (8.8%) was five times that in the crude extract (1.7%). Conversely, the relative abundance of most IAA metabolites (IAAsp, IAGlu, IAA-glc and oxIAA) in the ER fraction was lower than in the crude extract and total organelle suspension. The main auxin metabolite in all three sample types was oxIAA-glc, whose relative abundance was relatively stable and ranged from 70 to 80% (Figure 5b). Finally, we used the total protein content of each sample (determined by MS) to normalise the levels of the analytes in order to compare the concentrations of IAA and its metabolites in the ER-enriched fraction with those in the crude *Arabidopsis* extract. The levels of individual IAA metabolites relative to the total protein content for each sample type are presented in Table S6. Surprisingly, the ER-enriched fraction contained considerably higher levels of all studied analytes; levels of IAA metabolites were between 5 (IAAsp) and 12 (oxIAA-glc) times higher in the ER-enriched fraction than in the crude extract, and the level of free IAA in the ER was 62 times that in the crude extract (Figure 5c).

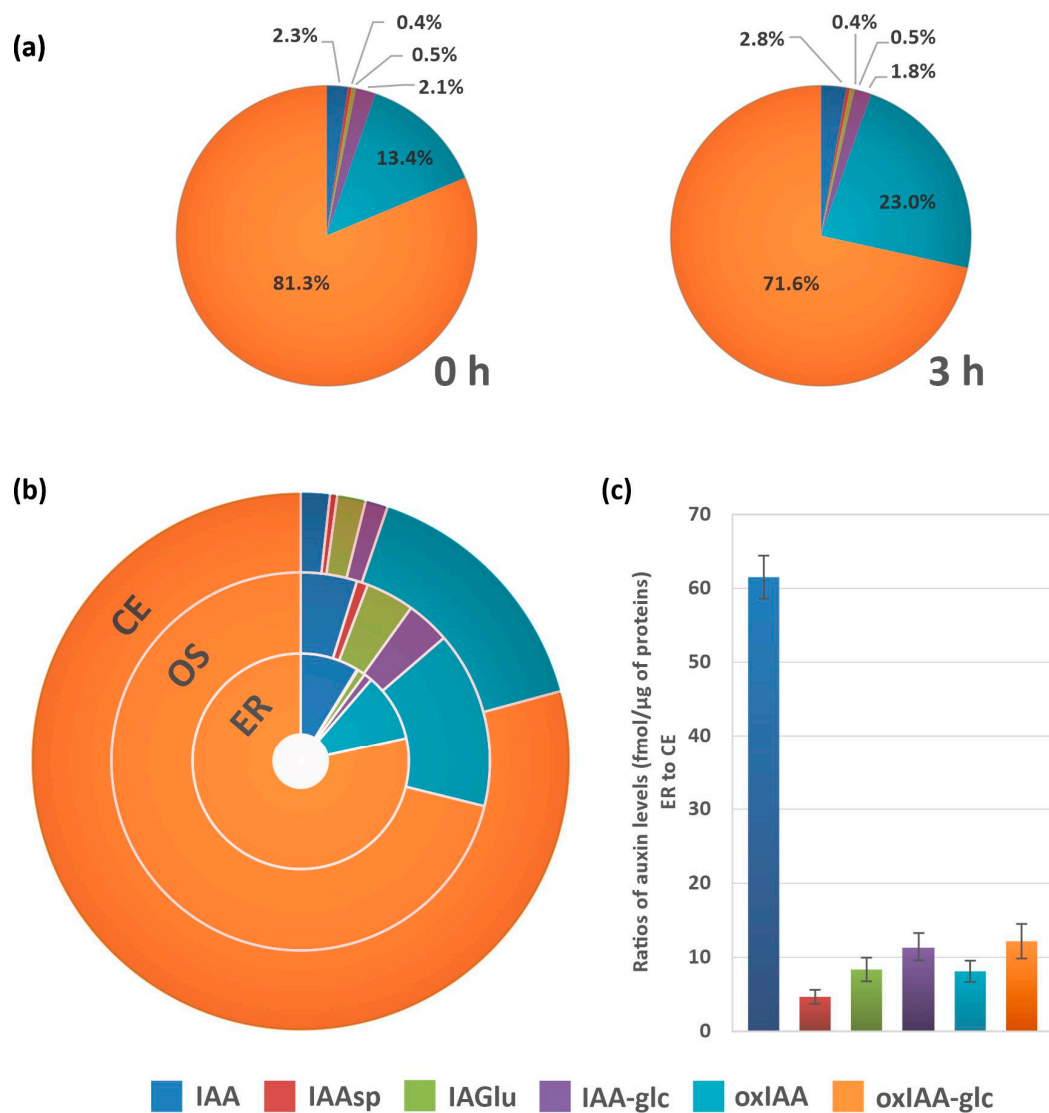


Figure 5. Determination of auxin metabolites in the Arabidopsis endoplasmic reticulum (ER). **(a)** Control of auxin metabolite profile stability. A homogenate prepared from 10-day-old seedlings was filtered and then centrifuged. The supernatant was immediately frozen or incubated in refrigerator at 4 °C for 3 h, as in the ER isolation process. Auxin metabolite profiles are expressed in percentages showing the relative abundance of each metabolite ($n = 3$). **(b)** Relative distribution of auxin metabolites in crude Arabidopsis extracts from 10-day-old seedlings, a total organelle suspension, and the ER-enriched fraction. ($n = 5$). **(c)** Abundance of auxin metabolites in ER. The enrichment of analytes is expressed as the ratio of the absolute level of each metabolite (fmol/μg of proteins) in the ER to that in the crude extract ($n = 5$). Error bars indicates. Crude extract (CE), organelle suspension (OS), Indole-3-acetic acid (IAA), IAA-aspartate (IAA_{sp}), IAA-glutamate (IAGlu), IAA-glucose (IAA-glc), 2-oxindole-3-acetic acid (oxIAA), oxIAA-glucose (oxIAA-glc).

3. Discussion

To perform ER-specific proteomic and IAA-metabolomic analyses, it is essential to start with a highly pure ER fraction with minimal contamination by other organelles. Additionally, the ER fraction must be isolated using a method that does not destroy the organelle while simultaneously achieving sufficient enrichment for subsequent metabolite determination. Most published protocols for ER isolation were developed and optimised to isolate enriched ER membrane samples in order to study membrane proteins. The purity of the fractions obtained using these protocols is rarely reported, however.

With the aim of preparing an ER fraction suitable for studying the IAA metabolome in the ER, we adapted the ER isolation protocol of Ding et al. [6], which is based on

ultracentrifugation in a discontinuous sucrose gradient. The individual steps of the protocol were optimised to maximise ER enrichment while minimising contamination by other organelles. Homogenisation with a mortar and pestle delivered a greater organelle yield than chopping the plants with a razor blade (Figure 3a) but was found to be unsuitable for our purposes because of the low purity of the final ER fraction. This low purity may be due to disintegration of organelle membranes caused by excessive homogenisation of plant tissue with the mortar and pestle, which prevents their fractionation [57]. It is also reasonable to assume that excessively rough homogenisation of plant material before ER isolation would cause leakage of the organelles' contents. Chopping the material with a razor blade proved to be a gentler but still adequate method of homogenisation prior to ER isolation (Figure 3a).

Chloroplasts were the main contaminants of the ER fraction obtained using the original method. Therefore, the initial centrifugation of the total organelle suspension and the subsequent density gradient ultracentrifugation were optimised to remove chloroplasts from the final fraction (Figure 3b). The optimisation strategy exploited the fact that chloroplasts are denser than the ER [58]; consequently, reducing the density of the gradient solutions caused sedimentation of chloroplasts at the bottom of the centrifugal tube and yielded a purer ER fraction. The final fraction obtained using the modified protocol contained no visible chloroplast marker signal (Figure 3a). However, Western blot analysis of the ER-enriched fraction isolated using the optimised ultracentrifugation protocol revealed the presence of GA and vacuolar marker proteins. The GA and the ER have similar biochemical characteristics and are difficult to separate on the basis of density [59]. Despite this, the signal of GA marker protein Sec21p was greatly weakened in the ER fraction, which was consistent with the results of a proteomic analysis (Figure 4). Conversely, both Western blotting and MS-based protein analysis revealed the presence of the vacuolar marker protein V-ATPase in the ER-enriched fraction (Figures 3a and 4c). However, this did not necessarily imply the presence of intact vacuoles in that fraction; although V-ATPase is a tonoplast-resident protein, it is synthesised in the ER and transported to the vacuole by intracellular trafficking [60]. It is thus possible that at least some of the V-ATPase signal was due to protein awaiting delivery to the vacuole rather than the presence of intact vacuoles in the ER fraction.

The successful analysis of the protein complement of our samples proved their ER enrichment and allowed us to draw several important conclusions. First, the high overlap of protein identifications in the analysed replicates indicated that our ER isolation protocol exhibits good reproducibility. This claim is greatly strengthened by the fact that the analysed samples were obtained from independently cultivated plants and independent ER isolations; in other words, they were true biological replicates. Second, the method allowed for plant ER enrichment. This was indicated not only by significant enrichment of established ER markers, such as BiP, CNX1, and calreticulin (CRT), but also by the ER-localisation of a substantial proportion (14 %) of the identified proteins. This proportion of ER-localised proteins was very high, given that ER proteins typically comprise about 1% of the total dataset in standard proteomic experiments [61]. As might be expected, this was accompanied by an overrepresentation of cellular processes associated with the ER including protein processing and post-translational modification as well as biosynthesis of secondary metabolites and phenylpropanoids [62]. Finally, extracts prepared using the optimised protocol were highly compatible with proteomic methods, and could thus provide important new and detailed information on the ER and its homeostasis. It also seems plausible that these extracts would be compatible with other modern "omics" techniques.

IAA metabolite profile analyses revealed considerable differences in the relative abundance of active IAA and its most abundant metabolites when comparing the ER-enriched fraction to other plant extracts. Specifically, free IAA accounted for a greater proportion of the total IAA metabolite pool in the ER fraction than in crude plant extracts or total organelle suspensions, and the opposite was true for most other IAA metabolites (Figure 5b). Control experiments were performed to determine the extent to which these differences

in metabolite distributions could be attributed to undesirable metabolic transformations occurring during the relatively lengthy isolation of the ER fraction. It was found that small changes in the relative abundance of some metabolites did occur during the incubation of organelle suspension—specifically, the relative abundance of free IAA and oxIAA increased, while that of IAA-glc and oxIAA-glc decreased, suggesting that some hydrolysis of IAA glucosyl esters occurred during sample preparation (Figure 5a). However, the relative abundance of IAA only increased by 0.5 percentage points during the control experiment; ER enrichment caused a much greater increase of four percentage points when compared to the total organelle suspension, and seven percentage points relative to the crude extract (Figure 5b). Additionally, whereas the relative abundance of oxIAA increased by 10 percentage points in the control experiments, its relative abundance in the ER-enriched fraction fell by five percentage points (Figure 5a,b). This suggests that the observed differences in the distribution of auxin metabolites were mainly due to the ER enrichment of the obtained fraction rather than undesirable metabolic changes during the ER isolation procedure.

The relative abundances of the various IAA metabolites in each sample type were also normalised against the samples' total protein contents, revealing that the absolute concentrations of IAA and all its metabolites in the ER-enriched fraction were substantially higher than in the crude whole-plant extract. Interestingly, this difference was most pronounced for free IAA (Figure 5c). One might reasonably expect IAA in its active form to accumulate in the ER and to eventually be transported to the nucleus, where the auxin signal is perceived and the signaling pathway is triggered, as suggested by Middleton et al. [9]. The lower relative abundance of most IAA metabolites in the ER (when compared to whole-plant and organelle extracts) may suggest that the formation and accumulation of IAA metabolites and conjugates occurs predominantly in other cell compartments. For example, analysis of the vacuolar IAA metabolite profile revealed that most of the total IAA in that organelle exists as the glycosyl ester (IAA-glc), a storage form that can be re-hydrolysed to the active form [15].

4. Materials and Methods

4.1. Plant Material and Growth Conditions

Ten-day-old *Arabidopsis thaliana* ecotype Col-0 were used as the material for experiments. Seeds were surface-sterilised using a 70% ethanol solution (Merck Life Science, Darmstadt, Germany) supplemented with 0.1% Tween-20 (Merck Life Science, Darmstadt, Germany) for 10 min, rinsed with sterile deionised water, and sowed on Murashige and Skoog solid media supplemented with 1% sucrose. After 3 days of stratification, the plates were arranged vertically and incubated under long-day conditions (16 h light/8 h dark) at 22 ± 1 °C.

4.2. Homogenisation

For the homogenisation process, 2 g (FW) of whole *Arabidopsis* seedlings were homogenised in 2 mL of ice-cold homogenisation buffer (0.5 M sucrose, 5 mM $\text{MgCl}_2 \cdot 6\text{H}_2\text{O}$, 0.1 M KH_2PO_4 , 1 mM 1,4-Dithiothreitol, 1 mM phenylmethylsulfonyl fluoride, 1 mM Roche cOmplete™ Protease Inhibitor Cocktail EDTA-free, pH 6.65; all components from Merck Life Science, Darmstadt, Germany). The plant material was transferred to a petri dish placed on ice. All subsequent steps were performed on ice using precooled solutions and implements. The sample was chopped using a razor blade for 5 min, or homogenised in a mortar containing quartz sand with a pestle and incubated for 5 min. The resulting homogenate was filtered into a 50 mL falcon tube through two layers of Miracloth pre-wetted with homogenisation buffer. Residual homogenised material was washed out of the petri dish or mortar with 4 mL of homogenisation buffer. An aliquot of the resulting total organelle suspension (500 μL) was collected and immediately frozen in liquid nitrogen and stored at -80 °C until Western blot or LC-MS/MS analysis. ER enrichment

was then performed according to the original protocol [6] or the optimised protocol as described below.

4.3. Optimisation of Initial Centrifugation

Arabidopsis seedlings were homogenised with a razor blade as described above. The filtrate was then centrifuged at $2000\times g$, $3000\times g$, $4000\times g$, $5000\times g$, $6000\times g$, $7000\times g$, $9000\times g$, or $12,000\times g$ (10 min, $4\text{ }^{\circ}\text{C}$), after which 1 mL of supernatant (S) was collected and immediately frozen in liquid nitrogen and stored at $-80\text{ }^{\circ}\text{C}$ until Western blot analysis.

4.4. Preparation of ER-Enriched Fraction—Original Protocol

The density gradient centrifugation protocol was adapted from that of Ding et al. [6]. The sucrose solutions used to establish the gradients were prepared by dissolving sucrose in the ER buffer (5 mM $\text{MgCl}_2\cdot 6\text{H}_2\text{O}$; 0.1 M KH_2PO_4 ; pH 6.65). The supernatant obtained after initial centrifugation at $4000\times g$ (S4000) was then divided into two aliquots of approx. 3 mL each. Each aliquot was then carefully loaded on top of a 3 mL ice-cold 1.3 M sucrose cushion in an ultracentrifuge tube to establish a two-step density gradient, after which the aliquot was supplemented with a further 3 mL of homogenisation buffer to prevent tube collapse. The two tubes were then loaded symmetrically into the centrifuge and spun at $108,000\times g$, $4\text{ }^{\circ}\text{C}$ for 90 min. After ultracentrifugation, the upper phase was removed without disrupting the focused microsomal fraction, which was then slowly overlaid with 3 mL of 1.1 M, 3 mL of 0.7 M, and 3 mL of 0.25 M sucrose solutions. The resulting four-step gradients were centrifuged at $108,000\times g$, $4\text{ }^{\circ}\text{C}$ for 90 min. The ER-enriched fraction located at the 1.1/1.3M interphase (1 mL) was then transferred into a new tube and frozen for phytohormone and protein extraction. Alternatively, collected fractions were ultracentrifuged again at $108,000\times g$ and $4\text{ }^{\circ}\text{C}$ for 50 min to concentrate the ER-enriched fraction. The supernatant was then removed and the pellet was resuspended in 50 μL of homogenisation buffer. The resulting ER-enriched fraction was immediately frozen in liquid nitrogen and stored at $-80\text{ }^{\circ}\text{C}$ until Western blot analysis was performed.

4.5. Preparation of ER-Enriched Fraction—Optimised Protocol

The two- and four-step gradient centrifugation processes were performed as described above, but the concentrations of the gradient-forming sucrose solutions were slightly reduced to 31%, 27%, 19%, and 8% (*w/w*). To determine the IAA metabolite profile of the ER, 1 mL of the ER-enriched fraction located at the interface of the 27% and 31% sucrose solutions was taken and processed as described above.

4.6. The SDS-PAGE Western Blot Assay

The samples were mixed with Laemmli Sample Buffer (Bio-Rad, Hercules, CA, USA) supplemented with 10% β -mercaptoethanol (Merck Life Science, Darmstadt, Germany) and incubated in a thermoblock at $70\text{ }^{\circ}\text{C}$ for 5 min. Samples were then centrifuged in a MiniSpin[®] centrifuge (Eppendorf, Hamburg, Germany) at 10,000 rpm for 5 min before separation of the protein mixtures on a 12% polyacrylamide gel (Bio-Rad, Hercules, CA, USA). Dual Color Standards (Bio-Rad, Hercules, CA, USA) was used as a molecular weight marker. Electrophoresis was performed first at 90 V for 30 min and then at 120 V until the end of the separation. After protein migration, the gel was rinsed for 5 min in transfer buffer (150 mM), and proteins were transferred for 2 h at 290 mA and $4\text{ }^{\circ}\text{C}$ onto 0.45 μm nitrocellulose membranes (Santa Cruz Biotechnology, Heidelberg, Germany). The membranes were then blocked with 5% low-fat milk in TBS-T for 1 h, cut into segments, and incubated for 1 h with rabbit primary antibodies (Agriserä, Vännäs, Sweden) against the organelle markers listed below: anti-BiP (1:2500; AS09 481), anti-CNX1/2 (1:2500; AS12 2365), anti-V-ATPase (1:2000; AS07 213), anti-H3 (1:5000; AS10 710), anti-Sec21p (1:1000; AS08 327), anti-PsbA (1:10,000; AS05 084), anti-GDC-H (1:5000; AS05 074), anti-GOGAT (1:1000; AS07 242), anti-ACT (1:2500; AS13 2640) and anti-H-ATPase (1:1000; AS07 260). All primary antibodies were diluted in 1% low-fat milk in TBS-T. Membrane

segments were then incubated with goat anti-rabbit IgG (H&L) HRP-conjugated secondary antibody (1:10,000; AS09 602) diluted in 1% low-fat milk in TBS-T for 1 h. Visualisation was performed with a chemiluminescence kit (SuperSignal™ West Pico Chemiluminescent Substrate (Thermo Fisher Scientific, Waltham, MA, USA) using a ChemiDoc MP Imaging System (Bio-Rad, Hercules, CA, USA).

4.7. Proteomic Analysis

Proteins in the retentate from sample partitioning on Amicon® Ultra centrifugal filter units (cut-off: 3 kDa) (Merck Millipore, Burlington, MA, USA) were precipitated with ice-cold acetone, recovered by centrifugation and digested *in solution* with commercially available trypsin as previously described [63]. Five biological replicates were processed in this way. As control samples, total protein extracts were prepared from 10-day-old *Arabidopsis* seedlings as described by Basal et al. [64] and digested in solution in the same way as the ER isolates (see above). Six control biological replicates were prepared and analysed. The tryptic peptides were purified on a home-made reversed-phase (C18) microcolumn according to Franc et al. [65] and analysed by LC-MS/MS using settings adapted from Chamrád et al. [66]. The collected MS data were processed and searched using MaxQuant software, version 1.6.17.0 [67] with the “Bruker QTOF” instrument parameter setting [68] and the Andromeda engine [69]. Protein identification was achieved using the *Arabidopsis thaliana* (cv. Columbia) protein database (UniProt, reference proteome UP000006548, 39,345 protein sequences, downloaded 8 March 2021) supplemented with 247 common laboratory contaminants. The iBAQ [54] was calculated to assess the relative abundances of the selected marker proteins, and the localisation of these proteins was investigated *in silico* using following predictors: BaCelLo [70]; iPSORT [71]; PProwler 1.2 [72]; PredSL [73]; SLPFA [74]; SLP-Local [75]; and TargetP 1.1 [76]. A consensus of at least four predictors was required for a protein to be assigned as ER-located. The enriched clusters of functional annotation GO terms and KEGG pathways related to the identified proteins were determined using DAVID Bioinformatics Resources 6.8 [77].

The total protein content of the samples was calculated from the MS data by integrating the area under the curve of the corresponding chromatogram. To this end, a series of protein digests with preset protein contents prepared from *Arabidopsis* seedlings were used for calibration.

All proteomics data were deposited with the ProteomeXchange consortium (<http://proteomecentral.proteomexchange.org>) via the PRIDE partner repository [78] with the dataset identifier PXD027522.

4.8. Optimisation of SPE Protocols

Sucrose solutions of 1.2 M, 0.8 M and 0.6 M prepared by dissolving sucrose in the ER-isolation buffer were divided into equal portions, which were supplemented with a mixture of auxin standards comprising IAA, IAA-glc, IAAsp, IAGlu, oxIAA and oxIAA-glc (1 pmol each). Some aliquots of each spiked sucrose solution were purified by SPE using Oasis™ HLB columns (30 mg/mL, Waters) following the protocol of Novák et al. [55]. Other aliquots were processed by in-tip μ SPE [56]. Eluates were evaporated to dryness *in vacuo* and stored at $-20\text{ }^{\circ}\text{C}$ until LC-MS/MS analysis.

4.9. Control of Auxin Metabolite Profile Stability

As described above, 2 g (FW) of whole *Arabidopsis* seedlings were homogenised, filtered, and centrifuged at $4000\times g$. The supernatant was divided into 1 mL aliquots and transferred into microtubes. Half of the samples were immediately frozen in liquid nitrogen and stored at $-80\text{ }^{\circ}\text{C}$. The other half were placed in a refrigerator ($4\text{ }^{\circ}\text{C}$) and incubated for 3 h. At the end of the incubation, these samples were frozen in liquid nitrogen and stored at $-80\text{ }^{\circ}\text{C}$ until SPE extraction.

Samples were slowly thawed on ice and centrifuged (15 min, $4\text{ }^{\circ}\text{C}$, $21,000\times g$), after which the following stable isotope-labelled internal standards were added to each sam-

ple: [$^{13}\text{C}_6$]IAA, [$^{13}\text{C}_6$]oxIAA, [$^{13}\text{C}_6$]oxIAA-glc, [$^{13}\text{C}_6$]IAA-glc, [$^{13}\text{C}_6$]IAAsp a [$^{13}\text{C}_6$]IAGlu (5 pmol per sample). The samples were then purified by the SPE protocol using OasisTM HLB columns [55]. Finally, the eluates were evaporated to dryness in vacuo and stored at $-20\text{ }^\circ\text{C}$ until LC-MS/MS analysis.

4.10. Extraction and Purification of IAA Metabolites

Samples of enriched ER fractions were slowly thawed on ice. The following stable isotope-labelled internal standards were added to each sample: [$^{13}\text{C}_6$]IAA, [$^{13}\text{C}_6$]oxIAA, [$^{13}\text{C}_6$]oxIAA-glc, [$^{13}\text{C}_6$]IAA-glc, [$^{13}\text{C}_6$]IAAsp and [$^{13}\text{C}_6$]IAGlu (5 pmol per sample). Amicon[®] Ultracentrifugal filters (cut-off: 3 kDa) were used to separate proteins from low molecular weight substances including auxin metabolites. Filtrates were purified by in-tip μSPE as described by Pěnčík et al. [56]. Each filtrate ($\sim 3\text{ mL}$) was divided into two equal parts, which were processed as independent replicates. Samples were acidified to pH 2.7 with 1 M hydrochloric acid, and two 500 μL aliquots were loaded onto a multi-StageTip column that had been activated with 50 μL of acetone (by centrifugation at 2200 rpm, 10 min, $4\text{ }^\circ\text{C}$), 50 μL of methanol (2200 rpm, 10 min, $4\text{ }^\circ\text{C}$), and 50 μL of redistilled water (2200 rpm, 15 min, $4\text{ }^\circ\text{C}$). The column was then washed with 50 μL of 0.1% acetic acid (3400 rpm, 15 min, $4\text{ }^\circ\text{C}$) and eluted with 50 μL of 80% methanol (3400 rpm, 15 min, $4\text{ }^\circ\text{C}$). Eluates from three columns were combined and evaporated to dryness in vacuo and stored at $-20\text{ }^\circ\text{C}$ until LC-MS/MS analysis. For quantification of IAA and its metabolites in Arabidopsis seedlings, samples containing 10 mg plant material (fresh weight) were extracted in 1 mL ice-cold sodium phosphate buffer (50 mM, pH 7.0, $4\text{ }^\circ\text{C}$) containing 0.1% diethyldithiocarbamic acid sodium salt. The mixture of internal standards (5 pmol per sample) was added to each sample. The samples were homogenised, extracted at $4\text{ }^\circ\text{C}$ with continuous shaking (10 min), centrifuged (15 min, $21,000\times g$ at $4\text{ }^\circ\text{C}$) and purified by in-tip μSPE as described above. Eluates were evaporated to dryness in vacuo and stored at $-20\text{ }^\circ\text{C}$ until LC-MS/MS analysis.

4.11. Quantification of IAA Metabolites

The evaporated samples processed by in-tip μSPE were dissolved in 30 μL of 10% methanol. Samples processed by SPE on OasisTM HLB columns (Waters Corp., Milford, CT, USA) were dissolved in 40 μL of 10% methanol. All samples were mixed, sonicated for 5 min, and filtered using a Micro-spin[®] filter tube (0.2 μm pore size; 3 min at 8000 rpm, Chromservis, Praha, Czech republic). Determination of auxin metabolites was performed using a high-performance liquid chromatography–electrospray tandem mass spectrometry with a 1260 Infinity II HPLC system (Agilent Technologies, Santa Clara, CA, USA) equipped with a reversed-phase column (Kinetex; 50 mm \times 2.1 mm, 1.7 μm ; Phenomenex) coupled to a 6495 Triple Quad detector (Agilent Technologies, Santa Clara, CA, USA). Individual analytes were detected in positive and negative ion mode using optimised conditions [56].

5. Conclusions

Although auxins were the first phytohormones to be discovered [79], they continue to be studied intensively. While the subcellular partitioning of auxin biosynthesis, signalling, storage, and deactivation processes suggests the existence of complex mechanisms for maintaining auxin homeostasis, the distribution of IAA and its metabolites within the plant cell remains largely unknown. By combining organelle separation by density gradient centrifugation with ultrasensitive mass spectrometry-based analysis, it may be possible to perform detailed organelle-level auxin profiling to shed light on this issue [80].

To this end, we developed an improved protocol for ER isolation from Arabidopsis seedlings to determine the content of auxin and its metabolites in this organelle. Herein we present the first reported auxin metabolite profile in a highly ER-enriched fraction. We found that active IAA was substantially more abundant in the ER than in total plant extracts, which is consistent with the hypothesised importance of ER in auxin metabolism and signalling modulation [9]. In addition, we were able to characterise the protein content

of the isolated ER fraction, confirming its enrichment with the desired organelle. Our improved ER isolation method could potentially enable further study of this organelle using other “omics” techniques, as well as more detailed studies on intracellular auxin transport.

Supplementary Materials: The following are available online at <https://www.mdpi.com/article/10.3390/ijms22179370/s1>, Figure S1: Procedure of ER-enriched fraction isolation by density gradient ultracentrifugation; Figure S2: Elimination of co-migrating chloroplast by optimisation of initial centrifugation prior to density-gradient separation; Figure S3: Reproducibility of ER isolations; Figure S4: KEGG pathway enrichment analysis; Figure S5: Total process efficiency (%) of solid-phase extraction (SPE) protocols; Table S1: Protein and peptide identification characteristics for analyses of ER isolates and control samples; Table S2: A list of all identified proteins assigned as ER-located; Table S3: Complete functional annotation clustering results for the proteins assigned as ER-located as downloaded from DAVID Bioinformatics Resources 6.8; Table S4: Complete results of KEGG pathways enrichment analysis for the proteins assigned as ER-located as downloaded from DAVID Bioinformatics Resources 6.8; Table S5: IAA metabolites levels and their relative distribution in Arabidopsis seedlings, organelle suspension and ER-enriched fraction; Table S6: Endogenous levels (fmol/μg of proteins) of auxin metabolites in Arabidopsis crude extract and ER-enriched fraction. Tables S1–S4 are available in attached in zip file.

Author Contributions: Conceptualisation, V.S., M.F.K., A.P. and O.N.; methodology, L.V., V.S., M.F.K., I.C. and A.P.; investigation, L.V., V.S., M.F.K., I.C., R.L., A.P. and O.N.; data curation, V.S., I.C., R.L. and A.P.; writing—original draft preparation, L.V., V.S., I.C. and A.P.; writing—review and editing, V.S., M.F.K., I.C., A.P. and O.N.; supervision A.P. and O.N. All authors have read and agreed to the published version of the manuscript.

Funding: This work was financially supported by the Czech Science Foundation (GA17-21581Y) and by the Ministry of Education, Youth and Sports of the Czech Republic (European Regional Development Fund-Project “Plants as a tool for sustainable global development” No. CZ.02.1.01/0.0/0.0/16_019/0000827). L.V. was supported by the Internal Grant Agency of Palacký University in Olomouc (IGA_PrF_2021_016). V.S. was supported by the Endowment fund of Palacký University in Olomouc.

Institutional Review Board Statement: Not applicable.

Informed Consent Statement: Not applicable.

Data Availability Statement: The data presented in the current study are available in the article and supplementary materials.

Acknowledgments: The authors would like to thank Ota Blahoušek for graphic editing of figures, and John Blackwell (Sees-editing Ltd.) for careful language revision of the manuscript.

Conflicts of Interest: The authors declare no conflict of interest.

References

1. Chen, J.; Doyle, C.; Qi, X.; Zheng, H. The endoplasmic reticulum: A social network in plant cells. *J. Integr. Plant Biol.* **2012**, *54*, 840–850. [[CrossRef](#)]
2. Spang, A. Retrograde traffic from the Golgi to the endoplasmic reticulum. *Cold Spring Harb. Perspect. Biol.* **2013**, *5*, a013391. [[CrossRef](#)] [[PubMed](#)]
3. Hawes, C.; Kiviniemi, P.; Kriechbaumer, V. The endoplasmic reticulum: A dynamic and well-connected organelle. *J. Integr. Plant Biol.* **2015**, *57*, 50–62. [[CrossRef](#)]
4. Dashek, W.V. Endoplasmic reticulum. In *Plant Cells and their Organelles*, 1st ed.; Dashek, W.V., Miglani, G.S., Eds.; Wiley: Hoboken, NJ, USA, 2017; pp. 42–60. [[CrossRef](#)]
5. Mravec, J.; Skůpa, P.; Bailly, A.; Hoyerová, K.; Křeček, P.; Bielach, A.; Petrášek, J.; Zhang, J.; Gaykova, V.; Stierhof, Y.-D.; et al. Subcellular homeostasis of phytohormone auxin is mediated by the ER-localized PIN5 transporter. *Nature* **2009**, *459*, 1136–1140. [[CrossRef](#)] [[PubMed](#)]
6. Ding, Z.; Wang, B.; Moreno, I.; Dupláková, N.; Simon, S.; Carraro, N.; Reemmer, J.; Pěnčík, A.; Chen, X.; Tejos, R.; et al. ER-localized auxin transporter PIN8 regulates auxin homeostasis and male gametophyte development in *Arabidopsis*. *Nat. Commun.* **2012**, *3*, 941. [[CrossRef](#)] [[PubMed](#)]
7. Bosco, C.D.; Dovzhenko, A.; Liu, X.; Woerner, N.; Rensch, T.; Eismann, M.; Eimer, S.; Hegermann, J.; Paponov, I.A.; Ruperti, B.; et al. The endoplasmic reticulum localized PIN8 is a pollen-specific auxin carrier involved in intracellular auxin homeostasis. *Plant J.* **2012**, *71*, 860–870. [[CrossRef](#)]

8. Barbez, E.; Kleine-Vehn, J. Divide et Impera—Cellular auxin compartmentalization. *Curr. Opin. Plant Biol.* **2013**, *16*, 78–84. [[CrossRef](#)] [[PubMed](#)]
9. Middleton, A.M.; Dal Bosco, C.; Chlap, P.; Bensch, R.; Harz, H.; Ren, F.; Bergmann, S.; Wend, S.; Weber, W.; Hayashi, K.-I.; et al. Data-Driven Modeling of Intracellular Auxin Fluxes Indicates a Dominant Role of the ER in Controlling Nuclear Auxin Uptake. *Cell Rep.* **2018**, *22*, 3044–3057. [[CrossRef](#)] [[PubMed](#)]
10. Caesar, K.; Thamm, A.M.K.; Witthöft, J.; Elgass, K.; Huppenberger, P.; Grefen, C.; Horak, J.; Harter, K. Evidence for the localization of the *Arabidopsis* cytokinin receptors AHK3 and AHK4 in the endoplasmic reticulum. *J. Exp. Bot.* **2011**, *62*, 5571–5580. [[CrossRef](#)] [[PubMed](#)]
11. Wulfetange, K.; Lomin, S.N.; Romanov, G.A.; Stolz, A.; Heyl, A.; Schmülling, T. The cytokinin receptors of *Arabidopsis* are located mainly to the endoplasmic reticulum. *Plant Physiol.* **2011**, *156*, 1808–1818. [[CrossRef](#)] [[PubMed](#)]
12. Chen, Y.-F.; Randlett, M.D.; Findell, J.L.; Schaller, G.E. Localization of the ethylene receptor ETR1 to the endoplasmic reticulum of *Arabidopsis*. *J. Biol. Chem.* **2002**, *277*, 19861–19866. [[CrossRef](#)] [[PubMed](#)]
13. Barbez, E.; Kubeš, M.; Rolčík, J.; Béziat, C.; Pěňčík, A.; Wang, B.; Rosquete, M.R.; Zhu, J.; Dobrev, P.I.; Lee, Y.; et al. A novel putative auxin carrier family regulates intracellular auxin homeostasis in plants. *Nature* **2012**, *485*, 119–122. [[CrossRef](#)] [[PubMed](#)]
14. Feraru, E.; Feraru, M.I.; Barbez, E.; Waidmann, S.; Sun, L.; Gaidora, A.; Kleine-Vehn, J. PILS6 is a temperature-sensitive regulator of nuclear auxin input and organ growth in *Arabidopsis thaliana*. *Proc. Natl. Acad. Sci. USA* **2019**, *116*, 3893–3898. [[CrossRef](#)] [[PubMed](#)]
15. Ranocha, P.; Dima, O.; Nagy, R.; Felten, J.; Corratgé-Faillie, C.; Novák, O.; Morreel, K.; Lacombe, B.; Martinez, Y.; Pfrunder, S.; et al. *Arabidopsis* WAT1 is a vacuolar auxin transport facilitator required for auxin homeostasis. *Nat. Commun.* **2013**, *4*, 2625. [[CrossRef](#)] [[PubMed](#)]
16. Béziat, C.; Barbez, E.; Feraru, M.I.; Lucyshyn, D.; Kleine-Vehn, J. Light triggers PILS-dependent reduction in nuclear auxin signalling for growth transition. *Nat. Plants* **2017**, *3*, 17105. [[CrossRef](#)]
17. Ljung, K. Auxin metabolism and homeostasis during plant development. *Development* **2013**, *140*, 943–950. [[CrossRef](#)]
18. Casanova-Sáez, R.; Mateo-Bonmatí, E.; Ljung, K. Auxin Metabolism in Plants. *Cold Spring Harb. Perspect. Biol.* **2021**, a039867. [[CrossRef](#)]
19. Stepanova, A.N.; Robertson-Hoyt, J.; Yun, J.; Benavente, L.M.; Xie, D.Y.; Doležal, K.; Schlereth, A.; Jürgens, G.; Alonso, J.M. TAA1-mediated auxin biosynthesis is essential for hormone crosstalk and plant development. *Cell* **2008**, *133*, 177–191. [[CrossRef](#)]
20. Tao, Y.; Ferrer, J.L.; Ljung, K.; Pojer, F.; Hong, F.; Long, J.A.; Li, L.; Moreno, J.E.; Bowman, M.E.; Ivans, L.J.; et al. Rapid synthesis of auxin via a new tryptophan-dependent pathway is required for shade avoidance in plants. *Cell* **2008**, *133*, 164–176. [[CrossRef](#)]
21. Kim, J.I.; Sharkhuu, A.; Jin, J.B.; Li, P.; Jeong, J.C.; Baek, D.; Lee, S.Y.; Blakeslee, J.J.; Murphy, A.S.; Bohnert, H.J.; et al. *yucca6*, a dominant mutation in *Arabidopsis*, affects auxin accumulation and auxin-related phenotypes. *Plant Physiol.* **2007**, *145*, 722–735. [[CrossRef](#)]
22. Kriechbaumer, V.; Botchway, S.W.; Hawes, C. Localization and interactions between *Arabidopsis* auxin biosynthetic enzymes in the TAA/YUC-dependent pathway. *J. Exp. Bot.* **2016**, *67*, 4195–4207. [[CrossRef](#)] [[PubMed](#)]
23. Kubeš, M.; Napier, R. Non-canonical auxin signalling: Fast and curious. *J. Exp. Bot.* **2019**, *70*, 2609–2614. [[CrossRef](#)] [[PubMed](#)]
24. Fendrych, M.; Akhmanova, M.; Merrin, J.; Glanc, M.; Hagihara, S.; Takahashi, K.; Uchida, N.; Torii, K.U.; Friml, J. Rapid and reversible root growth inhibition by TIR1 auxin signalling. *Nat. Plants* **2018**, *4*, 453–459. [[CrossRef](#)] [[PubMed](#)]
25. Korasick, D.A.; Enders, T.A.; Strader, L.C. Auxin biosynthesis and storage forms. *J. Exp. Bot.* **2013**, *64*, 2541–2555. [[CrossRef](#)]
26. Zhang, J.; Lin, J.E.; Harris, C.; Campos Mastrotti Pereira, F.; Wu, F.; Blakeslee, J.J.; Peer, W.A. DAO1 catalyzes temporal and tissue-specific oxidative inactivation of auxin in *Arabidopsis thaliana*. *Proc. Natl. Acad. Sci. USA* **2016**, *113*, 11010–11015. [[CrossRef](#)]
27. Jin, S.-H.; Ma, X.-M.; Han, P.; Wang, B.; Sun, Y.-G.; Zhang, G.-Z.; Li, Y.-J.; Hou, B.-K. UGT74D1 is a novel auxin glycosyltransferase from *Arabidopsis thaliana*. *PLoS ONE* **2013**, *8*, e61705. [[CrossRef](#)]
28. Staswick, P.E.; Serban, B.; Rowe, M.; Tiryaki, I.; Maldonado, M.T.; Maldonado, M.C.; Suza, W. Characterization of an *Arabidopsis* Enzyme Family that Conjugates Amino Acids to Indole-3-Acetic Acid. *Plant Cell* **2005**, *17*, 616–627. [[CrossRef](#)]
29. Cano, A.; Sánchez-García, A.B.; Albacete, A.; González-Bayón, R.; Justamante, M.S.; Ibáñez, S.; Acosta, M.; Pérez-Pérez, J.M. Enhanced Conjugation of Auxin by GH3 Enzymes Leads to Poor Adventitious Rooting in Carnation Stem Cuttings. *Front. Plant Sci.* **2018**, *9*, 566. [[CrossRef](#)]
30. Ostin, A.; Kowalczyk, M.; Bhalerao, R.; Sandberg, G. Metabolism of indole-3-acetic acid in *Arabidopsis*. *Plant Physiol.* **1998**, *118*, 285–296. [[CrossRef](#)]
31. Rampey, R.A.; LeClere, S.; Kowalczyk, M.; Ljung, K.; Sandberg, G.; Bartel, B. A family of auxin-conjugate hydrolases that contributes to free indole-3-acetic acid levels during *Arabidopsis* germination. *Plant Physiol.* **2004**, *135*, 978–988. [[CrossRef](#)]
32. Sanchez Carranza, A.P.; Singh, A.; Steinberger, K.; Panigrahi, K.; Palme, K.; Dovzhenko, A.; Dal Bosco, C. Hydrolases of the ILR1-like family of *Arabidopsis thaliana* modulate auxin response by regulating auxin homeostasis in the endoplasmic reticulum. *Sci. Rep.* **2016**, *6*, 24212. [[CrossRef](#)]
33. Di Mambro, R.; Svolacchia, N.; Dello Ioio, R.; Pierdonati, E.; Salvi, E.; Pedrazzini, E.; Vitale, A.; Perilli, S.; Sozzani, R.; Benfey, P.N.; et al. The Lateral Root Cap Acts as an Auxin Sink that Controls Meristem Size. *Curr. Biol.* **2019**, *29*, 1199–1205. [[CrossRef](#)] [[PubMed](#)]

34. Porco, S.; Pěňčík, A.; Rashed, A.; Voß, U.; Casanova-Sáez, R.; Bishopp, A.; Golebiowska, A.; Bhosale, R.; Swarup, R.; Swarup, K.; et al. Dioxygenase-encoding AtDAO1 gene controls IAA oxidation and homeostasis in *Arabidopsis*. *Proc. Natl. Acad. Sci. USA* **2016**, *113*, 11016–11021. [[CrossRef](#)]
35. Kai, K.; Horita, J.; Wakasa, K.; Miyagawa, H. Three oxidative metabolites of indole-3-acetic acid from *Arabidopsis thaliana*. *Phytochemistry* **2007**, *68*, 1651–1663. [[CrossRef](#)] [[PubMed](#)]
36. Jiskrová, E.; Novák, O.; Pospíšilová, H.; Holubová, K.; Karády, M.; Galuszka, P.; Robert, S.; Frébort, I. Extra- and intracellular distribution of cytokinins in the leaves of monocots and dicots. *New Biotechnol.* **2016**, *33*, 735–742. [[CrossRef](#)]
37. Polanská, L.; Vičánková, A.; Nováková, M.; Malbeck, J.; Dobrev, P.I.; Brzobohatý, B.; Vaňková, R.; Macháčková, I. Altered cytokinin metabolism affects cytokinin, auxin, and abscisic acid contents in leaves and chloroplasts, and chloroplast ultrastructure in transgenic tobacco. *J. Exp. Bot.* **2007**, *58*, 637–649. [[CrossRef](#)] [[PubMed](#)]
38. Benková, E.; Witters, E.; Van Dongen, W.; Kolář, J.; Motyka, V.; Brzobohatý, B.; Van Onckelen, H.A.; Macháčková, I. Cytokinins in tobacco and wheat chloroplasts. Occurrence and changes due to light/dark treatment. *Plant Physiol.* **1999**, *121*, 245–252. [[CrossRef](#)]
39. Thibivilliers, S.; Anderson, D.; Libault, M. Isolation of Plant Root Nuclei for Single Cell RNA Sequencing. *Curr. Protoc. Plant Biol.* **2020**, *5*, e20120. [[CrossRef](#)]
40. Somerville, C.R.; Somerville, S.C.; Ogren, W.L. Isolation of photosynthetically active protoplasts and chloroplasts from *Arabidopsis thaliana*. *Plant Sci. Lett.* **1981**, *21*, 89–96. [[CrossRef](#)]
41. Saxena, P.K.; Fowke, L.C.; King, J. An efficient procedure for isolation of nuclei from plant protoplasts. *Protoplasma* **1985**, *128*, 184–189. [[CrossRef](#)]
42. Antoniadis, I.; Skalický, V.; Sun, G.; Ma, W.; Galbraith, D.W.; Novák, O.; Ljung, K. Fluorescence activated cell sorting—A selective tool for plant cell isolation and analysis. *Cytom. Part A* **2021**. [[CrossRef](#)]
43. Muñoz, P.; Norambuena, L.; Orellana, A. Evidence for a UDP-glucose transporter in Golgi apparatus-derived vesicles from pea and its possible role in polysaccharide biosynthesis. *Plant Physiol.* **1996**, *112*, 1585–1594. [[CrossRef](#)]
44. Robert, S.; Zouhar, J.; Carter, C.J.; Raikhel, N. Isolation of intact vacuoles from *Arabidopsis* rosette leaf-derived protoplasts. *Nat. Protoc.* **2007**, *2*, 259–262. [[CrossRef](#)]
45. Keech, O.; Dizengremel, P.; Gardeström, P. Preparation of leaf mitochondria from *Arabidopsis thaliana*. *Physiol. Plant.* **2005**, *124*, 403–409. [[CrossRef](#)]
46. Seigneurin-Berny, D.; Salvi, D.; Dorne, A.-J.; Joyard, J.; Rolland, N. Percoll-purified and photosynthetically active chloroplasts from *Arabidopsis thaliana* leaves. *Plant Physiol. Biochem.* **2008**, *46*, 951–955. [[CrossRef](#)]
47. Lee, Y.H.; Tan, H.T.; Chung, M.C.M. Subcellular fractionation methods and strategies for proteomics. *Proteomics* **2010**, *10*, 3935–3956. [[CrossRef](#)] [[PubMed](#)]
48. De Araújo, M.; Huber, L.A.; Stasyk, T. Isolation of endocytic organelles by density gradient centrifugation. *Methods Mol. Biol.* **2008**, *424*, 317–331. [[CrossRef](#)] [[PubMed](#)]
49. Petrovská, B.; Jeřábková, H.; Chamrád, I.; Vrána, J.; Lenobel, R.; Uřinová, J.; Šebela, M.; Doležel, J. Proteomic analysis of barley cell nuclei purified by flow sorting. *Cytogenet. Genome Res.* **2014**, *143*, 78–86. [[CrossRef](#)] [[PubMed](#)]
50. Kuhnert, F.; Stefanski, A.; Overbeck, N.; Drews, L.; Reichert, A.S.; Stühler, K.; Weber, A.P.M. Rapid single-step affinity purification of HA-tagged plant mitochondria. *Plant Physiol.* **2020**, *182*, 692–706. [[CrossRef](#)] [[PubMed](#)]
51. Niehaus, M.; Straube, H.; Künzler, P.; Rugen, N.; Hegermann, J.; Giavalisco, P.; Eubel, H.; Witte, C.P.; Herde, M. Rapid Affinity Purification of Tagged Plant Mitochondria (Mito-AP) for Metabolome and Proteome Analyses. *Plant Physiol.* **2020**, *182*, 1194–1210. [[CrossRef](#)] [[PubMed](#)]
52. Deal, R.B.; Henikoff, S. The INTACT method for cell type-specific gene expression and chromatin profiling in *Arabidopsis thaliana*. *Nat. Protoc.* **2011**, *6*, 56–68. [[CrossRef](#)] [[PubMed](#)]
53. Boussardon, C.; Przybyla-Toscano, J.; Carrie, C.; Keech, O. Tissue-Specific Isolation of *Arabidopsis*/plant Mitochondria—IMTACT (Isolation of Mitochondria Tagged in specific Cell Types). *Plant J.* **2020**, *103*, 459–473. [[CrossRef](#)]
54. Schwanhüsser, B.; Busse, D.; Li, N.; Dittmar, G.; Schuchhardt, J.; Wolf, J.; Chen, W.; Selbach, M. Global quantification of mammalian gene expression control. *Nature* **2011**, *473*, 337–342. [[CrossRef](#)]
55. Novák, O.; Hényková, E.; Sairanen, I.; Kowalczyk, M.; Pospíšil, T.; Ljung, K. Tissue-specific profiling of the *Arabidopsis thaliana* auxin metabolome. *Plant J.* **2012**, *72*, 523–536. [[CrossRef](#)] [[PubMed](#)]
56. Pěňčík, A.; Casanova-Sáez, R.; Pilařová, V.; Žukauskaitė, A.; Pinto, R.; Luis Micol, J.; Ljung, K.; Novák, O. Ultra-rapid auxin metabolite profiling for high-throughput mutant screening in *Arabidopsis*. *J. Exp. Bot.* **2018**, *69*, 2569–2579. [[CrossRef](#)]
57. Song, Y.; Hao, Y.; Sun, A.; Li, T.; Li, W.; Guo, L.; Yan, Y.; Geng, C.; Chen, N.; Zhong, F.; et al. Sample preparation project for the subcellular proteome of mouse liver. *Proteomics* **2006**, *6*, 5269–5277. [[CrossRef](#)]
58. Vertommen, A.; Panis, B.; Swennen, R.; Carpentier, S.C. Challenges and solutions for the identification of membrane proteins in non-model plants. *J. Proteom.* **2011**, *74*, 1165–1181. [[CrossRef](#)]
59. Parsons, H.T.; Christiansen, K.; Knierim, B.; Carroll, A.; Ito, J.; Batth, T.S.; Smith-Moritz, A.M.; Morrison, S.; McInerney, P.; Hadi, M.Z.; et al. Isolation and Proteomic Characterization of the *Arabidopsis* Golgi Defines Functional and Novel Components Involved in Plant Cell Wall Biosynthesis. *Plant Physiol.* **2012**, *159*, 12–26. [[CrossRef](#)]

60. Viotti, C.; Kruger, F.; Krebs, M.; Neubert, C.; Fink, F.; Lupanga, U.; Scheuring, D.; Boutte, Y.; Frescatada-Rosa, M.; Wolfenstetter, S.; et al. The Endoplasmic Reticulum Is the Main Membrane Source for Biogenesis of the Lytic Vacuole in *Arabidopsis*. *Plant Cell* **2013**, *25*, 3434–3449. [[CrossRef](#)]
61. Hooper, C.M.; Castleden, I.R.; Tanz, S.K.; Aryamanesh, N.; Millar, A.H. SUBA4: The interactive data analysis centre for *Arabidopsis* subcellular protein locations. *Nucleic Acids Res.* **2017**, *45*, D1064–D1074. [[CrossRef](#)] [[PubMed](#)]
62. Biała, W.; Jasiński, M. The Phenylpropanoid Case—It Is Transport that Matters. *Front. Plant Sci.* **2018**, *9*, 1610. [[CrossRef](#)] [[PubMed](#)]
63. Leon, I.R.; Schwammle, V.; Jensen, O.N.; Sprenger, R.R. Quantitative assessment of in-solution digestion efficiency identifies optimal protocols for unbiased protein analysis. *Mol. Cell. Proteom.* **2013**, *12*, 2992–3005. [[CrossRef](#)] [[PubMed](#)]
64. Bassal, M.; Abukhalaf, M.; Majovsky, P.; Thieme, D.; Herr, T.; Ayash, M.; Tabassum, N.; Al Shweiki, M.R.; Proksch, C.; Hmedat, A.; et al. Reshaping of the *Arabidopsis thaliana* Proteome Landscape and Co-regulation of Proteins in Development and Immunity. *Mol. Plant* **2020**, *13*, 1709–1732. [[CrossRef](#)] [[PubMed](#)]
65. Franc, V.; Šebela, M.; Řehulka, P.; Končítiková, R.; Lenobel, R.; Madzak, C.; Kopečný, D. Analysis of N-glycosylation in maize cytokinin oxidase/dehydrogenase 1 using a manual microgradient chromatographic separation coupled offline to MALDI-TOF/TOF mass spectrometry. *J. Proteom.* **2012**, *75*, 4027–4037. [[CrossRef](#)]
66. Chamrád, I.; Simerský, R.; Běřešová, L.; Strnad, M.; Šebela, M.; Lenobel, R. Proteomic Identification of a Candidate Sequence of Wheat Cytokinin-Binding Protein 1. *J. Plant Growth Regul.* **2014**, *33*, 896–902. [[CrossRef](#)]
67. Tyanova, S.; Temu, T.; Cox, J. The MaxQuant computational platform for mass spectrometry-based shotgun proteomics. *Nat. Protoc.* **2016**, *11*, 2301–2319. [[CrossRef](#)]
68. Beck, S.; Michalski, A.; Raether, O.; Lubeck, M.; Kaspar, S.; Goedecke, N.; Baessmann, C.; Hornburg, D.; Meier, F.; Paron, I.; et al. The impact II, a very high-resolution quadrupole time-of-flight instrument (QTOF) for deep shotgun proteomics. *Mol. Cell. Proteom.* **2015**, *14*, 2014–2029. [[CrossRef](#)]
69. Cox, J.; Neuhauser, N.; Michalski, A.; Scheltema, R.A.; Olsen, J.V.; Mann, M. Andromeda: A peptide search engine integrated into the MaxQuant environment. *J. Proteome Res.* **2011**, *10*, 1794–1805. [[CrossRef](#)]
70. Pierleoni, A.; Martelli, P.L.; Fariselli, P.; Casadio, R. BaCelLo: A balanced subcellular localization predictor. *Bioinformatics* **2006**, *22*, e408–e416. [[CrossRef](#)]
71. Bannai, H.; Tamada, Y.; Maruyama, O.; Nakai, K.; Miyano, S. Extensive feature detection of N-terminal protein sorting signals. *Bioinformatics* **2002**, *18*, 298–305. [[CrossRef](#)]
72. Bodén, M.; Hawkins, J. Prediction of subcellular localization using sequence-biased recurrent networks. *Bioinformatics* **2005**, *21*, 2279–2286. [[CrossRef](#)] [[PubMed](#)]
73. Petsalaki, E.I.; Bagos, P.G.; Litou, Z.I.; Hamodrakas, S.J. PredSL: A tool for the N-terminal sequence-based prediction of protein subcellular localization. *Genom. Proteom. Bioinform.* **2006**, *4*, 48–55. [[CrossRef](#)]
74. Tamura, T.; Akutsu, T. Subcellular location prediction of proteins using support vector machines with alignment of block sequences utilizing amino acid composition. *BMC Bioinform.* **2007**, *8*, 466. [[CrossRef](#)]
75. Matsuda, S.; Vert, J.-P.; Saigo, H.; Ueda, N.; Toh, H.; Akutsu, T. A novel representation of protein sequences for prediction of subcellular location using support vector machines. *Protein Sci.* **2005**, *14*, 2804–2813. [[CrossRef](#)]
76. Emanuelsson, O.; Nielsen, H.; Brunak, S.; von Heijne, G. Predicting subcellular localization of proteins based on their N-terminal amino acid sequence. *J. Mol. Biol.* **2000**, *300*, 1005–1016. [[CrossRef](#)] [[PubMed](#)]
77. Huang, D.W.; Sherman, B.T.; Lempicki, R.A. Systematic and integrative analysis of large gene lists using DAVID bioinformatics resources. *Nat. Protoc.* **2009**, *4*, 44–57. [[CrossRef](#)]
78. Perez-Riverol, Y.; Csordas, A.; Bai, J.; Bernal-Llinares, M.; Hewapathirana, S.; Kundu, D.J.; Inuganti, A.; Griss, J.; Mayer, G.; Eisenacher, M.; et al. The PRIDE database and related tools and resources in 2019: Improving support for quantification data. *Nucleic Acids Res.* **2019**, *47*, D442–D450. [[CrossRef](#)]
79. Darwin, C.; Darwin, F. *The Power of Movement in Plants*; John Murray: London, UK, 1880.
80. Novák, O.; Napier, R.; Ljung, K. Zooming in on Plant Hormone Analysis: Tissue- and Cell-Specific Approaches. *Annu. Rev. Plant Biol.* **2017**, *68*, 323–348. [[CrossRef](#)]



Supplementary materials

Auxin Metabolome Profiling in the Arabidopsis Endoplasmic Reticulum Using an Optimised Organelle Isolation Protocol

Ludmila Včelařová †, Vladimír Skalický †, Ivo Chamrád, René Lenobel, Martin F. Kubeš ‡, Aleš Pěňčík *
and Ondřej Novák

Laboratory of Growth Regulators, Institute of Experimental Botany of the Czech Academy of Sciences, and Faculty of Science, Palacký University, Šlechtitelů 27, CZ-78371 Olomouc, Czech Republic; ludmila.vcelarova@upol.cz (L.V.); vladimir.skalicky@upol.cz (V.S.); ivo.chamrad@upol.cz (I.C.); rene.lenobel@upol.cz (R.L.); martin.kubes@uhk.cz (M.F.K.); ondrej.novak@upol.cz (O.N.).

* Correspondence: ales.pencik@upol.cz; Tel.: +420-585-634-853

† These authors contributed equally to this work.

‡ Current address: Department of Biology, Faculty of Science, University of Hradec Králové, Rokitanského 62, 500 03 Hradec Králové, Czech Republic.

Citation: Včelařová, L.; Skalický, V.; Chamrád, I.; Lenobel, R.; Kubeš, M.F.; Pěňčík, A.; Novák, O. Auxin Metabolome Profiling in the Arabidopsis Endoplasmic Reticulum Using an Optimised Organelle Isolation Protocol. *Int. J. Mol. Sci.* **2021**, *22*, 9370. <https://doi.org/10.3390/ijms22179370>

Academic Editor: Jutta Ludwig-Mueller

Received: 31 July 2021

Accepted: 25 August 2021

Published: 29 August 2021

Publisher's Note: MDPI stays neutral with regard to jurisdictional claims in published maps and institutional affiliations.



Copyright: © 2021 by the authors. Submitted for possible open access publication under the terms and conditions of the Creative Commons Attribution (CC BY) license (<http://creativecommons.org/licenses/by/4.0/>).

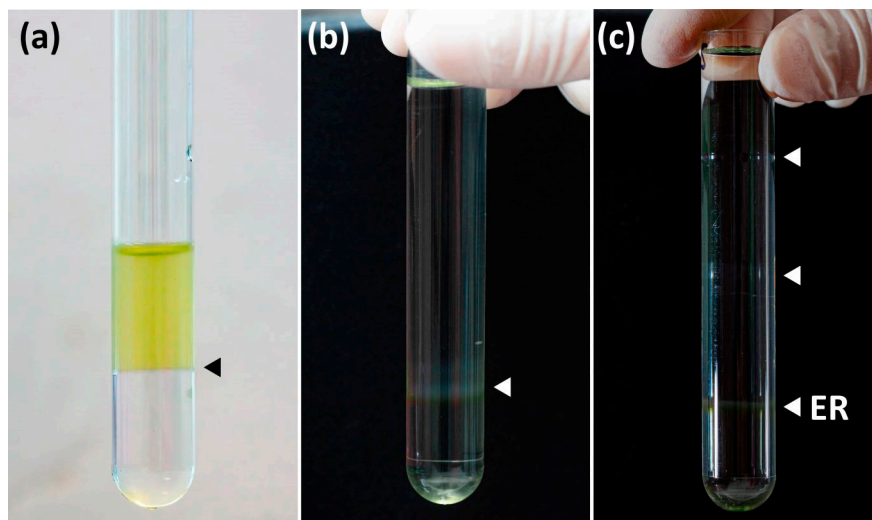


Figure S1. Procedure for isolating the ER-enriched fraction by density gradient ultracentrifugation. (a) A supernatant S4,000 loaded on the top of 31% (w/w) sucrose solution. (b) A two-step density gradient after ultracentrifugation. The supernatant was removed and focused microsomes were overlaid with 27%, 19%, and 8% (w/w) sucrose solutions. (c) A four-step gradient after the final ultracentrifugation. The 27/31% interface enriched with ER microsomes was collected. Arrows indicate interphases between the two gradient-forming solutions, ER – endoplasmic reticulum-enriched fraction.

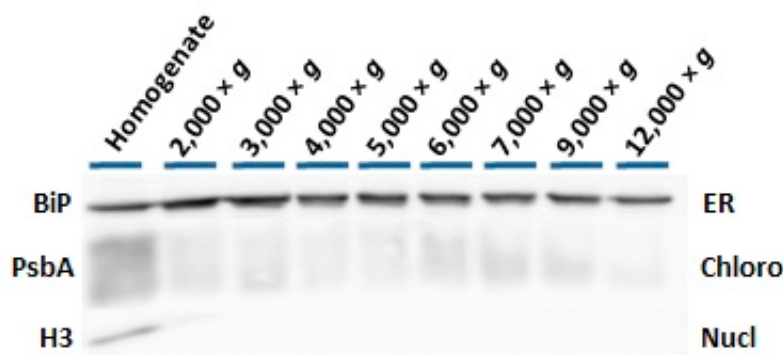


Figure S2. Elimination of co-migrating chloroplasts by optimizing the initial centrifugation prior to density-gradient separation. The crude homogenate was centrifuged at speeds between 2,000 and 12,000 \times g. The parent homogenate and the resulting supernatants were then subjected to Western blot analysis. The following organelle-specific markers were immunodetected: endoplasmic reticulum – ER (Lumena-binding protein, BiP), chloroplasts – Chloro (D1 protein of photosystem II, PsbA) and nuclei – Nucl (Histone 3, H3).

Isolation					
Replicate 1	Replicate 1				
Replicate 2	74.40	Replicate 2			
Replicate 3	76.40	76.80	Replicate 3		
Replicate 4	76.70	74.00	73.00	Replicate 4	
Replicate 5	68.20	67.00	71.90	69.70	Replicate 5

Figure S3. Reproducibility of ER isolations visualized using a histogram showing pairwise comparisons of protein identifications (in %).

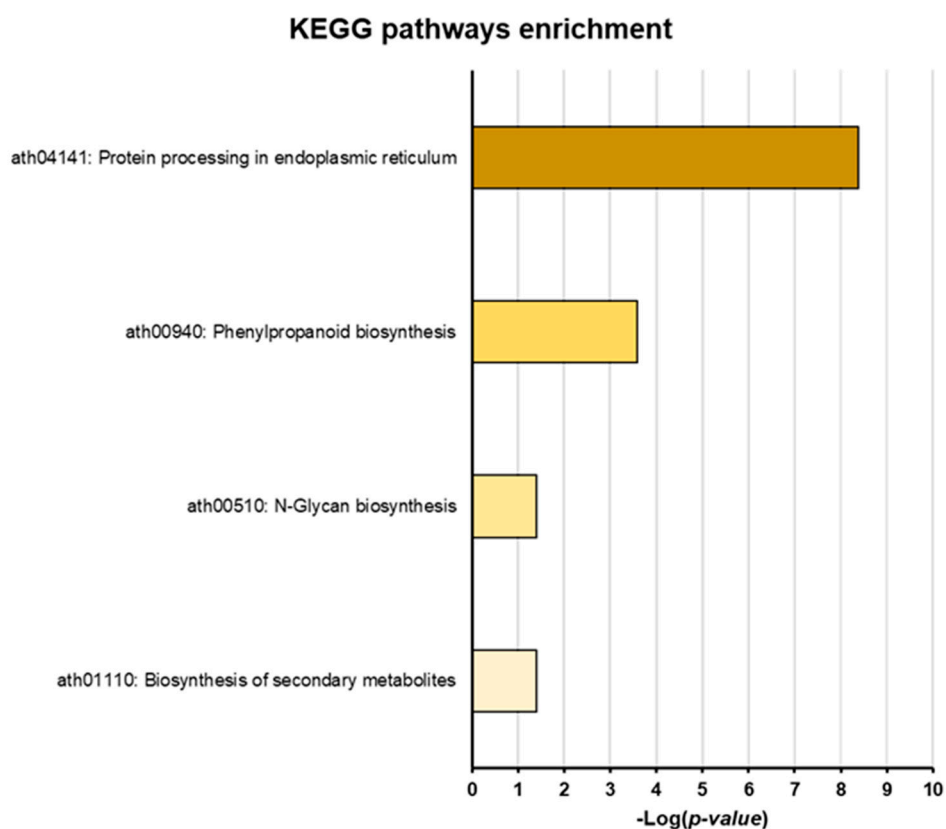


Figure S4. KEGG pathway enrichment analysis. Significantly enriched KEGG pathways are sorted according to the $-\log$ of their p-value.

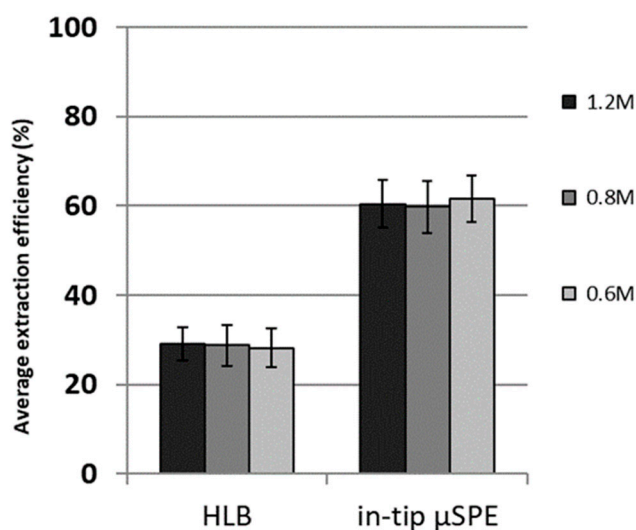


Figure S5. Total process efficiency (%) of solid-phase extraction (SPE) protocols. The recovery achieved using a conventional HLB column [1] was compared to that for an in-tip μ SPE protocol [2]. Gradient-forming sucrose solutions were spiked with a mixture of six auxin standards (1 pmol each). Recoveries of standards were evaluated by LC-MS/MS. Values are mean recoveries (%) of all tested auxin standards ($n=3$). Error bars indicate the s. d.

Tables S1–S4. Tables are available in attached in zip file.

Table S1. Protein and peptide identification characteristics for analyses of ER isolates and control samples (n=5 for both) as provided by MaxQuant software version 1.6.10.43 [3].

Table S2. A list of all identified proteins assigned as ER-located.

Table S3. Complete functional annotation clustering results for the proteins assigned as ER-located, as downloaded from DAVID Bioinformatics Resources 6.8 [4].

Table S4. Complete results of a KEGG pathways enrichment analysis for the proteins assigned as ER-located as downloaded from DAVID Bioinformatics Resources 6.8 [4].

Table S5. Levels of IAA metabolites levels and their relative abundance in Arabidopsis seedlings, an organelle suspension, and the ER-enriched fraction. Values are mean (n=5).

Compound	Crude extract		Organelle suspension		ER fraction	
	(<i>pmol/g FW</i>)	(%)	(<i>fmol/ml</i>)	(%)	(<i>fmol/ml</i>)	(%)
IAA	102.1	1.7	11,451.4	4.8	832.3	8.8
IAAsp	25.1	0.4	2,265.7	1.0	15.5	0.2
IAGlu	100.3	1.7	9,835.0	4.1	111.0	1.2
IAA-glc	78.2	1.3	8,883.5	3.7	118.3	1.2
oxIAA	909.2	15.6	36,105.3	15.2	975.6	10.3
oxIAA-glc	4,629.0	79.2	168,948.3	71.1	7,455.4	78.4

Table S6. Endogenous levels (*fmol/μg* of proteins) of auxin metabolites in the Arabidopsis crude extract and ER-enriched fraction. The mean abundance ± s.d. is given (n=5) for indole-3-acetic acid (IAA), IAA-aspartate (IAAsp), IAA-glutamate (IAGlu), IAA-glucose (IAA-glc), 2-oxoindole-3-acetic acid (oxIAA), oxIAA-glucose (oxIAA-glc)

Compound	Crude extract	ER fraction
	<i>fmol/μg of proteins</i>	
IAA	11.7 ± 0.9	718.1 ± 34.0
IAAsp	2.9 ± 0.1	13.3 ± 2.7
IAGlu	11.5 ± 0.9	95.7 ± 18.3
IAA-glc	8.9 ± 0.8	102.0 ± 16.6
oxIAA	103.9 ± 10.8	841.7 ± 150.0
oxIAA-glc	529.0 ± 13.7	6,432.1 ± 1,244.9

References

- Novák, O.; Hényková, E.; Sairanen, I.; Kowalczyk, M.; Pospíšil, T.; Ljung, K. Tissue-specific profiling of the Arabidopsis thaliana auxin metabolome. *Plant J.* **2012**, *72*, 523–36, doi:10.1111/j.1365-313X.2012.05085.x.
- Pěňčík, A.; Casanova-Sáez, R.; Pilařová, V.; Žukauskaitė, A.; Pinto, R.; Luis Micol, J.; Ljung, K.; Novák, O. Ultra-rapid auxin metabolite profiling for high-throughput mutant screening in Arabidopsis. *J. Exp. Bot.* **2018**, *69*, 2569–2579, doi:10.1093/jxb/ery084.

3. Tyanova, S.; Temu, T.; Cox, J. The MaxQuant computational platform for mass spectrometry-based shotgun proteomics. *Nat. Protoc.* **2016**, *11*, 2301–2319, doi:10.1038/nprot.2016.136.
4. Huang, D. W.; Sherman, B. T.; Lempicki, R. A. Systematic and integrative analysis of large gene lists using DAVID bioinformatics resources. *Nat. Protoc.* **2009**, *4*, 44–57, doi:10.1038/nprot.2008.211.



Article

Auxin metabolite profiling in isolated and intact plant nuclei

Vladimír Skalický¹, Tereza Vojtková¹, Aleš Pěňčík¹, Jan Vrána², Katarzyna Juzon³, Veronika Koláčková², Michaela Sedlářová⁴, Martin F. Kubes^{1,5,#,*} and Ondřej Novák^{1,*}

¹ Laboratory of Growth Regulators, Institute of Experimental Botany of the Czech Academy of Sciences & Faculty of Science of Palacký University, Šlechtitelů 27, 78371 Olomouc, Czech Republic; vladimir.skalicky@upol.cz, voj.te111@gmail.com, ales.pencik@upol.cz

² Centre of Plant Structural and Functional Genomics, Institute of Experimental Botany, Czech Academy of Sciences, Šlechtitelů 31, 779 00 Olomouc, Czech Republic; kolackova@ueb.cas.cz, jan.vrana@fno.cz

³ Department of Biotechnology, The Franciszek Górski Institute of Plant Physiology, Polish Academy of Sciences, Niezapominajek 21, 30-239 Krakow, Poland; k.juzon@ifp-pan.edu.pl

⁴ Department of Botany, Faculty of Science, Palacký University, Šlechtitelů 27, 78371 Olomouc, Czech Republic; michaela.sedlarova@upol.cz

⁵ School of Life Sciences, University of Warwick, Coventry CV4 7AL, United Kingdom;

Actual address: University of Hradec Králové, Faculty of Science, Department of Biology, Rokitanského 62, 500 03 Hradec Králové, Czech Republic

* Correspondence: novako@ueb.cas.cz, martin.kubes@uhk.cz; Tel.: +420-585-634-852, O.N.

Abstract: The plant nucleus plays an irreplaceable role in cellular control and regulation by auxin (indole-3-acetic acid, IAA) mainly because canonical auxin signaling takes place here. Auxin can enter the nucleus from either the endoplasmic reticulum or cytosol. Therefore, new information about the auxin metabolome (auxinome) in the nucleus can illuminate our understanding of subcellular auxin homeostasis. Different methods of nucleus isolation from various plant tissues have been described previously, but information about auxin metabolite levels in nuclei is still fragmented and insufficient. Herein, we tested several published nucleus isolation protocols based on differential centrifugation or flow cytometry. The optimized sorting protocol leading to promising yield, intactness and purity was then combined with an ultra-sensitive mass spectrometry analysis. Using this approach, we can present the first complex report on the auxinome of isolated nuclei from cell cultures of Arabidopsis and tobacco. Moreover, our results show dynamic changes in auxin homeostasis at the intranuclear level after treatment of protoplasts with free IAA, or indole as a precursor of auxin biosynthesis. Finally, we can conclude that the methodological procedure combining flow cytometry and mass spectrometry offers new horizons for the study of auxin homeostasis at the subcellular level.

Keywords: subcellular fractionation; flow cytometry; nucleus; auxin; auxin metabolism

Citation: Lastname, F.; Lastname, F.; Lastname, F. Title. *Int. J. Mol. Sci.* **2021**, *22*, x. <https://doi.org/10.3390/xxxxx>

Academic Editor: Firstname Lastname

Received: date

Accepted: date

Published: date

Publisher's Note: MDPI stays neutral with regard to jurisdictional claims in published maps and institutional affiliations.



Copyright: © 2021 by the authors. Submitted for possible open access publication under the terms and conditions of the Creative Commons Attribution (CC BY) license (<https://creativecommons.org/licenses/by/4.0/>).

1. Introduction

The processes of plant growth, development, growth and plasticity are driven mainly by plant hormones. Auxin, one of the plant hormone groups and represented by native indole-3-acetic acid (IAA), plays an irreplaceable role in all these aspects through the entire plant life span. Auxins act at the organ/tissue [1], the cellular [2,3] and the subcellular level [4]. Thus, precise control of the spatio-temporal distribution of IAA in both plant and cell is critical [5,6].

Auxin homeostasis is tightly regulated by the coordination of transport, biosynthesis and metabolism, which altogether regulate the availability of IAA. It seems that cellular and subcellular compartmentalization of auxin may be also functionally important for the control of physiological processes [4]. The canonical auxin signaling pathway occurs in nuclei, where IAA “glues” TRANSPORT INHIBITOR RESPONSE 1/AUXIN SIGNALING F-BOX (TIR1/AFB) proteins with AUXIN/INDOLE-3-ACETIC ACID (Aux/IAAs) in a co-

receptor complex. Subsequently, Aux/IAAs, which repress AUXIN RESPONSE FACTORS (ARFs), are degraded and auxin-responsive genes are transcribed. Recently, it was shown that TIR1/AFBs and ARF3, also known as ETTIN, are not found exclusively in the nucleus but also in cytosol. Thus, they may also be involved in non-transcriptional responses to auxin input known as non-canonical auxin signaling [7–11].

Several intracellular auxin transporters have been already described, such as the endoplasmic reticulum (ER) localized PIN-FORMED (PIN5, [12] and PIN8, [13,14], PIN-LIKES (PILS) [6,15] and tonoplast located WALLS ARE THIN1 (WAT1) [16]. However, the details of the regulation of intracellular IAA fluxes and thus of the control of subcellular homeostasis remain elusive. Recently, two possible routes – via the ER or via the cytosol – were proposed. IAA can enter the nucleus directly, although ER-to-nucleus flux dominates [17].

De novo IAA biosynthesis is mainly mediated via the TRYPTOPHAN AMINOTRANSFERASE OF ARABIDOPSIS/YUCCA (TAA/YUC) pathway including tryptophan (Trp) and indole-3-pyruvic acid (IPyA) as precursors in *Arabidopsis thaliana* [18]. The TAA/YUC enzyme complex has been shown to be anchored to the ER membrane and faced to cytosol [19]. However, the YUC enzyme family comprises homologues for which localization remains unclear. Additionally, three other IAA biosynthetic pathways have been described in Arabidopsis named according to their intermediates: indole-3-acetamide (IAM), tryptamine (TRA) and indole-3-acetaldoxime (IAOx) pathway [20]. A Trp-independent pathway for auxin synthesis has also been proposed [21].

Homeostasis of free IAA is likewise controlled by (ir)reversible conjugation with glucose (glc) or amino acids by UDP-glucosyl transferases or GRETCHEN HAGEN 3 (GH3), respectively [22–24]. Localization of IAA conjugation is not fully clear, however, it was recently published that GH3.17 occurs in cytosol [25]. IAA-glucose (IAA-glc) is believed to be a storage form enriched in vacuoles [16], whereas only some IAA amino conjugates can be reversibly transformed back to free IAA by amidohydrolases located mainly in ER [26,27]. DIOXYGENASE FOR AUXIN OXIDATION 1 (DAO1) catalyzes terminal IAA degradation producing 2-oxindole-3-acetic acid (oxIAA) in the cytosol [28,29] which can be also conjugated with amino acids or glucose (oxIAA-glc) [21].

Direct or indirect monitoring of the subcellular auxinome in plants has been a high interest of plant biologists for many decades [30]. An important prerequisite is an effective and robust method providing a pure, intact nuclear fraction. A classic biochemical method is differential centrifugation (DC), typically in combination with continuous or discontinuous density gradients. Nuclei are usually pelleted during an initial step at about 1000 – 2000× *g* as a crude nuclear fraction. For purer fractions, centrifugation using sucrose, Percoll, Ficoll, or other media offer density, osmolarity or viscosity gradients [31–33]. The detergent Triton X-100 was used successfully for endomembrane washing [32,34–36].

Other two available methods circumvent typical problems associated with biochemical purification techniques. Flow cytometry (FCM) enables isolation of nuclei from crude cell lysates [37–39]. Fluorescence from a wide range of organelle specific fluorescent dyes e.g. for nuclei 4',6-diamidino-2-phenylindole (DAPI) is used. A method called INTACT (Isolation of Nuclei TAgged in specific Cell Types) allows affinity-based isolation of nuclei. This technique combines specific labeling of a nuclear envelope protein by biotin in the cell type of interest and streptavidin-coated magnetic beads (micro or nano size) for biotin-labeled nucleus affinity purification (AP) [40,41].

In this work, we focus on two subcellular fractionation methods. We optimized methods with emphasis on nuclear intactness, purity and yield using fluorescence microscopy, immunoblots and 3D volume reconstruction. Finally, the auxinome of isolated nuclei from cell cultures of Arabidopsis and tobacco was determined by ultra-sensitive LC-MS/MS.

2. Results

2.1. Comparison of DC and FCM as nucleus isolation methods

Two cell cultures, *Arabidopsis thaliana* ecotype *Landsberg erecta* (Ath-Ler) and tobacco *Nicotiana tabacum* cv. Bright Yellow 2 (BY-2) were cultivated under the same standard conditions (see details in Methods section). The cell lines showed distinct characteristics, such as formation of cell clusters (Figure 1a,f), different growth parameters such as cell density and growth curves [42], and composition of cell wall [43]. Therefore, both lines were selected for our comparative study.

We tested various protocols for releasing nuclei from the plant cells. The first isolation protocol was based on grinding cell cultures using a Dounce homogenizer in combination with classical DC [44] (Method S1). Cell debris was present in the nuclear fraction (Figure S1,b) and so we decided to examine homogenization protocols based on protoplast isolation [34,45] (Figure 1b,g). A protoplasting protocol based on Saxena et al. [34] was optimized, although problems with quality and yields persisted. Therefore, we finally applied the well-established protocol published by Yoo et al. [45]. Importantly, plasma membrane rupture enabled soft release of intact subcellular compartments during the protoplast lysis step (Figure 1c,h). Samples were further processed to obtain purified, enriched intact nuclei (Figure 1d,i and Figure 1e,j).

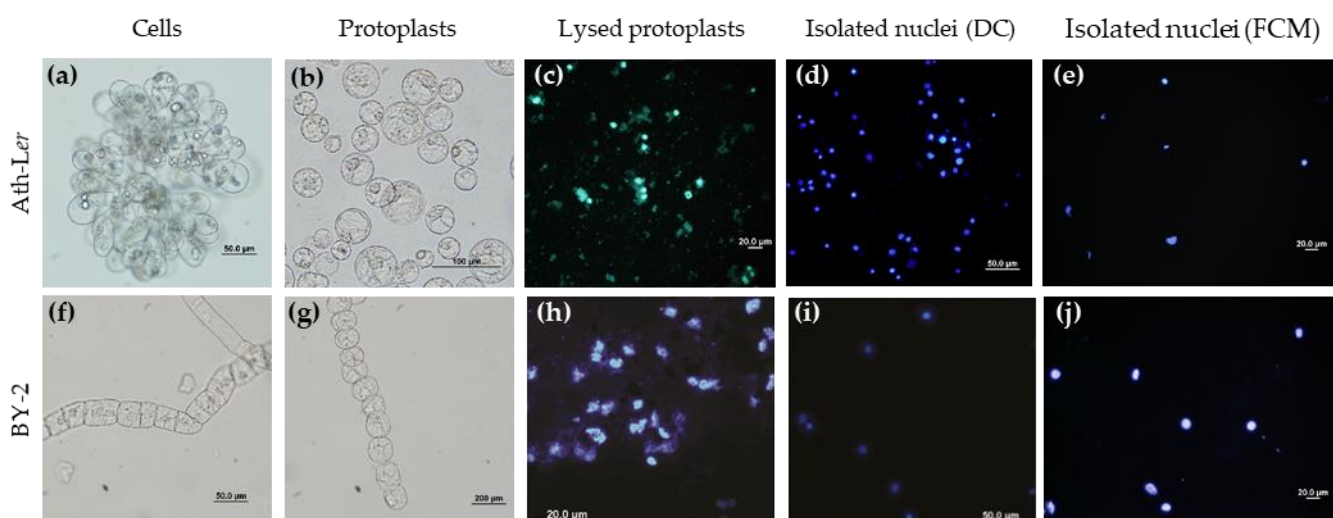


Figure 1. Microscopic analysis of nucleus isolation protocols. Isolations of nuclei from cell lines of (a–e) *Arabidopsis thaliana* ecotype *Landsberg erecta* (Ath-Ler) and (f–j) *Nicotiana tabacum* cv. BY-2 (BY-2) were performed by differential centrifugation (DC) or flow cytometry (FCM). (a) Ath-Ler cells, (b) Ath-Ler protoplasts, (c) Ath-Ler protoplasts after lysis, (d) Ath-Ler nuclei isolated by DC, (e) Ath-Ler nuclei isolated by FCM; (f) BY-2 cells, (g) BY-2 protoplasts, (h) BY-2 protoplasts after lysis, (i) BY-2 nuclei isolated by DC, (j) BY-2 nuclei isolated by FCM. Nuclei were stained with DAPI (2 μg/ml).

The purity of all nuclear fractions was evaluated by immunoblot analysis (Figure 2). Four representative organelle markers for nuclei (Histone 3, H3), ER (Lumena-binding protein, BiP), Golgi complex (Coatomer subunit gamma, Sec21p) and vacuole (Epsilon subunit of tonoplast H⁺ATPase, V-ATPase) were selected. Compared to the nuclear fractions isolated by the FCM method (Figure 2b), fractions isolated by the DC method showed the presence of contaminating organelle markers, mainly ER and Golgi complex (Figure 2a). Next, we performed volume analysis of sorted nuclei together with image processing and 3D-FISH according to Koláčková et al. [46] and Perníčková et al. [47] (Method S2). Our data clearly showed that cell nuclei isolated by FCM offers intactness, but also heterogeneity of 3D shapes. However, the calculated volumes based on 3D reconstructions suggest a low level of variability (Figure S2). In summary, FCM provides lower yields, but significantly higher purity of intact nuclei than the classical DC method. Moreover, the use of FCM can improve subsequent LC-MS/MS analysis [48].

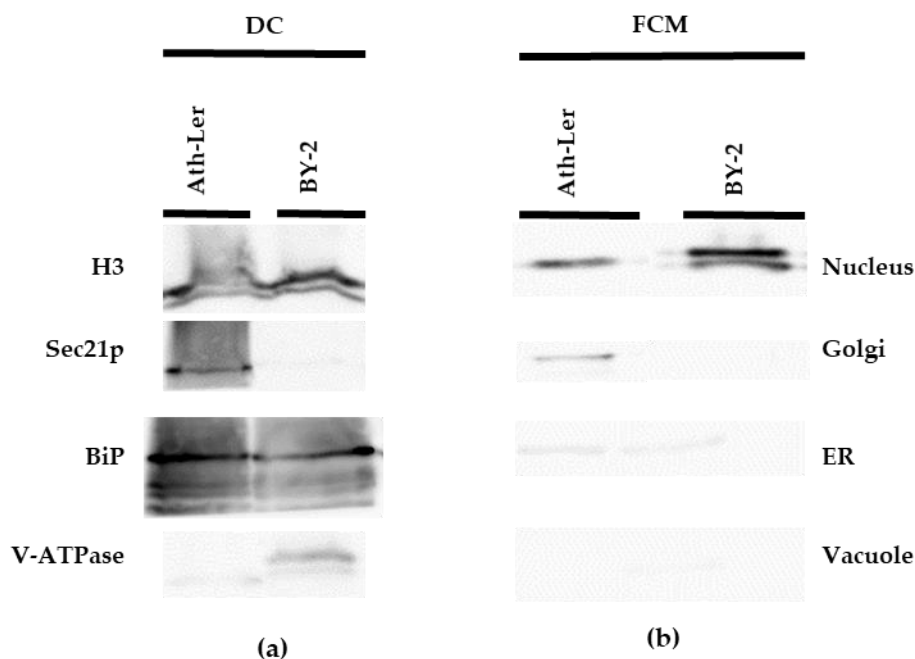


Figure 2. Purity control of nuclear fractions by immunoblotting. Nuclei were isolated from *Arabidopsis thaliana* Ler (Ath-Ler) and *N. tabacum* cv. BY-2 (BY-2) cell lines by (a) differential centrifugation (DC) and (b) flow cytometry (FCM). Nuclear extracts were immunoblotted using anti-Histone 3 (H3) to confirm enrichment of nuclei. The following antibodies were used to test for the presence of contaminating organelles: Anti-Coatomer subunit gamma (Sec21p) for presence of Golgi complex, anti-Luminal-binding protein (BiP) for presence of endoplasmic reticulum (ER), and anti-Epsilon subunit of tonoplast H⁺ATPase (V-ATPase) for presence of vacuole.

2.2. Auxinome of isolated nuclei

To reduce the time required for the preparation of individual samples and to improve nuclear intactness, a formaldehyde fixation-based method [49] (Method S1) was tested. Surprisingly, fixation was not compatible with auxin metabolic analysis. Formaldehyde cell fixation significantly reduced sensitivity and/or caused loss of MS signal, including the internal standards.

Therefore, a long-term stability control experiment was performed to evaluate the effect of the FCM procedure on auxin profiles in *A. thaliana* nuclei. All sorted fractions were analyzed by LC-MS/MS [50]. Surprisingly, no dramatic conversion between IAA, its main precursor (IPyA) and catabolite (oxIAA) was observed in sorted nuclei up to 14 h after protoplast lysis (Figure 3a). This finding indicates valid results of endogenous auxin levels in nuclear fractions isolated by FCM method.

A comparison of IAA metabolic profiles in *A. thaliana* nuclei isolated by DC or FCM showed that only six auxin metabolites were quantified in the fraction isolated by DC. The FCM approach gave a wider portfolio of compounds across the auxinome (Figure 3b). This optimized approach combining an enzymatic cell wall digestion and FCM combined with an ultra-sensitive MS-based analysis was further used to profile the auxinome in isolated nuclei from both Ath-Ler and BY-2 cell cultures. The analysis reveals not only IAA and relative metabolites, but also its precursors to give the first complex auxin metabolic profile for plant nuclei (Figure 1). Nine auxin related compounds were detected, although IAM was detected only in Ath-Ler nuclei (Table S1). Surprisingly, indole-3-acetonitrile (IAN) was not detected in the isolated nuclei compared to the analysis performed on Ath-Ler cells (Table S2). Moreover, IAA-glc and oxIAA-glc were not detected in nuclei or cells.

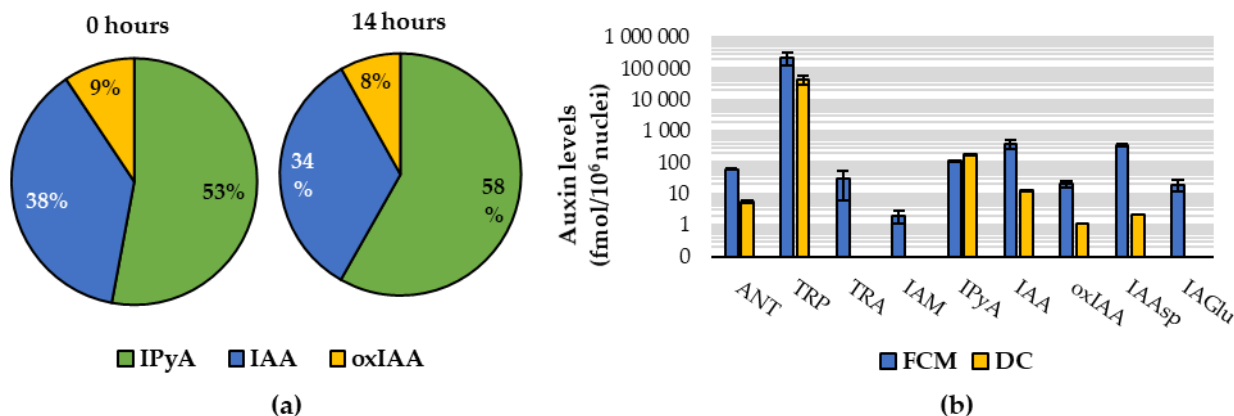


Figure 3. Auxin metabolite profiles in isolated nuclei. (a) Stability of auxin metabolite profile based on relative distribution of indole-3-pyruvic acid (IPyA), indole-3-acetic acid (IAA) and 2-oxoindole-3-acetic acid (oxIAA) in *Arabidopsis thaliana* nuclei sorted directly (0 h) or stored on ice (14 hours) after protoplast lysis. (b) The auxinome determined in *A. thaliana* nuclei obtained by differential centrifugation (DC) or flow cytometry (FCM). Anthranilate (ANT), tryptophan (TRP), tryptamine (TRA), indole-3-acetamide (IAM), IAA-aspartate (IAAsp), IAA-glutamate (IAGlu). Indole-3-acetonitrile, IAA-glucose and oxIAA-glucose were not detected. 5 and 4 biological replicates were analyzed for nuclei isolated by DC and FCM, respectively, except IPyA (n=2/3). Error bars indicate SD.

The dominant compound in all samples was tryptophan (99.6% and 99.8% of relative distribution in *Ath-Ler* and BY-2, respectively, Figure 4a). Interestingly, the BY-2 results showed a higher proportion of IAA precursors (IPyA; TRA; and anthranilate, ANT), whereas *Ath-Ler* profiles had significantly higher levels of IAA and its metabolites (oxIAA; IAA-aspartate, IAAsp; and IAA-glutamate, IAGlu) (Figure 4a and Table S1). In conclusion, our findings illustrate that we are able to detect credible nuclear auxin profiles from two plant cell models using an optimized isolation protocol based on the FCM technique.

2.3. Feeding experiments with indole and IAA

Finally, to demonstrate the reliability of the FCM-based isolation method, we decided to promote auxin metabolism in *A. thaliana* protoplasts by treatment with 10 μ M indole as a precursor of the Trp-dependent biosynthetic pathway [20]. The data were converted to the ratio of auxin levels in treated and untreated nuclei (Figure 4b). Our results showed that the level of indole precursor ANT was not elevated after indole treatment. Compared to the non-treated control, we clearly detected increased levels of IAA precursors (Trp, TRA, IAM and IPyA), in the range of 1.4- to 3.8-fold. As expected, IAN levels were below the limit of detection. Interestingly, the IAA level was not affected by indole treatment, however, slightly elevated levels of oxIAA and IAAsp were detected (Figure 4b). Due to the negligible increase in IAA and its metabolites, protoplasts were fed with 100 μ M IAA. Under our experimental conditions, levels of not only free IAA, but also other analyzed metabolites, such as oxIAA, IAAsp and IAGlu, were very significantly increased (Figure 4b). However, the levels of all IAA precursors were not affected by IAA treatment expect slight increase in IPyA level (Figure S3). Confirming our previous results, the glucose conjugates IAA-glc and oxIAA-glc were also not detected.

Overall, our results of the feeding experiment nicely showed the applicability of the organelle-isolation method based on FCM. In the near future, we should be able to quantify not only auxins, but also other plant hormones in sorted organelle populations.

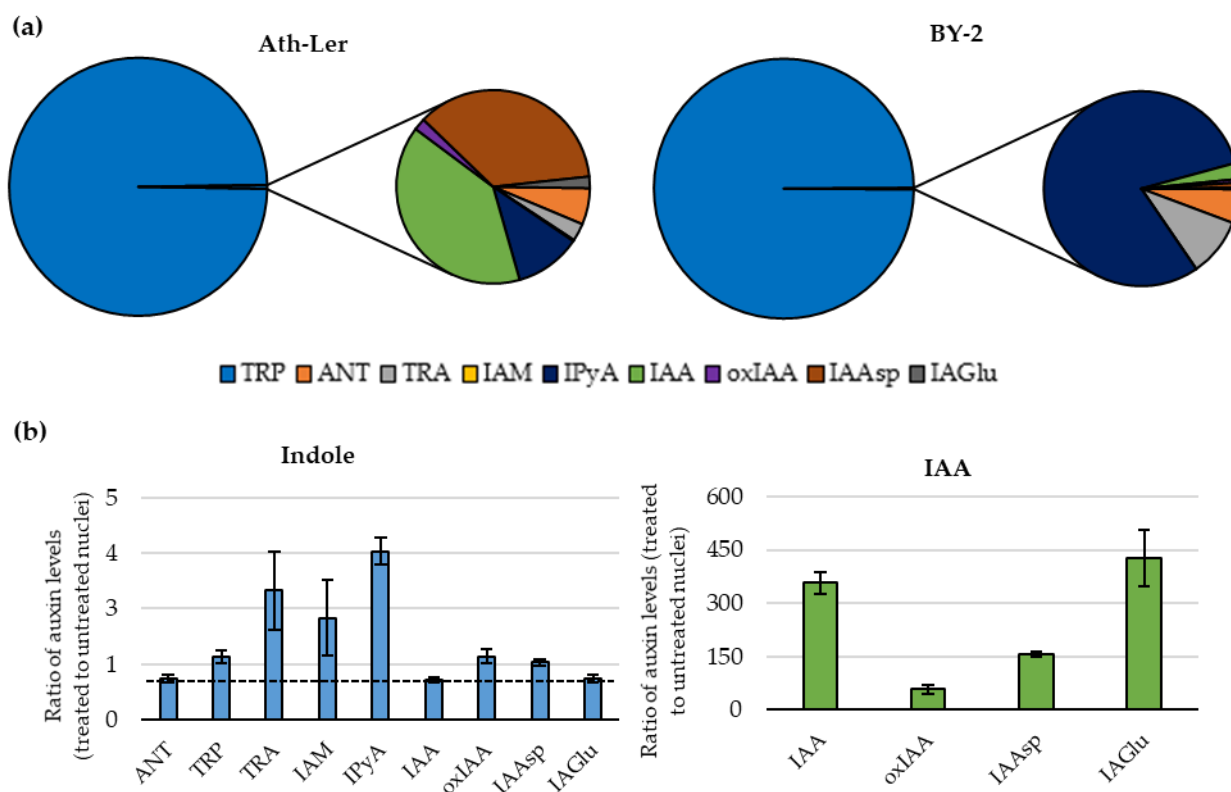


Figure 4. (a) Auxinomes in nuclei sorted by flow cytometry from *Arabidopsis thaliana* Ler (Ath-Ler; left) and *N. tabacum* cv. BY-2 (BY-2; right), (n=4). (b) Relative auxinomes in nuclei after treatment of Ath-Ler protoplasts with indole (left) and indole-3-acetic acid (IAA; right). The auxin concentration was calculated as fmol/1,000,000 nuclei, and the respective ratios (treated to untreated) were then determined (n=5-6). Anthranilate (ANT), tryptophan (TRP), tryptamine (TRA), indole-3-acetamide (IAM), indole-3-pyruvic acid (IPyA), IAA-aspartate (IAAsp), IAA-glutamate (IAGlu) and 2-oxoindole-3-acetic acid (oxIAA). Indole-3-acetonitrile (IAN), IAA-glucose and oxIAA-glucose were under limit of detection. Error bars indicate s.d.

3. Discussion

The maintenance of auxin homeostasis and its distribution within the plant cell remains elusive, because only few previous studies were focused on subcellular auxin analysis in chloroplasts [51], vacuoles [16] and recently ER [52], but none in nuclei. The nucleus represents a key organelle because it contains the process of canonical auxin signaling. Therefore, we decided to examine several protocols for nucleus isolation with subsequent auxin analysis by LC-MS/MS.

It is important to emphasize that the original nuclei isolation protocols were designed mainly for DNA or genomic studies [35,53]. Nevertheless, the intactness and high purity of the isolated nuclei are crucial for the auxin metabolic profiling. Release of nuclei from plant tissue or cell cultures can be achieved by various homogenization methods but a combination of enzymatic cell wall digestion and osmotic plasma membrane disruption was found to be most conducive for gentle release of nuclei. This protoplast preparation has been successfully employed for organelle isolation in previously published protocols [34,54,55] and the protoplast lysis step does not significantly change auxin metabolism [56] and our data show that this is stable long-term after nucleus isolation (Figure 3a). Immunoblot analysis and confocal microscopy verified the success of the protocols used (Figure 1 and 2). In general, DC showed low resolving power leading to the presence of contaminating organelles in the isolated nuclear fraction [33]. The FCM approach provides better purity (Figure 2) and 3D nuclei reconstruction showed that FCM nuclei were intact and with some shape heterogeneity (Figure S2).

Quantitative analysis of auxins at the cellular or even subcellular level is challenging [57] although recent improvements of plant sample purification protocols and mass spectrometry-based techniques have enabled the analysis of the auxinome in minute samples (~2 mg of fresh weight; [58]). The use of additional steps, such as nuclei isolation,

should further reduce the contents of pigments, lipids, phenolic compounds, and other interfering compounds. Overall, we observed a better signal during LC-MS/MS analysis in samples sorted by FCM compared to DC-delivered nuclei, indicating a reduced matrix effect. (Figure 3b).

Profiling of the auxinome in nuclear fluid revealed the presence not only of free IAA but also the precursors of three biosynthetic pathways (IPyA, IAM and TRA; [4,20]) as well as IAA main catabolite oxIAA and conjugates with Asp and Glu (Figure 4 a,b). Surprisingly, no ester-linked sugar conjugates IAA-glc and oxIAA-glc were detected in isolated nuclear fractions, even after the feeding with IAA. This, together with the fact that IAA-glc and oxIAA-glc have not been determined in whole *Ath-Ler* cells (Table S1), suggests that the *Ath-Ler* cell culture has a reduced ability to form ester-linked conjugates of IAA and oxIAA. How and why IAA precursors and metabolites are transported into the nucleus is still unclear, although Middleton et al. [17] showed that ER-to-nucleus auxin flux represents a major subcellular pathway controlling nuclear auxin levels, and that auxin diffusion from the cytosol via the nuclear pores plays only a minor role. Additionally, it was shown that PILSes can reduce nuclear auxin signaling in the apical hook leading to the de-repression of growth and the onset of hook through the direct regulation of PILS gene activity by phytochrome B-reliant light-signaling pathway [59].

We should also mention the roles of other organelles in auxin homeostasis. For example, Ranocha et al. [16] detected IAA, its precursors and metabolites in vacuoles and the importance of the ER has been included above. In fact, the biological importance and function of compartmentation in the nucleus and other organelles remains elusive and needs to be further studied.

4. Materials and Methods

4.1. Cultivation of cell cultures

Arabidopsis (*Arabidopsis thaliana* cv. Landsberg *erecta*) cell line (*Ath-Ler*) was grown in sterile Murashige-Skoog medium (4.4 g·L⁻¹, pH 5.8; Duchefa Biochemie, Haarlem, Netherlands) supplemented with vitamins, 3% sucrose, 0.232 μM kinetin and 5.37 μM 1-naphthaleneacetic acid (Merck Life Science, Darmstadt, Germany). Tobacco (*Nicotiana tabacum* cv. Bright Yellow 2) cell line (BY-2) was grown in sterile Murashige-Skoog medium (4.3 g·L⁻¹ pH 5.8) supplemented with 3% sucrose, 4 μM thiamin, 555 μM inositol, 1.47 mM KH₂PO₄ and 0.9 μM 2,4-dichlorophenoxyacetic acid (Merck Life Science, Darmstadt, Germany). Both cell lines were subcultured weekly into fresh media in volume ratio 1:10. The cells were cultivated at 23 °C in dark and shaken at 120 rpm. 5-day-old cells were used for all experiments. As a stock material, cell calli were cultivated on the same solidified media and subcultured monthly.

4.2. Protoplast preparation

The cells were gently filtered (0.45 μm nylon filter) using vacuum filtration. Protoplasts were prepared according to Yoo et al. [45] with minor modifications in enzyme combination and final concentrations. Exactly 6 g of cell material was resuspended in 60 ml of preheated protoplasting buffer (37 °C; 0.6 M mannitol, 10 mM KCl, 2 mM 4-morpholineethanesulfonic acid (MES), 2 mM CaCl₂, 0.1% (v/v) BSA, 2 mM MgCl₂, 20 U/ml cellulase Onozuka R-10, 7.5 U/ml macerozyme R-10, 0.3 U/ml pectolyase Y-23, and 45 U/ml celulysin pH 5.7; Merck Life Science, Darmstadt, Germany, enzymes were from Duchefa Biochemie, Haarlem, Netherlands). The suspension was shortly incubated at 37 °C to activate the enzymes and then incubated at 28 °C for 3 h with gentle and occasional hand-shaking. The enzyme solution with released protoplasts was then diluted with an equal volume of preheated W5 buffer (2 mM MES, 154 mM NaCl, 149 mM CaCl₂ and 5 mM KCl, pH 5.7, 28 °C) to stop enzymatic reaction. The protoplast suspension was gently filtered through a pre-wetted nylon mesh (70 μm) to remove undigested cell clusters and the released protoplasts were pelleted by centrifugation (100× g, 3 min, 20 °C). The pelleted protoplasts were gently washed twice in 2-3 ml of WI buffer (4 mM MES, 0.5 M mannitol, 20 mM KCl and 1% sucrose, pH 5.7) by repeating both centrifugation and

resuspension steps. The released protoplasts were finally stored on ice. A cell culture protoplasting protocol based on the protoplast lysis step published by Saxena et al. [34] was also tested.

For feeding experiments, the protoplast culture was incubated with 10 μM indole (final concentration) for 3 h. Compound added at the beginning of protoplast isolation protocol) or 100 μM IAA (final concentration) for last 1 h of protoplasting process.

4.3. Nuclei isolation by differential centrifugation

The protoplast culture was prepared based on a modified protocol from Yoo et al. [45] (for details see Chapter 4.2.) and subsequent nuclei isolation by DC was performed according to Saxena et al. [34] with minor modifications. All isolation steps were carried out at 4 $^{\circ}\text{C}$ and with pre-cooled buffers. Briefly, the protoplast pellet was resuspended in 1.5 ml of 0.6 M mannitol and 7.5 ml of 20 % (w/v) sucrose, which was added slowly to avoid mixing of the layers. The next step was centrifugation (100 \times g, 7 min, 4 $^{\circ}\text{C}$) to effectively separate the protoplasts into the mannitol phase. The collected ring of protoplasts was mixed with 13 ml of nuclear isolation buffer (NIB; 200 mM sucrose, 10 mM MES, 10 mM NaCl, 10 mM KCl, 0.1 % Triton X-100, 2.5 mM dithiothreitol and 0.1 mM spermine, pH 5.3; Merck Life Science, Darmstadt, Germany) and then incubated on ice for 15 min. To release a satisfactory number of nuclei, the suspension was mixed for 1 min on shaker, filtered through the pre-wetted 3 layers of Miracloth membrane (20–25 μm) and then pelleted by centrifugation (150 \times g, 8 min, 4 $^{\circ}\text{C}$). The obtained nuclear fraction was resuspended in 2 ml of NIB buffer without Triton X-100 and centrifuged (150 \times g, 8 min, 4 $^{\circ}\text{C}$). The final pellets of isolated nuclei were immediately used for microscopy analysis or frozen in liquid nitrogen and stored at -80 $^{\circ}\text{C}$.

4.4. Nuclei isolation by FCM

The nuclei were isolated from the protoplasts prepared as described in Chapter 4.2 using the FCM method according to Petrovská et al. [49] with minor modifications [48]. All samples were mixed with an equal volume of 0.7% NaCl to disrupt the protoplast plasma membranes. The released nuclei were then filtered through 20 μm nylon mesh and stained with DAPI (final concentration 2 $\mu\text{g}/\text{ml}$; Merck Life Science, Darmstadt, Germany). Sorting of nuclei was performed in 0.7% NaCl as a sheath fluid solution using a BD FACS Aria II SORP flow cytometer (BD Bioscience, NY, USA) equipped with a nozzle (70 μm diameter), filtration bandpass 450/30 nm for DAPI and 480/10nm for flow cytometry standard (FCS), system pressure 482.6 kPa, UV laser (355 nm, 100 mW) and blue laser (488 nm, 100 mW) for FCS (DAPI-A for sorting of nuclei population, DAPI-W vs. DAPI-A for sorting). The population of nuclei was selected according to following optical parameters: forward and side scatter in combination with DAPI specific fluorescence. Nuclear fractions were immediately used for fluorescent microscopy and/or frozen in liquid nitrogen.

4.5. Microscopy analysis

The purity of nuclear fraction and the intactness of isolated nuclei were verified by a fluorescent microscope Olympus IX51 (Olympus, Tokyo, Japan). Nuclei were stained with DAPI (final concentration 1 $\mu\text{g}/\text{ml}$). The number of nuclei isolated by DC was estimated using a Bürker counting chamber (~ 8–10 samples were calculated).

4.6. Immunoblot analysis

The purity of nuclear fractions isolated by DC or FCM were also checked by immunoblot analysis utilizing a set of antibodies against protein organelle markers. The pellet of nuclei (approx. 1–3 million) were suspended in Laemmli sample buffer and boiled at 95 $^{\circ}\text{C}$ for 5 min. Nuclear proteins were separated using SDS-PAGE on a 12% polyacrylamide resolving gel and a 4% stacking gel at 90 V for 0.5 h and then at 120 V for ~ 1.5 h [60] (Bio-Rad, Hercules, CA, USA). The separated proteins were electrophoretically transferred onto a 0.45 μm nitrocellulose membrane at 290 mA for 2 h (Santa Cruz Biotechnology, Heidelberg, Germany). The membrane was blocked in 5% low-fat milk dissolved in

TBST buffer for 1 h, incubated for 1 h with primary rabbit antibodies (Agrisera, Vännäs, Sweden): Sec21p (1:1000 diluted; AS08 327), CNX1/2 (1:2500 diluted; AS12 2365), BiP (1:2500 diluted; AS09 481), V-ATPase (1:2000 diluted; AS07 213), H3 (1:5000 diluted; AS10 710). After washing three times with TBST buffer for 5 min, the membrane was incubated with secondary antibody goat anti-rabbit IgG (H&L) conjugated with HRP (1:10,000 diluted; AS09 602) for 1 h. Proteins were visualized by SuperSignal® West Pico Chemiluminescent substrate (Thermo Scientific, Waltham, MA, USA) according to the manufacturer's instructions using using a ChemiDoc MP Imaging System (Bio-Rad, Hercules, CA, USA).

4.7. Auxin purification and determination

Full auxinome (IAA, its precursors and metabolites) were determined as described in Novák et al. [50]. First, the pelleted nuclei isolated by DC approach were suspended in 1 ml sodium-phosphate buffer (pH 7.0). Aliquots of around 1 million nuclei were used for each technical replicate. Next, the sorted nuclei (3 million nuclei for replicate) in sheath fluid (0.7% NaCl) were diluted with deionized water up to 1 ml. Prior auxin extraction, a cocktail of internal standards (50 pmol of [²H₅]TRA and [²H₄]TRA, 10 pmol of [²H₄]IAN and 5 pmol of [²H₄]ANT, [²H₅]IAM, [²H₄]IPyA, [¹³C₆]IAA, [¹³C₆]oxIAA, [¹³C₆]IAA_{asp}, [¹³C₆]IAGlu, [¹³C₆]IAA-glc and [¹³C₆]oxIAA-glc) were added to each sample. The extracts were acidified with HCl to pH 2.7 and then purified by solid-phase extraction (SPE) using Oasis™ HLB columns (30 mg/ml, Waters). For quantification of IPyA, separated samples were derivatized by cysteamine (0.25 M, pH 8.0) for 1 hour, acidified with HCl to pH 2.7 and purified by SPE. All analytes were eluted with 80 % methanol and the eluents were then evaporated to dryness. Auxin profiles were determined by an ultra-high-performance liquid chromatography–electrospray tandem mass spectrometry using an Acquity UPLCTM System (Waters Corp., Milford, CT, USA) equipped with Kinetex C18 (50 mm x 2.1 mm, 1.7 µm; Phenomenex) coupled to a triple-quadrupole mass spectrometer (Xevo TQ-S MS; Waters Corp., Milford, CT, USA) [50].

The long-term stability of auxin profiles in nuclei isolated by the FCM method was tested using two sets of nuclear isolated fractions. Samples (*Ath-Ler* cells) were sorted directly or stored on ice (14 hours) after protoplast lysis and then analyzed by LC-MS/MS.

Table 1. Methodology overview of various different methods of plant nucleus isolation. The comparison of their key parameters are distinguished accordingly to their (dis)advantages. Differential centrifugation (DC), gradient centrifugation (GC), flow cytometry (FCM), affinity purification (AP), genomics (G), proteomics (P), transcriptomics (T), metabolomics (M).

Parameters	DC	GC	FCM ¹	AP
Yield	+++	++	+	-
Purity	-	+	++	+++
Instrumentation	+++	+++	-	+
Duration	+	-	++	+++
Cell-type specificity	-	-	+++ ¹	+++
Simultaneous multi-organelle isolation	-	-	+++	-
Downstream application	G, P, (M)	G, T, P	G, P, T, M	G, T

¹ FCM is able also sort nuclei into different phases of the cell cycle.

5. Conclusions

An innovative combination of FCM with ultra-sensitive mass spectrometry analysis has been shown to provide a useful tool for monitoring of IAA and other related compounds at the subcellular level. Our methodology has given unprecedented information about the subcellular distributions of the auxinome, and thus should facilitate attempts to elucidate regulatory networks involved in plant developmental processes.

Finally, we summarized the main pros and cons of different nuclei isolation approaches, such as conventional biochemical methods of DC or density gradient centrifugation (GC), and modern methods exploiting technique of FCM or AP. We focused on five main parameters of cell nuclei isolation such as yield, purity, instrumentation, duration and cell-type specificity (Table 1). We want to point out that these techniques can be easily applied to most of cell organelles and the FCM technique could be used to sort more than one or two organelle populations from the same biological material simultaneously. FCM represents a powerful tool for subcellular fractionation with following downstream applications including various “omics” approaches [49,53,61,62].

Supplementary Materials: The following are available online at www.mdpi.com/xxx/s1, Figure S1: title, Table S1: Endogenous levels of auxin metabolites and their relative distribution in nuclear fractions isolated from Ath-Ler and BY-2 cells, Table S2: Endogenous levels of auxin metabolites in Ath-Ler cells, Method S1: Alternative methods of cell nuclei isolation, Method S2: Volume analysis of isolated cell nuclei by 3D reconstruction method.

Author Contributions: M.K., V.S., T.V., A.P. and O.N. developed the idea and outline of the paper. M.K., V.S., T.V., A.P., J.V., V.K. and K.J. performed experiments and data analysis. M.K., V.S., T.V., A.P. and O.N. discussed results and create outline of the paper. M.K., V.S., A.P., R.N. and O.N. wrote the manuscript. All authors read the manuscript before the submission.

Funding: This work was financially supported by by the Ministry of Education, Youth and Sports of the Czech Republic (European Regional Development Fund-Project “Plants as a tool for sustainable global development” No. 587 CZ.02.1.01/0.0/0.0/16_019/0000827), by the Internal Grant Agency of Palacký University in Olomouc (IGA_PrF_2021_011 and IGA_PrF_2021_016), by the Czech Science Foundation (17-21581Y). V.S. was partially supported by the Endowment fund of Palacký University in Olomouc and M.K. was supported by the EU MSCA-IF project CrispINs (792329).

Data Availability Statement: Data presented in the current study are available in the article and supplementary materials.

Acknowledgments: The authors would like to thank prof. Richard Napier for careful language revision, critical proof-reading and helpful comments, and to Ota Blahoušek for graphic editing of figures.

Conflicts of Interest: The authors declare no conflict of interest.

References

1. Brumos, J.; Robles, L. M.; Yun, J.; Vu, T. C.; Jackson, S.; Alonso, J. M.; Stepanova, A. N. Local Auxin Biosynthesis Is a Key Regulator of Plant Development. *Dev. Cell* **2018**, *47*, 306–318.e5, doi:10.1016/j.devcel.2018.09.022.
2. Di Mambro, R.; De Ruvo, M.; Pacifici, E.; Salvi, E.; Sozzani, R.; Benfey, P. N.; Busch, W.; Novak, O.; Ljung, K.; Di Paola, L.; Marée, A. F. M.; Costantino, P.; Grieneisen, V. A.; Sabatini, S. Auxin minimum triggers the developmental switch from cell division to cell differentiation in the Arabidopsis root. *Proc. Natl. Acad. Sci. U. S. A.* **2017**, *114*, E7641–E7649, doi:10.1073/pnas.1705833114.
3. Grones, P.; Majda, M.; Doyle, S. M.; Damme, D. Van; Robert, S. Fluctuating auxin response gradients determine pavement cell-shape acquisition. *Proc. Natl. Acad. Sci. U. S. A.* **2020**, *117*, 16027–16034, doi:10.1073/pnas.2007400117.
4. Skalický, V.; Kubeš, M.; Napier, R.; Novák, O. Auxins and Cytokinins-The Role of Subcellular Organization on Homeostasis. *Int. J. Mol. Sci.* **2018**, *19*, 3115, doi:10.3390/ijms19103115.
5. Tanaka, H.; Dhonukshe, P.; Brewer, P. B.; Friml, J. Spatiotemporal asymmetric auxin distribution: A means to coordinate plant development. *Cell. Mol. Life Sci.* **2006**, *63*, 2738–2754, doi:10.1007/s00018-006-6116-5.
6. Barbez, E.; Kubeš, M.; Rolčík, J.; Béziat, C.; Pěňčík, A.; Wang, B.; Rosquete, M. R.; Zhu, J.; Dobrev, P. I.; Lee, Y.; Zažímalová, E.; Petrášek, J.; Geisler, M.; Friml, J.; Kleine-Vehn, J. A novel putative auxin carrier family regulates

- intracellular auxin homeostasis in plants. *Nature* **2012**, *485*, 119–22, doi:10.1038/nature11001.
7. Dindas, J.; Scherzer, S.; Roelfsema, M. R. G.; Von Meyer, K.; Müller, H. M.; Al-Rasheid, K. A. S.; Palme, K.; Dietrich, P.; Becker, D.; Bennett, M. J.; Hedrich, R. AUX1-mediated root hair auxin influx governs SCFTIR1/AFB-type Ca²⁺ signaling. *Nat. Commun.* **2018**, *9*, doi:10.1038/s41467-018-03582-5.
 8. Fendrych, M.; Akhmanova, M.; Merrin, J.; Glanc, M.; Hagihara, S.; Takahashi, K.; Uchida, N.; Torii, K. U.; Friml, J. Rapid and reversible root growth inhibition by TIR1 auxin signalling. *Nat. plants* **2018**, *4*, 453–459, doi:10.1038/s41477-018-0190-1.
 9. Retzer, K.; Singh, G.; Napier, R. It starts with TIRs. *Nat. Plants* **2018**, *4*, 410–411, doi:10.1038/s41477-018-0196-8.
 10. Simonini, S.; Mas, P. J.; Mas, C. M. V. S.; Østergaard, L.; Hart, D. J. Auxin sensing is a property of an unstructured domain in the Auxin Response Factor ETTIN of *Arabidopsis thaliana*. *Sci. Reports* **2018**, *8*, 1–11, doi:10.1038/s41598-018-31634-9.
 11. Kubeš, M.; Napier, R. Non-canonical auxin signalling: Fast and curious. *J. Exp. Bot.* **2019**, *70*, 2609–2614.
 12. Mravec, J.; Skůpa, P.; Bailly, A.; Hoyerová, K.; Křeček, P.; Bielach, A.; Petrášek, J.; Zhang, J.; Gaykova, V.; Stierhof, Y.-D.; Dobrev, P. I.; Schwarzerová, K.; Rolčík, J.; Seifertová, D.; Luschnig, C.; Benková, E.; Zažímalová, E.; Geisler, M.; Friml, J. Subcellular homeostasis of phytohormone auxin is mediated by the ER-localized PIN5 transporter. *Nature* **2009**, *459*, 1136–40, doi:10.1038/nature08066.
 13. Bosco, C. D.; Dovzhenko, A.; Liu, X.; Woerner, N.; Rensch, T.; Eismann, M.; Eimer, S.; Hegermann, J.; Paponov, I. A.; Ruperti, B.; Heberle-Bors, E.; Touraev, A.; Cohen, J. D.; Palme, K. The endoplasmic reticulum localized PIN8 is a pollen-specific auxin carrier involved in intracellular auxin homeostasis. *Plant J.* **2012**, *71*, 860–870, doi:10.1111/j.1365-313X.2012.05037.x.
 14. Ding, Z.; Wang, B.; Moreno, I.; Dupláková, N.; Simon, S.; Carraro, N.; Reemmer, J.; Pěnčík, A.; Chen, X.; Tejos, R.; Skůpa, P.; Pollmann, S.; Mravec, J.; Petrášek, J.; Zažímalová, E.; Honys, D.; Rolčík, J.; Murphy, A. S.; Orellana, A.; Geisler, M.; Friml, J. ER-localized auxin transporter PIN8 regulates auxin homeostasis and male gametophyte development in *Arabidopsis*. *Nat. Commun.* **2012**, *3*, 941, doi:10.1038/ncomms1941.
 15. Feraru, E.; Vosolsobě, S.; Feraru, M. I.; Petrášek, J.; Kleine-Vehn, J. Evolution and Structural Diversification of PILS Putative Auxin Carriers in Plants. *Front. Plant Sci.* **2012**, *3*, 227, doi:10.3389/fpls.2012.00227.
 16. Ranocha, P.; Dima, O.; Nagy, R.; Felten, J.; Corratgé-Faillie, C.; Novák, O.; Morreel, K.; Lacombe, B.; Martinez, Y.; Pfrunder, S.; Jin, X.; Renou, J.-P.; Thibaud, J.-B.; Ljung, K.; Fischer, U.; Martinoia, E.; Boerjan, W.; Goffner, D. *Arabidopsis* WAT1 is a vacuolar auxin transport facilitator required for auxin homeostasis. *Nat. Commun.* **2013**, *4*, 2625, doi:10.1038/ncomms3625.
 17. Middleton, A. M.; Dal Bosco, C.; Chlap, P.; Bensch, R.; Harz, H.; Ren, F.; Bergmann, S.; Wend, S.; Weber, W.; Hayashi, K.-I.; Zurbriggen, M. D.; Uhl, R.; Ronneberger, O.; Palme, K.; Fleck, C.; Dovzhenko, A. Data-Driven Modeling of Intracellular Auxin Fluxes Indicates a Dominant Role of the ER in Controlling Nuclear Auxin Uptake. *Cell Rep.* **2018**, *22*, 3044–3057, doi:10.1016/j.celrep.2018.02.074.
 18. Zhao, Y. Auxin Biosynthesis: A Simple Two-Step Pathway Converts Tryptophan to Indole-3-Acetic Acid in Plants. *Mol. Plant* **2012**, *5*, 334–338, doi:10.1093/MP/SSR104.
 19. Kriechbaumer, V.; Wang, P.; Hawes, C.; Abell, B. M. Alternative splicing of the auxin biosynthesis gene YUCCA4 determines its subcellular compartmentation. *Plant J.* **2012**, *70*, 292–302, doi:10.1111/j.1365-313X.2011.04866.x.
 20. Ljung, K. Auxin metabolism and homeostasis during plant development. *Development* **2013**, *140*, 943–950, doi:10.1242/dev.086363.
 21. Casanova-Sáez, R.; Mateo-Bonmatí, E.; Ljung, K. Auxin Metabolism in Plants. *Cold Spring Harb. Perspect. Biol.* **2021**, a039867, doi:10.1101/cshperspect.a039867.
 22. Jin, S.-H.; Ma, X.-M.; Kojima, M.; Sakakibara, H.; Wang, Y. W.; Hou, B.-K. Overexpression of glucosyltransferase UGT85A1 influences trans-zeatin homeostasis and trans-zeatin responses likely through O-glucosylation. *Planta* **2013**, *237*, 991–999, doi:10.1007/s00425-012-1818-4.
 23. Staswick, P. E.; Serban, B.; Rowe, M.; Tiryaki, I.; Maldonado, M. T.; Maldonado, M. C.; Suza, W. Characterization of an *Arabidopsis* Enzyme Family That Conjugates Amino Acids to Indole-3-Acetic Acid. *PLANT CELL ONLINE* **2005**, *17*, 616–627, doi:10.1105/tpc.104.026690.
 24. Cano, A.; Sánchez-García, A. B.; Albacete, A.; González-Bayón, R.; Justamante, M. S.; Ibáñez, S.; Acosta, M.; Pérez-Pérez, J. M. Enhanced Conjugation of Auxin by GH3 Enzymes Leads to Poor Adventitious Rooting in Carnation Stem Cuttings. *Front. Plant Sci.* **2018**, *9*, doi:10.3389/fpls.2018.00566.
 25. Di Mambro, R.; Svolacchia, N.; Dello Ioio, R.; Pierdonati, E.; Salvi, E.; Pedrazzini, E.; Vitale, A.; Perilli, S.; Sozzani, R.; Benfey, P. N.; Busch, W.; Costantino, P.; Sabatini, S. The Lateral Root Cap Acts as an Auxin Sink that Controls

- Meristem Size. *Curr. Biol.* **2019**, *29*, 1199–1205.e4, doi:10.1016/j.cub.2019.02.022.
26. Sanchez Carranza, A. P.; Singh, A.; Steinberger, K.; Panigrahi, K.; Palme, K.; Dovzhenko, A.; Dal Bosco, C. Hydrolases of the ILR1-like family of Arabidopsis thaliana modulate auxin response by regulating auxin homeostasis in the endoplasmic reticulum. *Sci. Rep.* **2016**, *6*, doi:10.1038/srep24212.
27. Fu, Y.; Yang, Y.; Chen, S.; Ning, N.; Hu, H. Arabidopsis IAR4 modulates primary root growth under salt stress through ros-mediated modulation of auxin distribution. *Front. Plant Sci.* **2019**, *10*, doi:10.3389/fpls.2019.00522.
28. Porco, S.; Pěňčík, A.; Rashed, A.; Voš, U.; Casanova-Sáez, R.; Bishopp, A.; Golebiowska, A.; Bhosale, R.; Swarup, R.; Swarup, K.; Peňáková, P.; Novák, O.; Staswick, P. E.; Hedden, P.; Phillips, A. L.; Vissenberg, K.; Bennett, M.; Ljung, K. Dioxygenase-encoding AtDAO1 gene controls IAA oxidation and homeostasis in Arabidopsis. *Proc. Natl. Acad. Sci. U. S. A.* **2016**, *113*, 11016–21, doi:10.1073/pnas.1604375113.
29. Zhang, J.; Lin, J. E.; Harris, C.; Campos Mastrotti Pereira, F.; Wu, F.; Blakeslee, J. J.; Peer, W. A. DAO1 catalyzes temporal and tissue-specific oxidative inactivation of auxin in Arabidopsis thaliana. *Proc. Natl. Acad. Sci. U. S. A.* **2016**, *113*, 11010–5, doi:10.1073/pnas.1604769113.
30. Novák, O.; Napier, R.; Ljung, K. Zooming In on Plant Hormone Analysis: Tissue- and Cell-Specific Approaches. *Annu. Rev. Plant Biol.* **2017**, *68*, 323–348, doi:10.1146/annurev-arplant-042916-040812.
31. Pertoft, H. Fractionation of cells and subcellular particles with Percoll. *J. Biochem. Biophys. Methods* **2000**, *44*, 1–30, doi:10.1016/S0165-022X(00)00066-X.
32. Folta, K. M.; Kaufman, L. S. Isolation of Arabidopsis nuclei and measurement of gene transcription rates using nuclear run-on assays. *Nat. Protoc.* **2007**, *1*, 3094–3100, doi:10.1038/nprot.2006.471.
33. Lee, Y. H.; Tan, H. T.; Chung, M. C. M. Subcellular fractionation methods and strategies for proteomics. *Proteomics* **2010**, *10*, 3935–3956, doi:10.1002/pmic.201000289.
34. Saxena, P. K.; Fowke, L. C.; King, J. An efficient procedure for isolation of nuclei from plant protoplasts. *Protoplasma* **1985**, *128*, 184–189, doi:10.1007/BF01276340.
35. Zhang, H.-B.; Zhao, X.; Ding, X.; Paterson, A. H.; Wing, R. A. Preparation of megabase-size DNA from plant nuclei. *Plant J.* **1995**, *7*, 175–184, doi:10.1046/j.1365-313X.1995.07010175.x.
36. Vertommen, A.; Panis, B.; Swennen, R.; Carpentier, S. C. Challenges and solutions for the identification of membrane proteins in non-model plants. *J. Proteomics* **2011**, *74*, 1165–1181, doi:10.1016/j.jpro.2011.02.016.
37. Zini, N.; Matteucci, A.; Squarzone, S.; Galanzi, A.; Rizzoli, R.; Papa, S. Electron microscopy microsampling of isolated nuclei sorted by flow cytometry. *Cytometry* **1986**, *7*, 605–608, doi:10.1002/cyto.990070617.
38. Šimková, H.; Čiháliková, J.; Vrána, J.; Lysák, M. A.; Doležel, J. Preparation of HMW DNA from plant nuclei and chromosomes isolated from root tips. *Biol. Plant.* **2003**, *46*, 369–373, doi:10.1023/A:1024322001786.
39. Zhang, C.; Barthelson, R. A.; Lambert, G. M.; Galbraith, D. W. Global characterization of cell-specific gene expression through fluorescence-activated sorting of nuclei. *Plant Physiol.* **2008**, *147*, 30–40, doi:10.1104/pp.107.115246.
40. Deal, R. B.; Henikoff, S. A simple method for gene expression and chromatin profiling of individual cell types within a tissue. *Dev. Cell* **2010**, *18*, 1030–1040, doi:10.1016/j.devcel.2010.05.013.
41. Deal, R. B.; Henikoff, S. The INTACT method for cell type-specific gene expression and chromatin profiling in Arabidopsis thaliana. *Nat. Protoc.* **2011**, *6*, 56–68, doi:10.1038/nprot.2010.175.
42. Seifertová, D.; Klíma, P.; Pařezová, M.; Petrášek, J.; Zažímalová, E.; Opatrný, Z. Plant Cell Lines in Cell Morphogenesis Research. *Methods Mol. Biol.* **2014**, *1080*, 215–229, doi:10.1007/978-1-62703-643-6_18.
43. Gigli-Bisceglia, N.; Engelsdorf, T.; Hamann, T. Plant cell wall integrity maintenance in model plants and crop species-relevant cell wall components and underlying guiding principles. *Cell. Mol. Life Sci.* **2020**, *77*, 2049–2077, doi:10.1007/S00018-019-03388-8.
44. Xu, F.; Copeland, C. Nuclear Extraction from Arabidopsis thaliana. *BIO-PROTOCOL* **2012**, *2*, doi:10.21769/BIOPROT.306.
45. Yoo, S.-D.; Cho, Y.-H.; Sheen, J. Arabidopsis mesophyll protoplasts: a versatile cell system for transient gene expression analysis. *Nat. Protoc.* **2007**, *2*, 1565–1572, doi:10.1038/nprot.2007.199.
46. Koláčková, V.; Perníčková, K.; Vrána, J.; Duchoslav, M.; Jenkins, G.; Phillips, D.; Turkosi, E.; Šamajová, O.; Sedlářová, M.; Šamaj, J.; Doležel, J.; Kopecký, D. Nuclear Disposition of Alien Chromosome Introgressions into Wheat and Rye Using 3D-FISH. *Int. J. Mol. Sci.* **2019**, *20*, 4143, doi:10.3390/IJMS20174143.
47. Perníčková, K.; Koláčková, V.; Lukaszewski, A. J.; Fan, C.; Vrána, J.; Duchoslav, M.; Jenkins, G.; Phillips, D.; Šamajová, O.; Sedlářová, M.; Šamaj, J.; Doležel, J.; Kopecký, D. Instability of Alien Chromosome Introgressions in Wheat Associated with Improper Positioning in the Nucleus. *Int. J. Mol. Sci.* **2019**, *20*, 1448,

- doi:10.3390/IJMS20061448.
48. Antoniadis, I.; Plačková, L.; Simonovik, B.; Doležal, K.; Turnbull, C.; Ljung, K.; Novák, O. Cell-Type-Specific Cytokinin Distribution within the Arabidopsis Primary Root Apex. *Plant Cell* **2015**, *27*, 1955–67, doi:10.1105/tpc.15.00176.
 49. Petrovská, B.; Jeřábková, H.; Chamrád, I.; Vrána, J.; Lenobel, R.; Uřinová, J.; Šebela, M.; Doležel, J. Proteomic analysis of barley cell nuclei purified by flow sorting. *Cytogenet. ancyd genome Res.* **2014**, *143*, 78–86, doi:10.1159/000365311.
 50. Novák, O.; Hényková, E.; Sairanen, I.; Kowalczyk, M.; Pospíšil, T.; Ljung, K. Tissue-specific profiling of the Arabidopsis thaliana auxin metabolome. *Plant J.* **2012**, *72*, 523–36, doi:10.1111/j.1365-313X.2012.05085.x.
 51. Polanská, L.; Vičánková, A.; Nováková, M.; Malbeck, J.; Dobrev, P. I.; Brzobohatý, B.; Vaňková, R.; Macháčková, I. Altered cytokinin metabolism affects cytokinin, auxin, and abscisic acid contents in leaves and chloroplasts, and chloroplast ultrastructure in transgenic tobacco. *J. Exp. Bot.* **2007**, *58*, 637–49, doi:10.1093/jxb/erl235.
 52. Včelařová, L.; Skalický, V.; Chamrád, I.; Lenobel, R.; Kubeš, M.; Pěňčík, A.; Novák, O. Auxin Metabolome Profiling in the Arabidopsis Endoplasmic Reticulum Using an Optimised Organelle Isolation Protocol. *Int. J. Mol. Sci.* **2021**, *22*, 9370, doi:10.3390/IJMS22179370.
 53. Šafář, J.; Noa-Carrazana, J. C.; Vrána, J.; Bartoš, J.; Alkhimova, O.; Sabau, X.; Šimková, H.; Lheureux, F.; Caruana, M.-L.; Doležel, J.; Piffanelli, P. Creation of a BAC resource to study the structure and evolution of the banana (*Musa balbisiana*) genome. *Genome* **2004**, *47*, 1182–1191, doi:10.1139/g04-062.
 54. Somerville, C. R.; Somerville, S. C.; Ogren, W. L. Isolation of photosynthetically active protoplasts and chloroplasts from Arabidopsis thaliana. *Plant Sci. Lett.* **1981**, *21*, 89–96.
 55. Robert, S.; Zouhar, J.; Carter, C. J.; Raikhel, N. Isolation of intact vacuoles from Arabidopsis rosette leaf-derived protoplasts. *Nat. Protoc.* **2007**, *2*, 259–262, doi:10.1038/nprot.2007.26.
 56. Petersson, S. V.; Johansson, A. I.; Kowalczyk, M.; Makoveychuk, A.; Wang, J. Y.; Moritz, T.; Grebe, M.; Benfey, P. N.; Sandberg, G.; Ljung, K. An Auxin Gradient and Maximum in the Arabidopsis Root Apex Shown by High-Resolution Cell-Specific Analysis of IAA Distribution and Synthesis. *Plant Cell* **2009**, *21*, 1659–1668, doi:10.1105/tpc.109.066480.
 57. Tarkowská, D.; Novák, O.; Floková, K.; Tarkowski, P.; Turečková, V.; Grúz, J.; Rolčík, J.; Strnad, M. Quo vadis plant hormone analysis? *Planta* **2014**, *240*, 55–76, doi:10.1007/s00425-014-2063-9.
 58. Pěňčík, A.; Casanova-Sáez, R.; Pilařová, V.; Žukauskaitė, A.; Pinto, R.; Luis Micol, J.; Ljung, K.; Novák, O. Ultra-rapid auxin metabolite profiling for high-throughput mutant screening in Arabidopsis. *J. Exp. Bot.* **2018**, *69*, 2569–2579, doi:10.1093/jxb/ery084.
 59. Béziat, C.; Barbez, E.; Feraru, M. I.; Lucyshyn, D.; Kleine-Vehn, J. Light triggers PILS-dependent reduction in nuclear auxin signalling for growth transition. *Nat. plants* **2017**, *3*, 17105, doi:10.1038/nplants.2017.105.
 60. Laemmli, U. K. Cleavage of structural proteins during the assembly of the head of bacteriophage T4. *Nature* **1970**, *227*, 680–685, doi:10.1038/227680a0.
 61. Wolf, P. G.; Karol, K. G.; Mandoli, D. F.; Kuehl, J.; Arumuganathan, K.; Ellis, M. W.; Mishler, B. D.; Kelch, D. G.; Olmstead, R. G.; Boore, J. L. The first complete chloroplast genome sequence of a lycophyte, *Huperzia lucidula* (Lycopodiaceae). *Gene* **2005**, *350*, 117–28, doi:10.1016/j.gene.2005.01.018.
 62. Thibivilliers, S.; Anderson, D.; Libault, M. Isolation of Plant Root Nuclei for Single Cell RNA Sequencing. *Curr. Protoc. Plant Biol.* **2020**, *5*, doi:10.1002/cppb.20120.



Supplementary Material

Auxin metabolite profiling in isolated and intact plant nuclei

Vladimír Skalický¹, Tereza Vojtková¹, Aleš Pěničák¹, Jan Vrána², Katarzyna Juzon³, Veronika Koláčková², Michaela Sedlářová⁴, Martin F. Kubes^{1,5,#,*} and Ondřej Novák^{1,*}

¹ Laboratory of Growth Regulators, Institute of Experimental Botany of the Czech Academy of Sciences & Faculty of Science of Palacký University, Šlechtitelů 27, 78371 Olomouc, Czech Republic; vladimir.skalicky@upol.cz, voj.te111@gmail.com, ales.pencik@upol.cz

² Centre of Plant Structural and Functional Genomics, Institute of Experimental Botany, Czech Academy of Sciences, Šlechtitelů 31, 779 00 Olomouc, Czech Republic; kolackova@ueb.cas.cz, jan.vrana@fno.cz

³ Department of Biotechnology, The Franciszek Górski Institute of Plant Physiology, Polish Academy of Sciences, Niezapominajek 21, 30-239 Krakow, Poland; k.juzon@ifr-pan.edu.pl

⁴ Department of Botany, Faculty of Science, Palacký University, Šlechtitelů 27, 78371 Olomouc, Czech Republic; michaela.sedlarova@upol.cz

⁵ School of Life Sciences, University of Warwick, Coventry CV4 7AL, United Kingdom;

[#] Actual address: University of Hradec Králové, Faculty of Science, Department of Biology, Rokitanského 62, 500 03 Hradec Králové, Czech Republic

* Correspondence: novako@ueb.cas.cz, martin.kubes@uhk.cz; Tel.: +420-585-634-852, O.N.

Citation: Lastname, F.;
Lastname, F.; Lastname, F. Title.
Int. J. Mol. Sci. **2021**, *22*, x.
<https://doi.org/10.3390/xxxxx>

Academic Editor: Firstname
Lastname

Received: date
Accepted: date
Published: date

Publisher's Note: MDPI stays neutral with regard to jurisdictional claims in published maps and institutional affiliations.



Copyright: © 2021 by the authors.
Submitted for possible open access publication under the terms and conditions of the Creative Commons Attribution (CC BY) license (<https://creativecommons.org/licenses/by/4.0/>).

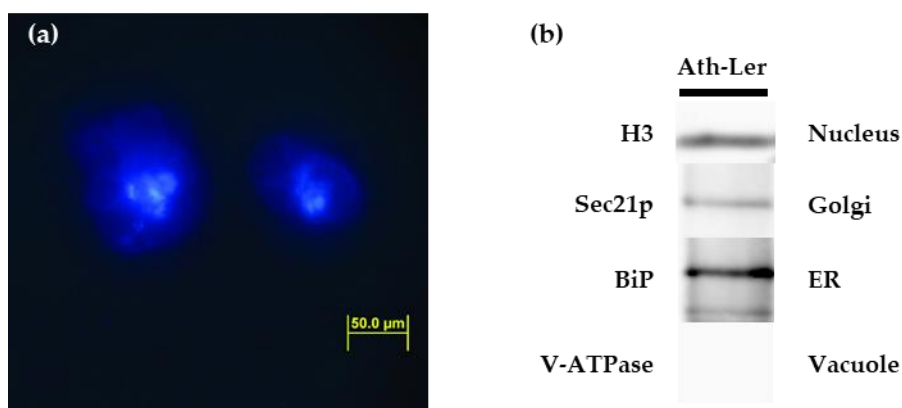


Figure S1. Isolation of nuclei according to the Method S1 [1] and purity control of isolated nuclei from *Arabidopsis thaliana* ecotype Landsberg *erecta* (Ath-Ler) cell line by immunoblotting. (a) Ath-Ler cells after lysis step with not properly released cell nuclei (stained with DAPI), (b) nuclear fraction was immunoblotted with anti-Histone 3 (H3) antibody to confirm enrichment of nuclei and following antibodies were used to disprove presence of contaminating organelles in particular fraction: Anti-Coatomer subunit gamma (Sec21p) for presence of Golgi complex, anti-Lumenal-binding protein (BiP) for presence of endoplasmic reticulum (ER) and finally anti-Epsilon subunit of tonoplast H⁺ATPase (V-ATPase) for presence of vacuole.

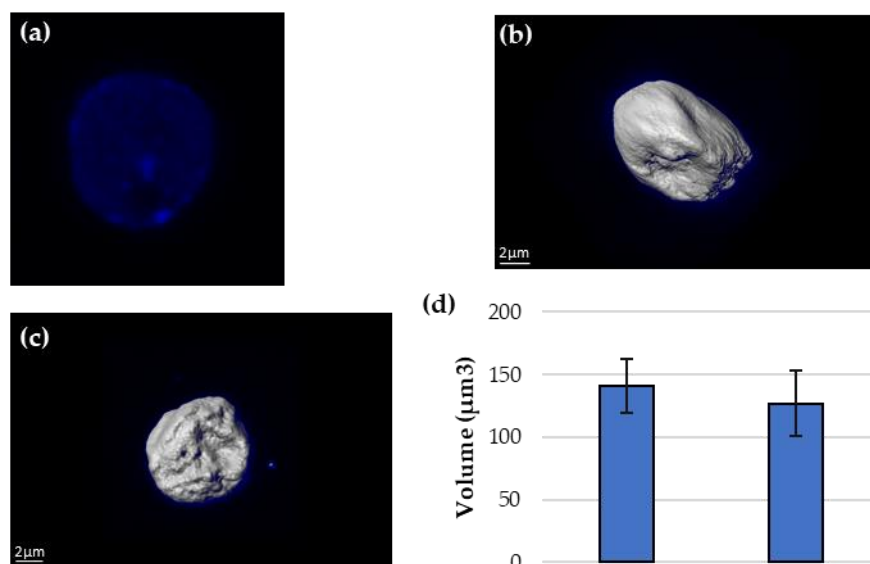


Figure S2. 3D reconstruction of nuclei from *Arabidopsis thaliana* ecotype Landsberg *erecta* (Ath-Ler) cell line isolated by flow cytometry method. (a) Detail of intact nuclei, (b,c) representative 3D reconstruction of nuclei, (d) average values of calculated nuclear volumes (two independent nucleus isolations). Volume analysis was done based on 200 3D reconstructed nuclei). Error bars indicate SD.

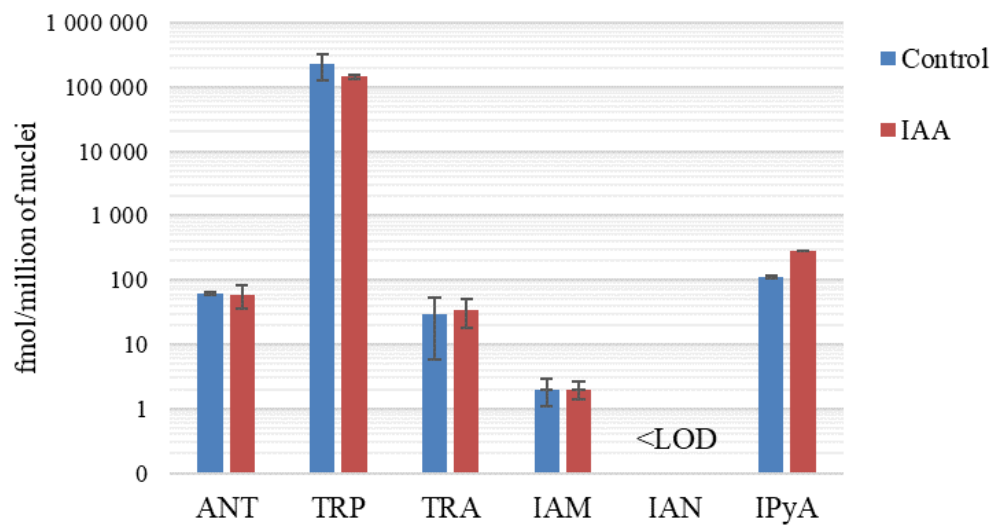


Figure S3. Endogenous levels (fmol/million nuclei) of auxin precursors in nuclei isolated from *Ath-Ler* protoplasts untreated (Control) and treated (IAA) with indole-3-acetic acid. Error bars indicate SD. (n=5-6)



Table S1. Endogenous levels (fmol/million nuclei) of auxin metabolites and their relative distribution in nuclear fractions isolated from *Ath-Ler* and BY-2 cells.

Compound	Ath-Ler cell line		BY-2 cell line	
	Auxin levels ¹ (fmol/1,000,000 nuclei)	Rel. Distribution (%)	Auxin levels ¹ (fmol/1x10 ⁶ nuclei)	Rel. Distribution (%)
ANT	61.09 ± 2.07	0.027%	58.22 ± 0.82	0.0085%
TRP	225,309.76 ± 100,381.48	99.6%	685,351.32 ± 185,482.78	99.8%
TRA	29.83 ± 23.99	0.013%	100.58 ± 9.59	0.015%
IAM	1.97 ± 0.89	0.0009%	n.d.	n.d.
IAN	n.d.	n.d.	n.d.	n.d.
IPyA	111.52 ± 3.69	0.049%	829.82 ± 190.86	0.12%
IAA	397.87 ± 124.09	0.18%	27.31 ± 13.69	0.0040%
oxIAA	20.15 ± 4.01	0.0089%	6.27 ± 3.06	0.0009%
IAAsp	362.24 ± 27.55	0.16%	8.80 ± 1.60	0.0013%
IAGlu	19.38 ± 7.04	0.0086%	2.12 ± 0.14	0.0003%
IAA-glc	n.d.	n.d.	n.d.	n.d.
oxIAA-glc	n.d.	n.d.	n.d.	n.d.

¹ Values are means ± SD (n=4); n.d. – not detected.



Table S2. Endogenous levels (pmol/g of fresh weight) of auxin metabolites in *Ath-Ler* cells.

Compound	Ath-Ler cell line	
	Auxin levels ¹ (pmol/g)	
ANT	n.d.	
TRP	18,233.64	1227.86
TRA	0.61	0.21
IAM	0.26	0.04
IAN	3.30	0.38
IPyA	102.22	19.54
IAA	1.35	0.66
oxIAA	7.60	4.55
IAAsp	2.35	0.41
IAGlu	n.d.	
IAA-glc	n.d.	
oxIAA-glc	n.d.	

¹Values are means \pm SD (n=5); n.d. – not detected.



Method S1. Alternative methods of cell nuclei isolation

S1.1. Alternative method of nuclei isolation using differential centrifugation

Samples of cell nuclei were prepared according to Xu and Copeland [1] with minor modifications. Briefly, cells were filtered and resuspended in cold lysis buffer (20 mM Tris-HCl pH 7.4, 25% (v/v) glycerol, 20 mM KCl, 2 mM EDTA pH 7.5, 2.5 mM MgCl₂, and 250 mM sucrose). 1 mM 1,4-dithiothreitol (DTT) and 2 mM phenylmethylsulfonyl fluoride (PMSF) were also added before experiment (alternatively, pH was adjusted to 5.3 as described in [2]). The cell suspension was homogenized by a Dounce homogenizer and then filtered through the pre-wetted 3 layers of Miracloth membrane (20–25 µm) and pelleted by centrifugation (1500× g, 10 min, 4 °C). The nuclear pellet was gently resuspended in nuclear resuspension buffer (20 mM Tris-HCl pH 7.4, 25% (v/v) glycerol, 2.5 mM MgCl₂ and 0.2% (v/v) Triton X-100) and centrifuged (1500× g, 10 min, 4 °C). The washing step was repeated twice. Finally, the pellet was gently resuspended in the same buffer without Triton X-100 (all components from Merck Life Science, Darmstadt, Germany). The isolated nuclei were immediately used for fluorescent microscopy and/or frozen in liquid nitrogen.

S1.2. Alternative method of nuclei isolation by flow cytometry

Samples of cell nuclei for sorting experiment were also prepared as described in Petrovská *et al.* [3] with minor modifications. Briefly, cells were fixed in 2% (v/v) formaldehyde, gently mixed, incubated for 10 min on ice, and then pelleted by centrifugation (500× g, 10 min, 4 °C). Cells were grinded in mortar with pestle in lysis buffer (15 mM Tris, 2 mM Na₂EDTA, 0.5 mM EGTA, 80 mM KCl, 20 mM NaCl, 0.1% (v/v) Triton X-100, 0.2 mM spermine and 0.5 mM spermidine pH 7.5; 14 mM 2-mercaptoethanol and 0.1 mM PMSF were added before experiment) in final ratio of 1:3. The released nuclei were filtered through 20 µm nylon mesh and stained with DAPI (4',6-Diamidino-2-phenylindole dihydrochloride; final concentration 2 µg/ml; all components from Merck Life Science, Darmstadt, Germany). Sorting of nuclei was performed in 0.7% (m/v) NaCl as a sheath fluid solution using BD FACS Aria II SORP flow cytometer (BD Bioscience, NY, USA). Flow cytometer was equipped with 70 µm nozzle tip, UV laser (355 nm, 100 mW) and blue laser (488 nm, 100 mW), 450/30 nm and 480/10 nm bandpass filter for DAPI and flow cytometry standard (FCS), respectively. Fluidic system was pressurized to 482.6 kPa. The population of nuclei was selected according to following optical parameters: forward and side scatter in combination with DAPI specific fluorescence. Nuclear fractions were immediately used for fluorescent microscopy and/or frozen in liquid nitrogen.

Method S2. Volume analysis of isolated cell nuclei by 3D reconstruction method

Volume analysis of sorted nuclei together with image processing and 3D-FISH were done accordingly to Koláčková *et al.* [4] and Perníčková *et al.* [5]. About 50,000 nuclei in G1, G2 or S phase of the cell cycle per sample were identified and sorted using a FACS Aria II SORP flow cytometer (BD Biosciences). Total genomic DNA was labelled with Texas Red using Nick Translation Kit (Roche Applied Science) according to manufacturer's instructions and applied as a probe. The probe was detected with anti-digoxigenin-fluorescein (Roche Applied Science).

Selected nuclei were optically sectioned using an inverted motorized microscope Olympus IX81 equipped with a Fluoview FV1000 confocal system (Olympus, Tokyo, Japan) and FV10-ASW software. For each nucleus, 80–120 optical sections in 160–200 nm step were taken and then merged into a 3D model. Subsequent analyses were performed using Imaris 9.2 software (Bitplane, Oxford Instruments, Zurich, Switzerland). The volume and centre of the nucleus were determined from the rendering of primary intensity of DAPI nuclei staining using function 'Surfaces'. 'Display Adjustment' was used to adjust the channel contrast, and thus to improve the visualization of all analyzed objects.

References

1. Xu, F.; Copeland, C. Nuclear Extraction from *Arabidopsis thaliana*. *BIO-PROTOCOL* **2012**, *2*, doi:10.21769/BIOPROTOC.306.
2. Saxena, P. K.; Fowke, L. C.; King, J. An efficient procedure for isolation of nuclei from plant protoplasts. *Protoplasma* **1985**, *128*, 184–189, doi:10.1007/BF01276340.
3. Petrovská, B.; Jeřábková, H.; Chamrád, I.; Vrána, J.; Lenobel, R.; Uřinová, J.; Šebela, M.; Doležel, J. Proteomic analysis of barley cell nuclei purified by flow sorting. *Cytogenet. ancyd genome Res.* **2014**, *143*, 78–86, doi:10.1159/000365311.
4. Koláčková, V.; Perníčková, K.; Vrána, J.; Duchoslav, M.; Jenkins, G.; Phillips, D.; Turkosí, E.; Šamajová, O.; Sedlářová, M.; Šamaj, J.; Doležel, J.; Kopecký, D. Nuclear Disposition of Alien Chromosome Introgressions into Wheat and Rye Using 3D-FISH. *Int. J. Mol. Sci.* **2019**, *20*, 4143, doi:10.3390/IJMS20174143.
5. Perníčková, K.; Koláčková, V.; Lukaszewski, A. J.; Fan, C.; Vrána, J.; Duchoslav, M.; Jenkins, G.; Phillips, D.; Šamajová, O.; Sedlářová, M.; Šamaj, J.; Doležel, J.; Kopecký, D. Instability of Alien Chromosome Introgressions in Wheat Associated with Improper Positioning in the Nucleus. *Int. J. Mol. Sci.* **2019**, *20*, 1448, doi:10.3390/IJMS20061448.

Fluorescence-activated multi-organelle sorting: A smart tool for subcellular mapping of auxins and cytokinins

Short title: Phytohormone subcellular mapping

Vladimír Skalický,^{a,1} Ioanna Antoniadi,^{b,1} Aleš Pěňčík,^a Ivo Chamrád,^a René Lenobel,^a Martin Kubeš,^{a,2} Miroslav Strnad,^a Karin Ljung,^{b,3} and Ondřej Novák^{a,b,3}

^a Laboratory of Growth Regulators, Faculty of Science, Palacký University and Institute of Experimental Botany of the Czech Academy of Sciences, CZ-78371 Olomouc, Czech Republic

^b Umeå Plant Science Centre, Department of Forest Genetics and Plant Physiology, Swedish University of Agricultural Sciences, SE-90183 Umeå, Sweden

¹ These authors contributed equally to this work.

² Current address: University Hradec Králové, Faculty of Science, Department of Biology, Rokitanského 62, CZ-50003 Hradec Králové, Czech Republic

³ Address correspondence to karin.ljun@slu.se or novako@ueb.cas.cz.

Abstract

Auxins and cytokinins are two major families of phytohormones which control and regulate most aspects of plant growth, development and plasticity. Their plant organ or tissue distribution is already well described but the importance of cell-type specific phytohormone homeostasis is still under intense investigation. Furthermore, distinct localization of transporters, receptors and enzymes related to auxin and cytokinin homeostasis maintenance suggests control of their allocation at the subcellular level. Gaining knowledge on the intracellular distribution of both phytohormones enable deeper understanding in their homeostasis maintenance and spatial-temporal signalling on cellular and organelle level. Therefore, we are introducing a Fluorescence-Activated Multi-Organelle Sorting (FAmOS), the innovative subcellular compartment separating technique based on principles of flow cytometry. Combination of the efficient FAmOS with the sensitive mass spectrometry-based method provides a unique approach for phytohormone profiling at the subcellular level. Our results present a method for simultaneous sorting of four different organelle populations based on the compartment-specific fluorescence parameters while monitoring organelle condition changes. Control experiments showed that neither sorting nor application of fluorescent dyes cause significant changes in both auxin and cytokinin profiles. Due to the high resolution of FAmOS, we also expect further use of this method for multiple-omics approaches.

INTRODUCTION

Plant bodies are organised hierarchically into organs, tissues and the smallest independent units – cells. Furthermore, cells are also divided into subcellular compartments. Intracellular partitioning enables separation of contradictory or different physiological processes like reactions of enzymes with substrates. Organelle-specific protein sets define their structure and functions (sumarized in Lee et al., 2010). Study of cell organisation and organelles' functions require their isolation in enriched and highly pure fractions. Subcellular fractionation methods have started developing since fifties of 20th century (De Duve et al., 1955). The majority of publications dealing, albeit partially, with organelle isolation exploited conventional density gradient (ultra)centrifugation protocols (Benková et al., 1999; Chen et al., 2002; Wulfetange et al., 2011; Ding et al., 2012; Jiskrová et al., 2016). However, the continuously increasing sensitivity of the downstream instrumental analysis over the last decades demands higher resolution power of these conventional approaches for organelle isolation. Therefore, novel methods based on affinity-capturing (Deal and Henikoff, 2011; Boussardon et al., 2020) or flow cytometry (Petrovská et al., 2014; Gaiero et al., 2018; Wolf et al., 2005) have been developed. Fluorescence-activated cell sorting (FACS) is a technique that has been also experiencing a bloom in plant sciences during the last decade. Cell sorting from different plant tissues has revealed valuable cell-specific transcriptomic (Kortz et al., 2019), proteomic (Petricka et al., 2012), metabolomic data (Pěňčík et

al., 2013; Petersson et al., 2009; Antoniadis et al., 2015; Petersson et al., 2015) and has undoubtedly lead to far more detailed insights into the regulation of plant development. Our focus has moved from plant organ- to tissue-, cell- and to now subcellular compartment-level. Rapid development and improvements of mass spectrometric methods as well as sample isolation techniques have enabled substantial progress in cell-type-specific and subcellular studies over the last decade (reviewed in Novák et al., 2017). Studies of regulatory processes at the subcellular level will shed light into a deeper understanding of cellular homeostasis maintenance as well as in intra- and inter-cellular communication.

We aimed to create a subcellular map of phytohormones distribution, especially auxins and cytokinins (CKs) which are master regulators in myriad physiological processes contributing in plant growth, development and plasticity (Schaller et al., 2015). These two major hormone families act synergistically (Hurný et al., 2020) but also antagonistically (Müller and Sheen, 2008) to control different physiological aspects. Moreover, their mutual homeostasis regulation has been proven (Šimášková et al., 2015; Di Mambro et al., 2019; Tessi et al., 2021). Auxin and CK relevant enzymes' and transporters' localizations indicate hormonal homeostasis control at the subcellular level (reviewed in Skalický et al., 2018), yet the existence of intracellular distribution gradients of phytohormones is completely unknown. Initial steps of auxin and CK biosynthesis occur mainly in chloroplasts (Skalický et al., 2018; Zürcher and Müller, 2016). The active auxin compound, indole-3-acetic acid (IAA), can be produced by parallel biosynthetic pathways in plants (Ljung, 2013). IAA can be (ir)reversibly conjugated with amino acid, glucose or modulated into methyl IAA (Casanova-Sáez et al., 2021). However, the major IAA catabolic pathway in Arabidopsis is oxidation to 2-oxindole-3-acetic acid (oxIAA) (Novák et al., 2012). CK nucleotides are the firstly synthesized cytokinin forms originating from adenine (Kakimoto, 2001; Takei et al., 2001). CK nucleotides can be then converted either directly to highly active free-bases or indirectly by the production of the intermediate riboside forms (Kurakawa et al., 2007). CK bases can be stored as CK O-glucosides (Jin et al., 2013; Šmehilová et al., 2016), inactivated into CK N-glucoside form (Wang et al., 2013) or irreversibly degraded back to adenine by cytokinin oxidase/dehydrogenase (Werner et al., 2006).

Herein, we are introducing an effective flow cytometry technique for subcellular fractionation, so-called Fluorescence-Activated multi-Organelle Sorting (FAMOS). This method is based on combination of general principles of flow cytometry and organelle specific fluorescent dyes. It is thus independent of time-consuming generation of transgenic plant lines expressing fluorescent protein(s). FAMOS enables studying of macromolecular as well as low molecular compounds of a plant sample in four simultaneously sorted organelles. This technique is thus time-efficient while it minimizes the demands on starting material and the risk for technical errors. Moreover, FAMOS offers isolated organelles within half an hour, universal handling conditions for all sorted organelles and their live status monitoring recorded. Here we present the combination of our

newly developed FAmOS tool with ultra-sensitive mass spectrometry-based methods providing a unique approach for organelle-specific phytohormone analysis. We employed FAmOS to simultaneously isolate nuclei, chloroplasts, mitochondria, and endoplasmic reticulum populations for metabolic profiling of auxin and cytokinin. Vacuoles, due to their large occupancy of the plant cell, have been in parallel isolated in order to complete the picture of our aimed phytohormone subcellular distribution.

RESULTS

Multi-organelle fluorescent staining design for FAmOS

Undifferentiated pluripotent cell line of *Arabidopsis thaliana* cultivated without exogenously applied phytohormones was chosen as a biological model for metabolic profiling (Pesquet et al., 2010). We expected that the suspension cell culture exhibits a higher level of uniformity compared to the plant tissue, in which phytohormone gradients between different cell types have been described (Petersson et al., 2009; Pěňčík et al., 2013; Antoniadis et al., 2015).

Chloroplasts are highly auto-fluorescent organelles and therefore chlorophyll facilitated their identification as their endogenous natural fluorochrome. For analysis of nuclei, endoplasmic reticulum and mitochondria, organelle-specific fluorescent dyes were employed. These fluorescent dyes were carefully selected for live staining according to their respective excitation and emission wavelengths with primary criteria being the spectra overlap prevention. Thus, we could achieve multicolour labelling of distinct healthy and intact organelles at the same time. Additional confidence for fluorochrome separation derived also by the FACS instrument armed with four lasers that are strategically built in a spatial sequence. The fluorescence emission caused by the excitation of each laser is perceived by a distinct detector, equipped with several band pass filters. The combination of the above criteria and FACS possibilities drove our selection into the following fluorescent dyes: Hoechst, ER-tracker Green and MitoTracker Orange excited by UV, Blue and Yellow-Green lasers, respectively (Figure 1A). Chlorophyll is excited mainly with the blue laser, same as ER-tracker Green. However, the two fluorophores emit fluorescence in different wavelengths that are further narrowed down by band pass filters and can be thus clearly separated during flow cytometry (Figure 1A).

Since the selected fluorescent dyes have been primarily designed for mammalian cells and organelles, their localization specificity was verified in plant cells. For this reason, we isolated protoplasts from three transgenic plant lines with endogenous expression of green or yellow fluorescent protein (GFP or YFP) in ER, mitochondria and nuclei, respectively (Matsushima et al., 2002; Logan and Leaver, 2000; Boisnard-Lorig et al., 2001). The protoplasts were then stained with the corresponding fluorescent dye and as shown in Figure 1B, the colocalization of endogenous and dye fluorescence was confirmed. Finally, wild-type protoplasts were stained with a mixture of three fluorescent dyes (ER-tracker Green, MitoTracker Orange and Hoechst) and

imaged for all four organelle fluorescence emissions (chloroplasts, ER, mitochondria and nuclei). Our results demonstrate the unequivocally specific labelling of each fluorescent dye and the absence of labelling artefacts or doubly stained organelles (Figure 1C).

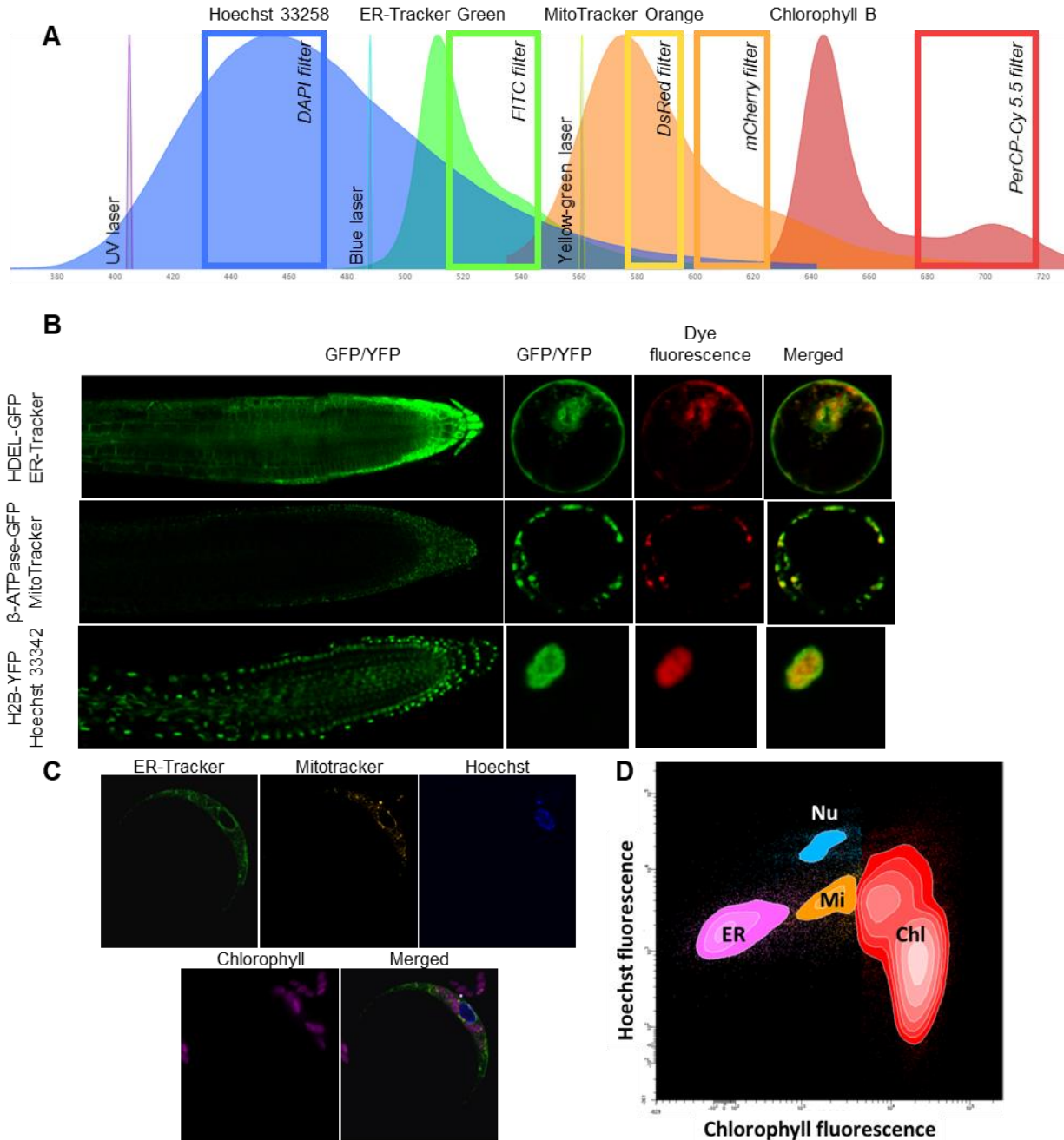


Figure 1. Selection of fluorescent dyes and verification of their specificity. **(A)** Non-normalised fluorescent spectra of selected fluorescent dyes with indication of laser wavelength. Rectangles indicate intervals of band pass filter wavelengths. **(B)** Co-localisation of organelle marker lines with fluorescent dyes. Image of root tip shows marker expression (right). Protoplast suspensions were then prepared from these lines and strained with relevant fluorescent dyes. **(C)** Co-staining protoplasts derived from 14-day-old cell culture with three fluorescent dyes. **(D)** Final representative separation of organelle population by FAmOS after set gate design.

Flow cytometry analysis and gate design for sorting four organelle populations

Fluorescence activated organelle sorting requires clear identification of the distinct organelle populations according to their measured optical characteristics, relevant size, granularity, complexity, and specific fluorescence. Based on these analysed characteristics we developed a sequential (three steps) gating strategy leading to identification and selection of four distinct organelle populations.

The first step was the discrimination and exclusion of debris and aggregates, which did not fit in the relevant organelle diameter size range of 2 – 10 μm . The relevant size estimation was facilitated by calibration beads with known diameters (2, 3 and 6 μm).

The second step of our gating strategy was the absolute identification of particular organelle populations based on their specific fluorophore signal, which was previously defined using appropriate negative control samples. For ER, mitochondria and nuclei, unstained samples were used as negative controls, while for chloroplasts we prepared a negative control organelle suspension from cells cultivated in the dark that were thus lacking chlorophyll (Figure S1). During this second step of our gating process, we incorporated a sequential exclusion strategy depending on the abundance and brightness of each fluorescent organelle. Since the identified chloroplasts population accounted for nearly 20 % of all measured particles, they were selected as the first organelle to gate and thus were further excluded from the organelle populations identification process. Following the same principal, the gate design was then sequentially continued for nuclei, ER and finally mitochondria. The selection of mitochondria as the last population for identification (after exclusion of debris, aggregates, chloroplasts, nuclei and ER) was not random. Mitochondria proved challenging to clearly distinguish from background noise over sorting time due to the fluorescent signal intensity of MitoTracker dye rapid deterioration. As a result, the number of identified mitochondria decreased significantly after 10 min of sorting. Our strategies to resolve this issue included both the above-mentioned fine design of their gate, where mitochondria were the last and most filtered designed gate, but also the time reduction between sample preparation and sorting to the minimum possible (Figure 2 and S2).



Figure 2. Summarized workflow of FAMOS with specified duration of each step as follows: (i) growth of plant cells in suspension culture, (ii) sample homogenization with a Potter-Elvehjem tissue grinder and staining with fluorescent dyes, (iii) fluorescence-activated multi-organelle sorting (FAMOS), (iv) phytohormone isolation by in-tip micro-solid phase extraction (in-tip μSPE), and (v) liquid chromatography-tandem mass spectrometry (LC-MS/MS) analysis. A detailed workflow is shown in Figure S2.

The third and the final step to our gating strategy was the distinction between contaminating doublets and true single organelles. To ensure that one drop contains only one organelle, we additionally analysed the ratio of each fluorescence signal width to the respective area (Suda et al., 2007). The designed gates finally allowed sufficient organelle separation and simultaneous sorting of mitochondria, nuclei, ER and chloroplasts populations in four individual vials (Figure 1D).

Identity of the sorted organelle populations

After completing the gate design (Figure S1), we performed several unbiased tests to prove the identity of the sorted organelle populations. This was achieved by preparing organelle suspensions from the plant lines expressing GFP or YFP in selected organelles as shown in Figure 1B. Prior to the flow cytometry analysis, the endogenously fluorescent organelle suspensions were additionally stained with the individual respective fluorescent dye. This resulted in double staining of a specific organelle by both GFP/YFP and fluorescent dye of different emission and/or excitation. Since both signals corresponded into the already created gates, the identity of the appropriate populations was verified. Ultimately, this also provided a proof of concept for our gating strategy as simultaneous isolation of chloroplasts, nuclei, ER and mitochondria was clearly achieved (Figure 1D).

Next, the sorted organelles were assessed by classical immunoblot analysis. Namely, we examined the presence of characteristic marker proteins – nuclear histone H3, chloroplast PsbA, reticular CNX1/2, mitochondrial GDC-H and the marker of Golgi apparatus, Sec21p, as a negative control (representative protein for an organelle that was not sorted). While these results confirmed substantial enrichment in chloroplast and nuclear fractions as shown in Figure S3A, no antibody signal was observed either in the ER or in the mitochondrial fraction. Importantly, this could be due to the combination of nanogram protein input and limited sensitivity of the antibodies used for immunoblotting.

To overcome this issue, we performed proteomic analysis with subsequent qualitative evaluation of the identified proteins in the isolated organelle fractions. Altogether, 401 *Arabidopsis* proteins were unambiguously identified in the examined samples (Figure 3A). Approximately 28% of these proteins were common for at least three fractions presumably originating from cytoplasmic and/or sorting background. However, characteristic function annotation clusters could be determined for each isolated organelle population (Figure 3B). Moreover, several well-known organelle marker proteins such as histone H3 and inner nuclear membrane protein Sun2, reticular chaperone BIP2 or mitochondrial porin VDAC3 were detected in the expected fractions. Altogether, it can be concluded that the FAmOS method presented here empowers simultaneous and sufficient enrichment of chloroplasts, nuclei, ER and mitochondria populations.

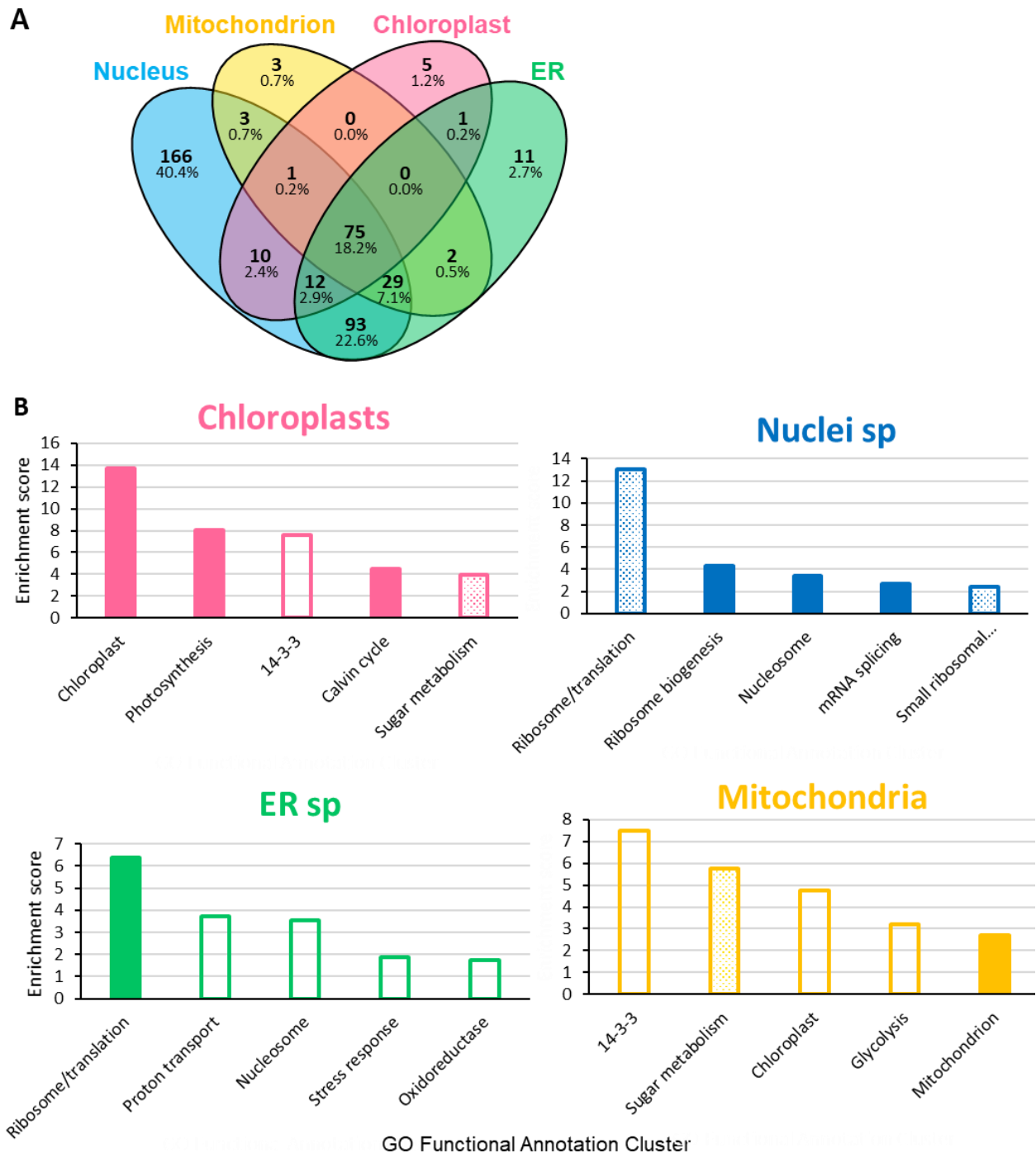


Figure 3. Identity determination of the sorted organelle populations. **(A)** Protein identification overlaps for the sorted organelle populations. Numbers show the total sums of protein identifications belonging to the particular population of the Venn diagram. **(B)** Gene ontology analysis of enriched functional annotation terms for the identified proteins in particular organelle identification.

Stability of Phytohormone Profiles during FAMOS

Sample preparation steps like cell wall and plasma membrane disintegration may cause alterations of intracellular homeostasis especially the one of tightly regulated phytohormones. To examine the potential influence of FAMOS on auxin and CK metabolisms, we performed a

series of control experiments. At first, imitation of the sorting process was performed, by incubation of the organelle suspension in sorting buffer at 4°C, and assessment of phytohormone profiles stability in several time points. While auxin metabolism showed no significant alteration over time (Figure 4A), CK precursors, nucleotides and ribosides, and respective active forms displayed increased levels after 2 h of incubation (Figure 4A). Although these changes were apparent within CK biosynthesis metabolic steps, sorting imitation did not result in any significant conversion in between different CK types (Figure 4C). Further control experiments showed that cytokinin and auxin concentrations remained unaffected in stained organelle suspension compared to the unstained sample meaning that fluorescent dyes pool had no impact to the phytohormone levels (Figure S4A).

To conserve endogenous levels of individual phytohormone metabolites during sample preparation and sorting procedure, we tested a number of chemical treatments. Initially, we tried mild fixation with formaldehyde to stop all metabolic processes (Petrovská *et al.*, 2014). Unfortunately, this step was detrimental for phytohormone detection by LC-MS/MS (Figure S4B) and was thus excluded from the process. Next, we applied sodium azide as ATP-dependent processes inhibitor (Tucker, 1993) or naphthylphthalamic acid (NPA) as auxin transport inhibitor (Petrášek *et al.*, 2006). Both inhibitors affected neither cytokinins nor auxin metabolic profiles in organelle suspension (Figure S4C, D). Parallel treatments with adenosine 5'-monophosphate, as substrate competitor of phosphatases, or with adenine, as CK transport antagonist (Bürkle *et al.*, 2003; Cedzich *et al.*, 2008) further enhanced CK nucleotides or CK ribosides diversion from endogenous levels (Figure S4E, F). Finally, we combined a mixture of phosphatase inhibitors, which was proven the most effective treatment in both ceasing CK precursors' production and further stabilizing auxin conjugation (Figures 4B).

Lastly, to inspect possible hormonal profile changes during the whole procedure, from sample homogenization to sorting, we performed FAmOS after spiking the sample with stable-isotope labelled standards of active auxin and cytokinin, [¹³C₆]IAA and [¹⁵N₄]isopentenyladenine ([¹⁵N₄]iP), respectively. For examination of the actual sorting procedure, 200,000 pieces of each sorted organelle population were collected and pooled to determine a representative distribution of isotopic labels in all sorted organelle populations. LC-MS/MS analysis showed 1.8 % and 0.8 % conversion of [¹³C₆]IAA and [¹⁵N₄]iP during sorting, respectively (Figure 4D). Moreover, as presented in Figure S4G we detected only a metabolic turn-over of 2.1 % and 0.2 % for the isotopically labelled IAA and iP during sample preparation, respectively. Altogether, metabolic turn-over of labelled IAA and iP during FAmOS did not exceed 4 % and 1 %, respectively. It can thus be concluded that the hormone profiles measured downstream of the developed method represent endogenous levels for auxin and CK metabolites.

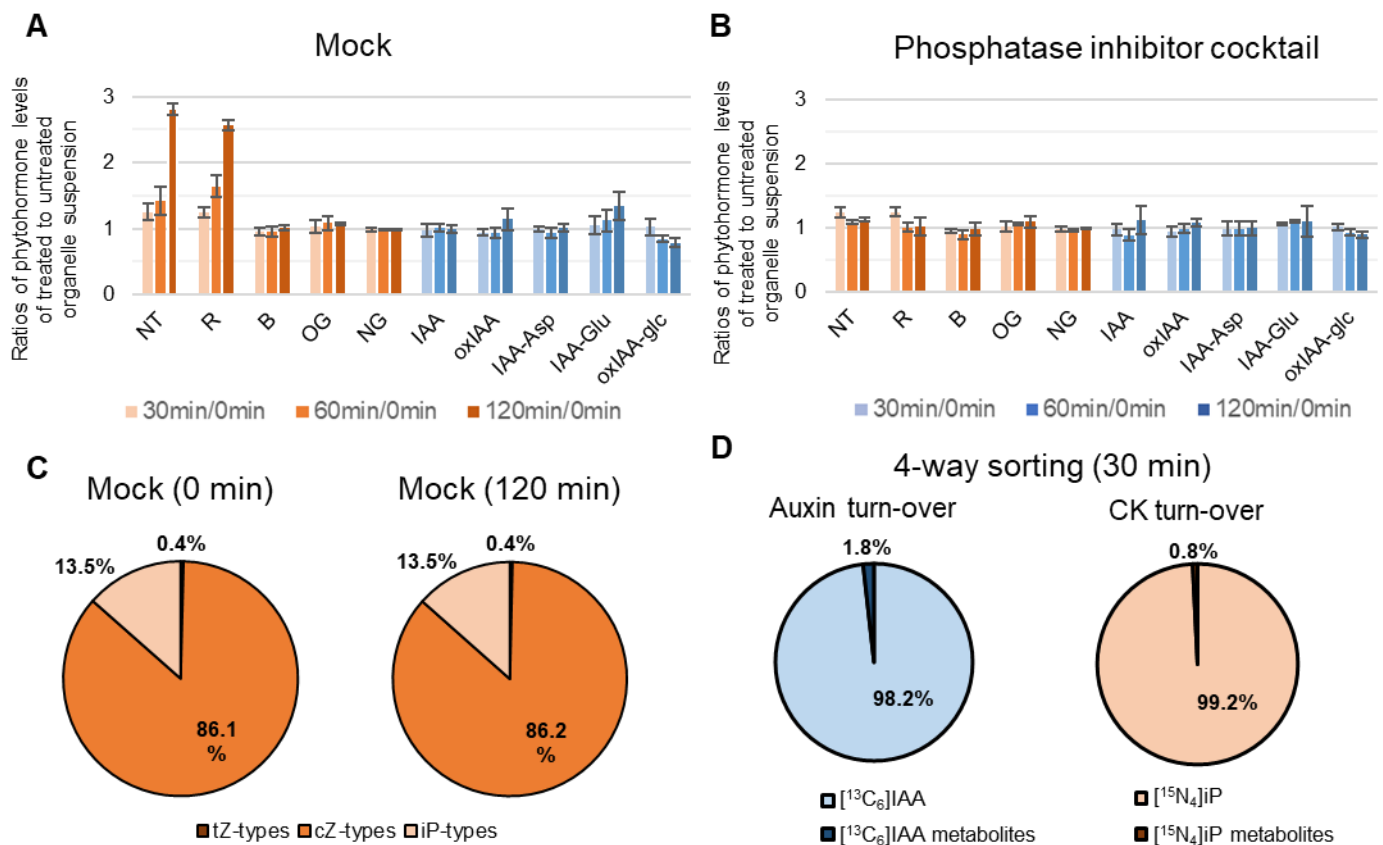


Figure 4. Evaluation of phytohormone profile stability. **(A-B)** Stability of cytokinin and auxin profiles in organelle suspension treated without **(A, Mock)** or with phosphatase inhibitor cocktail **(B)** and kept on ice for 2 hours to mimic the sorting process. The endogenous concentrations of auxins and cytokinins were calculated as fmol per 1,000,000 cells. The results are expressed as the respective ratios of metabolite concentration at time point to metabolite concentration at 0 min (n=4). IAA-glucose was not detected. **(C)** Monitoring of changes in the distribution of CK types (*tZ*, *trans*-zeatin; *cZ*, *cis*-zeatin; and *iP*, isopentenyladenine) in the organelle suspension after a 2-hour incubation. Metabolite profiles are expressed in percentages showing the relative abundance of each CK type (n=4). **(D)** Metabolic turn-over of isotopically labeled [$^{13}\text{C}_6$]IAA and [$^{15}\text{N}_4$]iP during 30-min four-way sorting process. The full profile of cytokinin and auxin metabolites labeled with the appropriate stable isotope was determined by LC-MS/MS, their concentration were calculated as fmol/1,000,000 sorted organelles and shown as the relative distribution of the respective stable isotope in the cytokinin and auxin metabolites. IAA – indole-3-acetic acid, oxIAA – 2-oxindole-3-acetic acid, IAA-Asp – IAA-Aspartate, IAA-Glu – IAA-Glutamate, oxIAA-glc – oxIAA-glucose, NT – CK nucleotides, R – CK ribosides, B – free bases, OG – O-glucosides, and NG – N-glucosides.

In conclusion, we adjusted our FAmOS workflow by adding the phosphatase inhibitor cocktail to ensure maintenance of hormone endogenous levels. Moreover, we shortened the procedure time to the minimum possible. This was achieved by freshly prepared sample every half an hour. As a result, the final FAmOS workflow included sample preparation and sorting procedure of less than 20 min and 30 min, respectively (Figure 2 and S2).

Subcellular Metabolic Profiling

With our fully established FAmOS method, we were able to get the first insight into the intracellular distribution of auxin and CK metabolites. We isolated substantially enriched fractions of 200,000 chloroplasts, nuclei, ER and mitochondria in four different tubes, deriving from the same sample, and then quantified endogenous auxin and CK metabolite levels in the sorted organelle populations (Figure 5). To confirm our results, we also performed FAmOS to samples that have been incubated with [¹⁵N₄]iP and [¹³C₆]IAA, respectively (Figure S5B and S6B). To obtain an overall picture of the distribution of phytohormones at subcellular levels, we also performed an analysis in vacuoles isolated by Ficoll density gradient centrifugation (Robert et al., 2007).

Due to the different size and number of organelles per plant cell, data normalization was essential for facilitation of phytohormone levels' comparisons between organelles. This data normalization process was based on protein content of organelle fraction (Table S1) (Včelařová et al., 2021) and the phytohormone map was finally expressed as the ratio of compound(s) level in particular organelle to compound(s) level in chloroplasts (Figure 5).

The generated auxin subcellular map exhibited in Figure 5B and S6, revealed an auxin gradient within the plant cell with concentration maxima in vacuoles. Interestingly, oxidized forms of IAA showed a similar pattern to free IAA. In comparison, auxin conjugated with amino acid were detected exclusively in vacuoles as their endogenous levels were below the detection limit in all other subcellular compartments isolated (Figure S6A). This could be probably due to low abundance of these metabolites in the amount of organelles collected in combination with detection limits of the LC-MS/MS method used. In the organelle suspension sample (prior sorting) auxin metabolites were unambiguously detected, except IAA-glc (Figure 4A). Labelled [¹³C₆]IAA confirmed the identified auxin gradient within the cell as well as rapid inactivation by conjugation and oxidation. Interestingly, all labelled IAA metabolites were found enriched in the vacuole and ER (Figure S6B). Moreover, increased oxIAA-glc content were also detected in nuclei and mitochondria.

As summarized in Figure 4C, the most abundant CK types in the organelle suspension sample were *cis*-zeatin-types (*cZ*) prevailing by an outstanding 88 %. The *iP*-types were only present as 12 % while the levels of *trans*-zeatin- (*tZ*) and dihydrozeatin-types were close to and/or below the detection limit of LC-MS/MS method. The intracellular CK map uncovered by FAmOS (Figure 5C), displayed a CK gradient with maxima pivotally in the vacuole and secondarily in the ER. Interestingly, cytokinin *O*-glucosides were detected exclusively in the vacuolar fraction, while CK nucleotides were below the detection limit in this compartment (Figure S5A). Our findings regarding the CK subcellular gradient were further supported by feeding experiment of labelled [¹⁵N₄]iP (Figure S5B). Surprisingly, labelled *iP* was found enriched not only in the vacuoles and ER but also in mitochondria. During one hour of the feeding experiment, *iP* was inactivated very

rapidly mainly as *N*-glucosides. The active CK form was also converted to riboside and ribotide, mainly enriched in vacuoles and ER.

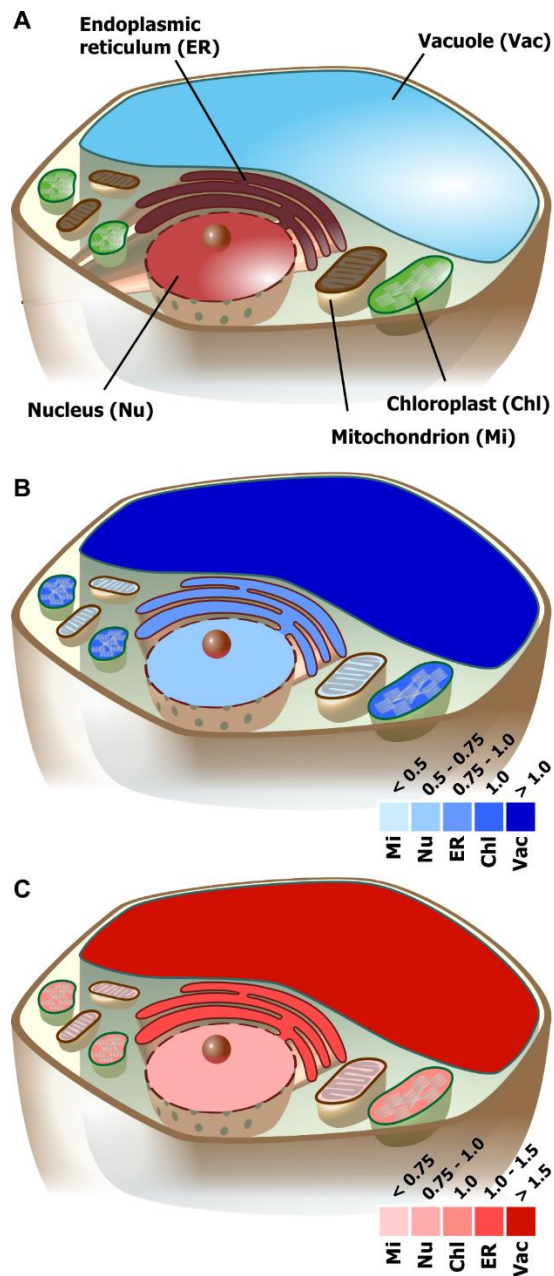


Figure 5. Subcellular map of endogenous phytohormones. (A) Scheme of a plant cell, (B) Relative distribution of IAA, (C) Relative distribution of CK sum. The phytohormone concentration was calculated as fmol/ μ g of proteins, and the ratios of respective organelle to chloroplast were determined.

DISCUSSION

Auxin and cytokinin homeostasis maintenance is a strictly regulated coordination of biosynthesis, metabolism, catabolism and transport. Although many aspects of this fine balance have been described during the last two decades (Schaller et al., 2015), its overview within the unit of one

cell yet remains elusive. Here we present a subcellular multi-fractionation technique, FAmOS, which can be coupled with several downstream analysis and thus pave the way for intracellular homeostasis investigations.

Previously introduced subcellular fractionation strategies or organelle isolation procedures have been based on distinct principles (reviewed in Lee et al., 2010) and most of them concerned only one type of organelle. Flow cytometry has been earlier used for cell sorting in human medicine (Adan et al., 2017) as well as in plant sciences (Carter et al., 2013). This technique has been also utilized for sorting of nuclei (Petrovská et al., 2014), chloroplasts (Wolf et al., 2005) or even smaller particles like chromosomes (Thind et al., 2017). Our newly developed FAmOS method achieved simultaneous and efficient separation and sorting of four distinct organelle populations deriving from a single sample. Our method was designed for versatile use, in terms of sample preparation and downstream application possibilities. This additionally empowers FAmOS as a compelling tool for various subcellular studies.

Organelles were stained with fluorescent dyes after confirming their labelling specificity in plant cells (Figure 1B, C). These dyes are commercially available and can be selected according to variety of spectral properties (Table 1). This way of labelling does not only facilitate fast and multi-staining strategies but also excludes the necessity for time-consuming generation and establishment of transgenic lines often used in methods based on affinity purification (Deal and Henikoff, 2011; Bousardon et al., 2020). Although the affinity-approach method is focused on cell-type-specific organelle isolation, FAmOS could be applied to incorporate such resolution power too. An advantageous aspect in FAmOS is that organelle sorting can be live-monitored, documented and in parallel analysed by several parameters. For example, the data generated during FAmOS include the number of particles that passed in front of the laser, their relative size and granularity/complexity and their (auto)fluorescent signal intensities. These values can be used for further calculations (organelle yield) or for normalized data projection (number of organelles sorted). Crucially, in this method one can always return to inspect the data derived from a specific sorted and analysed sample.

The identity of the sorted organelle populations was verified in a series of independent experiments comprising fluorescent co-staining, immunoblotting and qualitative proteomic analysis. When organelles from plant lines harboring GFP/YFP-tagged organelle protein markers (Figure 1B) were stained with the respective fluorescent dyes, a clear overlap of signals was evident in the designed gates during the sorting procedure (Figure 1D). In addition, various protein markers characteristic to the desired organelles were detected in the sorted populations by both immunoblotting (Figure S3) and LC-MS/MS-based-protein identification (Figure 3 and Table S1). Finally, specific functions could be associated with the sorted organelles by GO functional annotation clustering (Huang et al., 2009). It should be mentioned that these annotations were observed despite the presence of background proteins, which normally constitute even more than

80% of the total protein content of the photosynthetically active plant tissues (Bassal et al., 2020; Niehaus et al., 2020; Mergner et al., 2020) and easily enshroud signals of less abundant proteins (Huber et al., 2003). Hence, the appearance of GO terms belonging to scarce proteins that usually do not manifest without any enrichment nicely highlights the specific sorting ability of the developed FAmOS method. Interestingly, the successful identification of specific organelle proteins in the respective populations obtained by FAmOS implies its potential extension to other “omics” approaches.

After verifying that FAmOS can achieve isolation of chloroplasts, mitochondria, ER and nuclei fractions, we continued with a series of control experiments to understand how FAmOS process can possibly affect hormone profiles. Phytohormones are part of strictly regulated metabolic pathways. Therefore, tissue or cell disruptions may cause rapid responses or enzymes activation resulting in changes on the hormone concentrations and profiles. The control experiments performed here were inspired from two studies dealing with auxin and CK profiling in sorted plant protoplasts (Petersson et al., 2009; Antoniadis et al., 2015) and are included for first time in phytohormone profiling at subcellular level in comparison of previous studies (Benková et al., 1999; Polanská et al., 2007; Ranocha et al., 2013; Jiskrová et al., 2016).

During imitation of the sorting procedure, we did not observe any significant changes in auxin profile (Figure 4), but a sharp rise of CK precursors was detected (Figure 3). The observed increase of CK precursors was mainly attributed to CK nucleotides. Normally, cytokinin purification from plant tissues involves inactivation of enzymatic degradation by an organic solvent deactivated enzymatic degradation and thus stability of CK metabolites (Bielecki, 1964). Unfortunately, such buffer is not compatible with FAmOS technique, because organic solvent with acid would cause phospholipid membrane dissolution and protein precipitation. This could be the reason of increased tRNA degradation which could then explain the increased of the resulting CK nucleotides (Miyawaki et al., 2006). Since enzymatic inactivity could not be halted with the conventional way, we examined the possibility of halting all metabolic processes by performing several chemical treatments (Figure S4). For examples, mild tissue fixation with formaldehyde conserves organelles resulting in improved sorting procedure (Levi et al., 1986) as well as inactivating all metabolic processes (Petrovská et al., 2014). However, the applied formaldehyde fixation resulted in phytohormone analysis deterioration due to the cross-linking of IAA and CK ribosides with cellular structures (Friml et al., 2003). Finally, CK metabolism could be stabilized during sorting imitation process after application of a phosphatase inhibitor cocktail (Figure 5B). The use of this mixture was inspired by its functionality during protein extraction processes.

A final overview on the subcellular phytohormone profiles stability during the whole FAmOS procedure was achieved by the additional metabolism monitoring control experiment based on fluxomic principles (Xu et al., 2020). Metabolic turn-over of isotopically labelled [¹³C₆]IAA and [¹⁵N₄]iP during FAmOS was estimated in total to be 4 % and 1 %, respectively. Importantly, these

results indicate that determination of phytohormonal subcellular profile is minimally burdened by artificial changes during our method.

Auxin and cytokinin distribution within primary root apex at cell-type-specific level has been previously described (Pettersson et al., 2009; Pěňčík et al., 2013; Antoniadis et al., 2015). The subcellular localization of the enzymes involved in auxin and CK metabolism, perception and signalling suggest that there could be a hormonal gradient also within the plant cells (reviewed in Skalický et al., 2018). For this reason, we decided to push the boundaries and create a first sketch of the auxin and cytokinin subcellular map in *Arabidopsis* cell. While these two phytohormone levels have been already measured in chloroplasts and vacuoles (Benková et al., 1999; Polanská et al., 2007; Jiskrová et al., 2016; Ranocha et al., 2013), the divergent normalization methods and sample preparation processes used does not allow comparison of the data between the two organelles. With FAmOS development, we could rise above these challenges. Sorting of four different intracellular compartments simultaneously that have undergone identical isolation procedure was achieved. The downstream quantification of 14 endogenous hormonal metabolites in these four organelle fractions was accomplished using ultra-sensitive LC-MS/MS. However, it was still critical to identify a functional way to compare phytohormone distribution in organelle types of different size, shape, and abundance per cell. Therefore, the total protein content was quantified in each organelle fraction (Table S1) and used as normalization method enabling comparison between the obtained organelle hormonal data (Včelařová et al., 2021).

We could then finally express intracellularly the phytohormone gradient maps for auxin and cytokinins (Figure 5). The concentration gradients revealed within the cell supported our hypothesis that phytohormone distribution is in good agreement with relevant enzymes' and transporters' localizations (Skalický et al., 2018). Our results indicate that in both cases of auxin and CK metabolism, vacuoles play important role potentially as a storage compartment. That is because all detected phytohormone forms were accumulated in this compartment or even exclusively present there (Figure S5 and S6).

Interestingly, the hormonal gradients FAmOS uncovered was observed even between endoplasmic reticulum and nuclei, supporting the hypothesis that ER regulate IAA flux to nucleus (Middleton et al., 2018). CK O-glucosides detection exclusively in vacuoles, is in accordance with the hypothesis that cytokinin storage form locate to this compartment (Šmehilová et al., 2016). The absence of CK nucleotides in vacuoles is in agreement with the respective enzymatic localization of CK biosynthesis enzymes ISOPENTENYL-TRANSFERASEs (IPTs). These genes, responsible for cytokinin biosynthesis (cytokinin nucleotides), post-translationally do not localize in vacuoles (reviewed in Skalický et al., 2018). Cytokinin active compounds, CK bases, have been also found abundant in ER compared to mitochondria, chloroplasts and nuclei populations. This is in agreement with the presence of the majority of CK receptors in the ER (Ceasar et al., 2011, Wulfetange et al., 2011, Lomin et al., 2017).

It should be noted that these first intracellular hormone maps presented here (Figure 5) depict situations in individual and independent cells as we are using plant cell culture. Future FAmOS work will shed light on respective results when samples derive from plant tissues and organs. A big advantage of FAmOS method is that it can be directly applied in different genotypes, plant species and combined with different downstream applications. It is a groundbreaking method that can enhance our understanding on the role of different organelles in specific plant functions as it can involve respective mutants and overexpressor transgenic lines.

METHODS

Plant Material and Growth Conditions

Arabidopsis (*Arabidopsis thaliana*) Col-0 cell suspension cultures were grown in liquid Murashige and Skoog media with addition of 3% sucrose, pH adjusted to 5.7, in darkness at 22 °C. Plant cells were weekly subcultured into fresh media in ratio 1:10. For confocal microscopy, 7-day-old and 14-day-old cells cultivated under continuous light with fully-developed chloroplasts (Dubreuil et al., 2018) were used. Green 14-days old cells grown in continuous light were used for all control and sorting experiments. *A. thaliana* lines expressing organelle-specific markers: β -ATPase:GFP (Logan and Leaver, 2000) in mitochondria, HDEL:GFP in endoplasmic reticulum (Matsushima et al., 2002) and H2B:YFP in nuclei (Boisnard-Lorig et al., 2001) were utilized for confocal microscopy and for organelle sorting (FAmOS gating strategy verification). Seeds were sterilized in 70% ethanol with 0.01% Tween-20 for 10 min, then rinsed 5-times with sterile water and sown on square Petri dishes containing solid Murashige and Skoog medium with 1% sucrose, 2.5mM MES and 1% agar. After stratification in darkness at 4 °C, seeds were placed vertically in growth chamber for 5 days (for confocal microscopy) or 10 days (for sorting) in long-day conditions (16 h light and 8 h darkness) and at 22 °C.

Protoplast isolation and staining with fluorescent dyes

Roots of 5-day-old *Arabidopsis* transgenic lines β -ATPase:GFP, HDEL:GFP and H2B:YFP were separately harvested and immediately submerged into protoplasts isolation buffer. Their root protoplasts were extracted according to Yoo et al. (2007) with slight modifications (Antoniadi et al., 2015). The isolated protoplasts from each line were then stained with the corresponding fluorescent dye that would label the same organelle endogenously expressing GFP or YFP according to the transgene. Therefore, root protoplasts originated from β -ATPase:GFP line were treated with 0.1 μ M MitoTracker Deep Red FM (Thermo Fisher Scientific; double labelling of mitochondria), the ones from HDEL:GFP line with 1 μ M ER-Tracker red (Thermo Fisher Scientific; double labelling of ER) and from H2B:YFP line with 1 μ g/ml Hoechst 33342 (Thermo Fisher Scientific; double labelling of nuclei). After 10 min of staining, the microscopy slides were covered with a thin layer of poly-L-lysine and the confocal imaging took place. Protoplasts from cell culture

cultivated under light condition were also isolated and stained with all dyes simultaneously (0.1 μ M MitoTracker Orange CMTMRos, 1 μ M ER-Tracker green and 1 μ g/ml Hoechst 33342) to image the dyes' specificity and spectra overlap including the autofluorescence in chloroplasts.

Confocal Microscopy

For confocal experiments imaging protoplasts co-stained with a mixture of fluorescent dyes, fluorescence was recorded using a Zeiss LSM 880 inverted fast Airyscan microscope with the objective C-Apochromat 40x NA 1.20 W Korr FCS M27. Pinhole was set to 183.2 μ m and the images were taken in two fluorescence tracks. Track 1 included ER-Tracker green or GFP or YFP and Chlorophyll excitations with 488 nm blue laser and respective emissions detection between 499-535 nm and 638-721 nm, respectively. Track 2 accommodated excitations of Hoechst 33342 (405 nm violet laser) and MitoTracker Orange CMTMRos (561 nm yellow-green laser) with respective emissions detected between 410-483 nm and 570-633 nm.

For confocal experiments imaging co-localization of the fluorescent dye and endogenous fluorescent of transgenic GFP lines, fluorescence was recorded using a Zeiss LSM 780 CLSM with inverted stand microscope. The objective used was C-Apochromat 40x/1.20 W Korr M27 and the parameters are reported in Table 1.

Table 1 List of used marker lines and fluorescent dyes

		Excitation (nm)	Emission (nm) detected	Pinhole (μ m)
Nuclei	H2B:YFP line	514	523-620	242
	Hoechst 33342 dye	405	441-506	
Mitochondria	β -ATPase:GFP line	488	493-568	89
	Mitotracker Deep Red FM dye	633	611-711	
ER	HDEL:GFP line	488	493-556	82
	ER tracker Red dye	561	568-690	

Sample Preparation for FAmOS

Green cells were pelleted by gravity at room temperature. During the following steps all components were kept on ice and all manipulations were performed with precooled equipment. Cells were washed twice with 0.7% NaCl and then grinded in 0.7% NaCl supplemented with 1 mM phenylmethanesulfonyl fluoride (PMSF) and phosphatase inhibitor cocktail (final concentrations: 1mM Na_3VO_4 , 4mM sodium tartrate dibasic dihydrate, 10mM NaF, 1mM Na_2MoO_4 , 5mM glycerol 2-phosphate disodium salt hydrate, 1 mM sodium pyrophosphate decahydrate) in glass tube with Potter-Elvehjem PTFE pestle by 15 strokes. Released organelles were filtered through three layers of prewetted Miracloth to remove unbroken cells and cell debris.

Organelles were stained with mix of fluorescent dyes (final concentrations: 1 μ M ER-Tracker Green, 0.1 μ M Mitotracker Orange CMTMRos and 0.2 μ g/ml Hoechst 33258) for 10 min in dark.

Organelle Sorting

Fluorescently-stained organelles were analysed and sorted utilizing BD FACS Aria III flow cytometer equipped with four lasers (BD Biosciences). BD FACSDiva software version 7.0 was used for cytometer handling and data analysis. Organelle suspension was loaded in the cell sorter (4 °C, mild agitation 100 rpm) and forced through the cuvette in a single-file stream, where laser lights intercepted the stream at the sample interrogation point. After passing through the cuvette, the stream entered the integrated 85 μ m nozzle tip, where the drop drive broke the stream into the droplets for sorting. Detection and recording of the interrogated particles deriving from the organelle suspension took place as described in Table 2. The forward scatter (FSC) of light was initially filtered through a 1.5 neutral density filter and then perceived by a photodiode detector with a 488/10 bandpass filter.

The sorted samples were collected in polypropylene tubes that were kept at 4°C during the sorting process. Simultaneous sorting of four organelle populations required some further optimization. The sheath fluid 0.7% NaCl that has been so far used for its compatibility with downstream LC-MS/MS applications (Antoniadi et al., 2015) was lacking the appropriate viscosity for the required four-way sorting process. Therefore, we have changed the sheath fluid composition and optimized its dilution to the key balance between viscosity and LC-MS/MS affinity.

Table 2 Cytometer configuration for FAmOS

	Laser	Excitation (nm)	Detector	Band Pass Filter (nm)	Long Pass Mirror (nm)
Side Scatter (SSC)	Blue	488	Tringon-Blue	488/10	-
ER-Tracker Green				530/30	-
Chlorophyll				695/40	655
Mitotracker Orange	Yellow-Green	561	Octagon- Yellow Green	582/15	-
Hoechst 33258	Violet	405	Octagon-Violet	510/50	502

Organelle Sorting

Fluorescently-stained organelles were analysed and sorted utilizing BD FACS Aria III flow cytometer equipped with violet (405 nm), blue (488 nm), yellow-green (561 nm) and red (633 nm) lasers (BD Biosciences). Organelle suspension was loaded in the cell sorter (4 °C) and passed

individually through 85 µm nozzle (Becton Dickinson and Company) using 70% Sheath Fluid BD FACSTFlow™ as a sorting buffer.

Protoplasts and Vacuoles Isolation

Protoplasts and vacuoles were isolated from 14-days-old suspension cells according to modified protocol from Robert *et al.* (2007). 10 mL of suspension cells was sedimented by gravity and medium was removed. Cells were resuspended in 30 ml enzyme solution containing 0.3 units/mL pectolyase and 45 units/mL cellulysin without β-Mercaptoethanol for 4 hours in dark. At the beginning of incubation, vacuum was applied to suspension for 1 min. For the feeding experiment, cell suspension was treated with 10 µM [¹³C₆]IAA, 10 µM [¹⁵N₄]iP or the 96% ethanol as a mock and incubated for 2 hours. Protoplasts were passed through 100 µm collector tissue sieve and two times washed and collected by gentle centrifugation. Vacuoles were released by adding of lysis buffer and purified through three-step Ficoll gradient by ultracentrifugation at 71 000 × g at 10 °C for 55 min. Amounts of protoplasts or vacuoles were calculated using Bürker counting chamber. All collected samples were immediately frozen in liquid nitrogen and stored at -80 °C.

Control Experiments

Organelle suspension was prepared as described above and treated with either 3 mM NaN₃, 10 µM adenine, 40 µM naphthylphthalamic acid, 10 µM adenosine 5'-monophosphate, phosphatase inhibitor cocktail, mixture of fluorescent dyes or the DMSO control and incubated on ice in dark. Organelle suspension was frozen at four following timepoints: 0 min, 30 min, 1h and 2 h in liquid nitrogen. For the feeding experiment, cells were washed from media and spiked with 10 µM [¹⁵N₄]iP and [¹³C₆]IAA before grinding. Then cells were prepared as was described above. Organelle suspension was aliquoted and frozen in liquid nitrogen. Organelle suspension was prepared as was described above and spiked with 10 µM [¹⁵N₄]iP and [¹³C₆]IAA before sorting. From treated organelle suspension, it was sorted 200,000 of each organelle population. These sorted samples were pooled and divided into aliquots comprising 200,000 of organelles and frozen in liquid nitrogen.

Auxin and Cytokinin Analysis

Auxins and cytokinins were purified according to by in-tip solid-phase microextraction protocol described by Svačinová *et al.* (2012) with modification according to Antoniadi *et al.* (2015). Firstly, samples were thawed on ice, aliquoted into 200.000 sorted organelles or vacuoles and frozen in liquid nitrogen to rupture membranes. Samples were diluted with deionised water at a ratio of 3:1 (v/v) and acidified with 1M HCl to pH≤2.7. Prior to extraction isotope-labeled internal standards (Olchemim) were added to each sample as follows: 0.5 pmol [¹³C₆]IAA, [¹³C₆]oxIAA, [¹³C₆]IAAsp, [¹³C₆]IAGlu, [¹³C₆]IAA-glc, [¹³C₆]oxIAA-glc; 0.2 pmol of [¹³C₅]cZ, [¹³C₅]tZ, [²H₃]DHZ, [²H₆]iP, [²H₅]tZR, [²H₃]DHZR, [²H₆]iPR, [²H₅]tZ7G, [¹⁵N₄]cZ7G, [²H₆]iP7G, [²H₅]tZ9G, [²H₃]DHZ9G, and

[²H₆]iP9G; 0.5 pmol of [²H₅]tZOG, [²H₇]DHZOG, [²H₅]tZROG, [²H₅]tZRMP, [²H₃]DHZRMP, and [²H₆]iPRMP. After application of the sample, microcolumn was washed with deionised water and auxins were eluted with methanol and cytokinins with 0.5 mM NH₄OH in 60% (v/v) methanol. Eluates were evaporated to dryness and then dissolved in 10% methanol. Auxin and cytokinin content was determined by ultra-performance liquid chromatography coupled with electro-spray-tandem mass spectrometry as described by Pěňčík *et al.* (2018) and Svačinová *et al.* (2012), respectively. Data were normalized according to protein content of organelle fraction and the phytohormone maps were expressed as the ratio of compound(s) level in particular organelle to compound(s) level in chloroplasts. To specifically estimate O-glucosides and IAA amino-conjugates level ratio in vacuoles in comparison with chloroplasts, we used 2/3 of the detection limit normalized per protein amount for each compound.

Proteomic Analysis

The sorted samples (organelle suspensions) were first concentrated employing a centrifugal filter unit with 3K cut-off and then, proteins were precipitated by four volumes of ice cold acetone. Protein pellets were collected by centrifugation and digested in-solution with commercially available trypsin as described elsewhere (Leon *et al.*, 2013). The incurred digests were purified using a home-made reversed-phase (C18) microcolumn as published by Franc *et al.* (2012) and subjected to LC-MS/MS analysis with settings adapted from Chamrad *et al.* (2014). Processing of the acquired MS data for the protein identification was performed with the use of MaxQuant software version 1.6.10.43 (Tyanova *et al.*, 2016) with an instrument parameter setting “Bruker QTOF” (Beck *et al.*, 2015) and Andromeda search engine (Cox *et al.*, 2011). The data were searched against *Arabidopsis thaliana* (cv. Columbia) protein database (UniProt, reference proteome UP000006548, 39,346 protein sequences, downloaded 2019/07/25) supplemented with 247 common laboratory contaminant proteins. To evaluate relative abundances of the identified proteins, the iBAQ method (Schwanhäusser *et al.*, 2011) was utilized. For the determination of the enriched functional annotation themes (particularly GO terms) connected with the identified proteins, DAVID Bioinformatics Resources 6.8 (Huang *et al.*, 2009) was used. The total protein content of the analyzed samples was determined from the MS data by integration of the area under a curve of the corresponding chromatogram. To this end, a series of protein digests with pre-set protein content prepared from *A. thaliana* cell culture was employed as a calibration (Figure S3B). The MS/MS proteomics data have been deposited to the ProteomeXchange consortium (<http://proteomecentral.proteomexchange.org>) via the PRIDE partner repository (Perez-Riverol *et al.*, 2019) with the dataset identifier PXDxxxxxx.

REFERENCES

- Adan, A., Alizada, G., Kiraz, Y., Baran, Y., and Nalbant, A.** (2017). Flow cytometry: basic principles and applications. *Crit. Rev. Biotechnol.* **37**: 163–176.
- Antoniadi, I., Plačková, L., Simonovik, B., Doležal, K., Turnbull, C., Ljung, K., and Novák, O.** (2015). Cell-Type-Specific Cytokinin Distribution within the Arabidopsis Primary Root Apex. *Plant Cell* **27**: 1955–67.
- Bassal, M. et al.** (2020). Reshaping of the Arabidopsis thaliana Proteome Landscape and Co-regulation of Proteins in Development and Immunity. *Mol. Plant* **13**.
- Beck, S. et al.** (2015). The impact II, a very high-resolution quadrupole time-of-flight instrument (QTOF) for deep shotgun proteomics. *Mol. Cell. Proteomics* **14**: 2014–2029.
- Benková, E., Witters, E., Van Dongen, W., Kolář, J., Motyka, V., Brzobohatý, B., Van Onckelen, H.A., and Macháčková, I.** (1999). Cytokinins in tobacco and wheat chloroplasts. Occurrence and changes due to light/dark treatment. *Plant Physiol.* **121**: 245–52.
- Bieleski, R.L.** (1964). The problem of halting enzyme action when extracting plant tissues. *Anal. Biochem.* **9**: 431–442.
- Boisnard-Lorig, C., Colon-Carmona, A., Bauch, M., Hodge, S., Doerner, P., Bancharel, E., Dumas, C., Haseloff, J., and Berger, F.** (2001). Dynamic analyses of the expression of the HISTONE::YFP fusion protein in arabidopsis show that syncytial endosperm is divided in mitotic domains. *Plant Cell* **13**: 495–509.
- Boussardon, C., Przybyla-Toscano, J., Carrie, C., and Keech, O.** (2020). Tissue-Specific Isolation of Arabidopsis/plant Mitochondria- IMTACT (Isolation of Mitochondria TAgged in specific Cell Types). *Plant J.* **103**: 459–473.
- Bürkle, L., Cedzich, A., Döpke, C., Stransky, H., Okumoto, S., Gillissen, B., Kühn, C., and Frommer, W.B.** (2003). Transport of cytokinins mediated by purine transporters of the PUP family expressed in phloem, hydathodes, and pollen of Arabidopsis. *Plant J.* **34**: 13–26.
- Carter, A.D., Bonyadi, R., and Gifford, M.L.** (2013). The use of fluorescence-activated cell sorting in studying plant development and environmental responses. *Int. J. Dev. Biol.* **57**: 545–552.
- Casanova-Sáez, R., Mateo-Bonmatí, E., and Ljung, K.** (2021). Auxin Metabolism in Plants. *Cold Spring Harb. Perspect. Biol.*: a039867.
- Cedzich, A., Stransky, H., Schulz, B., and Frommer, W.B.** (2008). Characterization of cytokinin and adenine transport in Arabidopsis cell cultures. *Plant Physiol.* **148**: 1857–1867.
- Chamrád, I., Simerský, R., Bérešová, L., Strnad, M., Šebela, M., and Lenobel, R.** (2014). Proteomic Identification of a Candidate Sequence of Wheat Cytokinin-Binding Protein 1. *J. Plant Growth Regul.* **33**: 896–902.
- Chen, Y.-F., Randlett, M.D., Findell, J.L., and Schaller, G.E.** (2002). Localization of the ethylene receptor ETR1 to the endoplasmic reticulum of Arabidopsis. *J. Biol. Chem.* **277**: 19861–6.
- Cox, J., Neuhauser, N., Michalski, A., Scheltema, R.A., Olsen, J. V., and Mann, M.** (2011). Andromeda: A peptide search engine integrated into the MaxQuant environment. *J. Proteome Res.* **10**: 1794–1805.
- Deal, R.B. and Henikoff, S.** (2011). The INTACT method for cell type-specific gene expression and

- chromatin profiling in *Arabidopsis thaliana*. *Nat. Protoc.* **6**: 56–68.
- Ding, Z. et al.** (2012). ER-localized auxin transporter PIN8 regulates auxin homeostasis and male gametophyte development in *Arabidopsis*. *Nat. Commun.* **3**: 941.
- Dubreuil, C., Jin, X., Barajas-López, J. de D., Hewitt, T.C., Tanz, S.K., Dobrenel, T., Schröder, W.P., Hanson, J., Pesquet, E., Grönlund, A., Small, I., and Strand, Å.** (2018). Establishment of Photosynthesis through Chloroplast Development Is Controlled by Two Distinct Regulatory Phases. *Plant Physiol.* **176**: 1199–1214.
- De Duve, C., Pressman, B.C., Gianetto, R., Wattiaux, R., and Appelmans, F.** (1955). Tissue fractionation studies. 6. Intracellular distribution patterns of enzymes in rat-liver tissue. *Biochem. J.* **60**: 604–17.
- Franc, V., Šebela, M., Řehulka, P., Končítíková, R., Lenobel, R., Madzak, C., and Kopečný, D.** (2012). Analysis of N-glycosylation in maize cytokinin oxidase/dehydrogenase 1 using a manual microgradient chromatographic separation coupled offline to MALDI-TOF/TOF mass spectrometry. *J. Proteomics* **75**: 4027–4037.
- Friml, J., Vieten, A., Sauer, M., Weijers, D., Schwarz, H., Hamann, T., Offringa, R., and Jürgens, G.** (2003). Efflux-dependent auxin gradients establish the apical-basal axis of *Arabidopsis*. *Nature* **426**: 147–53.
- Gaiero, P., Šimková, H., Vrána, J., Santiñaque, F.F., López-Carro, B., Folle, G.A., van de Belt, J., Peters, S.A., Doležel, J., and de Jong, H.** (2018). Intact DNA purified from flow-sorted nuclei unlocks the potential of next-generation genome mapping and assembly in *Solanum* species. *MethodsX* **5**: 328–336.
- Huang, D.W., Sherman, B.T., and Lempicki, R.A.** (2009). Systematic and integrative analysis of large gene lists using DAVID bioinformatics resources. *Nat. Protoc.* **4**: 44–57.
- Huber, L.A., Pfaller, K., and Vietor, I.** (2003). Organelle Proteomics: Implications for Subcellular Fractionation in Proteomics. *Circ. Res.* **92**: 962–968.
- Hurný, A. et al.** (2020). SYNERGISTIC ON AUXIN AND CYTOKININ 1 positively regulates growth and attenuates soil pathogen resistance. *Nat. Commun.* **11**: 2170.
- Jin, S.-H., Ma, X.-M., Kojima, M., Sakakibara, H., Wang, Y.W., and Hou, B.-K.** (2013). Overexpression of glucosyltransferase UGT85A1 influences trans-zeatin homeostasis and trans-zeatin responses likely through O-glucosylation. *Planta* **237**: 991–999.
- Jiskrová, E., Novák, O., Pospíšilová, H., Holubová, K., Karády, M., Galuszka, P., Robert, S., and Frébort, I.** (2016). Extra- and intracellular distribution of cytokinins in the leaves of monocots and dicots. *N. Biotechnol.* **33**: 735–742.
- Kakimoto, T.** (2001). Identification of plant cytokinin biosynthetic enzymes as dimethylallyl diphosphate:ATP/ADP isopentenyltransferases. *Plant Cell Physiol.* **42**: 677–85.
- Kortz, A., Hochholdinger, F., and Yu, P.** (2019). Cell Type-Specific Transcriptomics of Lateral Root Formation and Plasticity. *Front. Plant Sci.* **10**: 21.
- Kurakawa, T., Ueda, N., Maekawa, M., Kobayashi, K., Kojima, M., Nagato, Y., Sakakibara, H., and Kyojuka, J.** (2007). Direct control of shoot meristem activity by a cytokinin-activating enzyme. *Nature* **445**: 652–655.

- Lee, Y.H., Tan, H.T., and Chung, M.C.M.** (2010). Subcellular fractionation methods and strategies for proteomics. *Proteomics* **10**: 3935–3956.
- Leon, I.R., Schwammle, V., Jensen, O.N., and Sprenger, R.R.** (2013). Quantitative assessment of in-solution digestion efficiency identifies optimal protocols for unbiased protein analysis. *Mol. Cell. Proteomics* **12**: 2992–3005.
- Levi, M., Tarquini, F., Sgorbati, S., and Sparvoli, E.** (1986). Determination of DNA content by static cytofluorimetry in nuclei released from fixed plant tissue. *Protoplasma* **132**: 64–68.
- Ljung, K.** (2013). Auxin metabolism and homeostasis during plant development. *Development* **140**: 943–950.
- Logan, D.C. and Leaver, C.J.** (2000). Mitochondria-targeted GFP highlights the heterogeneity of mitochondrial shape, size and movement within living plant cells. *J. Exp. Bot.* **51**: 865–71.
- Di Mambro, R. et al.** (2019). The Lateral Root Cap Acts as an Auxin Sink that Controls Meristem Size. *Curr. Biol.* **29**: 1199-1205.e4.
- Matsushima, R., Hayashi, Y., Kondo, M., Shimada, T., Nishimura, M., and Hara-Nishimura, I.** (2002). An Endoplasmic Reticulum-Derived Structure That Is Induced under Stress Conditions in Arabidopsis. *Plant Physiol.* **130**: 1807–1814.
- Mergner, J. et al.** (2020). Mass-spectrometry-based draft of the Arabidopsis proteome. *Nature* **579**: 409–414.
- Middleton, A.M. et al.** (2018). Data-Driven Modeling of Intracellular Auxin Fluxes Indicates a Dominant Role of the ER in Controlling Nuclear Auxin Uptake. *Cell Rep.* **22**: 3044–3057.
- Miyawaki, K., Tarkowski, P., Matsumoto-Kitano, M., Kato, T., Sato, S., Tarkowská, D., Tabata, S., Sandberg, G., and Kakimoto, T.** (2006). Roles of Arabidopsis ATP/ADP isopentenyltransferases and tRNA isopentenyltransferases in cytokinin biosynthesis. *Proc. Natl. Acad. Sci. U. S. A.* **103**: 16598–603.
- Müller, B. and Sheen, J.** (2008). Cytokinin and auxin interaction in root stem-cell specification during early embryogenesis. *Nature* **453**: 1094–7.
- Niehaus, M., Straube, H., Künzler, P., Rugen, N., Hegermann, J., Giavalisco, P., Eubel, H., Witte, C.P., and Herde, M.** (2020). Rapid Affinity Purification of Tagged Plant Mitochondria (Mito-AP) for Metabolome and Proteome Analyses. *Plant Physiol.* **182**: 1194–1210.
- Novák, O., Hényková, E., Sairanen, I., Kowalczyk, M., Pospíšil, T., and Ljung, K.** (2012). Tissue-specific profiling of the Arabidopsis thaliana auxin metabolome. *Plant J.* **72**: 523–36.
- Novák, O., Napier, R., and Ljung, K.** (2017). Zooming In on Plant Hormone Analysis: Tissue- and Cell-Specific Approaches. *Annu. Rev. Plant Biol.* **68**: 323–348.
- Pěňčík, A. et al.** (2013). Regulation of auxin homeostasis and gradients in Arabidopsis roots through the formation of the indole-3-acetic acid catabolite 2-oxindole-3-acetic acid. *Plant Cell* **25**: 3858–70.
- Pěňčík, A., Casanova-Sáez, R., Pilařová, V., Žukauskaitė, A., Pinto, R., Luis Micol, J., Ljung, K., and Novák, O.** (2018). Ultra-rapid auxin metabolite profiling for high-throughput mutant screening in Arabidopsis. *J. Exp. Bot.* **69**: 2569–2579.
- Perez-Riverol, Y. et al.** (2019). The PRIDE database and related tools and resources in 2019: Improving support for quantification data. *Nucleic Acids Res.* **47**: D442–D450.

- Pesquet, E., Korolev, A. V, Calder, G., and Lloyd, C.W.** (2010). The Microtubule-Associated Protein AtMAP70-5 Regulates Secondary Wall Patterning in Arabidopsis Wood Cells. *Curr. Biol.* **20**: 744–749.
- Petersson, S. V, Johansson, A.I., Kowalczyk, M., Makoveychuk, A., Wang, J.Y., Moritz, T., Grebe, M., Benfey, P.N., Sandberg, G., and Ljung, K.** (2009). An Auxin Gradient and Maximum in the Arabidopsis Root Apex Shown by High-Resolution Cell-Specific Analysis of IAA Distribution and Synthesis. *Plant Cell* **21**: 1659–1668.
- Petersson, S. V, Lindén, P., Moritz, T., and Ljung, K.** (2015). Cell-type specific metabolic profiling of Arabidopsis thaliana protoplasts as a tool for plant systems biology. *Metabolomics* **11**: 1679–1689.
- Petrášek, J. et al.** (2006). PIN proteins perform a rate-limiting function in cellular auxin efflux. *Science* **312**: 914–8.
- Petricka, J.J., Schauer, M.A., Megraw, M., Breakfield, N.W., Thompson, J.W., Georgiev, S., Soderblom, E.J., Ohler, U., Moseley, M.A., Grossniklaus, U., and Benfey, P.N.** (2012). The protein expression landscape of the Arabidopsis root. *Proc. Natl. Acad. Sci. U. S. A.* **109**: 6811–6818.
- Petrovská, B., Jeřábková, H., Chamrád, I., Vrána, J., Lenobel, R., Uřinová, J., Šebela, M., and Doležel, J.** (2014). Proteomic analysis of barley cell nuclei purified by flow sorting. *Cytogenet. Genome Res.* **143**: 78–86.
- Polanská, L., Vičánková, A., Nováková, M., Malbeck, J., Dobrev, P.I., Brzobohatý, B., Vaňková, R., and Macháčková, I.** (2007). Altered cytokinin metabolism affects cytokinin, auxin, and abscisic acid contents in leaves and chloroplasts, and chloroplast ultrastructure in transgenic tobacco. *J. Exp. Bot.* **58**: 637–49.
- Ranocha, P. et al.** (2013). Arabidopsis WAT1 is a vacuolar auxin transport facilitator required for auxin homeostasis. *Nat. Commun.* **4**: 2625.
- Robert, S., Zouhar, J., Carter, C.J., and Raikhel, N.** (2007). Isolation of intact vacuoles from Arabidopsis rosette leaf-derived protoplasts. *Nat. Protoc.* **2**: 259–262.
- Schaller, G.E., Bishopp, A., and Kieber, J.J.** (2015). The yin-yang of hormones: cytokinin and auxin interactions in plant development. *Plant Cell* **27**: 44–63.
- Schwanhüusser, B., Busse, D., Li, N., Dittmar, G., Schuchhardt, J., Wolf, J., Chen, W., and Selbach, M.** (2011). Global quantification of mammalian gene expression control. *Nature* **473**: 337–342.
- Šimášková, M. et al.** (2015). Cytokinin response factors regulate PIN-FORMED auxin transporters. *Nat. Commun.* **6**: 8717.
- Skalický, V., Kubeš, M., Napier, R., and Novák, O.** (2018). Auxins and Cytokinins-The Role of Subcellular Organization on Homeostasis. *Int. J. Mol. Sci.* **19**: 3115.
- Šmeřilová, M., Dobrušková, J., Novák, O., Takáč, T., and Galuszka, P.** (2016). Cytokinin-Specific Glycosyltransferases Possess Different Roles in Cytokinin Homeostasis Maintenance. *Front. Plant Sci.* **7**: 1264.
- Suda, J., Kron, P., Husband, B.C., and Trávníček, P.** (2007). Flow Cytometry and Ploidy: Applications in Plant Systematics, Ecology and Evolutionary Biology. In *Flow Cytometry with Plant Cells* (Wiley), pp. 103–130.

- Svačinová, J., Novák, O., Plačková, L., Lenobel, R., Holík, J., Strnad, M., and Doležal, K.** (2012). A new approach for cytokinin isolation from Arabidopsis tissues using miniaturized purification: pipette tip solid-phase extraction. *Plant Methods* **8**: 17.
- Takei, K., Sakakibara, H., and Sugiyama, T.** (2001). Identification of Genes Encoding Adenylate Isopentenyltransferase, a Cytokinin Biosynthesis Enzyme, in Arabidopsis thaliana. *J. Biol. Chem.* **276**: 26405–26410.
- Tessi, T.M., Brumm, S., Winklbauer, E., Schumacher, B., Pettinari, G., Lescano, I., González, C.A., Wanke, D., Maurino, V.G., Harter, K., and Desimone, M.** (2021). Arabidopsis AZG2 transports cytokinins in vivo and regulates lateral root emergence. *New Phytol.* **229**: 979–993.
- Thind, A.K., Wicker, T., Šimková, H., Fossati, D., Moullet, O., Brabant, C., Vrána, J., Doležal, J., and Krattinger, S.G.** (2017). Rapid cloning of genes in hexaploid wheat using cultivar-specific long-range chromosome assembly. *Nat. Biotechnol.* **35**: 793–796.
- Tucker, E.B.** (1993). Azide treatment enhances cell-to-cell diffusion in staminal hairs of *Setcreasea purpurea*. *Protoplasma* **174**: 45–49.
- Tyanova, S., Temu, T., and Cox, J.** (2016). The MaxQuant computational platform for mass spectrometry-based shotgun proteomics. *Nat. Protoc.* **11**: 2301–2319.
- Včelařová, L., Skalický, V., Chamrád, I., Lenobel, R., Kubeš, M., Pěňčík, A., and Novák, O.** (2021). Auxin Metabolome Profiling in the Arabidopsis Endoplasmic Reticulum Using an Optimised Organelle Isolation Protocol. *Int. J. Mol. Sci.* **22**: 9370.
- Wang, J., Ma, X.M., Kojima, M., Sakakibara, H., and Hou, B.K.** (2013). Glucosyltransferase UGT76C1 finely modulates cytokinin responses via cytokinin N-glucosylation in Arabidopsis thaliana. *Plant Physiol. Biochem.* **65**: 9–16.
- Werner, T., Köllmer, I., Bartrina y Manns, I., Holst, K., and Schmülling, T.** (2006). New insights into the biology of cytokinin degradation. *Plant Biol. (Stuttg.)* **8**: 371–81.
- Wolf, P.G., Karol, K.G., Mandoli, D.F., Kuehl, J., Arumuganathan, K., Ellis, M.W., Mishler, B.D., Kelch, D.G., Olmstead, R.G., and Boore, J.L.** (2005). The first complete chloroplast genome sequence of a lycophyte, *Huperzia lucidula* (Lycopodiaceae). *Gene* **350**: 117–28.
- Wulfetange, K., Lomin, S.N., Romanov, G.A., Stolz, A., Heyl, A., and Schmülling, T.** (2011). The cytokinin receptors of Arabidopsis are located mainly to the endoplasmic reticulum. *Plant Physiol.* **156**: 1808–1818.
- Xu, J., Martien, J., Gilbertson, C., Ma, J., Amador-Noguez, D., and Park, J.O.** (2020). Metabolic flux analysis and fluxomics-driven determination of reaction free energy using multiple isotopes. *Curr. Opin. Biotechnol.* **64**: 151–160.
- Yoo, S.-D., Cho, Y.-H., and Sheen, J.** (2007). Arabidopsis mesophyll protoplasts: a versatile cell system for transient gene expression analysis. *Nat. Protoc.* **2**: 1565–1572.
- Zürcher, E. and Müller, B.** (2016). Cytokinin Synthesis, Signaling, and Function-Advances and New Insights. In *International Review of Cell and Molecular Biology*, K.W. Jeon, ed (Academic Press Inc. Elsevier Science: Amsterdam, Netherlands), pp. 1–38.

Supplementary materials

Table S1 Protein identifications and total protein content for sorted plant organelle fractions (Mean \pm SD, n=4)

Organele fraction	Identified Proteins	Organelle Specific Annotated Proteins	Specific Protein Mass (%)	Amount of proteins (ng)
Chloroplasts	161	100	91	219 \pm 4
Nuclei	43	14	74	356 \pm 59
ER	174	57	48	198 \pm 2
Mitochondria	162	45	14	332 \pm 18
Vacuoles	-	-	-	13 \pm 3

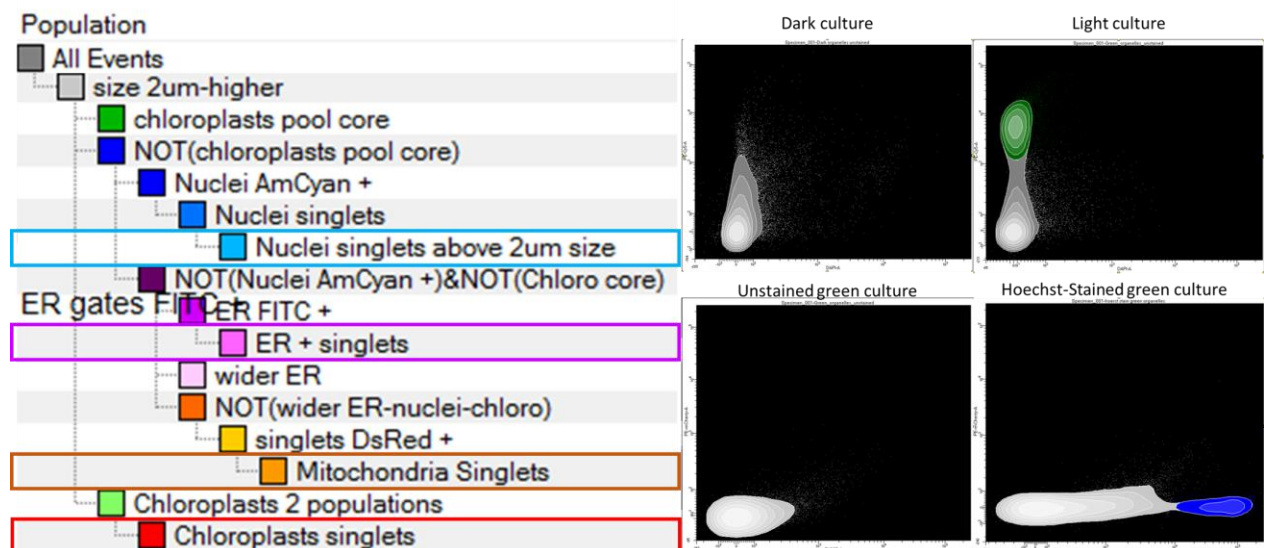


Figure S1. Selection of organelle population, which were selected hierarchically after analysis of stained sample and negative control. In case of chloroplasts, organelles released from cell culture cultivated in dark was used as negative control.

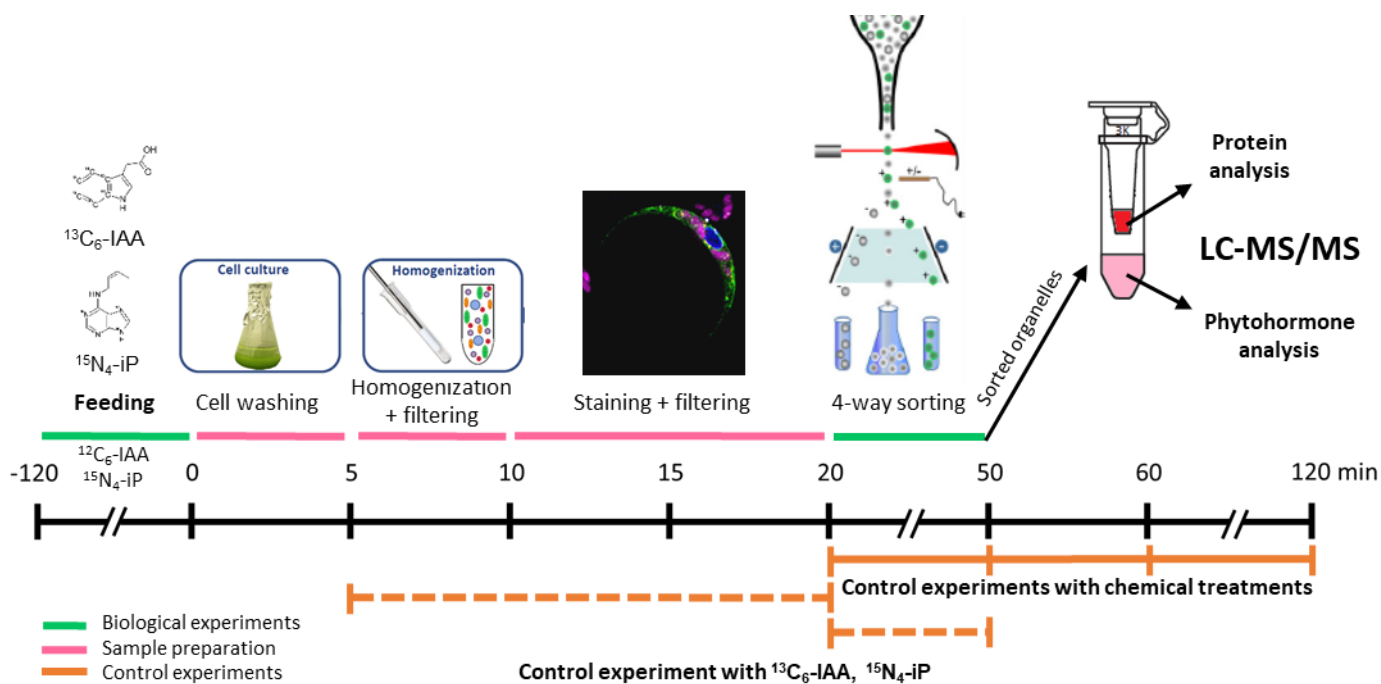


Figure S2. Detailed workflow of FAMOS.

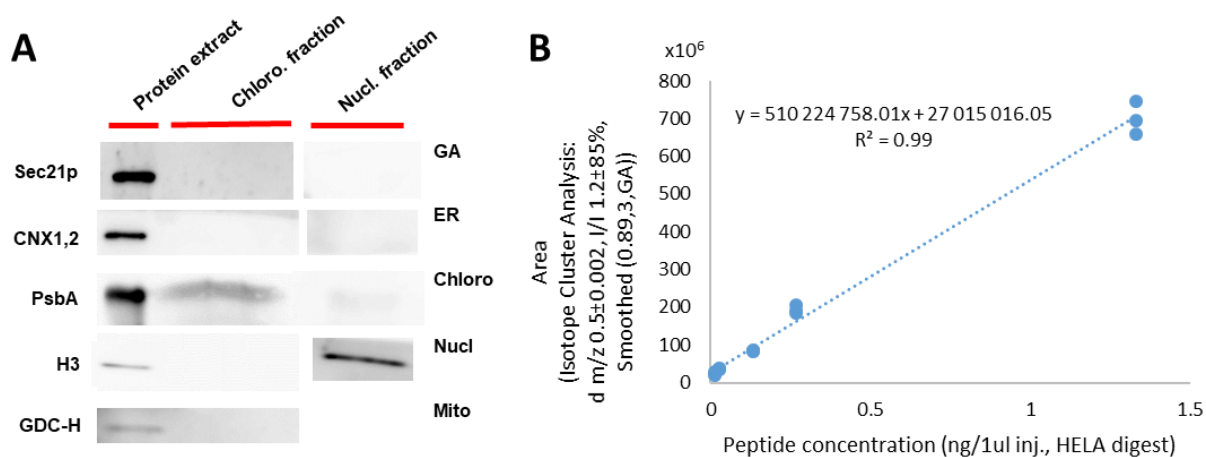


Figure S3. (A) Western blot analysis of sorted chloroplast and nuclei population. The following organelle-specific markers were immunodetected: Golgi apparatus–GA (Coatomer subunit gamma, Sec21p), Endoplasmic reticulum – ER (Lumena-binding protein, BiP and Calnexin homolog 1/2, CNX1/2), chloroplasts – Chloro (D1 protein of photosystem II, PsbA), nucleus – Nucl (Histone 3, H3), mitochondria–Mito (H protein of glycine decarboxylase complex, GDC-H). (B) Calibration curve for quantification of protein content in particular organelle population.

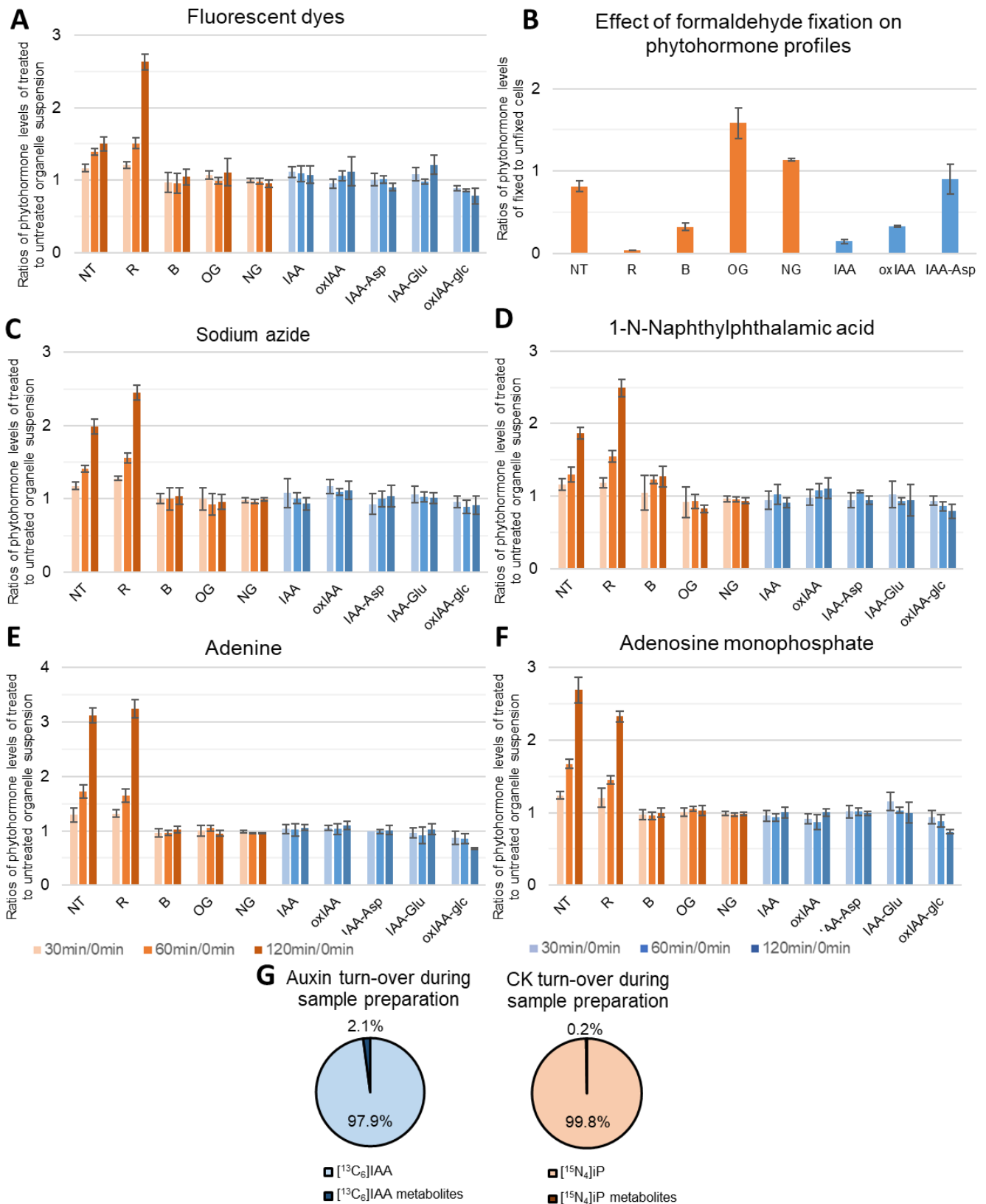


Figure S4. Evaluation of phytohormone profile stability. Selected agents were tested as follows: (A) Mixture of fluorescent dyes, (B) Formaldehyde (IAA-Glu was not detected in fixed cells), (C) Sodium azide, (D) 1-N-naphthylphthalamic acid, (E) adenine, (F) adenosine monophosphate. (G) Metabolic turn-over of isotopically labeled $[^{13}\text{C}_6]$ IAA and $[^{15}\text{N}_4]$ iIP during sample preparation (20 min).

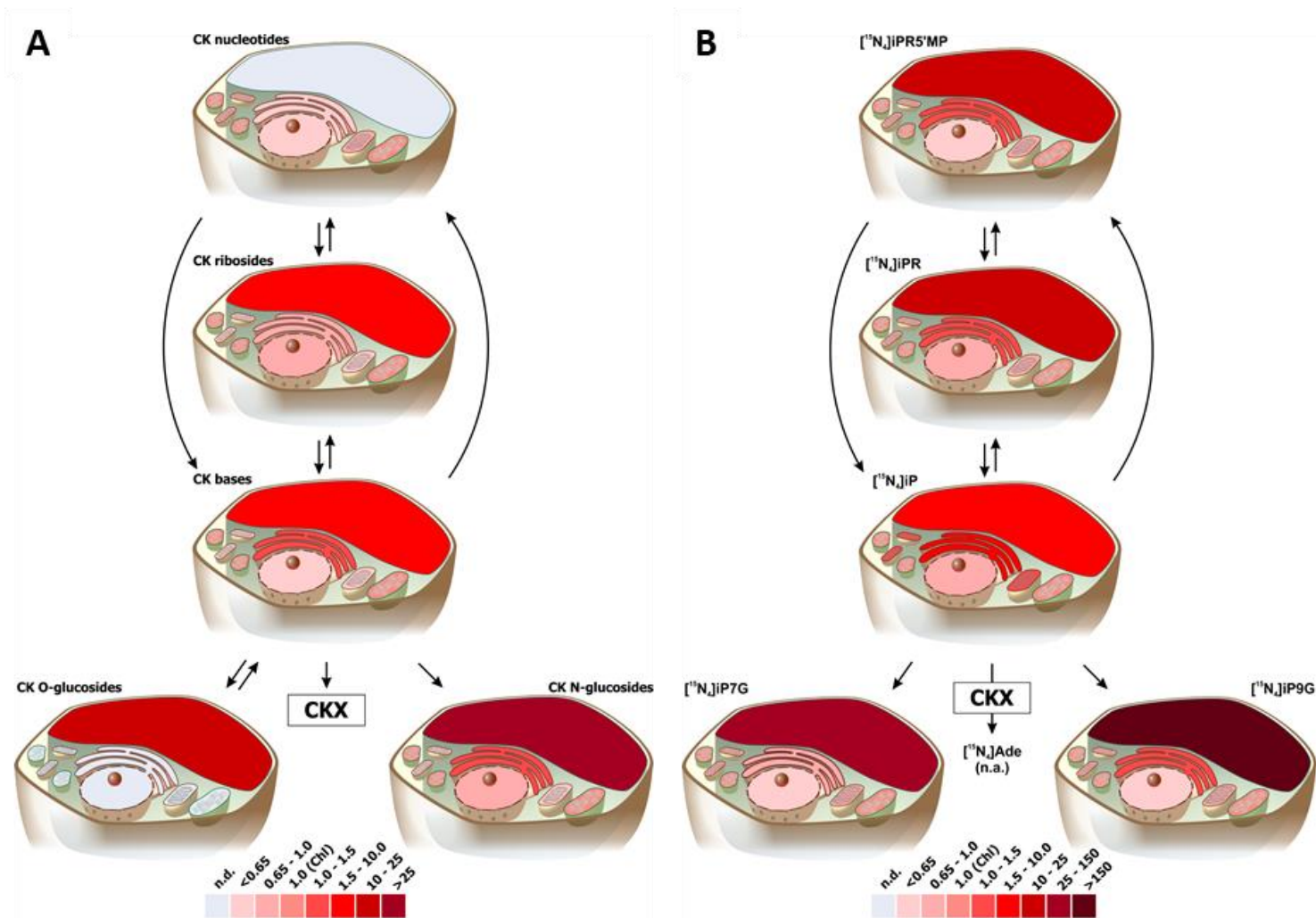


Figure S5. Subcellular map of (A) CK metabolites and (B) [¹⁵N₄]iP and relative metabolites (cell culture was treated with 10 μM [¹⁵N₄]iP for 1 h prior sorting). The phytohormone concentration was calculated as fmol/μg of proteins, and the ratios of respective organelle to chloroplast were determined. To estimate ratio of n.d. compounds in comparison with level in chloroplasts, 2/3 of the detection limit normalized per protein amount for each compound was used. Ade – adenine, CKX – cytokinin oxidase/dehydrogenase, n.a. – not analysed, n.d. – not detected.

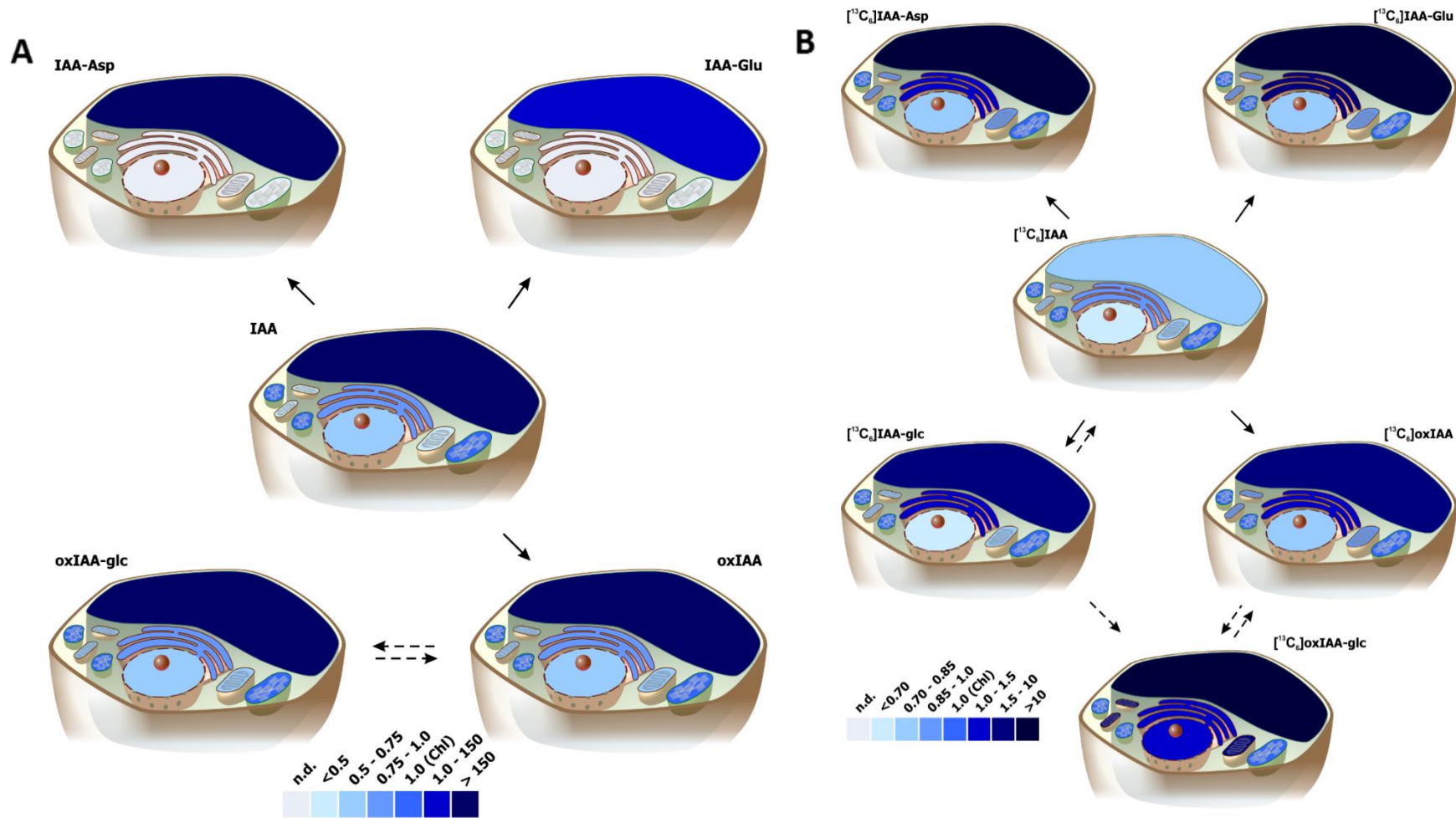


Figure S6. Subcellular map of (A) IAA and its metabolites, and (B) $[^{13}\text{C}_6]$ IAA and its metabolites (cell culture was treated with $10\ \mu\text{M}$ $[^{13}\text{C}_6]$ IAA for 1 h prior sorting). The phytohormone concentration was calculated as fmol/ μg of proteins, and the ratios of respective organelle to chloroplast were determined. To estimate ratio of n.d. compounds in comparison with level in chloroplasts, 2/3 of the detection limit normalized per protein amount for each compound was used. IAA-glc was not detected. IAA – indole-3-acetic acid, IAA-Asp – IAA-aspartate, IAA-Glu – IAA-glutamate, oxIAA – 2-oxoindole-3-acetic acid, oxIAA-glc – oxIAA-glucose, n.d. – not detected.



Palacký University Olomouc

Faculty of Science

Laboratory of Growth Regulators & Department of Chemical Biology

Vladimír Skalický

Summary of the Doctoral Thesis

**Metabolic profiling of phytohormones in subcellular
compartments using LC-MS techniques**

P1527 Biology

1501V019 Experimental Biology

Supervisor

doc. Mgr. Ondřej Novák, Ph.D.

Olomouc

2021

This Ph.D. thesis was realized in the Laboratory of Growth Regulators within the framework of internal Ph.D. Study of Experimental Biology, guaranteed by the Laboratory of Growth Regulators, Faculty of Science, Palacký University in Olomouc, between the years 2015-2021.

Ph.D. candidate: **Mgr. Vladimír Skalický**

Supervisor: **doc. Mgr. Ondřej Novák, Ph.D.**
Laboratory of Growth, Faculty of Science of Palacký University & Institute of Experimental Botany of the Czech Academy of Sciences, Olomouc, Czech Republic

Consultant: **Ioanna Antoniadis, Ph.D.**
Umeå Plant Science Centre, Department of Forest Genetics and Plant Physiology, Swedish University of Agricultural Sciences, Umeå, Sweden

Opponents: **Hélène Robert-Boisivon, Ph.D.**
Mendel Centre for Genomics and Proteomics of Plant Systems, CEITEC – Central European Institute of Technology, Masaryk University, Brno, Czech Republic

Prof. RNDr. Břetislav Brzobohatý, CSc.

Department of Molecular Biology and Radiobiology, Faculty of AgriSciences, Mendel University in Brno, Czech Republic.

Prof. RNDr. Ivana Macháčková, CSc.

Institute of Experimental Botany, Czech Academy of Science, Prague, Czech Republic

The evaluation of this Ph.D. thesis was written by **Prof. Ing. Miroslav Strnad, CSc. DSc.**, Laboratory of Growth Regulators, Faculty of Science, Palacký University in Olomouc.

The oral defence will take place on **14. 12. 2021 at 11:00** before the Commission for the Ph.D. thesis of the Study Program Experimental Biology, **Building 52 – Seminary room**, Šlechtitelů 27, Olomouc – Holice.

The PhD. thesis and expert reviews will be available 14 days before the defence in the Study Department of Faculty of Science (Mgr. M. Karásková), Palacký University, 17. listopadu 12, Olomouc.

After the defense, the Ph.D. thesis will be stored in the Library of the Biological Departments of Faculty of Science, Palacký University, Šlechtitelů 27, Olomouc – Holice.

Prof. Ing. Miroslav Strnad, CSc. DSc.

Chairman of the Commission for the Ph.D. thesis,
Study Program Experimental Biology,
Faculty of Science, Palacký University in Olomouc

CONTENT

1. INTRODUCTION	- 4 -
2. AIMS AND SCOPES	- 5 -
3. MATERIAL AND METHODS	- 6 -
3.1 Chemicals.....	- 6 -
3.2 Plant material and growth conditions	- 6 -
3.3 Equipment	- 7 -
4. SURVEY OF RESULTS	- 8 -
4.1 Revealing auxin metabolome in the endoplasmic reticulum isolated by density- gradient ultracentrifugation.....	- 8 -
4.2 Comparison of isolation methods for auxin metabolome determination in nucleus..	-
10 -	
4.3 Auxin and cytokinin subcellular map.....	- 11 -
5. CONCLUSION AND PERSPECTIVES	- 14 -
6. REFERENCES	- 15 -
7. LIST OF AUTHOR'S PUBLICATIONS	- 16 -
8. SOUHRN (SUMMARY, IN CZECH)	- 18 -

1. INTRODUCTION

Auxins and cytokinins (CKs) are the best-described plant hormones that regulate a variety of physiological processes in plants. Therefore, they play a crucial role in proper plant development and growth. Homeostasis of these phytohormones is tightly regulated by coordination of biosynthesis, transport, and metabolism. This leads to different distributions of auxin and CK within the plant body, organ, or tissue. In addition, the distinct enzymes and transporters' localization involved in the maintenance of homeostasis within the cell indicates a further level of complex regulation. To date, the organelle-specific profile of auxin or CK has only been described in chloroplasts and vacuoles. Nevertheless, a comprehensive view of this issue is still missing.

Several subcellular fractionation approaches such as differential centrifugation, density-gradient ultracentrifugation (DGU), affinity purification, and flow cytometric sorting have been developed. However, many of them focus only on one type of organelle. In addition, DGU is the gold standard for organelle isolation, but its resolving power may not be appropriate for phytohormone profiling.

This doctoral thesis describes the development of a method of subcellular fractionation based on DGU and flow cytometry (FCM) followed by profiling of phytohormones in isolated organelles by sensitive mass spectrometric methods. Flow cytometric method enabled simultaneous sorting of chloroplasts, nuclei, mitochondria, and endoplasmic reticulum (ER) from one sample. Combination of these approaches can shed light on the regulation mechanisms that maintain phytohormone homeostasis within the plant cell.

2. AIMS AND SCOPES

Auxins and CKs are master regulators of myriad physiological and developmental processes *in planta*. Their distribution within plant organs and tissues is already well described, but the importance of cell-type specific phytohormone homeostasis is currently under intense investigation. Moreover, intracellular auxin and CK dislocation and mechanisms of homeostasis maintenance are still elusive. Therefore, this doctoral thesis deals with auxin and CK metabolic profiling at the subcellular level.

The main aims of the work described and discussed in this thesis were as follows:

- to review the homeostasis of auxin and CK at the subcellular level and subcellular fractionation approaches,
- to develop and optimize protocols for subcellular compartments isolation with view to subsequent phytohormone analysis,
- to optimize the purification protocol for auxin and CKs analysis from isolated organelles,
- to analyse the profiles of auxin and CK in particular plant organelles,
- to create the subcellular map of auxin and CK concentrations.

3. MATERIAL AND METHODS

3.1 Chemicals

- All chromatographic solvents and chemicals for hormonal analysis were of hypergrade purity from Sigma-Aldrich Chemie GmbH (Steinheim, Germany), Merck Life Science (Darmstadt, Germany) and Roche Diagnostics (Mannheim, Germany).
- Standards of tested chemicals were obtained from Olchemim Ltd (Olomouc, Czech Republic), Sigma-Aldrich Chemie GmbH (Steinheim, Germany), CDN Isotopes (Quebec, Canada), or purchased from the Chembridge identification number.
- Chemical used for experiments were purchased from Sigma-Aldrich Chemie GmbH (Steinheim, Germany), Merck Life Science (Darmstadt, Germany), Duchefa Biochemie (Haarlem, Netherlands), Thermo Fisher Scientific (MA, USA), BD Bioscience (NY, USA).

3.2 Plant material and growth conditions

- Arabidopsis WT – *Arabidopsis thaliana* Columbia ecotype (Col-0)
- Arabidopsis lines expressing organelle-specific markers – β -ATPase:GFP (Logan and Leaver, 2000) in mitochondria, HDEL:GFP in ER (Matsushima et al., 2002), and H2B:YFP in nuclei (Boisnard-Lorig et al., 2001).
- Cell suspension cultures – *A. thaliana* Col-0, *A. thaliana* cv. Landsberg *erecta* (Ler), *Nicotiana tabacum* cv. Bright Yellow 2 cell line (BY-2)
- Arabidopsis seeds were surface-sterilised using a 70% ethanol solution (Merck Life Science, Germany) supplemented with 0.1% Tween-20 (Merck Life Science) for 10 min, rinsed with sterile deionised water. Seeds were sowed on solid Murashige and Skoog medium (4.4 g/L) (Duchefa Biochemie) supplemented with 1% sucrose (Sigma Aldrich) and 1% plant agar (Duchefa Biochemie). After 3 days of stratification at 4 °C in dark, the plates with seeds were arranged vertically and incubated for 10 days under long-day conditions (16 h light/8 h dark) at 22 °C.
- Cell suspension cultures of *A. thaliana* cv. Ler was grown in liquid Murashige-Skoog medium (4.4 g/L) supplemented with 3% sucrose, 0.232 μ M kinetin and 5.37 μ M 1-naphthaleneacetic acid. BY-2 was grown in Murashige-Skoog medium (4.4 g/L) supplemented with 3 % sucrose, 4 μ M thiamine, 555 μ M inositol, 1.47 mM KH₂PO₄ and 0.9 μ M 2,4-dichlorophenoxyacetic acid. Both cell lines were subcultured weekly into

fresh media in volume ratio 1:10. The cells were cultivated at 23 °C in dark and shaken at 120 rpm. 5-day-old cells were used for all experiments.

- Arabidopsis Col-0 cell suspension culture was grown in liquid Murashige and Skoog media with addition of 3% sucrose, pH adjusted to 5.7, in the dark at 22 °C and shaken at 120 rpm. Cells were weekly subcultured into fresh media in ratio 1:10. For all control and sorting experiments, 14-days old cells cultivated under continuous light ($150 \mu\text{mol photons m}^{-2} \text{s}^{-1}$) with fully-developed chloroplasts were used (Dubreuil et al., 2018).

3.3 Equipment

- Subcellular fractionation based on differential centrifugation and DGU was done using Centrifuge Heraeus Biofuge Stratos Thermo Fisher Scientific (MA, USA) and Ultracentrifuge CP 90 WX with swinging-bucket rotor P40ST-2054 Hitachi Koki (Tokyo, Japan).
- Organelle sorting was performed using BD FACSAria II and BD FACSAria III flow cytometer BD Bioscience (NY, USA). The software used for data processing was BD FACSDiva BD Bioscience (NY, USA).
- Auxin quantitative analysis was based on a LC-MS/MS analysis using a 1290 Infinity LC system and a 6495B Triple Quadrupole LC/MS system equipped with Jet Stream and Dual Ion Funnel systems Agilent Technologies (CA, USA) equipped with reversed-phase column (Kinetex C18 100A, length 50 mm, diameter 2.1 mm, particle size 1.7 μm ; Phenomenex; CA, USA) according to Pěnčík et al. (2018). All MS data were processed by MassHunter software Agilent Technologies (CA, USA).
- CK quantitative analysis was performed using an ACQUITY UPLC I-Class system combined with a triple quadrupole mass spectrometer Xevo TQ-S Waters (Manchester, UK) equipped with reversed-phase column (Acquity UPLC BEH C18, 1.7 μm , 2.1 \times 50 mm; Waters, Manchester, UK) according to Svačinová et al. (2012). All MS data were processed by Masslynx software Micromass (Manchester, UK).

4. SURVEY OF RESULTS

The current model of auxin and CK homeostasis maintenance at the subcellular level has been fully reviewed in (Skalický et al., 2018). The distinct localization of transporters, receptors, and enzymes related to auxin and CK suggests another layer of their complex regulation. The distribution of these phytohormones within plant organs or tissues is already well described but the importance of cell-type specific or intracellular phytohormone homeostasis is still poorly understood.

To shed light on phytohormone distribution within the plant cell, it is necessary to employ subcellular fractionation approaches. Differential centrifugation and DGU are possible conventional methods for isolation of cells and organelles. However, the use of advanced flow cytometric sorting as an ultra-selective tool for cell-type- and organelle-specific resolution analyses has been discussed (Galbraith et al., 2021; Antoniadi et al., 2021).

This doctoral thesis is focused on the metabolic profiling of phytohormones at the subcellular level utilizing approaches based on (ultra)centrifugation and flow cytometry (FCM) in combination with ultra-sensitive LC-MS/MS methods. To achieve this, several protocols dealing with organelle isolation were tested and optimised for subsequent phytohormone analysis. Moreover, a cutting-edge subcellular compartment separating technique based on principles of FCM has been developed.

4.1 Revealing auxin metabolome in the endoplasmic reticulum isolated by density-gradient ultracentrifugation

The endoplasmic reticulum (ER) plays a pivotal role in auxin distribution within the plant cell and auxin transport carriers have been identified to reside at this subcellular compartment. To elucidate the involvement of the ER in auxin homeostasis maintenance, an isolation protocol based on DGU has been optimized.

Initially, the effectivity and gentleness of two different homogenization methods were investigated. Grinding of 10-days old Arabidopsis seedlings with mortar and pestle in presence of quartz crystals showed more efficient organelle extraction compared to razor blade chopping. However, subsequent isolation of the ER via a discontinuous sucrose gradient was unsuccessful because the ER failed to focus properly at the expected

interphase. In addition, Western blot analysis showed the presence of other co-migrating organelles which impaired the purity of the isolated fraction. Finally, ER isolation was more effective after chopping of the seedling by razor blade as homogenization method.

However, our ER-enriched fraction still contained contaminants, especially chloroplasts or thylakoid membranes. Due to the fact that chloroplasts should be denser than ER the densities of gradient-forming sucrose solutions were slightly decreased. This resulted in chloroplast sedimentation to the bottom of centrifugal tubes. Finally, the described optimization of the isolation procedure resulted in elimination of unwanted co-migrating organelles in ER-enriched fraction. The collected ER-enriched fractions were then partitioned to high- and low-molecular weight subfractions containing proteins and auxins, respectively. Subsequent LC-MS/MS analysis of proteins extracted from the isolated ER confirmed the enrichment of the respective fraction with only minor contaminants.

DGU is a time-consuming process and auxin levels can be undesirably altered during ER isolation. Therefore, a control experiment was designed to examine possible changes. Released organelles from plant material were incubated at the same conditions mimicking the isolation of ER by DGU for 0 h and 3 h, and the relative abundance of individual auxin metabolites was compared at the selected time points. Importantly, only minimal changes in the auxin profile were observed. Finally, the ER-specific auxin profile was determined for the first time. Interestingly, auxin analysis revealed indole-3-acetic acid (IAA) enrichment in ER fraction compared to crude extract. However, the most dominant auxin metabolite in the crude extract (whole seedlings) as well as in the ER-enriched fraction was oxIAA-glc. We found the same relative proportion of oxIAA-glucosyl ester in both types of samples (79%). Altogether, we improved a protocol for ER isolation from *Arabidopsis* seedlings and for the first time reported for the first time the content of auxin and its metabolites in a highly ER-enriched fraction.

All data are summarized in:

Včelařová L, Skalický V, Chamrád I, Lenobel R, Kubeš FM, Pěnčík A, Novák O (2021). Auxin metabolome profiling in the Arabidopsis endoplasmic reticulum using an optimised organelle isolation protocol. Int. J. Mol. Sci. 22 (17), 9370.

4.2 Comparison of isolation methods for auxin metabolome determination in nucleus

The bioavailability of active IAA in the nucleus is crucial for triggering canonical auxin signalling. Direct monitoring of IAA levels and related metabolites in the nucleus may unravel a mechanism of spatial homeostasis maintenance. For accurate analysis of nuclear auxin content, two isolation methods were optimized. This study aimed to compare the pros and cons of nuclei isolation by conventional differential centrifugation and advanced FCM sorting from Arabidopsis and tobacco cell suspension cultures with respect to subsequent auxin analysis.

The cell suspension culture could not be homogenized by razor blade. Therefore, enzymatic digestion of the rigid cell wall in combination with protoplast lysis by osmotic shock was chosen as a homogenization method leading to gentle release of nuclei. Subsequently, nuclei were isolated by differential centrifugation or FCM. Western blot analysis showed that purer nuclear fractions were obtained after sorting than after centrifugation-based isolation. Moreover, FCM sorting allowed live monitoring of the organelle's condition changes, high reproducibility and easy quantification of collected organelles. On the other hand, the advantages of differential centrifugation are high yield, simplicity, and low expenses compared to FCM. Nevertheless, the low resolving power of differential centrifugation led to the presence of contaminating organelles in the nuclear fraction, mainly endomembranous compartments such as the ER or Golgi apparatus. Therefore, FCM sorting was chosen as the final isolation technique prior auxin analysis.

In addition to IAA detection, MS-based profiling of the isolated nuclei fraction also revealed the presence of auxin precursors and metabolites. The most abundant analyte in both nuclear samples isolated from Arabidopsis and tobacco cell suspension cultures was Tryptophan (Trp) as a primary metabolite (more than 99 % of relative distribution). Surprisingly, IAA and its metabolites prevailed in Arabidopsis nuclei, whereas auxin precursors predominated mainly in tobacco nuclei.

To confirm the applicability of FCM method, auxin metabolism was further promoted by feeding of the protoplasts with indole – a precursor of Trp – or active IAA. Indole treatment caused a high elevation of IAA precursors levels. Interestingly, only a slight increase in auxin metabolites was observed, but levels of free IAA were not altered in

Arabidopsis nuclei. After IAA treatment, levels of IAA as well as other analysed metabolites, such as 2-oxindole-3-acetic acid, IAA-aspartate and IAA-glutamate, were significantly increased. Overall, the combination of FCM with MS-based analysis has been shown to provide a useful tool for monitoring IAA and its metabolites at the subcellular level. Our methodology should help clarify the regulatory networks involved in plant development processes.

All data are summarized in:

Skalický V, Vojtková T, Pěňčík A, Vrána J, Katarzyna J, Koláčková V, Sedlářová M, Napier R, Kubeš MF, Novák O. (2021) Auxin profiling in isolated intact plant nuclei. Int. J. Mol. Sci. (submitted).

4.3 Auxin and cytokinin subcellular map

Conventional organelle isolation methods are focused on only one or at maximum of two types of organelles. Moreover, DGU-based protocols are time consuming (within hours). Therefore, a novel subcellular fractionation technique based on principles of FCM, so-called Fluorescence-Activated multi-Organelle Sorting (FAMOS), has been developed. FAMOS enabled the simultaneous sorting of 4 different organelle populations from one biological sample. Cell suspension culture of *Arabidopsis Col-0* was used as a simplified plant model. It was expected that the cell suspension culture exhibits a higher level of uniformity compared to the plant tissue, in which phytohormone gradients between different cell types were described (Pettersson et al., 2009; Pěňčík et al., 2013; Antoniadi et al., 2015).

First, a combination of organelle-specific fluorochromes was designed with respect to their excitation, emission, and minimisation of spectra overlap. Organelle populations were then identified based on the specific fluorescent signal of the organelles and the respective negative controls. Thus, the populations of chloroplast, nuclei, mitochondria, and ER were identified and a hierarchical gating strategy for their selection and subsequent sorting was established.

Furthermore, the identity of four sorted organelle-enriched fractions was examined by Western blot analysis. However, due to the impossibility of detecting all organelle marker proteins, the collected organelle populations were subjected to a much more sensitive LC-MS/MS based proteomic analysis. Importantly, our results showed an enrichment of the individual organelle fractions.

To disprove the changes in phytohormone profiles or analyte degradations during FAmOS, a set of control experiments covering the experimental design, from sample preparation to organelle sorting, was performed. The overall auxin profiles were not altered under our experimental conditions. However, levels of CK precursors (nucleotides and ribosides) have been shown to increase rapidly during sample preparation. Therefore, the homogenization buffer was supplemented with enzymatic or transport inhibitors to prevent undesirable increase of CK precursors levels. Finally, the use of a mixture of phosphatase inhibitors resulted in minimal changes in CK profiles during sample preparation. In addition, samples were spiked with isotopically labelled [$^{13}\text{C}_6$]IAA and [$^{15}\text{N}_4$]iP prior homogenization or sorting to monitor metabolic turn-over. The results showed that some negligible enzymatic activity persisted. As further measure to avoid altering the endogenous phytohormonal profile, the whole procedure was shortened to the minimum possible time. This was mainly achieved by preparing a fresh sample every half hour, followed by only 30 min of sorting. The sorted samples were then sub-fractionated for protein and phytohormone analyses. Each fraction was purified and analysed separately by LC-MS/MS methods. Finally, our FAmOS workflow was optimised to achieve high-resolution intracellular information about auxin and CK levels from a single sorted sample.

The FAmOS procedure was utilized to separate and collect the population of chloroplasts, nuclei, mitochondria, and ER. To create an overall phytohormonal map of a plant cell, vacuoles were isolated in parallel by a well-established DGU method (Robert et al., 2007). Employing ultra-sensitive MS-based methods, phytohormones were detected in only 200.000 pcs of collected organelles. Due to the different organelle sizes, the levels of the measured phytohormones concentrations were finally normalized according to each compartment's protein content. The concentration gradient of phytohormones was then expressed as subcellular heat maps of the ratio of auxin and cytokinin levels to the level of respective analyte in chloroplasts. Interestingly, auxins and CKs revealed different subcellular distributions within the plant cell. The highest concentration of both IAA and CKs was detected in vacuoles. In detail, CK *O*-glucosides, IAA-aspartate and IAA-glutamate were observed only in this organelle. Our findings point to a potential role of vacuoles as auxin and CK storage compartments. Further, CKs were also enriched in the ER, the place of their perception, while higher concentrations of IAA were measured in chloroplasts. The lowest concentrations of CKs and IAA were found in mitochondria.

In conclusion, the combination of efficient FAmOS with a sensitive MS-based method provides a unique approach for phytohormone profiling at the subcellular level. Our results present a way to simultaneously sort four different organelle populations based on the compartment-specific fluorescence parameters. Moreover, control experiments showed that neither sorting nor application of fluorescent dyes caused significant changes in both auxin and cytokinin profiles. Due to the high resolution of FAmOS, we also expect further use of this method for multiple omics approaches.

All data are summarized in:

Skalický V, Antoniadis I, Pěnčík A, Chamrád I, Lenobel R, Kubeš FM, Strnad M, Ljung K, Novák O. (2021) Fluorescence-activated multi-organelle sorting: A smart tool for subcellular mapping of auxins and cytokinins. (in preparation).

5. CONCLUSION AND PERSPECTIVES

This thesis deals with development and optimization of subcellular fractionation methods for subsequent high-resolution organelle-specific analysis of auxin and CK profiles. The combination of highly resolving fractionation techniques with ultra-sensitive LC-MS/MS analysis supplemented with modern approaches of molecular biology can elucidate the spatiotemporal coordination of phytohormone homeostasis maintenance at the subcellular level.

The most important outcomes of the described work are:

- Optimised isolation of ER by DGU can be utilized for phytohormone profiling. Auxin analysis revealed considerably higher levels of IAA in the ER-enriched fraction than in the whole plant.
- The FCM method provided higher purity of sorted nuclei than the differential centrifugation approach. Surprisingly, not only IAA but also its precursors and metabolites were detected in the nuclear fraction. However, Arabidopsis nuclei contains higher relative distribution of IAA and its metabolites whereas IAA precursors predominate in tobacco nuclei.
- Subcellular fractionation based on FCM enabled simultaneous sorting of 4 organelles. Moreover, FAmOS is a suitable tool for phytohormone profiling at the organelle level.
- One collected sample of sorted organelles can be subjected to auxin, cytokinin and proteomic analysis.
- A subcellular heat map of auxin and CKs revealed concentration gradients between different organelles.

Revealed concentration gradients of analysed phytohormones within the plant cell support our hypothesis that the distribution of phytohormone is in good agreement with relevant enzymes' and transporters' localizations (Skalický et al., 2018). However, the future involvement of respective loss-of-function mutants or overexpression lines of phytohormone transporters, receptors, biosynthetic or metabolic enzymes in profiling at the subcellular level can further shed light to regulation of homeostasis maintenance. The developed FAmOS is an innovative technique and a valuable tool not only for subcellular phytohormone analysis, but also for other “omics” approaches in plant sciences.

6. REFERENCES

- Antoniadi, I., Plačková, L., Simonovik, B., Doležal, K., Turnbull, C., Ljung, K., and Novák, O.** (2015). Cell-Type-Specific Cytokinin Distribution within the Arabidopsis Primary Root Apex. *Plant Cell* **27**: 1955–1967.
- Antoniadi, I., Skalický, V., Sun, G., Ma, W., Galbraith, D.W., Novák, O., and Ljung, K.** (2021). Fluorescence activated cell sorting—A selective tool for plant cell isolation and analysis. *Cytom. Part A: cyto.a.24461*. doi: 10.1002/cyto.a.24461.
- Boisnard-Lorig, C., Colon-Carmona, A., Bauch, M., Hodge, S., Doerner, P., Bancharel, E., Dumas, C., Haseloff, J., and Berger, F.** (2001). Dynamic analyses of the expression of the HISTONE::YFP fusion protein in arabidopsis show that syncytial endosperm is divided in mitotic domains. *Plant Cell* **13**: 495–509.
- Dubreuil, C., Jin, X., Barajas-López, J. de D., Hewitt, T.C., Tanz, S.K., Dobrenel, T., Schröder, W.P., Hanson, J., Pesquet, E., Grönlund, A., Small, I., and Strand, Å.** (2018). Establishment of Photosynthesis through Chloroplast Development Is Controlled by Two Distinct Regulatory Phases. *Plant Physiol.* **176**: 1199–1214.
- Galbraith, D.W. et al.** (2021). Best practices in plant cytometry. *Cytom. Part A* **99**: 311–317.
- Logan, D.C. and Leaver, C.J.** (2000). Mitochondria-targeted GFP highlights the heterogeneity of mitochondrial shape, size and movement within living plant cells. *J. Exp. Bot.* **51**: 865–871.
- Matsushima, R., Hayashi, Y., Kondo, M., Shimada, T., Nishimura, M., and Hara-Nishimura, I.** (2002). An Endoplasmic Reticulum-Derived Structure That Is Induced under Stress Conditions in Arabidopsis. *Plant Physiol.* **130**: 1807–1814.
- Pěňčík, A. et al.** (2013). Regulation of auxin homeostasis and gradients in Arabidopsis roots through the formation of the indole-3-acetic acid catabolite 2-oxindole-3-acetic acid. *Plant Cell* **25**: 3858–3870.
- Pěňčík, A., Casanova-Sáez, R., Pilařová, V., Žukauskaitė, A., Pinto, R., Luis Micol, J., Ljung, K., and Novák, O.** (2018). Ultra-rapid auxin metabolite profiling for high-throughput mutant screening in Arabidopsis. *J. Exp. Bot.* **69**: 2569–2579.
- Petersson, S. V., Johansson, A.I., Kowalczyk, M., Makoveychuk, A., Wang, J.Y., Moritz, T., Grebe, M., Benfey, P.N., Sandberg, G., and Ljung, K.** (2009). An Auxin Gradient and Maximum in the Arabidopsis Root Apex Shown by High-Resolution Cell-Specific Analysis of IAA Distribution and Synthesis. *Plant Cell* **21**: 1659–1668.
- Robert, S., Zouhar, J., Carter, C.J., and Raikhel, N.** (2007). Isolation of intact vacuoles from Arabidopsis rosette leaf-derived protoplasts. *Nat. Protoc.* **2**: 259–262.
- Skalický, V., Kubeš, M., Napier, R., and Novák, O.** (2018). Auxins and Cytokinins-The Role of Subcellular Organization on Homeostasis. *Int. J. Mol. Sci.* **19**: 3115.
- Svačinová, J., Novák, O., Plačková, L., Lenobel, R., Holík, J., Strnad, M., and Doležal, K.** (2012). A new approach for cytokinin isolation from Arabidopsis tissues using miniaturized purification: pipette tip solid-phase extraction. *Plant Methods* **8**: 17.

7. LIST OF AUTHOR'S PUBLICATIONS

Papers published in scientific journals:

- **Skalický V**¹, Kubeš M¹, Napier R, Novák O. (2018) Auxins and cytokinins—the role of subcellular organization on homeostasis. *Int. J. Mol. Sci.* **19** (10), 3115.
- Galbraith D, Loureiro J, Antoniadou I, Bainard J, Bureš P, Cápál P, Castro M, Castro S, Čertner M, Čertnerová D, Chumová Z, Doležel J, Giorgi D, Husband BC, Kolář F, Koutecký P, Kron P, Leitch IJ, Ljung K, Lopes S, Lučanová M, Lucretti S, Ma W, Melzer S, Molnár I, Novák O, Poulton N, **Skalický V**, Sliwinska E, Šmarda P, Smith TW, Sun G, Talhinhos P, Tárnok A, Temsch EM, Trávníček P, Urfus T. (2021) Best practices in plant cytometry. *Cytometry A.* **99** (4), 311-317.
- Antoniadou I, **Skalický V**, Sun G, Ma W, Galbraith DW, Novák O, Ljung K. (2021) Fluorescence Activated Cell Sorting – A selective tool for plant cell isolation and analysis. *Cytometry A.* **99** (Online ahead of print) doi: 10.1002/cyto.a.24461.
- Včelařová L¹, **Skalický V**¹, Chamrád I, Lenobel R, Kubeš FM, Pěňčík A, Novák O. (2021) Auxin metabolome profiling in the Arabidopsis endoplasmic reticulum using an optimised organelle isolation protocol. *Int. J. Mol. Sci.* **22** (17), 9370.

Papers in preparation:

- **Skalický V**, Vojtková T, Pěňčík A, Vrána J, Katarzyna J, Koláčková V, Sedlářová M, Napier R, Kubeš MF, Novák O. (2021) Auxin profiling in isolated intact plant nuclei. *Int. J. Mol. Sci.* (submitted)
- **Skalický V**¹, Antoniadou I¹, Pěňčík A, Chamrád I, Lenobel R, Kubeš FM, Strnad M, Ljung K, Novák O. (2021) Fluorescence-activated multi-organelle sorting: A smart tool for subcellular mapping of auxins and cytokinins. (in preparation)

¹ These authors contributed equally to the presented works.

Published abstracts

- **DSEBR** – 13th Student Days of Experimental Plant Biology in Brno (Czech Republic), 2015 – oral presentation (*Isolation of Arabidopsis Endoplasmic Reticulum by Sucrose Gradient Ultracentrifugation and Its Proteomic Characterization*)
- **Growth regulators on the way** in Malá Morávka (Czech Republic), 2016 – oral presentation (*Auxin and Cytokinin Metabolome Profiling on the Subcellular Level*)
- **TNPR** – Trends in Natural Products Research: A Young Scientist Meeting of PSE and IUNG PIB in Pulawy (Poland), 2016 – poster (*Auxin Metabolome Profiling in Vacuoles*)
- **PBE** – Plant Biology Europe EPSO/FESPB Congress in Prague (Czech Republic), 2016 – poster (*Auxin Metabolome Profiling in Vacuoles*)
- **ICCB** – 12th International Congress of Cell Biology in Prague (Czech Republic), 2016 – poster (*Auxin Metabolome Profiling in Nuclei*)
- **Rooting 2017** – 8th International Symposium on Root Development in Umeå (Sweden), 2017 – poster (*Sorting of Plant Organelles via Flow Cytometer*)
- **ACPD** – International Symposium of Auxins and Cytokinins in Plant Development in Prague (Czech Republic), 2018 – poster (*Subcellular phytohormone profiling in Arabidopsis based on FAOS technique*)
- **G4G** – Plant Biotechnology: Green for Good in Olomouc (Czech Republic), 2019 – poster (*Subcellular phytohormone mapping in Arabidopsis based on mFAOS technique*)
- **IPGSA** – The 23rd International Conference on Plant Growth Substances in Paris (France), 2019 – poster (*Subcellular phytohormone mapping in Arabidopsis based on mFAOS technique*)
- **SPPS** – Scandinavian Plant Physiology Conference in Umeå (Sweden), 2019 – poster (*Subcellular phytohormone mapping in Arabidopsis based on mFAOS technique*)
- **CKFR** – Cytokinin forefront research in Prague (Czech Republic), 2020 – oral presentation (*Cytokinin subcellular mapping in Arabidopsis*)
- **CBPRS** – Chemistry and biology of phytohormones and related substances in Malenovice (Czech Republic), 2021 – oral presentation (*Metabolic profiling of phytohormones in subcellular compartments using LC-MS techniques*)
- **FEBS** – Plant Organellar Signalling Workshop in Priomošten (Czech Republic), 2021 – selected oral presentation (*Metabolic profiling of phytohormones in subcellular compartments using LC-MS techniques*)

8. SOUHRN (SUMMARY, IN CZECH)

Předložená disertační práce s názvem „Metabolické profilování rostlinných hormonů v buněčných organelách pomocí LC-MS technik“ se věnuje problematice udržování homeostázy auxinů a cytokininů na subcelulární úrovni. Auxiny a cytokininy jsou důležité fytohormony regulující nespočet fyziologických procesů vedoucích k vývoji a růstu rostlin. Dále ovlivňují jejich plasticitu tedy schopnost rostlin reagovat na vnější i vnitřní biotické a abiotické podněty. Pro studium distribuce auxinů a cytokininů v rámci buňky bylo třeba vyvinout a optimalizovat nové metody pro izolaci organel rostlinného materiálu pomocí diferenciální centrifugace, diskontinuální hustotně-gradientové ultracentrifugace a metod založených na průtokové cytometrii (FCM).

Nejprve byla optimalizována metoda pro izolaci endoplazmatického retikula (ER) v sacharózovém hustotním gradientu. Obohacení ER bylo sledováno pomocí imunoblotu, kde byla sledována přítomnost proteinových markerů ER, ale také ostatních organel. Výsledky z imunoblot analýzy bylo následně ověřené proteomickou analýzou založené na technikách kapalinové chromatografie ve spojení s tandemovou hmotnostní spektrometrií (LC-MS/MS). V ER-obohacených frakcích byl následně stanoven auxinový profil. Bylo zjištěno, že v ER je obohacena aktivní forma auxinu tedy indolyl-3-octové kyseliny (IAA) oproti celé klíčící rostlině.

Dále byly porovnány dva rozdílné přístupy izolace jader založené na diferenciální centrifugaci a moderní FCM. Po optimalizaci obou metod bylo zjištěno, že jaderná frakce získaná tříděním pomocí FCM vykazuje vyšší čistotu. Proto byla tato metoda následně využita pro třídění jader ze suspenzní buněčné kultury *A. thaliana* Ler a tabákové suspenzní kultury BY-2. Bylo zjištěno, že v jádrech se nevyskytuje pouze IAA, ale i její prekurzory a metabolity. Z výsledků kvantitativního stanovení auxinů lze usoudit, že FCM je vhodná metoda pro subcelulární frakcionaci a následné metabolické profilování fytohormonů.

Z tohoto důvodu byla vyvinuta metoda zvaná Fluorescence-Activated multi-Organelle Sorting (FAMOS). FAMOS umožňuje současné třídění až 4 populace různých subcelulárních kompartmentů z jednoho vzorku, v tomto případě chloroplastů, jader, mitochondrií a endoplazmatického retikula ze suspenzní buněčné kultury *A. thaliana* Col-0. Tříděné organely byly následně podrobeny analýze proteinů, auxinů a cytokininů. Dosažené výsledky nakonec umožnili sestavení subcelulární mapy fytohormonů ukazující

koncentrační gradient v buňce. Pro ověření spolehlivosti metody, byly buňky před sortováním ošetřeny izotopicky značenou IAA, nebo isopentenyladeninem umožňující sledovat metabolismus fytohormonů. Analýza izotopicky značených fytohormonů a jejich metabolitů ukázala jejich odlišnou distribuci v buňce. Je pravděpodobné, že technika FAmOS bude využitelná i v dalších vědních odvětví založených na „omických“ přístupech jako transkriptomika, proteomika, metabolomika se subcelulárním rozlišením.